Dissertation zur Erlangung des Doktorgrades der Fakultät für Chemie und Pharmazie
der Ludwig-Maximilians-Universität München

Aggregation of Therapeutic Antibodies in the Course of Downstream Processing

vorgelegt von

Eva Rosenberg

aus Stuttgart

Februar 2010

Erklärung

Diese Dissertation wurde im Sinne von § 13 Abs. 3 bzw. 4 der Promotionsordnung vom 29. Januar 1998 von Herrn Prof. Dr. Gerhard Winter betreut.

Ehrenwörtliche Versicherung

Diese Dissertation wurde selbständig, ohne unerlaubte Hilfe erarbeitet.

München, am 02. Februar 2010

(Eva Rosenberg)

Dissertation eingereicht am 02. Februar 2010

1. Gutachter: Prof. Dr. Gerhard Winter

2. Gutachter: Prof. Dr. Wolfgang Frieß

Mündliche Prüfung am 26. Februar 2010

Acknowledgements

The presented thesis has been acquired within a research cooperation between the Department of Pharmacy, Pharmaceutical Technology and Biopharmaceutics at the Ludwig-Maximilians-University Munich and Roche Diagnostics GmbH in Penzberg under the supervision of Prof. Dr. Gerhard Winter.

First of all, I would like to express my gratitude to my supervisor Prof. Dr. Gerhard Winter for the possibility to join his research group, especially for his professional guidance and the scientific input and advice he gave me over the years. Furthermore, I highly appreciate his ongoing interest in the progress of my work as well as the opportunity to participate in numerous scientific meetings. Thank you for the pleasant working climate and the different social events encompassing barbecues, skiing and hiking tours.

Moreover, I want to thank Prof. Dr. Wolfgang Frieß for taking over the co-referee and for participating in discussions during scientific meetings.

Special thanks to all present and former colleagues from the research group of Prof. Dr. Winter and Prof. Dr. Frieß. Thank you all for the warm welcome, the convenient and friendly atmosphere as well as the support whenever I stayed at the institute.

From the Department of Physical Chemistry of the Ludwig-Maximilians-University Munich, I would like to thank Dr. Steffen Schmidt for conducting the SEM measurements.

I am very grateful to the Department of Pharmaceutical Biotechnology Development for Recovery and Downstream processing at Roche Diagnostics, Penzberg, for the outstanding cooperation, the provision of different IgGs and the financial support.

Particularly, I acknowledge Dr. Wolfgang Kuhne for giving me the opportunity to work within this interesting project and for his dedicated inspirations, numerous fruitful discussions and the freedom to operate. Thank you for always being interested and encouraging.

In addition, I would like to dedicate special thanks to Dr. Stefan Hepbildikler for his support and the opportunity to conduct the main part of the practical work in his lab. Stefan, I am truly indebted for your general scientific support as well as your friendly and honest guidance. Thank you for the accurate proof-readings of divers manuscripts and your encouragement over the years.

To all other colleagues from Roche, I am deeply indebted for your support and kind assistance during the years. Karin Christa, Jürgen Lang, Bernard Sallier, Monika Schweigler and Michael Tischler for being my lab companions and for introducing me to the field of practical protein purification. Alexander Kurtenbach has to be mentioned for his dedicated input concerning the buffer solute quantification assays.

Special thanks are addressed to Katrin Heinrich for her dedicated and accurate work concerning the concentration method development.

Juliane Adelmann, Andreas Adlberger, Stephanie Kanzler, Bernd Maier, Alexandra Leiss, Angelika Strauch and others are also highly acknowledged for assistance and introduction in several analytical techniques.

Many thanks to Prof. Dr. Georg-Burkhard Kresse and Dr. Alexander Skolaut for the collaboration concerning the preparation of divers patent applications and the release of scientific publications including this thesis.

Furthermore, I would like to acknowledge Dr. Michael Frenz (Micromeritics GmbH, Mönchengladbach) for conducting the BET specific surface area determination by gas adsorption analysis.

Thanks are also extended to PD Dr. Stefan Zahler, Prof. Dr. Franz Bracher, Prof. Dr. Franz Paintner and Prof. Dr. Frank Böckler for serving as members of my thesis advisory committee.

Beside the above mentioned persons from university and industry, I especially want to thank my parents for their enduring love and their belief in me. Thank you for the encouragement and support you gave me over all the years of studying.

Finally, I want to thank Jochen for his love and mental support. Thank you for being the most important person in my life.

Für meine Eltern

Table of content

Chapter I General introduction

1 Therapeutic antibodies

With 29 US Food and Drug Administration (FDA)-approved mAbs, sales of monoclonal antibodies (mAbs) constitute 35 % of the total biologics market in 2009 (Aggarwal 2009). Nearly all of them are of the immunoglobulin isotype G (IgG) and the subclass IgG1 (Nissim and Chernajovsky 2008; Piggee 2008). The foundation of this triumphal procession was the generation of the first murine mAb by using the hybridoma technology (Koehler and Milstein 1975). This was the initiation to make mAbs available in large-scale for the specific treatment of various diseases mainly in the field of transplantation, oncology, inflammatory, infection and auto-immunogenicity.

To date, cancer therapeutics dominate the field (Pavlou and Reichert 2004). Several technology improvements have provided different approaches to overcome drawbacks for the broad therapeutically application in man. Clinical studies revealed that mAbs of murine origin triggered human immune responses (Shawler et al. 1985). After the injection of mouse mAbs into humans it is very likely that a HAMA (Human Anti Mouse Antibody) response will be developed (Khazaeli et al. 1994), limiting therapeutic efficacy of the product to the first or, at most, second dose administration. Moreover, it was realized that binding and hence affinity of the mAb to a specific antigen is not a sufficient condition for antitumor effect and efficacy. Mediated effector functions by Fc receptor binding are needed but are not fully provided by the murine mAb. These effector functions include on the one hand complement activation triggering a cascade of enzymatic reactions. This enzymatic reaction leads to a recruitment of phagocytes and a formation of a membrane-attack complex resulting in lysis of tumor cells (Gelderman et al. 2004). This effector function is termed complement dependent cytotoxicity (CDC). On the other hand, effector cells like natural killer cells and other leucocytes can respond via antibody dependent cellular cytotoxicity (ADCC) (Hessell et al. 2007). After interaction of their Fcγ receptors with

the Fc proportion of the tumor cell-bound antibodies a lytic attack of the potentially cytotoxic cells leads to death of the targeted tumor cells.

Genetic engineering provided a way to make these mechanisms accessible by implementing a human Fc proportion in the molecule (Walsh 2003; Walsh 2004). The reshaping can end up in chimeric as well as in humanized molecules. Chimeric mAbs only include xenogenetic variable regions (V_H and/ or V_L) whereas humanized molecules have solely a hyper variable antigen-binding region (complementarity determining regions: CDR) of murine origin grafted into the human immunoglobulin scaffold (Saldanha 2007). See Figure I-1 for the general introduction to the structure of IgG.

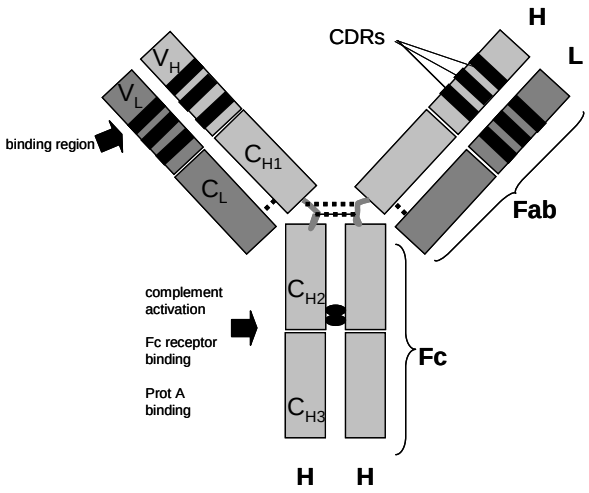

Figure I-1: **General introduction to antibody structure and function**
IgG is a protein composed of two identical heavy chains (H, 50 kDA) and light chains (L, 25 kDa) assembled by disulfide bonds (dashed lines). The Fab fragments (50 kDa) comprise the binding region for the specific antigen. The two antigen-contacting domains of the Fab are the variable region of the heavy (V_H) and light (V_L) chain. Three complementarity determining regions (CDR) per variable chain form the surface composed of hyper variable loops. The constant domains C_{H3} and C_{H2} of the two heavy chains form the Fc proportion. C_{H2} mediates complement activation and Protein A binding. It contains a polysaccharide component at a conserved asparagine in each heavy chain (black ball). C_{H2} and C_{H3} together mediate the binding to cell surfaces and induce cellular immune responses.

Usually humanized mAbs are significantly less immunogenic than chimeric molecules, however it is reported that some patients generate human antichimeric antibodies (HACA) after administration (Hwang and Foote 2005). Moreover, humanized mAbs show in most cases a concomitantly prolonged half-life but a compromized affinity in comparison to the chimeric ones (Luo et al. 2003). Humanized full length human antibodies can be obtained

by genetically engineering the immune system of the mouse. One basic idea was introduced in the 1990s, to generate an immune response in IgG-knock-out mice after inserting human antibody gene repertoires into the mouse genome. Afterwards the hybridoma technology was used to fuse spleen cells of the transgenic mouse with myeloma cells (Roque et al. 2004). But none of the molecules derived from these mice have yet made it into the market.

The first entirely human recombinant IgG1 antibody was approved in 2006 (Adalimumab, Humira©) inhibiting tumor necrosis factor alpha. The approach of generating a specific antibody from human antibody gene repertoires completely in vitro was applied by using the phage-display technology (Winter et al. 1994). The antibody fragments such as Fab or the single variable fragments V_H or V_L domains are cloned as a fusion with phage coat protein, resulting in libraries of phage, each displaying an antibody fragment. The selection of numerous antibody fragments of different specificity against a target is afterwards possible without the laborious generation of hybridoma cells. Moreover, the resulting link between phenotype and genotype (binding affinity and gene sequence) allows simultaneous recovery of the gene encoding the antibody of choice (Hoogenboom 2005).

The choice of the expression system depends on the intended use, required yield, preset costs and needed effector functions of the therapeutically used mAb. For the commercial production of fully length antibodies today, mainly mammalian cell culture is applied beside transgenic organisms like plants or animals (Chadd and Chamow 2001; Roque et al. 2004). For the production of the approved therapeutic chimeric or humanized therapeutic antibodies either Chinese Hamster Ovary (CHO) or mouse myeloma (NS0) cell lines are used (Chadd and Chamow 2001).

Unlike for bacterial expression, the potential to produce glycosylation patterns of the Fc region similar to those resulting from human cells is given. The degree of galactosylation and fucosylation and the proportion of bisecting N-acetyl-glucosamine residues have all been implicated in modulating effector functions (Yamane-Ohnuki and Satho 2009). By glyco-engineering of CHO cells a glycosyltransferase (GnTIII) catalyzes the formation of bisecting N-acetyl-glucosamine residues inhibiting the introduction of the core fucose in the Fc N-glycans. This leads to improved ADCC (Ferrara et al. 2006; Umana et al. 1999). Further, a knockout CHO cell line has been developed which was shown to stably produce non-fucosylated antibodies with enhanced ADCC (Niwa et al. 2005).

2 The purification process of therapeutic antibodies

The coding gen-sequence of mAbs is usually expressed in mammalian cells. In comparison to bacterial hosts which are capable to conduct some post-translational metabolic reactions such as lipidation, proteolysis or phosphorylation, mammalian cells have the ability to perform N- and O-glycosylation, too. Moreover, this expression system provides the target molecule usually properly folded and fully functional. The molecule is directly secreted into the cell culture medium and no disruption of the host cells and no solubilization and refolding is required in order to harvest the target protein. As a consequence, there are less isoforms, indigenous proteins expressed by the host cell (called host cell proteins: HCPs), DNA and cellular components present and hence the purification process is usually less complex compared to processes from bacterial hosts like E. coli (Prouty et al. 1975).

On the other side both, mammalian cell culture systems and proteins produced in mammalian cell culture are generally more complex than those of bacterial origin. Various process supplements may have to be added to the culture media including vitamins, lipids, serum, growth hormones, mineral salts, amino acids or antibiotics (Birch and Racher 2006).

The process to separate the target protein of interest from the cell free supernatant containing different impurities and to deliver the purified protein in a concentrated matrix required for administration is referred to as downstream processing (DSP).

Impurities are usually defined as process and product related. Product related impurities are molecule variants arising during manufacturing or storage which do not have properties comparable to those of the desired product with respect to activity, efficacy, and safety. Truncated forms, aggregates, precursors, deamidated or oxidized species can be subsumed here. Process related impurities encompass those that are derived from the manufacturing process and which are related to the cell substrate, the cell culture or the purification process. Table I-1 shows a summary of the process and product related impurities based on ICH Q6B guideline named "Specifications: Test procedures and acceptance criteria for biotechnological/ biological product" (ICH Q6B 1999a).

Classification according to ICH Q6B guideline	Impurities related to	Characteristics
Process-related impurities	Cell substrate	Host Cell Proteins (HCPs)
		Host Cell DNA
		Proteases
		Virus-like particles
	Cell culture	Process supplements
		Cell culture media components
	Downstream	Chromatographic leachables, ligands (like Protein A)
		Chemical and biochemical processing reagents
		Inorganic salts
		Solvents
		Endotoxins
Product-related impurities	Manufacturing and/ or storage	Truncated forms
		Precursors
		Other modified forms: deamidated, isomerized, S-S linked, oxidized or altered conjugated forms
		Aggregates

Table I-1: List of process- and product related impurities
According to the ICH guideline Q6B.

In addition, to product- and process related impurities, molecular entities and variants referring to the desired product can be removed or accumulated during manufacturing. These species are considered as product-related substances and can be formed during the manufacturing process or during storage. They have properties comparable to the product concerning activity, efficacy and safety. Due to the biosynthetic process used by living organisms an inherent degree of structural heterogeneity is predefined in protein products. Therefore, the desired product can be a mixture of defined product and product-related substances which are e.g. glycoforms occurring due to incomplete post-translational modification.

Finally, foreign contaminants introduced during the manufacturing process, such as microbial species, e.g. adventitious viruses or mycoplasma, as well as their chemical and

biochemical products (e.g. microbial proteases) need to be removed during the several steps of the DSP.

The level of process-related impurities like HCPs has to be significantly reduced during downstream processing. Since these impurities are potentially antigenic and thus elicit an undesirable immune response in the patient (Eaton 1995), they have to be eliminated or reduced to a level that will not cause an immune response. Regulatory guidelines require that HCP levels have to be routinely monitored using suitable analytical assays but it is impossible to set a common limit for all approved products due to the fact that reagents of the analytical test used are product and production system related and their sensitivity and selectivity is not comparable (CPMP 1997).

Residual host cell DNA from continuous mammalian cell lines (CCLs) was considered to be a risk factor for safety because of concerns that residual host DNA may be tumorigenic. Data published in the 1990s revealed that milligram amounts of human tumor cell DNA containing an activated oncogene did not cause tumors in primates (Wierenga et al. 1995). Hence, CCL DNA possesses much less a risk than thought and should be therefore considered today as a general impurity. For this, the removal to a low level up to 10 ng of residual CCL DNA per dose of the purified product is considered acceptable (CPMP 2001; WHO Expert Committee 1998).

Beside purity, the primary considerations during DSP are yield, robustness, reliability and scalability which are mandatory for a well-developed purification process.

2.1 Preparative chromatography

There are a variety of preparative modes of chromatography which have been employed for the process-scale purification. A purification strategy for any protein can be divided into three sequential stages: capture, intermediate purification and polishing.

2.1.1 Capture

In this stage the target protein is initially separated from the harvested cell culture fluid. The major goal is to concentrate the target protein and to concomitantly remove as much of the contaminants as possible.

In the purification of full length mAbs, affinity chromatography applying bacterial Fc receptors is the most common technique (Huse et al. 2002). Numerous cells and viruses have proteins on their surfaces which bind selectively to the Fc part of the immunoglobulin.

Different bacterial Fc receptors have been described including Protein A from Staphylococcus aureus and Protein G from Streptococcus subspecies. Today, mostly Protein A is used as an affinity ligand in preparative chromatography. IgG of human origin and most animal derived ones bind well, with exception of mouse IgG1. Generally, all IgG subclasses bind with high affinity except for IgG 3 which is weakly bound (Huse et al. 2002; Langone 1982).

Both, the native Protein A and a recombinant one from E. coli are applicable. Beside the full sequenced ligand, the recombinantly derived fragment without the cell wall domain is available (Hammond et al. 1990). Moreover, a tetramer of the IgG binding domains of Protein A is commonly used, since amino acids particularly sensitive to alkali were substituted for more stable ones in this construct.

Protein A has been immobilized via different linkers to all macro-porous chromatographic matrices suited for protein chromatography, such as cross linked agarose, polymethacrylate, polystyrene-divenylbenzene or porous glass (Boschetti and Jungbauer 2000; Hahn et al. 2003). After matrix activation several linkers can be covalently bound to the matrix via a large number of hydroxyl groups carried on the surface. Initially, Protein A was immobilized on CNBr activated agarose. Today, coupling of Protein A is commonly carried out by applying epoxy chemistry. Here, the matrix is activated by using bis-oxirane 1,4 bis-(2,3-epoxypropoxy-)butane. Afterwards the ligand is attached to the matrix via a C-terminal cystein favoring an orientated thioether coupling. A description of activating agents used with hydroxyl-containing matrices explaining the different ligand coupling reactions, mostly based on nucleophilic reactions, is detailed elsewhere (Boschetti 1994).

Especially, engineered Protein A derived recombinantly from E. coli is stable over a wide pH range of 2 to 11 and is able to refold after denaturation. This is important since urea, guanidine salts or sodium hydroxide are applied for regeneration and cleaning in place of the chromatographic resin.

Association between IgG and Protein A is affected by pH (Cuatrecasas and Anfinsen 1971). Binding conditions in Protein A chromatography are usually at pH 5-7, whereas protein desorption is performed at more acidic pH values of 3.0-4.5 (Shukla et al. 2007).

The interaction of Protein A with the IgG molecule is characterized by hydrophobic interaction together with some hydrogen bonds and two salt bridges (Li et al. 1998b). A positively charged histidyl residue at a pH < 6 located in both, the binding site of the Fc proportion and the Protein A, is involved in the dissociation of the two molecules, based on electrostatic repulsion (Burton 1985; Lindmark et al. 1977). Concomitantly, the hydrophobic counteract between the molecules is weakened. At alkaline or neutral pH the hydrophobic character of the uncharged imidazole rings contributes to net hydrophobicity at the interface of the two molecules, strengthening association.

The lower the pH, the higher the yield during elution. Concomitantly, the risk to affect conformational integrity or increase aggregation or fragmentation increases (Arakawa et al. 2004; Ejima et al. 2006; Vermeer and Norde 2000). Therefore, defined desorption conditions have to be individually optimized for every molecule to improve yield and concomitantly ensure stability.

Several attempts have been described to avoid the low pH elution by adding chaotropic salts, hydrophobic competitors to the dilution buffer like ethylene glycol, or arginine and arginine derivates (Arakawa et al. 2004; Ejima et al. 2005; Shukla et al. 2005). Only limited success was achieved on the one hand due to reduced yield and prolonged elution times in the case of arginine and arginine derivatives. On the other hand conformational changes of the eluted protein in the case of chaotropic salts like guanidine hydrochloride are reported.

2.1.2 Intermediate purification and polishing

Once the target protein has been captured, usually small amounts of impurities are present in the capture pool of a mAb purification process. After optimized Protein A chromatography frequently an overall purity of nearly 97-99 % can be achieved according to analytical size exclusion chromatography (Fahrner et al. 1999). During the subsequent steps purification has to be completed. In most mAb manufacturing processes Protein A affinity chromatography is followed by two further chromatography steps for intermediate purification and polishing (Shukla et al. 2007).

Chromatography techniques used should resolve the target protein from impurities on the basis of small differences in a single physicochemical attribute. High yield and high resolution are additionally important (Williams 2005).

Ion-exchange (IEX) chromatography is widely used after capturing the target protein. IEX chromatography separates biomolecules on the basis of charge characteristics. Charged groups on the surface of a protein interact with oppositely charged groups immobilized on the chromatographic medium. The charge of a protein depends on the pH of the environment. When operating at pH above the isoelectric point (IP) of the target protein, the target protein will be negatively charged and should bind to anion-exchange media which are positively charged. At an operating pH lower than the IP, the target protein will be positively charged and should bind to cation-exchange media which are negatively charged. Therefore, the IP of the target protein is the key to develop an IEX chromatography step.

Instead of binding the target protein to the matrix, binding of the impurities is possible while the target protein remains in the flow-through (Williams and Frasca 2001). Therefore, it is also valuable to know the IP of the impurities present. In both cases the conditions for binding and elution have to be optimized regarding pH and conductivity to ensure the separation of the target protein. Moreover, resolution, capacity and yield have to be optimized.

During anion-exchange (AEX) chromatography host cell DNA, virus-like particles, leached Protein A, HCPs or endotoxins can be removed. For removal of DNA, endotoxin and retrovirus-like particles, mostly product flow-through applications are effective (Curtis et al. 2003; Strauss et al. 2009b) since these impurities are negatively charged and bind to these resins while the mAbs do not. Leached Protein A and HCPs can also be effectively reduced in product-binding mode using the ability to elute the mAb within a sodium chloride gradient at much lower conductivity than HCPs or Protein A. At a pH near the IP of the mAb which is usually between pH 8 and 9, these impurities are much more negatively charged than the mAb due to their IP of around 5 (Sjoequist et al. 1972). Hence, a higher amount of salt is needed to remove them from the column compared to the removal of the mAb.

Conversely, an operating pH of around 8 leads to affinity complexes of IgG and Protein A complicating purification (Gagnon 2007). Moreover, product-binding mode is often limited by lower capacity and operating at a pH above 7 elevates the risk of deamidation and proteolysis (Geiger and Clarke 1987; Robinson and Rudd 1974).

Cation-exchange (CEX) chromatography in product-binding mode is usually performed at pH of 4.5-5.5. At this pH range a high product binding capacity is achieved due

to the enhanced positive net charge of the mAb. Concomitantly, a charge complementarity to strongly electronegative impurities is enhanced as well. This leads to stable charge complexes between the mAb and the polyphosphorylated impurity DNA. Therefore, CEX chromatography is effective in Protein A, HCPs and aggregate removal but not in DNA removal (Ansaldi and Lester 2005).

Hydrophobic interaction chromatography (HIC) is highly effective in aggregate removal (Guse et al. 1994; Lu et al. 2009). Considering the manufacturing of biomolecules mostly aqueous salt solutions are used here as mobile phase. Retention is achieved through interactions between non-polar ligands and hydrophobic patches accessible on the surface of the native protein (Jungbauer 2005). By increasing the salt concentration these hydrophobic portions of the molecule can interact with the HIC ligand, encompassing functional groups like phenyl- or butyl-residues. Operated in product flow-through mode the salt concentration can be reduced. Impurities such as HCPs and aggregates bind to the HIC media at reduced salt concentration due to their higher hydrophobicity (Wang and Ghosh 2008).

Ceramic hydroxyapatite (CHT) which is a special form of calcium phosphate sintered to a spherical particle, has been applied for protein purification (Giovannini and Freitag 2001; Jungbauer 2005). Protein binding is mediated by electrostatic interactions of carboxyl- and amino functions with calcium and phosphate groups of the chromatographic matrix. The majority of applications use a phosphate or chloride gradient to remove leached Protein A, DNA, virus-like particles and endotoxin (Gagnon 2009b). Elution with a chloride gradient in the presence of low phosphate concentration is known to remove IgG aggregates (Guerrier et al. 2001). A constant low level of phosphate between 5-15 mM weakens calcium affinity interactions but leaves ionic interactions relatively unaffected. During chloride gradient elution ionic bonds can be dissociated. The native IgG elutes before the aggregated species do.

Size exclusion chromatography (SEC) is a very robust technique to remove aggregates by a size based separation mechanism. Therefore, it is usually used for product quality monitoring during DSP development. However, its use for preparative purposes is limited. Since only 5-10 % of the column volume can be applied to the column, the huge column dimensions required at manufacturing scale are difficult to handle.

2.2 Viral clearance

Viral contaminants in the final product can arise either from adventitious introduction of viruses during processing or from the rodent cell expressing copies of endogenous retroviral genomes (Lieber et al. 1973). Retrovirus-like particles from CHO cells are not infectious and have not been associated with any disease in humans. However, murine-derived retroviral agents have been linked to tumorigenesis (Donahue et al. 1992). In order to minimize the presence of viral contaminants complementary approaches to inactivate and remove viral impurities are used in accordance to the ICH guideline "Viral safety evaluation of biotechnology products derived from cell lines of human or animal origin" (ICH Q5A (R1) 1999b) and the "Points to Consider" (PTC) of the FDA (CBER 1993; CBER 1997).

Usually, subsequent to Protein A chromatography the pH of the pool material is lowered to < 3.7 over ≥ 30 minutes at room temperature to inactivate especially lipid-enveloped viruses, e.g. xenotropic murine leukemia virus (X-MuLV), a model for rodent endogenous retrovirus (Brorson et al. 2003). Beside low pH treatment, other solvents as well as detergents are applied to inactivate potential viral impurities. In the blood plasma industry detergents like Polysorbate 80, Triton X-100 or solvent additives like tri-n-butyl phosphate (TNBP) are applied for virus inactivation (Roberts 2008; Roberts and Dunkerley 2003).

Moreover, inactivation by heat or UV-C irradiation, as well as removal by nanofiltration are possible steps within the purification process which are in addition dedicated to viral clearance but can potentially introduce demage to the molecule (Li et al. 2005; Marques et al. 2009).

The virus removal capacity of chromatographic steps has been demonstrated, although by some health authorities they are not considered as robust as solvent/ detergent inactivation, inactivation by heat or nano-filtration (CBER 1997) since the virus reduction factor can vary with pH and/ or conductivity of column buffer. Protein A affinity chromatography and anion-exchange chromatography can provide 10^4-fold of viral clearance capacity (Fahrner et al. 2001). Anion-exchange chromatography is known to remove a wide range of viruses including rodent viruses like minute virus of mice (MVM) or X-MuLV, as well as other model viruses like simian virus 40 (SV40) (Strauss et al. 2009a). Mostly product flow-through mode is applied (Strauss et al. 2009b). In general, the purification process has to provide a safety margin of ≥ 10^6 for the patients treated, e.g. less than 1 in 10^6 doses may potentially contain one retrovirus-like particle.

2.3 Filtration

Normal flow filtration (NFF) in which the feed flow is going perpendicular to the filter surface, is frequently employed during the purification process. Microfiltration membranes with a pore size of 0.1-0.2 μm are used to reduce the bioburden of process intermediates and to support sterility of the final formulated drug product. In addition, particles can be removed which is helpful to prevent fouling of the chromatographic columns. Moreover, nano-filtration is conducted in order to remove viral contaminants by using a pore size of 20 (-50) nm. Depth filtration can remove particles and larger aggregates of product or process related impurities like HCPs or DNA. Due to interception, internal impaction and diffusion, particles as small as 0.01 μm can be retained mainly in the depth of the filter matrix (Cheryan 1998).

2.3.1 Tangential flow filtration

In tangential flow filtration (TFF) the feed is going tangentially to the length of the membrane surface. Thus, as an alternative term for TFF, cross flow filtration is frequently used. Two streams are leaving the filtration device, the so-called retentate and the permeate. The nominal molecular weight cut-off (NMWC) determines which molecules remain in the cycled retentate and which molecules pass through the membrane and enter the permeate. Figure I-2 shows a schematic presentation of a TFF process.

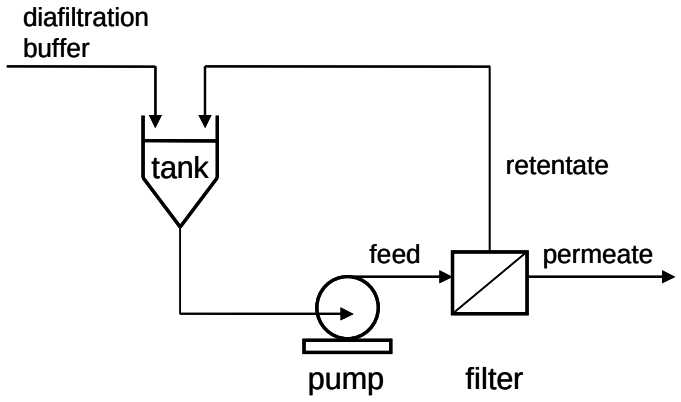

Figure I-2 Schematic presentation of a TFF process

In mAb purification processes usually the mAb is in the retentate whereas buffer ions and other diffusible compounds form the permeate. During the multi-step purification of therapeutic IgG ultrafiltration (UF) membranes with a normal molecular weight cut-off (NMWC) of 10–50 kDa are frequently applied. This ensures the reliable retention of the mAb in the retentate due to its molecular weight of about 150 kDa. UF operations are usually conducted between orthogonal chromatographic steps or prior to final formulation to concentrate the protein, exchange buffer, remove low molecular weight impurities or simply salts (Herb and Raghunath 2007). During UF concentration and diafiltration a high throughput is desired to allow short process time (Ahrer et al. 2006). The throughput of non-retained components like water and buffer solutes is termed permeate flux and is influenced by physical and physico-chemical factors. Physical factors refer to the system hydrodynamics while physico-chemical factors include properties of the membrane and the feed solution (Huisman et al. 2000).

2.3.2 System hydrodynamics

Especially during concentration processes retained protein or particles are concentrated at the membrane surface, causing a decrease in permeate flux over time. These compounds, being largely rejected by the membrane, tend to deposit on the surface and thus their local concentration increases. This concentration polarization is installing an additional layer on the membrane surface which is known as gel layer or cake layer (Howell and Velicangil 1982; Suki et al. 1984; Suki et al. 1986). In addition, solutes diffuse back to the bulk solution where the concentration is lower according to Fick's law of diffusion (Wilkes 2006).

The film theory is the simplest and most widely used theory to model permeate flux in mass transfer controlled UF which is shown schematically in Figure I-3. The well known schema as well the following Equations I-1, I 2 and I-3 are taken according to Cheryan and Porter (Cheryan 1998; Porter 1972).

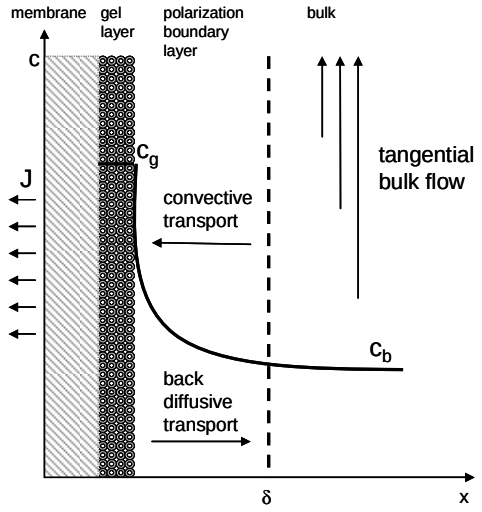

Figure I-3: **Film theory model schematically**
Concentration polarization of colloidal and macromolecular solutes on a membrane surface during UF: The build-up of the gel layer of a concentration cg and the associated boundary layer is shown. C_b is the concentration of the bulk solution.

The model assumes that permeate flux (J) is controlled by the gel layer resistance when the convective transport J_{con} ($J \cdot c$) of retained solutes to the membrane surface is equal to back-diffusive transport J_{back} ($D\ (dc/dx)$). This steady state can be described as:

$$J \cdot c = D\frac{dc}{dx} \qquad \text{Equation I-1}$$

Where c is the concentration of retained species in the bulk and $\frac{dc}{dx}$ is the concentration gradient. Integrating equation (1) over the boundary layer ends in:

$$J = \frac{D}{\delta}\ln\frac{c_g}{c_b} = k\ln\frac{c_g}{c_b} \qquad \text{Equation I-2}$$

Where δ is the thickness of the polarization boundary layer over which the concentration gradient exists, c_g is the concentration of the gel layer and k is the mass transfer coefficient calculated as:

$$k = \frac{D}{\delta} \qquad \text{Equation I-3}$$

D is the diffusion coefficient of Brownian motion. Since the values of c_g and c_b are mostly fixed by physicochemical properties of the feed, the permeate flux can only be improved

by increasing k and thus reducing the thickness of the boundary layer. It is important that this model does not consider the hydrodynamic action of particles in the concentrated layer due to shear flow of the layer during tangential flow operations (Davis and Leighton 1987).

In NFF there are on the one hand permeation drag and sedimentation forcing the retained solutes to deposit on the surface. On the other hand, diffusive transport of solutes back into the bulk solution is based on Brownian motion (Chan 2002). Beside the hydrodynamic forces acting on the retained solutes in NFF, TFF results in additional forces. Figure I-4 shows schematically the hydrodynamic forces acting on retained solutes during TFF.

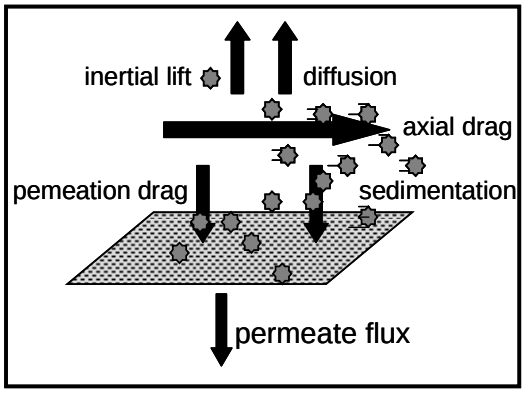

Figure I-4: Hydrodynamic forces acting on retained solutes during TFF

Shear-induced hydrodynamic diffusion processes are lifting particles in the concentrated layer away from the membrane exceeding by far the diffusion coefficient for Brownian motion. An axial drag results from tangential feed flow causing the retained solutes to move over the length of the membrane. When shear induced diffusion is sufficient to offset opposing sedimentation and permeation drag the polarization boundary layer on the membrane is reduced thus resulting in higher permeate flux (Belfort et al. 1994).

In membrane filtration processes the system hydrodynamics are directly affected by operating parameters like transmembrane pressure (TMP) (Aimar et al. 1989; Bacchin and Aimar 2005), permeate flux (Kim et al. 1992) and retentate (cross flow) velocity (Meireles et al. 1991). Thus, the adjustment of these parameters affects solute deposition on the membrane surface.

Permeation drag is mainly influenced by the TMP:

$$TMP = \frac{(p_i + p_o)}{2} - p_p \qquad \text{Equation I-4}$$

Where p_i is the inlet (feed) pressure, p_o is the outlet (retentate) pressure and p_p is the permeate pressure. According to Darcy´s law (Equation I-5) the permeate flux increases proportionally with TMP:

$$J = \frac{TMP}{\mu R} \qquad \text{Equation I-5}$$

Whereas an increase in intrinsic membrane resistance R_M (the product of bare membrane resistance R and viscosity μ of the permeate) results in permeate flux decline. R_M increases with filtration time due to concentration polarization and gel layer formation. This is accounted for by the addition of a further resistance term, R_G, referring to the gel layer, following the resistance model (Cheryan 1998):

$$J = \frac{TMP}{R_M + R_G} \qquad \text{Equation I-6}$$

The proportional relation between permeate flux and TMP is only valid if low pressure values and low feed concentration are applied. Increasing permeate flux due to increased TMP results in high permeation drag forcing retained solutes to deposit on the membrane surface. Hence the built up of the gel layer is enforced and flux becomes independent of pressure. Then the mass transfer limited model (film theory model) adequately reflects the factor influencing permeate throughput, i.e. the thickness of the boundary layer, as described above.

Figure I-5 shows the correlation of applied TMP and permeate flux depending on the concentration of the protein in the retentate. Flux increases linearly with increased TMP, according to Equation I-6. Beyond a certain TMP, a higher TMP does not result in increased permeate flux. The gel layer is formed and overall resistance increases. Consequently, at high TMP, the permeate flux reaches a maximum and becomes constant and independent from pressure. The complete constitution of the gel layer varies with concentration at a constant tangential feed flow rate.

The knee-point of the curve can be used to identify the actual values of TMP beyond which the permeate flux remains constant. Moreover, every deviation from the straight line of clean water flux indicates the onset of gel layer build-up. This can be used to iden-

tify critical flux values beyond which the permeation drag forces the retained solutes to deposit on the membrane surface. Hereby, critical flux values can be determined by considering the slope deviation which is than called *critical flux identification in the strong form*. If the slope deviation is neglected and solely the knee-point is considered, this refers to *critical flux identification in the weak form* (Field et al. 1995; Wu et al. 1999).

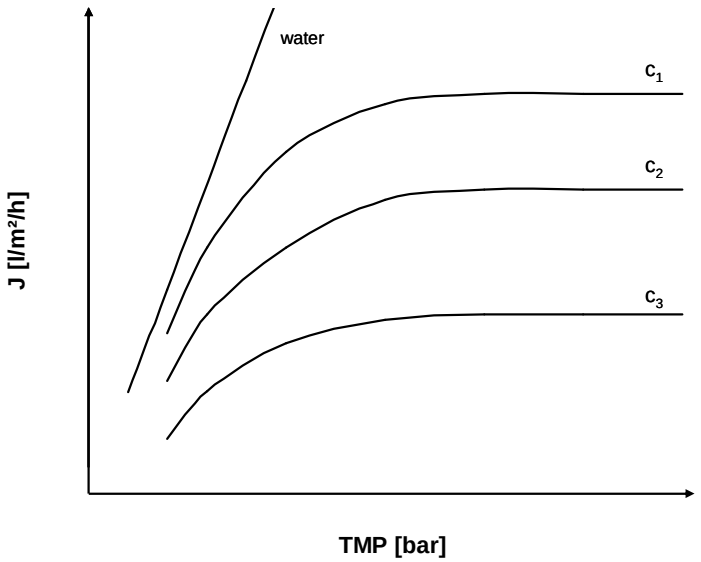

Figure I-5 : The correlation of applied TMP and permeate flux (J) with increasing protein concentration in the retentate ($c_1 > c_2 > c_3$) is shown schematically
The permeate flux increases with increasing protein concentration at a constant feed flow rate Q_1.

The thickness of the boundary layer can be reduced by increasing axial drag and hydrodynamic diffusion processes. In TFF operations this is achieved by increasing the feed flow rate (Q) and/ or the pressure drop (Δp) between feed (p_i) and retentate (p_o). Equation I-7 shows the proportional relation between Q and Δp according to the Poiseuille equation for laminar flow (Tutunjian 1983):

$$\Delta p = \frac{k_1 \mu L Q}{d^4} \qquad \text{Equation I-7}$$

Where μ is the viscosity of the retentate solution, L the length of the membrane, d the height of the fluid channel and k_1 is a constant depending on channel geometry. In addition, the proportional relation between Δp and the retentate flow Qr is based on Equa-

tion I-7 as well. Figure I-6 shows the correlation of permeate flux and TMP depending on the applied feed flow rate $\dot{Q}$.

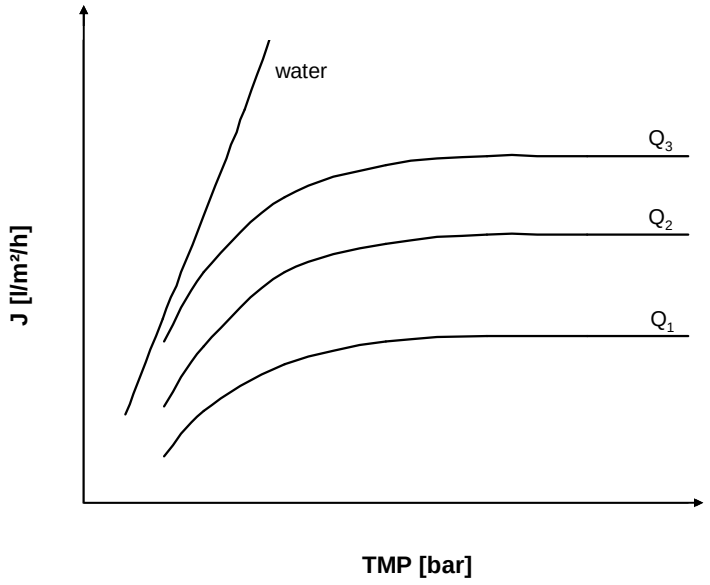

Figure I-6 : **The correlation of applied TMP and permeate flux (J) with increasing feed flow rate ($Q_1 > Q_2 > Q_3$) is shown schematically**
The permeate flux increases with increasing feed flow rate at a constant protein concentration c_3 in the retentate.

Permeate flux increases linearly at lower TMP and becomes constant at higher levels when the gel layer is completely built up. The level of final pemeate flux increases with tangential feed flow rate due to increased mass transfer, according to Equation I-3.

2.3.3 Physico-chemical effects

Beside hydrodynamics of the process, the physico-chemical properties of the membrane and the feed solution are the main factors which have influence on the deposition of retained solutes on the membrane and hence the permeate flux (Huisman et al. 2000; Mondor et al. 2004).

Due to attractive protein-membrane and protein-protein interactions the deposition of protein on the membrane can be affected. Electrostatic interactions, as well as hydrophobic interactions can be involved. Electrostatic interactions between the individual protein molecules and between the protein and the membrane depend on the prevailing solution conditions (Fane et al. 1983; Palecek and Zydney 1994). At pH values above or below

the IP of the protein the net charge of the protein increases with the distance of pH away from the IP. Hence, electrostatic charge repulsion between the protein molecules and charged membrane surfaces results in reduced deposition. Moreover, the charge repulsion between the protein occupied membrane and non-adsorbed protein reduces ongoing deposition on the surface.

Usually commercially available membrane materials used for UF steps during manufacturing of therapeutic mAbs are not ionic in nature. The membrane materials applied are mainly polysulfone (PS), polyethersulfone (PES) or regenerated cellulose (RC) (Rubin and Christy 2002; Van Reis et al. 1999). Especially PES membranes have a wide pH and temperature tolerance (Deanin 1972) which makes them a robust material in terms of cleaning and sterilizing in place. Due to their hydrophobicity compared to RC these membranes tend to interact strongly with a variety of solutes making them prone to adsorption of protein which can result in yield loss. Especially, at the pH equal to the IP of the protein, increased deposition of protein has been observed accompanied by reduced permeate flux (Fane et al. 1983; Koehler et al. 1997; Palacio et al. 1999; Salgin 2007).

It was reported that the charge of a membrane can be affected by pH or solutes, whether the material is ionic or not (Maenttaeri et al. 2006). As the material itself is not ionic it has been suggested that the apparent zeta potential of the membrane is affected by specific adsorption of ions on the membrane surface from the circulating solution (Nystroem et al. 1989). Streaming potential measurements are commonly used to characterize the interface of the membrane and an electrolyte. The external pressure (Δp) causes movement of the liquid and thus ions are stripped off along the shear plane and a streaming current is formed. The resulting electrical field is generated due to accumulation of charge on the downstream side (Ariza et al. 2001). The measurable electrical potential differences (ΔV) between the two ends of the solid/ liquid system gives direct information about the electrostatic charge at the shear plane and thus the so-called apparent zeta potential can be calculated (see chapter V and VI).

Benavente and Johnson showed that the apparent zeta potential of a PS membrane varied in the same way as that of the protein. The zeta potential of both, the protein and the membrane depends on the prevailing pH and salt concentration of the processed bovine serum albumin (BSA) solution (Benavente and Jonsson 1998). Results revealed that membrane permeability decreases strongly when the salt concentration increases or the pH decreases, having its minimum at the IP of BSA. Concomitantly, the apparent zeta poten-

tial values of the membrane decrease with increasing pH and salt concentration showing again a minimum when the pH is equal to the IP of BSA.

In summary, the surface chemistry of the membrane as well as the solution conditions have influence on the deposition of a specific protein on the membrane surface and hence permeate flux. The presence of salts and the pH alter the effective charge on the protein surface and the apparent zeta potential of the membrane.

Moreover, the growth and the hydraulic permeability of the deposited layers have influence on permeate flux. Both, surface charge of the protein and the character and concentration of the salts used, have impact on the permeability of the deposited layers. The permeability of the protein deposits was reported to decrease with increased ionic strength of the feed at a pH above and below the protein IP (Fane et al. 1983; Palecek et al. 1993; Palecek and Zydney 1994). This reflects the decrease in electrostatic repulsion between the proteins due to charge shielding effects of the salt. Permeability was relatively independent of ionic strength at the isoelectric point in the < 0.5 M salt concentration range (Palecek et al. 1993; Salgin 2007). Generally, at a pH equal to the IP it is suggested that more compact packing of the uncharged molecules occurs, resulting in a denser polarized layer than under electrostatic repulsion. This leads to more pronounced permeate flux decline (Nakatsuka and Michaels 1992).

Beside the influence of pH and salts, Kelly and Zydney reported that existing aggregates in the feed solution have an impact on the permeability of the membrane. Enhanced deposition of BSA was caused by the attachment of native protein molecules on existing aggregates on the membrane resulting in flux decline. After physical deposition of the aggregated species, chemical attachment of native BSA was reported. This chemical addition appeared to occur via the formation of an intermolecular disulfide linkage. Permeate flux increased when 1 mM dithiothreitol was added to the feed solution or s-cysteinylated BSA was applied (Kelly and Zydney 1995).

3 Stability during processing

Due to their size, complex structure and the correlation between their structure and function, proteins have a limited stability and are prone to degradation. In general, proteins are

known to be susceptible to chemical and physical instability (Brange 2000; Goolcharran et al. 2000; Manning et al. 1989b).

Chemical instability refers to modifications of covalent bonds, encompassing deamidation reactions, oxidation reactions or cleavage of peptide bonds. Physical instability or degradation refers to changes in secondary or tertiary structure, adsorption to surfaces, aggregation and precipitation.

Concerning aggregation, there are different types of aggregates previously mentioned in the literature, although there is no consistent definition used in general (Cromwell et al. 2006; Philo 2006). The type of aggregate can be categorized regarding size, type of bond, reversibility and protein conformation (Mahler et al. 2009).

For the purpose of this work, aggregates are divided in different types on the basis of their physical properties, as regards solubility and size. Aggregates which are not visible as discrete particles and can not be removed by a filter with a pore size of 0.1-0.2 μm are referred to as soluble higher molecular weight species (HMWs). Usually these aggregates of a size < 0.1 μm are analyzed by size exclusion chromatography. Aggregates which can be removed by 0.1-0.2 μm filtration are referred to as insoluble aggregates. Hence, these aggregates have a size of > 0.1 μm up to several hundred μm. This category encompasses particles which are visible to the unaided eye, as well as those particles which are subvisible, since it is reported that the human eye is able to resolve objects slightly smaller than 100 μm at a distance of 25 cm (Blackwell 1946).

Subvisible aggregates and particles are only partly addressed in the pharmacopeial monographs for sub-visible particles present in a pharmaceutical preparation (EDQM 2001a; EDQM 2001b; USPC 2002), since the document only refers to the species of ≥ 10 μm and ≥ 25 μm. Hence, particles between 0.1 μm and 10 μm are not addressed here. It is currently under discussion that actually these particles have the potential to impact safety and efficacy of the protein product. They appear during processing as well as during handling, storage and shipment in the final product container (Carpenter et al. 2009).

Beside this classification regarding size and solubility, aggregates can be characterized by their reversibility mentioned above. Aggregates being covalently linked over chemical bonds are usually more stable than reversible aggregates. If they are cross linked over disulfide bridges (Andya et al. 2005; Van Buren et al. 2008), reducing conditions are required to resolve them. Reversible aggregates can result from electrostatic protein interactions leading to self-association affected by solution conditions, e.g. pH (Liu et al. 2005).

Several chemical conditions including pH, ionic strength, redox potential and co-solvents may be used in DSP to separate the mAb from product and process related impurities. Often the used environmental conditions for the protein are far from physiologic in vivo and therefore may provoke chemical as well as physical instability. The low pH during Protein A elution and subsequent low pH incubation for viral inactivation is known to potentially provoke aggregation (Ejima et al. 2006; Shukla et al. 2005). Therefore, during process development it is important to find a combination of parameters which ensures both, stability and maximum purity at the same time.

Moreover, throughout manufacturing, the protein is exposed to several physical stress principles. The exposure to air-liquid interfaces (Kiese et al. 2008; Sluzky et al. 1991), to solid surfaces of different hydrophobic or hydrophilic materials (Mollmann et al. 2005; Randolph and Carpenter 2007), to temperature variations during freeze-thawing (Cao et al. 2003; Kueltzo et al. 2008) or to UV-light sources (Kerwin and Remmele 2007; Qi et al. 2008; Roy et al. 2009) can provoke aggregation.

Moreover, mechanical stress during pumping is known to potentially induce aggregation. Meireles at al. (1991) studied the effect of different pump heads and observed an increase in turbidity of an albumin preparation with pumping time at room temperature by using a screw pump. Likewise it was observed that the use of a peristaltic pump enhanced aggregation (Chandavarkar 1990). Particle formation of an IgG was eliminated by replacing a radial piston pump with a rolling diaphragm pump (Cromwell et al. 2006). A combination of physical stress principles can be involved in aggregation as well. Cavitations during pumping creating and destroying air bubbles and hence increasing the air-water interface is reported to enhance the formation of protein aggregates. Concomitantly, a higher shear stress during pumping was observed to contribute to aggregation (Gomme et al. 2006).

3.1 Conformational aspects of aggregation

It is reported that proteins can form aggregates with predominantly native structure as well as with predominantly non-native structure. The latter ones can be termed non-native aggregates. The native secondary structure of mAbs mainly consists of anti-parallel β-sheet structure as analyzed by Fourier transformed infrared spectroscopy (FT-IR) and small angle X-ray scattering (Cleland et al. 2001; Costantino et al. 1997).

Aggregates can be formed in response to thermal, chemical or physical stress or in the absence of any stress factors, showing concomitantly conformational changes in secondary structure. The formation of an intermolecular hydrogen-bonded anti-parallel β-sheet structure was observed during heat induced association of several molecules, regardless of the initial secondary structure composition of the native protein (Dong et al. 1995; Van Stokkum et al. 2002). Moreover, some molecular regions of the protein, like hydrophobic regions or free SH-groups, become accessible to new intermolecular interactions forming aggregates through non-covalent or disulfide bonds. Especially during heating the secondary and tertiary structure becomes more flexible and therefore more reactive towards its neighbors (Militello et al. 2004).

Several studies revealed that rather partially unfolded molecules are involved in aggregation than complete unfolded ones (Fink 1995; Fink 1998; Grillo et al. 2001; Kendrick et al. 1998a; Kim and Yu 1996). The classic three-stage model describing the denaturation process reflects that protein molecules do not solely exist in the native form (*N*) or completely unfolded (Dill and Shortle 1991; Dobson 1992).

A third state is defined where the molecules are not completely unfolded and therefore appear more compact. Only a small expansion of the native surface can be observed (Fink 1995; Kendrick et al. 1998a). For this, the intermediates are additionally termed molten globules or compact intermediates (*AI*). Today it is known that protein molecules can pass more than one intermediate state until they are completely unfolded. The stability of the intermediates and hence their detectability can depend on the molecular weight of the protein (Bam et al. 1998; Clarke and Waltho 1997). The unfolding is described as a continuous process in which the molecule passes a reversible transition state (*TS*) after activation. Hydrophobic patches are identified on the surface of these intermediates which are prone to aggregation (AI_{n+1} and $n\,AI$) to minimize thermodynamically unfavorable interactions with water (Cleland et al. 1993; Fink 1998; Sluzky et al. 1991). Lumry and Eyring (1954) described the pathway of non-native protein aggregation. Summarized, it involves a reversible conformational change of *N* forming an aggregation-competent species *AI*. This is followed by irreversible assembly of the non-native molecules *AI*. A schema of this process is presented here:

$$N \leftrightarrow TS \rightarrow AI \qquad \text{(step 1)}$$

$$AI + n\,AI \rightarrow AI_{n+1} \qquad \text{(step 2)}$$

Aggregation considered within the Lumry-Eyring framework shows a rate limitation within the unfolding (step 1) explaining the first order kinetics of aggregation reported for recombinant human Interferon γ (rhIFN γ) (Kendrick et al. 1998b; Mulkerrin and Wetzel 2002; Webb et al. 2001). The subsequent aggregation of the non-native species follows a second or higher order process. Thus, according to this model, aggregation does not seem to be limited by the protein concentration and hence protein-protein collision.

In contrast, aggregation of recombinant human Granulocyte-Colony Stimulating Factor (rhGCSF) was reported to follow a second-order reaction, suggesting that the aggregate-competent species is composed of at least two non-native molecules (AI_2) (Chi et al. 2003b; Krishnan et al. 2002). The dimeric aggregation-competent species can afterwards undergo irreversible assembly to form larger aggregates (AI_{n+2}). In addition, the transition species (TS) can react with an already formed aggregate (AI_n) to form larger aggregates. In this model the concentration of the non-native species is the rate limiting step of aggregation. A schema of the described process is presented here:

$$2N \leftrightarrow 2TS \rightarrow AI_2 \qquad \text{(step 1)}$$

$$AI_2 + nAI \rightarrow AI_{n+2} \qquad \text{(step 2a)}$$

$$AI_n + TS \rightarrow AI_{n+1} \qquad \text{(step 2b)}$$

3.2 Colloidal aspects of aggregation

As reported above, protein molecules undergo both, conformational changes and an assembly process to form aggregates. The assembly process is a result of attractive intermolecular interactions leading to self-association. The total interaction forces in aqueous colloidal systems are mainly described as attractive hydrophobic van der Waals- and repulsive Coulombic electrostatic interaction (Scopes 1994). The sum of these forces represents the total interaction energy acting on two spherical particles, as described in the Derjaguin-Landau-Verwey-Overbeck (DLVO) theory on colloidal stability.

For proteins, the distribution of hydrophobic and hydrophilic residues as well as charged residues on the surface of the molecules mainly determines the overall intermolecular interactions in solution. As described above, hydrophobic amino acid residues are exposed on the surface of the protein molecules during unfolding. In the native state these

residues are usually buried internally (Damodaran and Kinsella 1981). The exposure of these residues can accelerate molecular assembly due to more pronounced hydrophobic interactions (Fink 1995; Kendrick et al. 1998a).

But conformational alteration is not a basic prerequisite for the formation of aggregates. An overall charge near zero minimizes electrostatic repulsion whether the protein is unfolded or of native conformation. In any case, the molecules are prone to association due to pronounced attractive hydrophobic interaction forces or reduced electrostatic repulsion. In the case of an IgG1, aggregates are reported to be mainly of native structure after stressing the protein by shaking and stirring (Kiese et al. 2008). Recombinant human granulocyte colony stimulating factor (rhGCSF) has been prevented from aggregation even in the partially unfolded state. At pH 3.0, no aggregation was observed when 0.9 % benzyl alcohol was added which is known to cause partial unfolding of the protein (Thirumangalathu et al. 2006). At pH 3 the protein carries an allover positive charge resulting in enhanced colloidal stability and inhibited the formation of aggregates (Chi et al. 2003a).

Electrostatic interactions are generally affected by pH and ionic strength of the solution. Electrostatic interactions between isocharged surfaces are always repulsive suppressing the self-association. Non-charged surfaces are present when the pH of the solution is equal to the IP of the protein. In addition, at a pH unequal to the IP, the presence of salt can reduce charge-charge repulsion by charge shielding. Figure I-7 shows a schema of the total overall interaction energy of two isocharged surfaces in accordance to the DLVO theory depending on pH and salt concentration (Chi et al. 2003a; Israelachvili and Wennerstrom 1996).

When the distance between two isocharged surfaces, e.g. two protein particles, is reduced, a maximum interaction energy barrier (ΔW_{max}) has to be overcome to bring them in physical contact. Afterwards, attractive forces result in coagulation and thus aggregation. The higher ΔW_{max} the more kinetically stable is the colloidal system and dispersed particles are present in solution. With increasing salt concentration electrostatic repulsion is screened and ΔW_{max} is lowered. When the ionic strength is high enough, ΔW_{max} becomes negative which results in coagulation.

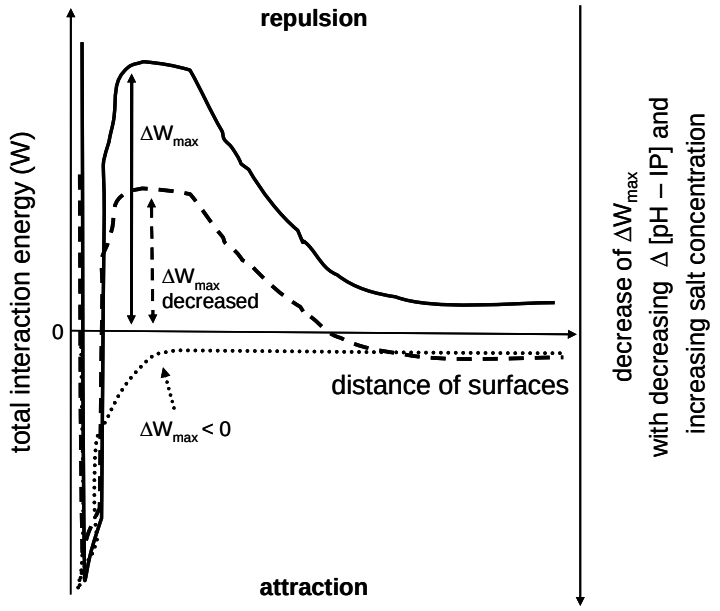

Figure I-7: **Schema of total interaction energy (W) of two isocharged surfaces resulting from the sum of attractive and repulsive net forces depending on pH and salt concentration (according to Chi et al 2003a and Israelachvili and Wennerstrom 1996)**
ΔW_{max} is the maximum interaction energy barrier of two particles (black arrow). A decrease of ΔW_{max} (dashed arrow) occurs with increased salt concentration or by decreasing the absolute value of the difference between solution pH and IP of the protein (Δ [pH-IP]). A $\Delta W_{max} < 0$ (dotted arrow) results in coagulation and aggregation.

Concomitantly, the higher the difference between solution pH and IP of the protein (Δ [pH-IP]) is, the higher is the value of ΔW_{max}. This results in a more kinetically stable system having again dispersed particles present in the solution. Coagulation occurs at $\Delta W_{max} < 0$, e.g. when the pH of the system is equal to the IP of the protein.

For rhGCSF aggregation was induced by the addition of 150 mM sodium chloride at pH 3.5 by shielding charge-charge repulsion present at this pH (Chi et al. 2003a). Advant and coworkers reported that self association of recombinant human Interleukin-2 (rhIL-2) was enhanced at pH 3.6 which is close to the IP of the protein. This resulted in the formation of differently sized aggregates. At a pH of 6.5 and 8.6 the formation of dimers was reduced (Advant et al. 1995).

In general, protein self-association is linked to environmental conditions regarding protein concentration, temperature, pH, and type and amount of added salts (Przybycien

and Bailey 1989). The self-associating species can be either of native conformation or structurally altered.

The added salts can have influence on both, the conformational stability of the protein and the colloidal stability of the system. According to the Hofmeister-Series salting-in electrolytes preferentially bind to the protein and thus increase the net charge of the protein. The resulting increased electrostatic free energy of the protein causes a decrease in stability and the protein tends to denature in the presence of these electrolytes (Von Hippel and Schleich 1969). Concomitantly, electrostatic repulsive forces prevent protein association and aggregation, or in other words increase the solubility of the protein in aqueous solutions.

On the other hand, electrolytes like sodium-, magnesium or ammonium sulfate are termed salting-out additives since the solubility of the protein decreases sharply at high molar salt concentrations preserving concomitantly the native conformation of the protein (Arakawa and Timasheff 1982; Arakawa and Timasheff 1984). These salts increase the surface tension of water and are therefore depleted from the surface layer. This preferential exclusion of the salt from the surface of the protein leads to the observation of a preferentially hydrated protein surface enriched in water as well as an increase in the total free energy of the system (Timasheff 1993). Since the preferential exclusion of the salt per subunit protein is reduced in the agglomerated state, precipitation of the protein is thermodynamically favored over the dispersed protein in solution. This principle has been widely used for selective precipitation and crystallization of proteins for purification purposes (McDonald et al. 2009).

3.3 Concentration dependent aggregation

By looking at aggregation as a simple association of at least two molecules, this bimolecular process is considered to be concentration dependent. This can be explained by increased encounter frequency and decreased dissociation tendency in crowded systems (Minton 2005). Crowded systems contain macromolecules at concentrations occupying a large fraction of the total volume of fluid. The formation of aggregates is reported to be enhanced even though a second molecular species is added to the system contributing to a general increase in macromolecular concentration. Therefore, self-association as well as hetero-association can be facilitated in crowded fluids (Zimmerman and Minton 1993).

Rivas et al. (1999) showed that the formation of dimers and larger oligomers of fibrinogen can be induced in the presence of > 40 g/l BSA without significant hetero-association of fibrinogen and BSA. The amount of higher ordered aggregates was increased when an IgG was reconstituted from a dried powder to a protein concentration of 200 mg/ml. Almost no aggregates appeared, when a concentration of 5 mg/ml was prepared (Dani et al. 2007).

Especially under quiescent shelf-life setting, aggregation was observed to increase with higher protein concentration (Alford et al. 2008a; Treuheit et al. 2002). However, agitation induced aggregation was observed to decrease with higher protein concentration. This was explained by the reduced air-water interface to protein ratio with increased protein concentration. After occupation of the total interface, the protein remaining in solution is protected from surface interaction which is known to greatly enhance aggregate formation on the basis of conformational changes (Donaldson et al. 1980; Henson et al. 1970).

In contrast, macromolecular crowding is expected to stabilize the native structure of the protein. Especially in concentrated solutions, the molecules are assumed to exclude volume to one another on the basis of steric repulsion and thus reducing the systems entropy. As a consequence, the systems free energy is increased and the most favored state will be the one excluding the least volume. Therefore, the compact native state is favored over the extended unfolded states of the protein. Moreover, macromolecular compaction and association is enforced since aggregated molecules exclude less volume to another than an equal number of isolated molecules (Minton 1980; Minton 1998).

Protein aggregation based on increasing collision frequency may further depend on the diffusional mobility of the molecules. Crowding is considered to reduce the diffusional mobility of the molecules, since viscosity is observed to increase with a higher macromolecular concentration (Liu et al. 2005). Therefore, diffusional limitations can define an upper limit of bimolecular reaction rates at a higher total macromolecular concentration (Zimmerman and Minton 1993).

Beside the diffusional mobility of the protein molecules, the diffusional mobility of the solutes is affected at a higher protein concentration. This can be important considering the concentration methods which are applied to obtain highly concentrated solutions in manufacturing scale. As described in section 2.3.1 of this chapter, UF in TFF-mode is the method of choice retaining the protein on the retentate side and concomitantly allowing the pass through of soluble solutes to the permeate side. It is known that the concentra-

tion of the diffusible charged solutes on the permeate and the retentate side is theoretically equal leading to the same defined composition of soluble solutes in the retentate before and after UF. Due to an increasing concentration of a charged protein on the retentate side the partitioning of charged solutes across the semipermeable membrane is affected. This thermodynamic non-ideality can result from intermolecular charge-charge based interactions between the charged protein molecules and the charged solutes affecting the partitioning of the solute. This is termed the Donnan-effect and Stoner and coworkers (2004) related these facts to the process development environment of different therapeutic proteins.

In general, a high total concentration of macromolecules in solution is known to affect the equilibria and kinetics of macromolecular reactions. Due to volume exclusion an effect on protein stability including protein folding as well as protein aggregation is reported.

3.4 Nucleation aspects of aggregation

Aggregation can be considered as a nucleation and growth phenomenon (Chi et al. 2003b). It was observed that aggregation in solution can start suddenly. Afterwards, aggregation proceeds and the aggregated species increase in number and size. Concomitantly, the monomeric protein population is depleted.

It is assumed that protein molecules assemble and locally accumulate, eventually exceeding their solubility limit and precipitate. To create such a new solid-liquid interface, assembly is allowed after the system has raised the free energy required. To achieve that, a stable critical-sized species has to be formed by spontaneous coalescence consisting of n molecules (Andrews and Roberts 2007; Li et al. 2009; Rotter et al. 2005). This species is called embryo or critical nucleus. The time until the nuclei are build up is described as a lag phase in aggregation and is caused an energy barrier to assembly. When the critical size of the nucleus is reached where energy barrier is highest then growth of the nucleus occurs and a new phase is formed spontaneously (Chi et al. 2003b; Debenedetti 1996). Such nucleation which occurs in the interior of a uniform substance is called homogeneous nucleation and is reported to increase with increasing concentration or increased temperature (Powers and Powers 2006).

Nucleation which occurs at nucleation sites on surfaces contacting the liquid is termed heterogeneous nucleation. At such preferential sites the effective surface energy is lower, thus the free energy barrier is diminished and nucleation is facilitated (Apfel 1970; Debenedetti 1996).

Figure I-8 shows a schema of homogeneous and heterogeneous nucleation leading to the further propagation of larger protein aggregates. When a critical nucleus is formed in solution (A), on the surface of an existing aggregate (B) or a foreign surface (C), this species grows into larger agglomerates. After exceeding a defined size the new aggregated species is separated from the nucleation site. The newly formed aggregates are afterwards able to serve as a nucleation site by themselves.

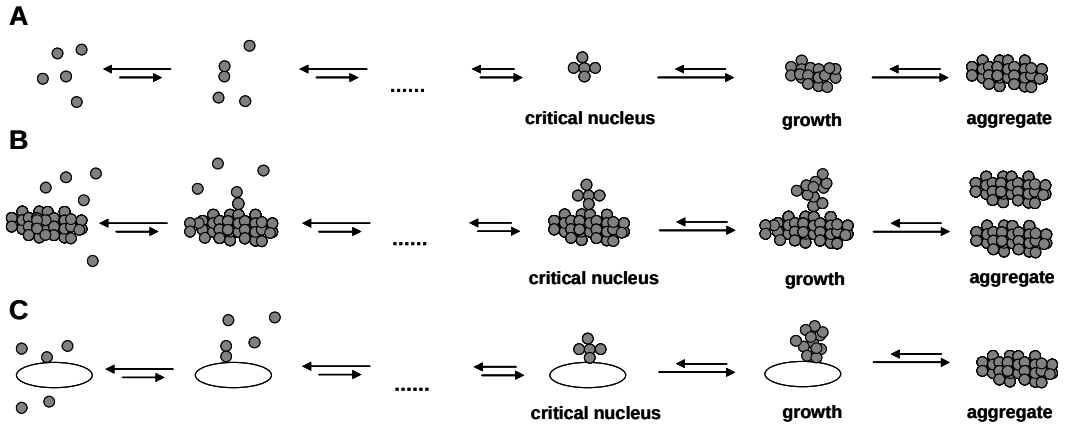

Figure I-8: **Nucleation schema (based in parts on Mirchev and Ferrone 1997)**
Homogeneous nucleation where the critical nucleus is formed from solution (A), heterogeneous nucleation where the critical nucleus is formed on the surface of an existing aggregate (B) and heterogeneous nucleation where the critical nucleus is formed on the surface of a foreign material (C).

For proteins it is reported that critical nuclei are often soluble aggregates that rapidly grow and form insoluble aggregates (Cleland et al. 1993; Reithel 1964; Wood et al. 1999). For α-synuclein the critical nucleus was a dithyrosine cross-linked dimer which was formed due to protein oxidation. When the species exceeded a level of 1-2 % the formation of fibril shaped aggregates started. Moreover, after spiking the preformed dimer into an aggregate free solution the fibril formation started as well. Due to the inhibition of dimer formation by adding methionine as an anti-oxidant, fibril formation was prevented (Krishnan et al. 2003). The formation of the dimer in the aggregate free solution was not detected during 15 days incubation at accelerated temperature. This lag phase until aggregate growth pro-

ceeds was observed for a number of other proteins, as well as the sudden induction of aggregation by spiking the proteinaceous nucleus reducing the lag time (Chi et al. 2003b; Harper and Lansbury 1997; Nielsen et al. 2001).

Ferrone and coworkers reported that sickle cell hemoglobin polymerizes as a consequence of both types of nucleation. On the one hand, homogeneous nucleation creates aggregates followed by a growth reaction forming polymerized molecules. On the other hand, heterogeneous nucleation on preexisting polymers via a specific binding site on the surface of the polymers was observed, too (Ferrone et al. 2002; Mirchev and Ferrone 1997).

Considering heterogeneous nucleation Chi et al. revealed that recombinant human platelet-activating factor acetylhydrolase (rhPAF-AH) did not aggregate after spiking of preformed proteinaceous nuclei. In contrast, extensive aggregation was induced rapidly when exogenous nano-sized hydrophilic silica particles were added (Chi et al. 2005b). After adsorption to the hydrophilic silica surface, aggregation occurred without detectable changes in secondary or tertiary structure. Decreasing the extent or affinity of rhPAF-AH adsorption to the particles by adding surfactant or increasing the pH, aggregation was repressed.

Moreover, Tyagi et al. (2008) reported that the formation of IgG particles was observed during vial filling by using a positive displacement piston pump. By performing spiking experiments it was shown that the pump shed nano-particles of stainless steel which served as heterogeneous nuclei inducing the formation of protein micro-particles. In this study a slight perturbation in secondary structure of the proteinaceous particles was observed.

In general, micro- and nano-sized particles of different materials can be shed or abraded from almost all bioprocessing equipment with which the protein solution is in contact. Pumps, tubing or filters can be considered as sources for these particles (Tyagi et al. 2008). In addition, containers or closures of different foreign wetted materials can shed particles which can induce aggregation potentially by a heterogeneous nucleation-controlled mechanism. Particles of glass, rubber or silicone oil droplets are known to cause aggregation of several proteins (Chi et al. 2005b; Jones et al. 2005; Thirumangalathu et al. 2009). Teflon particles were observed to cause aggregation of insulin (Sluzky et al. 1991). Tungsten micro-particles are involved in precipitation of an IgG1 solution in acidic buffer (below pH 6.0) without affecting secondary structure (Bee et al. 2009b).

Bee et al. (2009a) studied adsorption and aggregation by incubating an IgG1 with micro-particles of different materials. Glass, cellulose, stainless steel and ferric oxide particles were used. By applying stainless steel micro-particles irreversible adsorption was observed accompanied by the formation of soluble aggregates. Glass, cellulose and ferric oxide were shown to adsorb the protein, however protein aggregation was not observed. In all cases the secondary structure appeared nearly native.

Beside these already mentioned particles derived from the bioprocessing equipment, containers or closures, proteinaceous species like HCPs are suspected to potentially induce heterogeneous nucleation dependent aggregation (Arakawa et al. 2006).

Almost every study regarding heterogeneous nucleation dependent aggregation describes the formation of nearly native aggregates in the presence of nano- or micro-sized particles apart from the studies concerning silicon droplets. Here, the protein molecules being adsorbed to the oil-water interface showed a slight pertubation in tertiary structure (Thirumangalathu et al. 2009).

Adsorption to solid surfaces is in general known to potentially induce protein aggregation. The adsorption process is mostly driven by either hydrophobic interactions or electrostatic interactions between the surfaces and the protein protein (Norde 1995; Norde and Lyklema 1978). Due to partial unfolding of the protein on the surface, structurally perturbed molecules can potentially form aggregates on the surface or in the bulk solution after desorption. An increase in α-helical structures accompanied by a reduction in β-sheet and β-turn conformations is reported after adsorption of a mAb to Teflon particles (Vermeer et al. 1998). Formulated Interleukin-2 (IL-2) was shown to adsorb to silicone rubber tubing undergoing concomitantly conformational changes regarding secondary structure. Moreover, a loss in activity was observed (Tzannis et al. 1997).

In the case of heterogeneous nucleation partial unfolding is hardly involved in aggregation. Aggregation can be prevented, if the protein is hindered to adsorb to the surface and hence to form a critical nucleus. This was shown for hydrophilic glass particles and silicon oil droplets by adding surfactant to the protein solutions (Chi et al. 2005b; Thirumangalathu et al. 2009).

Chapter II Objectives of the thesis

This thesis aimed to gain more insight in mainly physical instability of therapeutic mAbs occurring during the purification process and especially at its interface to final formulation. The evaluation of critical factors leading to aggregation as well as the development of strategies to improve the quality of the purified bulks were focused. Particularly, the tangential UF processing of concentrated mAb bulks intended for subcutaneous administration of highly concentrated therapeutic formulations was examined. Moreover, the role of exogenous impurities which may be present in the purification intermediates was investigated considering their potential to facilitate aggregation.

The following objectives were predominantly addressed:

(I) Evaluation of operational parameters in UF concentration processes of IgGs affecting aggregation. The development of a method to produce highly concentrated solutions was aimed ensuring a high end-concentration. At first, a technique being applicable in lab scale as well as in manufacturing scale had to be elaborated to achieve a protein concentrations exceeding 100-200 mg/ml. Concomitantly, a short processing time and a reduced level of aggregates in the final bulk was mandatory during and after processing.

(II) Investigation of the storage stability of highly concentrated mAb solutions considering applied operational parameters during UF processing. The physical stability of an IgG bulk had to be investigated regarding aggregation as well as conformational changes. The influence of the UF method used and the protein concentration of the bulk had to be focused. Moreover, aggregation behavior due to the presence of preformed aggregates and particles induced by different UF strategies was required.

(III) Investigation of thermodynamic non-ideality during UF operations of IgGs. Thermodynamic non-ideality known to result from intermolecular charge-charge based interactions between macromolecular polyions and small charged solutes had to be examined during UF of IgGs. Potential correlation of pH and conductivity during the UF concentration process and the partitioning characteristics of soluble solutes across the semi permeable membrane were arrogated. The impact on chemical and physical stability of the highly concentrated protein solutions at the interface of DSP and final formulation should be evaluated.

(IV) MAb aggregation caused by exogenous process related impurities potentially present in the purification intermediates. The physical stability of an IgG monitored in the presence of nano- and macro-sized chromatographic particles should be evaluated regarding potential heterogeneous nucleation dependent aggregation. Aggregate formation as well as conformational changes due to the contact to different chromatographic surfaces need to be examined. In addition, the presence of indigenous proteinaceous species derived from a specific host cell system and their role in mAb aggregation was of special interest.

Chapter III Highly concentrated mAb solutions: Optimized operational parameters in UF minimizing aggregation

Abstract

For the production of highly concentrated mAb intermediate solutions in the course of downstream processing, ultrafiltration is the industry standard. Key challenges are to achieve high end concentrations and to reduce both process time and aggregate formation, particularly for therapeutic proteins intended for subcutaneous administration. Therefore, in this study the effects of operational parameters on permeate flux and aggregation in the concentrated solutions were investigated.

An optimized ultrafiltration concentration method was developed based on systematic screening of retentate flow rate and transmembrane pressure at different protein concentrations in the retentate. In this method flow and pressure values are adjusted depending on the prevailing retentate concentration. The resulting three stage protocol reduces process time and assures a low aggregate burden compared to concentration processes operated at constant flow and pressure conditions. Flow and pressure profiles were set and recorded in lab scale using an automated tangential flow filtration system which has been shown to adequately reflect process conditions at manufacturing scale.

The formation of IgG aggregates was monitored by turbidity measurement, SE-HPLC, light obscuration, dynamic light scattering and a microscopic method. These techniques allow the characterization of a wide range of aggregate sizes of soluble and insoluble aggregates that can occur during processing. In addition, FT-IR spectroscopy was performed to investigate the secondary structure of the aggregates, revealing different quanti-

ties of structurally perturbed protein which depend on applied flow and pressure conditions during UF.

Finally, the concentrated material derived from the optimized method showed improved processability at sterile filtration which is an important manufacturing step prior to storage.

1 Introduction

There is an unbroken demand for highly concentrated low volume formulations of mAbs for subcutaneous administration, especially in the field of chronic disease therapy, to improve patient convenience and compliance by offering outpatient treatment (Harris et al. 2004; Shire et al. 2004). Not only these high dose/ low volume dosage formulations, but also concentrated intermediate solutions of different purification steps are highly desired in the course of downstream processing. Low volume batches allow economic handling and storage and increase flexibility of hard-piped GMP manufacturing suites with fixed vessel volumes. To produce mAb solutions with a concentration of at least 100 mg/ml in large scale, reliable UF processes are required. The challenge is to achieve high end-concentration, short process time and high quality of the API at the same time (Harris et al. 2004; Luo et al. 2006).

Throughout manufacturing of biopharmaceutics, proteins are prone to chemical and physical instability as reported in chapter I. Hence, every step of the manufacturing process has to be evaluated regarding the potential formation of protein aggregates and aggregate precursors in order to diminish the risk of adverse effects in patients (Schellekens 2003) or loss in efficacy (Schellekens 2005) and to increase API stability during storage.

During UF the protein faces a combination of physical stress principles like pumping, flow induced shear stress or extensive contact to membrane surfaces. In addition, the protein reaches extremely high concentrations in the gel and polarization boundary layer near the membrane which is considered to support aggregation as well (Kiefhaber et al. 1991; Wang et al. 2007a).

Moreover, concentrated gel and polarization boundary layers near the membrane are leading to decreased permeate flux (Howell and Velicangil 1982; Kim et al. 1992; Pradanos et al. 1996; Suki et al. 1984; Suki et al. 1986). Therefore, a lower level of protein aggregates

should reduce additional membrane clogging. Especially if the protein concentration exceeds approximately 50 mg/ml, the viscosity will exponentially increase which affects permeate flux in addition adversely (Liu et al. 2005; Turker and Hubble 1987). On the one hand, the feed flow going tangentially to the membrane surface helps to remove deposited material from the membrane surface if enhanced back diffusion and lift velocity are sufficient to offset opposing sedimentation and permeation drag forces (Belfort et al. 1994; Davis and Leighton 1987). On the other hand, high shear rates in the flow channel potentially provoke aggregates which can be transported to the retentate solution and can adversely affect bulk quality.

In this study, the influence of applied shear stress during the UF concentration process on aggregation, permeate flux and concentration time was investigated using the proportional correlation between the pressure drop Δp ($p_i - p_0$) and the shear stress τ_w in the flow channel of the membrane module. This correlation has been presented before by using Equation III-1 (Ahrer et al. 2006):

$$\tau_w = \frac{d_H (p_i - p_o)}{4L}$$ Equation III-1

d_H is the hydraulic diameter of the flow channel, p_i is the inlet pressure, p_o is the outlet pressure and L is the length of the membrane (Gerhart et al. 1993). The hydraulic diameter d_H which behaves proportionally to τ_w was kept constant for all UF experiments by using the same cassette module for each experiment. The hydraulic diameter d_H can be calculated by Equation III-2 where a is the width and b is the height of the flow channel (Cheryan 1998):

$$d_H = 4\frac{ab}{2(a+b)}$$ Equation III-2

The second approach in the present study considers additionally that increased concentration during the UF process is detrimental to permeate flux and hence increase process time. In order to reflect this, the optimal values of cross flow rate and transmembrane pressure at different protein concentrations in the retentate were systematically determined. The aim was to develop an UF method offering improved permeate flux during the concentration process and thus reducing concentration time. Concomitantly, the formation of aggregates in the concentrated mAb solutions should be reduced.

2 Materials and methods

2.1 Materials

A capture pool of a chimeric human Fc (IgG4)/ rat Fab antibody in citrate buffer pH 5.5 (IgG A) was taken for the concentration experiments. In addition, completely purified bulk of two chimeric human Fc (IgG1)/ mouse Fab antibodies (IgG B and IgG C) in histidine buffer pH 6.0 were used. All mAbs were provided by Roche Diagnostics GmbH (Penzberg, Germany). Before UF processing the solutions of 5 mg/ml protein concentration were filtered through a 0.2 μm membrane cartridge (Sartorius, Goettingen, Germany). All chemicals and reagents used were at least analytical grade. Citric acid, sodium hydroxide and hydrochloric acid from Merck KG (Darmstadt, Germany) were employed. L-histidine from Ajinomoto (Raleigh, USA) was used.

2.2 Methods

2.2.1 Ultrafiltration concentration procedure

For the preparation of concentrated mAb solutions the automated TFF system ÄKTAcrossflow (GE Healthcare, Uppsala, Sweden) was used (Liten and Cohen 2007). The system was operated using the Unicorn software (GE Healthcare, Uppsala, Sweden). A Sartocon Slice flat sheet cassette with a Hydrosart membrane of regenerated cellulose, a nominal NMWC of 30 kDa and a membrane area of 0.02 m^2 was provided by Sartorius (Goettingen, Germany). Total membrane loading was about 400 g/m^2 for each experiment. After concentration the membrane module was cleaned with 1 M sodium hydroxide. The normalized flux rate for water (NWF) was determined after every cleaning cycle and compared to the obtained value before initial use. The cassette was only applied for the next experiments, if the NWF decline in ($l/m^2/h$)/ 1 bar at 20 °C was below 10 % of the initial value to ensure complete cleaning and comparable membrane properties.

2.2.2 Concentration determination

Concentration was determined by using the photometric absorbance at 280 nm and 320 nm after buffer blank subtraction (UV-Vis spectrophotometer Evolution 500, Thermo

Fisher Scientific, Waltham, USA). The absorbance at 320 nm was subtracted from the absorbance at 280 nm and this value was used to calculate the protein content according to the law of Lambert-Beer.

2.2.3 Turbidity measurements

Turbidity was determined as photometric absorbance after buffer-blank subtraction of the undiluted concentrate at 350 nm and 550 nm, where no intrinsic chromophores of the mAb absorb (UV-Vis spectrophotometer Evolution 500, Thermo Fisher Scientific, Waltham, USA) (Capelle et al. 2007). The samples were mixed before measuring in order to avoid a decrease in absorbance due to the settlement of large particles. Turbidity was used to determine the relative amount of particles encompassing colloidal and subvisible protein aggregates (Mahler et al. 2005).

2.2.4 Size exclusion high pressure liquid chromatography

Size exclusion high pressure liquid chromatography (SE-HPLC) analysis was conducted with a TSK 3000 SWXL column (Tosoh Biosep, Stuttgart, Germany) on a Summit HPLC-system (Dionex, Idstein, Germany). The elution peaks were monitored at 280 nm by the UV diode array detector UVD170U from Dionex (Idstein, Germany). Isocratic chromatography was conducted at room temperature using an aqueous buffer composed of 200 mM potassium phosphate and 250 mM potassium chloride at pH 7.0 and a flow-rate of 0.5 ml/min. Each sample contained 100 µg mAb per injection. The chromatograms were integrated manually by using the Chromeleon software (Dionex, Idstein, Germany). This is shown exemplarily in Figure III-1. The percentage of higher molecular weight species (HMWs) includes dimers and larger soluble oligomers. It was determined as relative area (mAU·min) of the respective peaks referred to total area of all peaks including the monomer peak and the peak of the lower molecular weight species (LMWs).

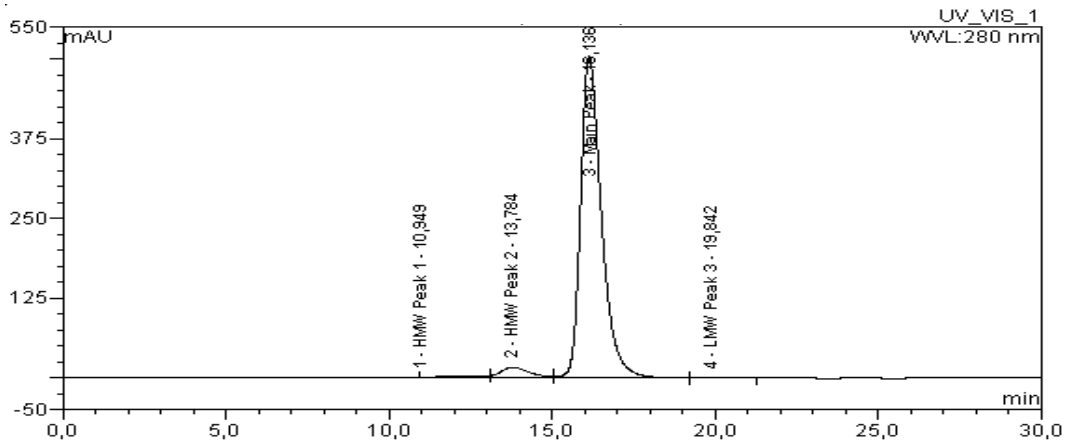

Figure III-1: Integration borders and retention times of the SE-chromatogram
HMWs elute first between 10 min (oligomers) and 15 min (dimers). Subsequently, the monomer elutes after about 16 min followed by LMWs.

Total recovery was monitored throughout the analysis by comparing the total peak area of the respective sample to the total peak area of a control sample.

2.2.5 Light obscuration particle counting

Light obscuration (LO) was used to monitor the formation of particles in a range of 1-200 µm similar to the method <788> Particulate Matter of Injection in the United States Pharmacopoeia and the European Pharmacopoeia method 2.9.1. (EDQM 2001a; USPC 2002). The particle counter SVSS-C (PAMAS Partikelmess- und Analysesysteme, Rutesheim, Germany) was equipped with a laser diode and a photodiode detector in order to determine the residual photocurrent after particles have passed the course of the beam. The HCB-LD-25/25 was applied as particle sensor. Concentrates of a higher content of particles than 120 000/ ml where diluted with buffer to match the specified capacity of the used sensor. Three measurements of a volume of 0.5 ml for each sample were analyzed after an equilibrating flush of 0.3 ml. Results were calculated as mean value of three measurements and referred to a sample volume of 1.0 ml. Before diluting the concentrates the buffer was filtered using Stericup Express plus 0.1 µm filter devices (Millipore, Billerica, USA) and the particle burden was determined as described before.

2.2.6 Fitration/ staining method

The method was applied according to Li et al. (2007) to investigate the level of insoluble aggregates in the concentrated solutions. 2 ml of the concentrated mAb solutions were filtered through a buffer-wetted 0.2 µm cellulose acetate membrane (Sartorius, Goettingen, Germany) with a diameter of 47 mm under vacuum. Then 10 ml of citrate buffer pH 5.5 were added three times and vacuumed away. 2 ml Reversible Protein Detection Kit solution from Sigma-Aldrich (Steinheim, Germany) were added on the membrane and kept in contact for 3 minutes and then drained. After that, the membrane was rinsed with 3 x 10 ml buffer and 3 x 10 ml water and then dried in air. Subsequently, the membranes with the retained and stained particles were examined under a stereomicroscope MZ 12 (Leica, Wetzlar, Germany) equipped with a digital camera DC 100 (Leica, Wetzlar, Germany) under 80-times magnification.

2.2.7 Dynamic light scattering

The Zetasizer Nano S dynamic light scattering (DLS) instrument (Malvern Instruments, Worcestershire, UK) was used to monitor colloidal species in the size range of a hydrodynamic diameter between 1 nm and 6 µm. The scattering information is detected at an angle of 173 ° operating with a 4 mW He-Ne-laser at 633 nm using the non-invasive backscatter technique (NIBS) (Kaszuba and Connah 2006). The samples were analyzed undiluted in a temperature controlled precision quartz cuvette (Hellma, Müllheim, Germany) at 25 °C. The size distribution by intensity was calculated from the time-dependent correlation function using the multiple narrow mode of the DTS software (Version 5.0, Malvern Instruments, Worcestershire, UK). The relative light intensity of the detected peaks is presented as mean values of three measurements.

2.2.8 FT-IR spectroscopy

FT-IR spectra were recorded with the Tensor 27 (Bruker Optics, Ettlingen, Germany) applying the MIRacle attenuated total reflection (ATR) cell with a Germanium crystal (Bruker Optics, Ettlingen, Germany) to investigate the washed insoluble aggregates separated from the concentrated retentate by centrifugation. In addition, the protein adsorbed to the UF membrane was investigated after the concentration process. For this, the Sartocon Slice flat sheet cassette was dismantled and the Hydrosart membranes were cut out,

washed with buffer and were applied to the crystal. The transmission cell AquaSpec (Bruker Optics, Ettlingen, Germany) was used to investigate the liquid solutions.

For each spectrum which was recorded from 850-4000 cm^{-1} a 120-scan interferogram was collected at a double sided acquisition mode with a resolution of 4 cm^{-1}. The reference spectrum of buffer and wetted membrane respectively was subtracted to obtain the protein spectrum.

The transmission spectra were edited by a vector normalization followed by the generation of the second derivative smoothed using a 13-point Savitsky-Golay smoothing function. To obtain the spectral characteristic of heat induced aggregation a Bio-ATR II unit with Silicium crystal (Bruker Optics, Ettlingen, Germany) was applied and a mAb solution of 100 mg/ml was heated up to 90 °C. The absorption spectra recorded in ATR mode were corrected concerning band intensity and band position to allow the comparison to spectra recorded in transmission mode. Therefore the extended ATR-correction of the software OPUS 6.0 (Bruker Optics, Ettlingen, Germany) according to Fringeli (1992) was used, to overcome wave number dependent anomalous dispersion (Goldberg and Chaffotte 2005; Grdadolnik 2002).

2.2.9 Sterile filtration experiments

A filtration line composed of a stainless steel in-line filter housing (Sealkleen, Pall, Dreieich, Germany) and a Millex VV PVDF filter unit with a pore size of 0.1 µm and a filtration area of 4.52 cm^2 (Millipore, Billerica, USA) were used and operated under constant pressure of 0.75 bar. The filtrate flow rate over time was determined at 90 mg/ml protein concentration. Every filtration was carried out at room temperature and the flow-through was recorded over ten minutes. The results are presented as mean values of three runs ± SD.

3 Results and discussion

3.1 The ÄKTAcrossflow: A representative TFF system

For the development of purification processes, representative scale down models are necessary which adequately reflect manufacturing conditions up to 10 000 liter scale. This assures the implementation of reliable chromatographic and filtration procedures. Moreover, online monitoring of process control parameters is desired. For TFF processes the monitoring of pH, conductivity, temperature, fill level, introduced air, pressure and flow parameters are considered to be highly valuable since theses parameters have impact on protein stability and hence quality (Carpenter et al. 1999). Further, an automated system is favored to ensure reproducibility of optimized operating conditions.

In this work the ÄKTAcrossflow, an automated TFF lab-scale system was used which meets all the requirements mentioned above. The effects of operational parameters on aggregation, end-concentration and process time were investigated. The system is composed of three piston pumps achieving a feed flow rate of 1-600 ml/min. The pump heads are made of a borosilicate tube and a piston of PTFE. The maximum system pressure is 5.2 bar. As reported in chapter I, different studies revealed that pumping can cause aggregation (Chandavarkar 1990; Meireles et al. 1991). Cromwell et al. (2006) described that the use of a piston pump during filling operations of a liquid IgG formulation caused an increase in the number of particles and in turbidity.

Therefore, we examined the effect of the ÄKTAcrossflow piston pumps on aggregation by recycling an IgG1 solution of 18 mg/ml for one hour at 25 °C. No UF membrane cassette was applied and the permeate side was closed. In addition, we performed the same experiments by using a diaphragm pump which is usually known to cause no protein aggregation (Cromwell et al. 2006). This type of pump can be applied in pilot or manufacturing scale and has an output of about ten fold compared to the ÄKTAcrossflow. Therefore, the feed flow rate was adjusted to 300 ml/min for the piston pumps of the ÄKTAcrossflow and to 3 000 ml/min for the diaphragm pump QF 1000S (Quattroflow Fluid Systems, Hardegsen-Hevensen, Germany). Samples were taken every 15 min during pumping and were analyzed by turbidity measurement and SE-HPLC in order to monitor insoluble larger aggregates and soluble HMWs. Figure III-2 and Figure III-3 show the analytical results for both pump types over 60 min total pumping time.

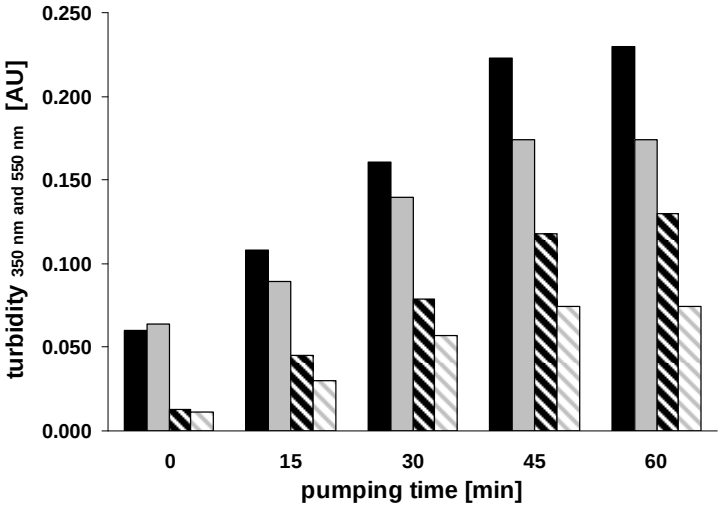

Figure III-2: Effect of pump type on turbidity of a cycled IgG solution at 18 mg/ml
Turbidity at 350 nm (and 550 nm) monitored over 60 min: Values for the ÄKTAcrossflow piston pumps are presented in black (black striped) and for the diaphragm pump in grey (grey striped).

With pumping duration a general increase in turbidity at both wave lengths was observed. The turbidity values at both wave lengths are slightly but consistently higher when the piston pumps of the ÄKTAcrossflow were used. After 45 min no further significant increase in turbidity with pumping time was observed for both pump types.

The amount of HMWs during pumping was not affected by either using a piston pump or a diaphragm pump. For the starting protein material processed by using the diaphragm pump a higher content of HMWs was identified which can be ascribed to a stability issue since this sample was stored at room temperature before processing (Figure III-3).

Since the pistons themselves did not induce the formation of HMWs during pumping and only a slight increase in the turbidity of the pumped solution was observed compared to the diaphragm pump, the ÄKTAcrossflow was chosen as a suitable TFF system to investigate the effect of system hydrodynamics on aggregation.

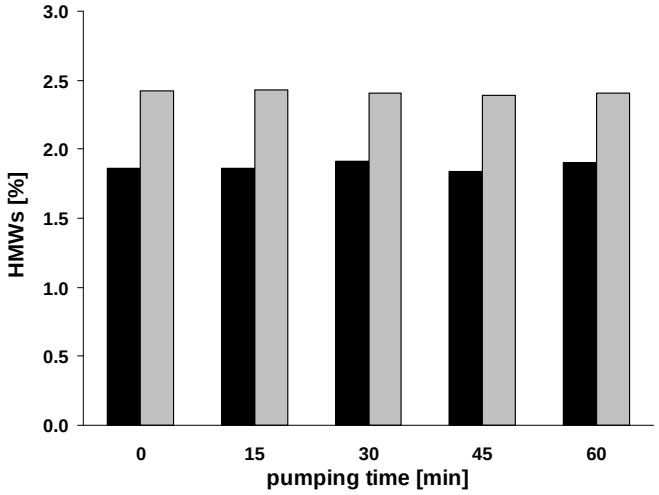

Figure III-3: Effect of pump type on the level of HMWs in an IgG solution at 18 mg/ml determined by SE-HPLC
HMWs [%] monitored over 60 min: Values for the ÄKTAcrossflow piston pump are presented in black and for the diaphragm pump in grey.

In order to potentially allow the transfer of our applied operational conditions to a larger scale system, the Reynolds numbers (Re) in the flow channel of the described lab-scale equipment were calculated and compared to the values of a pilot scale system. As pilot scale system the automated TFF system Uniflux 10 (GE Healthcare, Uppsala, Sweden) was chosen equipped with four diaphragm pumps to drive the feed.

The pilot-scale system was equipped with a 0.1 m² Sartocon Slice Cassette with 30 kDa NMWC (Sartorius, Goettingen, Germany). The membrane modules in lab scale and pilot scale module have identical flow path geometry ensuring defined fluid dynamics in the membrane module independent of scale (Van Reis et al. 1997).

The Reynolds numbers were calculated according to the commonly used equation presented by Cheryan (1998):

$$\mathrm{Re} = \frac{d_h \, u_0 \rho}{\mu} \qquad \text{Equation III-3}$$

Where d_h is the hydraulic diameter of the flow channel calculated according to Equation III–2, μ is the dynamic viscosity of the solution, ρ is the density of the solution and u_0 is the mean feed flow velocity calculated as:

$$u_0 = \frac{Q}{a \cdot b} \qquad \text{Equation III-4}$$

Where Q is the feed flow rate in m^3/s, a is the width and b is the height of the flow channel. In Table III-1 the Reynolds numbers are displayed for both systems, lab- and pilot scale, under typical operating conditions.

It has to be noticed that all Sartocon Slice devices are composed of multiple membrane layers. Therefore, the values given for mean velocities as well as for the Reynolds numbers were divided by three for Sartocon Slice 200 and twenty-five respectively for Sartocon Slice Cassette, since these devices are composed of three and twenty-five individual channels respectively. The dimensional analysis of fluid dynamics by using Reynolds numbers was performed to evaluate the quality of the scale-down model.

TFF system	Scale	Pump type	Δp [bar]	Re [ ]	Q [m^3/s]	u_0 [m/s]
ÄKTAcross-flow	lab	piston pump	1.2, 0.6	48.53, 23.65	2.66×10^{-6}, 1.30×10^{-6}	0.049, 0.025
Uniflux 10	pilot/ manufacturing	diaphragm pump	1.3	72.69	3.33×10^{-5}	0.076

Table III-1: Reynolds numbers for the ÄKTAcrossflow lab scale system equipped with 0.02 m² Sartocon Slice module and for the Uniflux 10 pilot scale system equipped with the 0.1 m² Sartocon Slice Cassette module
For calculation purposes a 50 mg/ml mAb solution with a dynamic viscosity value of 1.14 mPa s and a density of 1.014 g/ml was applied.

The determined numbers at different scales revealed that operating conditions applied in the lab scale system chosen can in general be transferred to a larger scale system. Reynolds numbers are used when performing dimensional analysis of e.g. fluid dynamics, and can be used to determine dynamic similitude between different experimental cases, where a fluid is in relative motion to a surface (Wilkes 2006). Moreover, Reynolds numbers are used to indicate the flow regime by evaluating the relative importance of inertial effects to viscous effects. Laminar flow occurs at low Reynolds numbers below 2000 (Wilkes 2006) where viscous forces dominate. Turbulent flow occurs at higher Reynolds numbers. There, inertial forces dominate which can produce random eddies, vortices and other flow fluctuations known to provoke protein aggregation (Bee et al. 2009c; Gomme et al. 2006). In the presented study, the Reynolds numbers are clearly lower than 2000 indicating that the operated lab scale model, as well as the pilot scale model show comparable flow regimes which are clearly laminar.

3.2 Effects of applied shear stress

UF concentration runs were conducted from 5 mg/ml up to 140 mg/ml target concentration. Four different UF methods were applied each of them using a different Δp value. According to Equation III–1, a higher Δp value is attributed to a higher τ_w value. Thus a Δp of 0.7, 1.2, 1.8 and 3.0 bar was applied resulting in a calculated τ_w of 126, 216, 325 and 541 Pa. The TMP, defined in Equation I–4, was kept constant at 0.6 bar for all experiments. Table III-2 shows the operational parameters as well as the calculated τ_w values for the four different methods used at a glance (method: Δp 0.7 bar, Δp 1.2 bar, Δp 1.8 bar and Δp 3.0 bar).

UF method	c [mg/ml]	Δp [bar]	TMP [bar]	τ_w [Pa]	Qr [l/m²/h]	Concentration time [min]
Δp 0.7 bar	5-90	0.7	0.6	126	270[a]	150[b]
Δp 1.2 bar	5-140	1.2	0.6	216	310 [a]	130
Δp 1.8 bar	5-140	1.8	0.6	325	465[a]	130
Δp 3.0 bar	5-90	3.0	0.6	541	845[a]	120[b]

[a] Average calculated from Qr values during the whole process
[b] Target concentration of 140 mg/ml was not reached

Table III-2: Overview of selected operating conditions of the different UF concentration methods
The indicated end concentrations (c) that were actually reached by the applied concentration method were determined before flushing the membrane with one dead volume.

The influence of shear stress (τ_w) on permeate flux and concentration time during UF up to 140 mg/ml target concentration was evaluated. Permeate flux versus protein concentration indicates that the permeate flux was improved by increasing the Δp from 0.7 bar to 1.2 bar (Figure III-4). Moreover, the target concentration of 140 mg/ml was achieved and the concentration time was reduced from 150 min to 130 min (Table III-2). When the Δp exceeded the value of 1.2 bar neither a further improvement in permeate flux nor a reduction in concentration time was recognized. At a Δp value of 3.0 bar an end concentration of only 90 mg/ml was reached due to high inlet pressure leading to an abortion of the UF process.

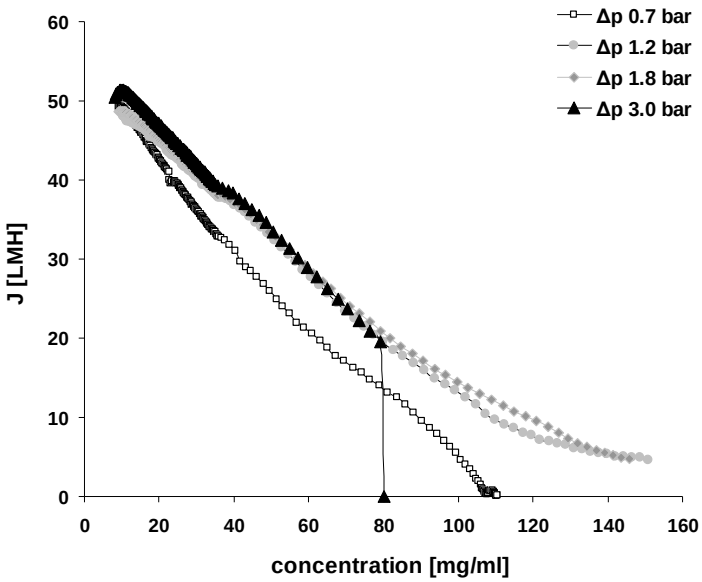

Figure III-4: Permeate flux (J) versus protein concentration operated at a fixed Δp of 0.7, 1.2, 1.8 and 3.0 bar (TMP = 0.6 bar for all experiments)
For the method operating under a Δp of 3.0 bar the end concentration of 140 mg/ml was not reached due to high inlet pressure.

At the same time, a slight but steady increase in soluble higher molecular weight species (HMWs) with increasing Δp was determined by SE-HPLC analysis. It was shown before that an increase in HMWs is not introduced by the piston pumps of the used TFF system It has to be noted that the increase in the HMW level is moreover pronounced by the increased protein concentration, comparing the levels at 5 mg/ml (before UF concentration) and at 90 mg/ml. However, the increase in the HMW level was observed at comparable protein concentrations of 90 mg/ml with increasing Δp (Figure III-5). The concentrates obtained from the Δp 0.7 bar method revealed an increase in HMWs from 0.4 % up to 0.6 %. By further increasing the Δp up to 3.0 bar the HMW level only slightly stepped up to about 0.8 %.

Concomitantly, a substantial decrease in total peak area of the monomer and the HMWs in the SE-chromatograms was observed. This can be explained by the retention of large protein aggregates and precipitated molecules by the SE-column resulting in the inability to detect them.

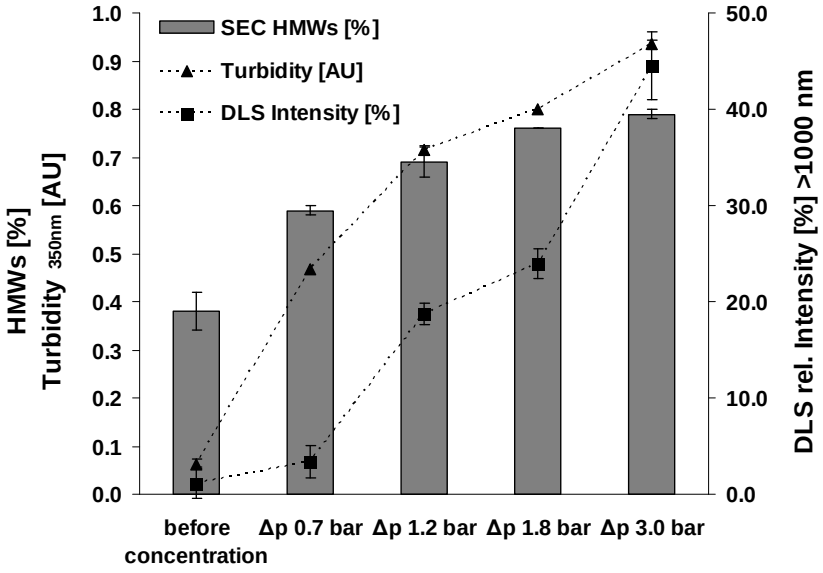

Figure III-5: Aggregates analyzed by SE-HPLC (grey bars, referring to the left scale), turbidity at 350 nm (black triangles, referring to the left scale) and relative intensity of the peak >1000 nm hydrodynamic diameter determined by DLS (black squares, referring to the right scale)
At 5 mg/ml (before concentration) and at 90 mg/ml protein concentration obtained after UF at Δp of 0.7, 1.2, 1.8 and 3.0 bar; experimental data is presented as mean values of three measurements ± SD.

However, their presence is accounted for by looking at the decline of total peak area compared to a control sample. The concentrates obtained from the 0.7 bar method showed a decrease in total peak area of about 6 % which stepped up to about 15 % when a Δp of 3.0 bar was applied. Additionally, the decrease in total peak area with increasing Δp was accompanied by an increase in the turbidity of the concentrated mAb solutions (Figure III-5). An increase in turbidity was ascribed before by Mahler et al. (2005) to the presence of subvisible particles of probably up to 1 μm and 2 μm in size. This appearance of particles larger 1 μm was as well observed by looking at the DLS relative intensity of an aggregated species presented by a peak at >1000 nm hydrodynamic diameter which was increasing with higher Δp values (Figure III-5).

Moreover, LO measurements were conducted since this technique is accounted for the detection of particles of 1 μm to 200 μm in size. LO revealed that an increase in particles larger 1 μm was observed with increasing Δp (Figure III-6) underlining the results obtained from total peak area evaluation of the SE-chromatograms, turbidity measurements and DLS.

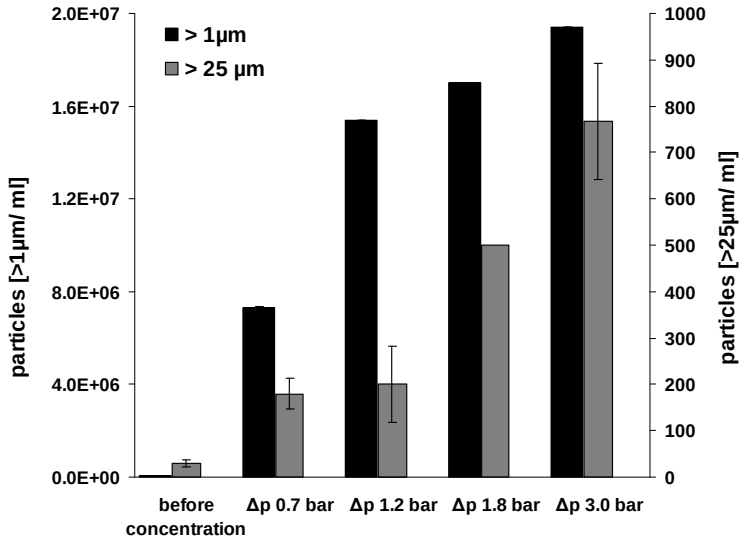

Figure III-6: LO data for particles per ml larger 1 µm (black bars, referring to the left scale) and 25 µm (grey bars, referring to the right scale)
At 5 mg/ml (before concentration) and at 90 mg/ml protein concentration obtained from UF at Δp of 0.7, 1.2, 1.8 and 3.0 bar; experimental data is presented as mean values of three measurements ± SD.

Moreover, the formation of very large particles exceeding 25 µm was observed with increasing Δp. A higher level of particles is additionally obvious when the protein concentration increases from 5 mg/ml (before UF concentration) to 90 mg/ml showing again that the formation of particles is in general enhanced at a higher protein concentration as reported in chapter I..

Summarized, an increased level of HMWs and particles in the retentate during UF processing depends on the applied Δp. These aggregates potentially contribute to membrane clogging resulting in permeate flux decline over time which is generally observed during all experiments as shown in Figure III-4. At a Δp of 3.0 bar, i.e. at highest shear stress referring to Equation III-1, the highest burden of aggregates in the retentate is recognized and accompanied by a sudden flux decline due to membrane clogging. As a consequence, the target concentration of 140 mg/ml was not reached (Table III-2).

If particles are completely rejected by the membrane their surface accumulation is equal to the difference between particles moving back to the retentate and particles convectively transferred to the surface (Youravong et al. 2003). It is reported that particle movement away from the membrane is proportional to wall shear stress due to enforced diffusion or inertial lift, depending on particle size and hydrodynamic conditions (Gésan-

Guiziou et al. 1999). In our case, we observed that the wall shear stress should not exceed 1.2 bar since sufficient back transport and therefore improved permeate flux especially at very high retentate concentrations were achieved. For values larger 1.2 bar no improvement of permeate flux was achieved (Figure III-4). This is in accordance with the model of Davis and Leighton (1987; Porter 1972), showing that low shear rates or high feed concentration reduce the permeate flow rate. At the same time shear-induced transport has to be limited to avoid the generation of aggregates of different sizes and especially their removal from the membrane surface adversely affecting bulk quality as shown in Figure III-5 and Figure III-6.

It has to be mentioned that factors like turbulence promoter or entrance/exit design of the used membrane cassette are not represented in the simplified calculation concerning shear stress (Equation III-1). Hence, the calculations should be considered an estimation.

3.3 Systematic variation of operational parameters: The optimized method

As reported, UF operations conducted at constant pressure and flow conditions result in rapid flux decline due to high permeation drag, aggravated membrane fouling and a rapidly increased protein concentration near the membrane. This is accompanied by an rapidly increasing protein concentration in the retentate and hence viscosity during the processing (Bacchin and Aimar 2005; Vladisavljevic and Rajkovic 1999).

The results in section 3.2 of this chapter underline that permeate flux decline was generally inevitable during the UF concentration process at fixed pressure and flow conditions. Therefore, an adaptation of pressure and flow conditions depending on the protein concentration in the retentate was considered successful to modify the system hydrodynamics and thus improve permeate flux over time. In contrast, one constant Δp during the whole UF process results in a defined feed flow rate Q and retentate flow rate Qr respectively, according to Equation I-7. Moreover, it results in a fixed shear rates τ_w, according to Equation III-1. Hence, the increasing protein concentration and its contribution to permeate flux decline during processing is not considered. It assumed e.g. that with higher protein concentration and thus membrane polarization a higher retentate flow rate and thus wall shear stress is suitable to remove deposited protein from the surface of the membrane.

Since the TMP is known to have a large impact on permeation drag and the retentate flow rate directly influences the shear rate over the surface as presented above, these parameters were chosen as key parameters influencing permeate flux during UF concentration. To improve flux during the concentration process, the optimal flux at a specific retentate flow rate and TMP was systematically screened at defined protein concentrations in the retentate. In contrast to common approaches where these experiments are only carried out at a single concentration (Luo et al. 2006), the increase in concentration during the UF was mimiced. Experiments were conducted at a protein concentration of 5-180 mg/ml. The minimal and maximal retentate flow rates were defined according to the preliminary experiments revealing that a Δp of 1-2 bar and a retentate flow rate of about 200-500 l/m²/h respectively is suitable to provide enough wall shear stress to improve permeate flux without supporting aggregation.

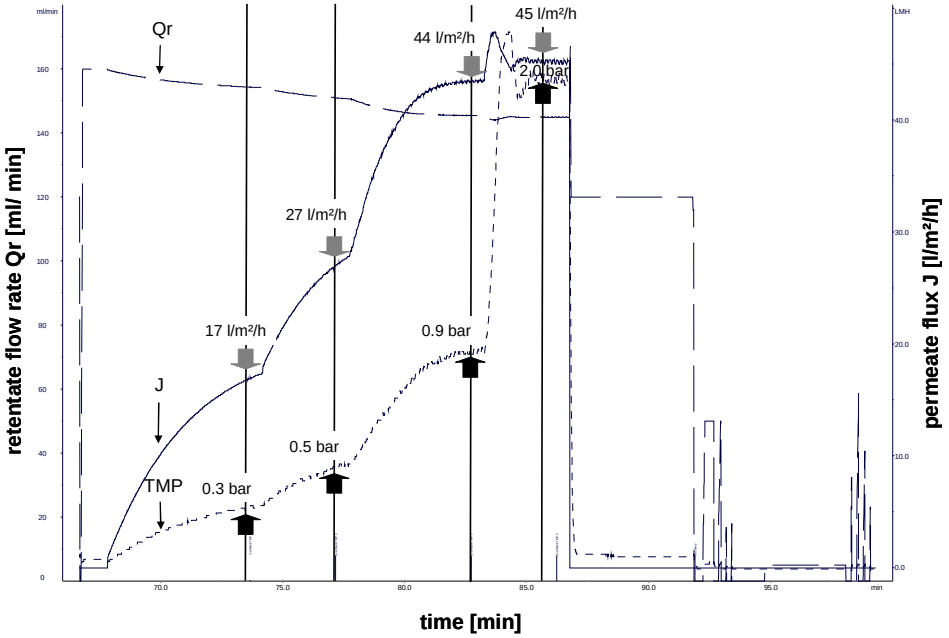

Figure III-7: Flow and pressure diagram of the ÄKTAcrossflow at 45 mg/ml protein concentration under total retentate recycling
A retentate flow rate (Qr) of 450 l/m²/h was applied in combination with a TMP of 0.3-2.0 bar (black arrows); the grey arrows mark the point at which the permeate flux (J) was determined.

A TMP of 0.3-2.0 bar was applied. Under total retentate recycling (closed permeate) each solution with a protein concentration of 25, 45, 90 and 180 mg/ml was processed using a TMP of of 0.3, 0.5, 0.9 and 2.0 bar at a retentate flow rate of 150, 240, 390 and 450 l/m²/h in series.

Figure III-7 shows the flow and pressure diagram recorded with the ÄKTAcrossflow for the solution at 45 mg/ml IgG concentration and a retentate flow rate of 450 l/m²/h exemplarily. The maximum permeate flux (grey arrows) was determined when the defined TMP value was reached and concomitantly stable over 1 min (black arrows). The experiments and the evaluation of maximum permeate flux were repeated at a retentate flow rate of 150, 240 and 390 as well as at the other protein concentrations reported above. Afterwards, the determined permeate flux was plotted against TMP for all experiments resulting in the curves shown in Figure III-8 and Figure III-9.

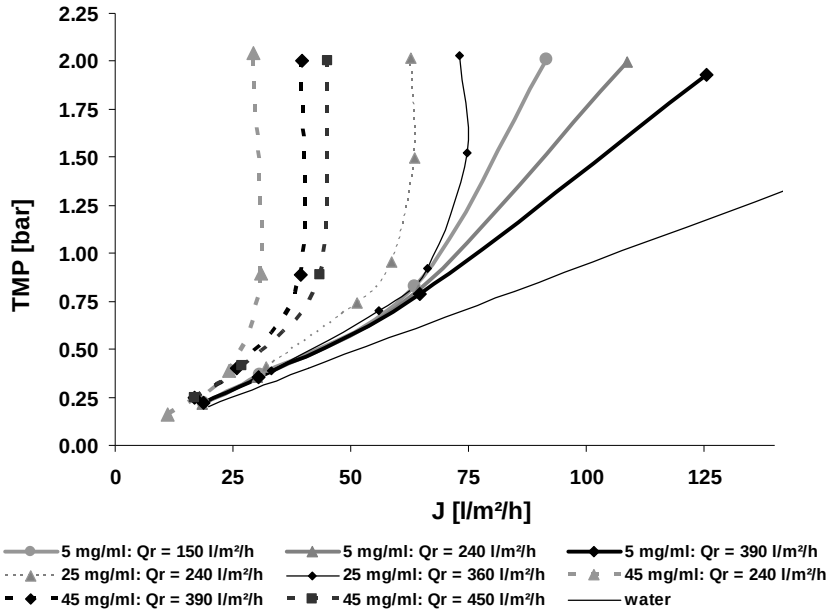

Figure III-8: Transmembrane pressure (TMP) versus permeate flux (J) for a concentration of 5 mg/ml (solid lines), 25 mg/ml (fine lines) and 45 mg/ml (dotted lines)
Retentate flow rate (Qr) was adjusted consecutively to 150, 240, 360, 390 and 450 l/m²/h. TMP was adjusted consecutively to 0.3, 0.5, 0.9 and 2.0 bar. The fine black line indicates the clean water flux at the same TMP and cross flow values.

Based on this permeate flux versus TMP plot the values of retentate flow and TMP at each concentration were identified from the knee point of the curves where permeate flux is at its maximum. In this plot it is obvious that a further increase in TMP and retentate flow rate does not result in further permeate flux improvement. The described evaluation plot closely follows the hypothesis of critical flux in the weak form in which any deviation of

the straight line of clean water flux, without considering the slope, indicates the onset of multilayer fouling (Field et al. 1995; Wu et al. 1999).

No knee point was reached by the applied retentate flow rate and TMP values for the starting concentration of 5 mg/ml (Figure III-8). Therefore, the results for 25 mg/ml were considered as well. No flux improvement was observed by increasing the TMP beyond 1.25 bar at a retentate flow rate of 240 and 360 l/m²/h. Considering the previous findings that higher shear stress during UF can result in an increased aggregate level of the concentrated solutions we identified a retentate flow rate of 240 l/m²/h and a TMP of 1.25 bar as the optimal condition at the beginning of the UF process for a concentration of 5 to 25 mg/ml.

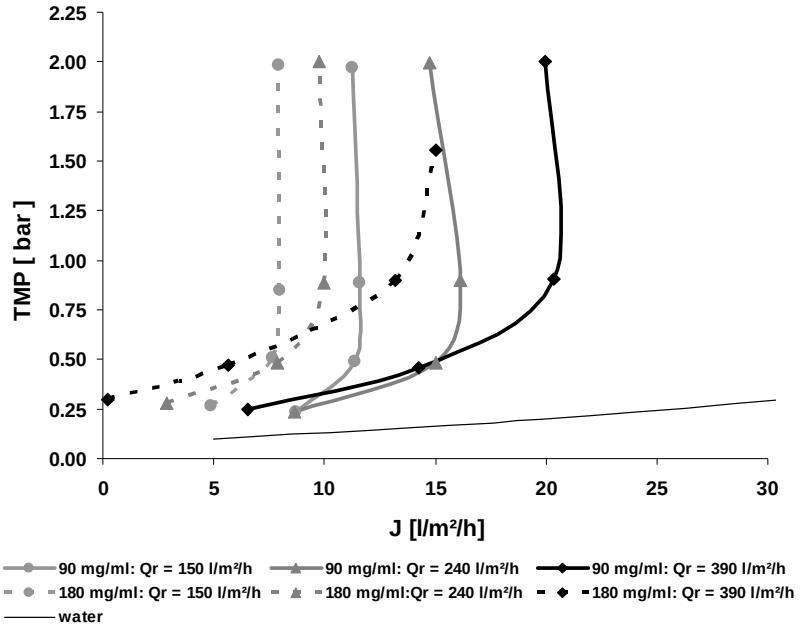

Figure III-9: Transmembrane pressure (TMP) versus permeate flux (J) for a concentration of 90 mg/ml (solid lines) and 180 mg/ml (dotted lines)
Retentate flow rate (Qr) was adjusted consecutively to 150, 240, 360, 390 and 450 l/m²/h. TMP was adjusted consecutively to 0.3, 0.5, 0.9 and 2.0 bar. The fine black line indicates the clean water flux at the same TMP and retentate flow rate.

From 25 to 50 mg/ml the TMP was lowered to 0.85 bar because the 45 mg/ml experiments did not reveal an improved permeate flux beyond this TMP value. In addition, the retentate flow rate was increased to 450 l/m²/h, bringing the permeate flux from 30 up to 45 l/m²/h at 0.85 bar TMP.

For a concentration range from 50 mg/ml up to the target concentration of 140 mg/ml a TMP of 0.85 bar and an increased retentate flow rate of 390 l/m²/h were chosen. No improvement of flux was observed exceeding a TMP of 0.85 bar (Figure III-9). However, an increased cross flow velocity was successful to achieve a higher permeate flux up to a retentate concentration of 180 mg/ml.

Table III-3 summarizes the TMP and retentate flow values for an UF concentration process from 5-180 mg/ml considered suitable to achieve maximal permeate flux during processing. This three stage process was titled optimized method (optMeth).

UF method	c [mg/ml]	Δp [bar]	TMP [bar]	τ_w [Pa]	Qr [l/m²/h]	Concentration time [min]
optMeth	5-25	0.6	1.25	108	240	
	25-50	1.2	0.85	216	450	110
	50-140	1.6	0.85	288	390	

Table III-3: Overview of selected operating conditions of the optimized UF concentration methods (optMeth)

The set of curves in Figure III-8 and Figure III-9 shows that at a defined concentration a further increase in TMP ends in constant permeate flux. This is visualized by a permeate flux plateau indicating that a pressure independent region is reached. This is in accordance with the concentration polarization model based on the film theory (Porter 1972; Sablani et al. 2001) presented in chapter I. The data shows improved permeate flux with increased retentate flow rate in the TMP independent region. This clearly varies with protein concentration in the retentate, underlining that the model theory does not consider the hydrodynamic interactions in the concentrated boundary layer due to shear flow of the layer during tangential flow operations (Davis and Leighton 1987; Fradin and Field 1999; Li et al. 1998a; Madaeni et al. 1999). Taking into account that permeate flux at a defined TMP and retentate flow rate is decreasing with higher concentration during UF processing the importance of changing operational conditions, depending on the prevailing concentration in the retentate is obvious in order to improve permeate flux and to reduce concentration time.

The optMeth offers an improved permeate flux compared to a method operating constantly under a fixed Δp of 1.2 bar and a fixed TMP of 0.6 bar (method: Δp 1.2 bar). Moreover, the permeate flux curve of the optMeth converges to a method with an in-

creased TMP of 1.0 bar (method: Δp 1.2 bar/ TMP 1.0 bar) but the predetermined concentration was reached and no membrane clogging was observed leading to an abortion of the UF process (Figure III-10).

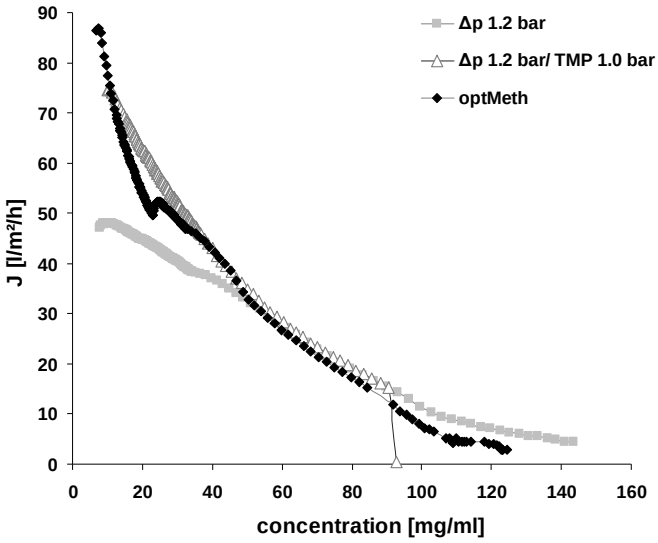

Figure III-10: Permeate flux (J) versus protein concentration for different concentration methods
For the method operating under increased TMP of 1.0 bar the end concentration of 140 mg/ml was not reached due to high inlet pressure.

This corresponds to literature dealing with critical flux operations and showing that uncontrolled convection of solutes towards the membrane surface due to a permanently increased TMP causes strong concentration polarization and thus rapid flux decline (Aimar et al. 1989). By reducing the TMP during the concentration process, following the concept of the optMeth, the point at which concentration polarization proceeds is less imminent compared to method operating at fixed pressure conditions. At the same time, an increase in retentate flow rate accelerates shear-induced back-diffusion. This is considered suitable to explain the approximately 20 % reduction in process time when the optMeth is used compared to the UF methods operating at constant pressure and flow conditions.

Table III-4shows the recorded concentration times for the optMeth as well as the different UF method operating under constant flow and pressure conditions at a glance.

UF method	c [mg/ml]	Δp [bar]	TMP [bar]	τ_w [Pa]	Qr [l/m²/h]	Concentration time [min]
Δp 0.7 bar	5-90	0.7	0.6	126	270 [a]	150[b]
Δp 1.2 bar	5-140	1.2	0.6	216	310 [a]	130
Δp 1.8 bar	5-140	1.8	0.6	325	465 [a]	130
Δp 3.0 bar	5-90	3.0	0.6	541	845[a]	120 [b]
Δp 1.2 bar/ TMP 1.0	5-90	1.2	1.0	216	480 [a]	100 [b]
optMeth	5-25	0.6	1.25	108	240	
	25-50	1.2	0.85	216	450	110
	50-140	1.6	0.85	288	390	

[a] Average calculated from Qr values during the whole process
[b] Target concentration of 140 mg/ml was not reached

Table III-4: Overview of the operating conditions of the different UF concentration methods used
The indicated end concentrations (c) that were actually reached by the applied concentration method were determined before flushing the membrane with one dead volume.

It is assumed that the systematically defined operational conditions of the optimized concentration process (optMeth) avoid aggregation and thus high inlet pressure, leading finally to the abortion of the UF process. This contributes to the significantly reduced processing time concomitantly reaching the target concentration of 140 mg/ml in the retentate.

3.4 Effect of defined operational parameters on aggregation

The amount of aggregated protein was monitored during the concentration process by using several analytical methods like LO, turbidity measurement, DLS and SE-HPLC (Hawe and Friess 2008) in order to allow the characterization of differently sized aggregates in the processed protein solutions.

Large aggregates may be excluded, resolved or modified during SE-HPLC due to the interaction with the column matrix or changes in the sample buffer matrix during dilution in the mobile phase (Stulík et al. 2003). In order to monitor the formation of soluble HMWs in the end-concentrated solutions SE-HPLC was applied. Moreover, DLS measurements were conducted using time-dependent fluctuation of a scattered light signal to calculate the hydrodynamic diameter of aggregates as well as their relative amount (Demeester et al. 2005). This method is particularly valuable to detect aggregated species even in small traces. Samples during the UF experiments were taken every time the protein concentration doubled and were analyzed by LO and turbidity measurement to detect larger aggregates (Figure III-11).

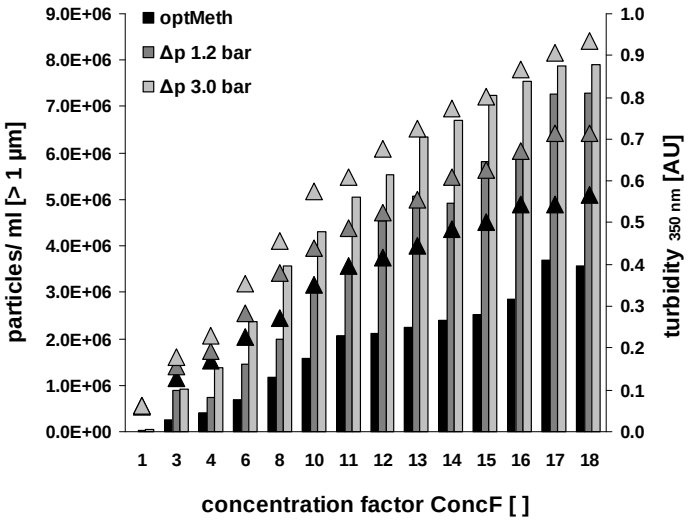

Figure III-11: Turbidity measurement (triangles, referring to the right scale) and number of particles larger than 1 µm (bars, referring to the left scale) during UF concentration from 5-90 mg/ml
Samples were taken every time the retentate concentration doubled.

LO revealed that by using the optMeth the lowest particle burden is generated over the whole process at comparable protein concentrations. The data is supported by turbidity measurements at 350 nm since it is known that an increase in particles of up to 1-2 µm in size is in good correlation with an increase in turbidity, as reported above (Mahler et al. 2005).

During the UF processing not only particles of proteinaceous nature can be generated but also particles of non-proteinaceous origin can be leached or abraded from tubing, pump heads or fittings (Arakawa et al. 2006; Tyagi et al. 2008). Both types o aggregates contribute to higher turbidity values as well as a higher number of particles determined by

LO. Tyagi et al. reported that stainless steel particles shed by the piston pump caused the formation of protein micro-particles after incubation at room temperature.

To identify the source and type of particles, a filtration/ staining method was used as described by Li et al. (2007). This method distinguishes between proteinaceous and unspecific particulate matter independent on rheological or optical properties of the sample and is therefore particularly suitable for high concentrations. Solely the proteinaceous particles are stained with the metal chelat stain pyrogallol red-molybdate which is known to be able to stain proteins immobilized on solid-phase supports (Shojaee et al. 1996). The aromatic functionalities of the dye enhance association with proteins through hydrophobic interactions and the dye contains a domain that reversibly binds to proteins, consisting of one or more anionic sulfonate residue for selective electrostatic interaction with amino side chains at acidic pH (Patton et al. 1999).

The filtered buffer solution did not show any retained and stained particles on the surface of the 0.2 µm filter (Figure III-12A).

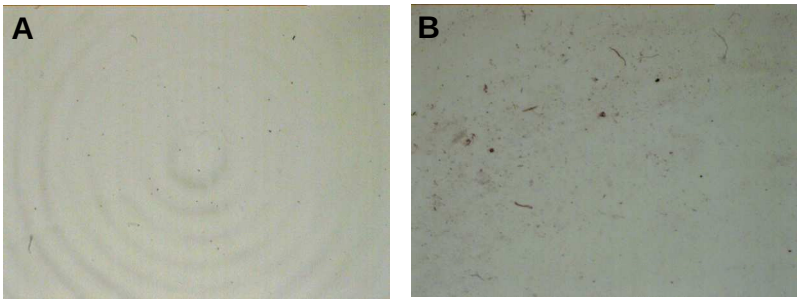

Figure III-12: Optical microscopy images of stained insoluble aggregates separated from the solution by 0.2 µm filtration
Buffer after recirculation (A) and 5 mg/ml protein solution before UF (B).

The buffer solution was taken from the equilibration run of the ÄKTAcrossflow after 30 min recirculation in the system. Moreover, the protein solution before UF showed only a few retained proteinaceous particles which are visible as stained purple dots on the filter surface (Figure III-12B).

An increased level of insoluble protein aggregates was clearly visible on the filter surface when the concentrated mAb solutions obtained from the different UF methods were investigated (Figure III-13). The concentrates of the most stressful Δp 3.0 bar mode showed the highest aggregate burden (Figure A). In comparison, the concentrates derived

from the optMeth (Figure C) showed a reduced level of stained insoluble proteinaceous particles on the filter surface with respect to number and size. This was shown as well in comparison to the concentrates derived from the Δp 1.2 bar method. Hence, this analysis underlines the results obtained from LO and turbidity measurements that the optMeth shows the lowest level of large proteinaceous aggregates.

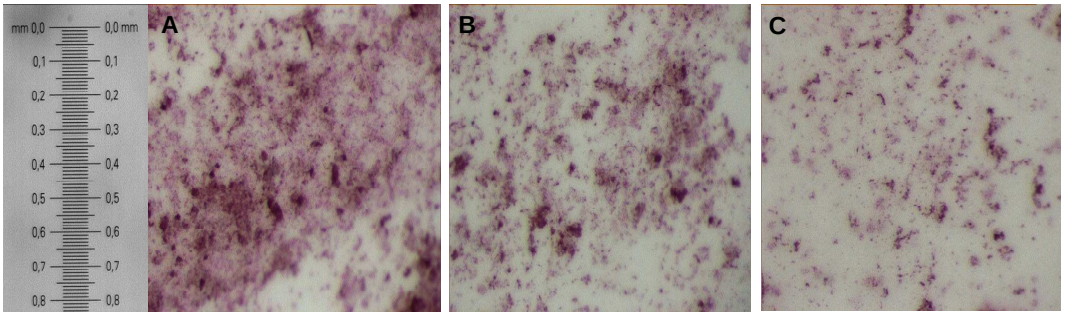

Figure III-13: Optical microscopy images of stained insoluble aggregates separated from the concentrates by 0.2 µm filtration
Concentrated solutions of 90 mg/ml after UF using the Δp 3.0 bar method (A), the Δp 1.2 bar method (B) and the optMeth (C).

Based on SE-HPLC data, almost no improvement in the quality of the concentrates was detected by applying the optMeth compared to the method operating at a constant Δp of 1.2 bar (Figure III-14). By referring to the method applying a Δp of 3.0 bar, a slight improvement considering the level of HMWs was detected by SE-HPLC if the optMeth or the Δp = 1.2 bar method were used.

A decline in total peak area of the SE-chromatograms was recognized when the differently concentrated samples were analyzed. Total recovery of the samples derived from both UF methods, the optMeth and the Δp = 1.2 bar method, were quite comparable with a value of about 8-10 %. Again, the decrease in total peak area stepped up to about 15 % when the Δp = 3.0 bar method was applied.

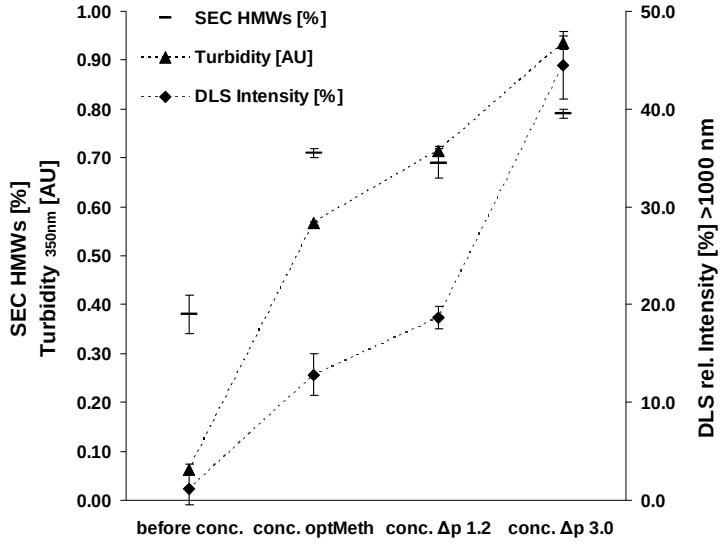

Figure III-14: Aggregates monitored by SE-HPLC, turbidity measurement and DLS relative intensity of the peak > 1000 nm (referring to the right axis)
For 90 mg/ml mAb solutions received from the optMeth compared to two other methods operating under constant Δp of 1.2 bar and 3.0 bar; experimental data is presented as mean values of three measurements ± SD.

By evaluating the DLS relative intensity, the concentrates of the optMeth show a clearly reduced level of aggregates larger than 1000 nm mean diameter. In general, larger aggregates present in trace levels are detectable with high sensitivity by using DLS, because the intensity of scattered light increases exponentially with the hydrodynamic radius according to the Rayleigh equation considering spherical particles (Ahrer et al. 2003; Demeester et al. 2005). This analytical method is again suitable to detect aggregates which are retained by the SE-column. Thus, aggregates are accessible by this method which are not detectable by SE-HPLC and are only reflected by the decline in total peak area of the chromatogram.

The monomer of an IgG is represented by the first peak at about 10 nm mean hydrodynamic diameter. The aggregates in the concentrated solutions appear at a hydrodynamic diameter larger than 1000 nm (Figure III-15).

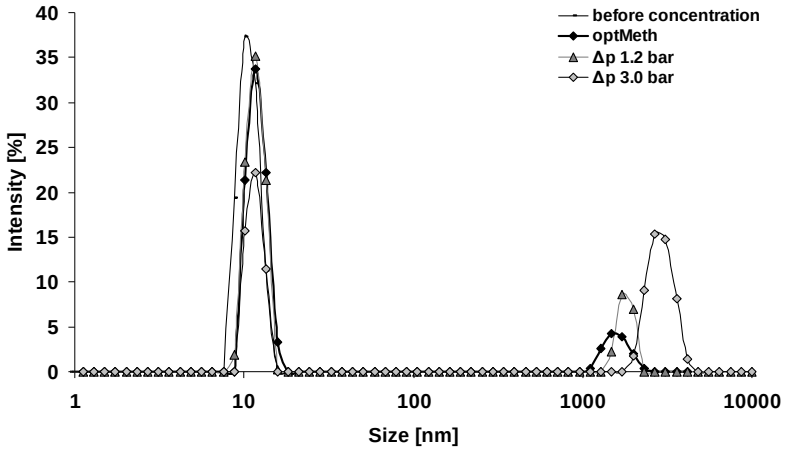

Figure III-15: DLS size distribution by intensity for 90 mg/ml mAb solutions derived from the optMeth compared to two other methods operating under constant Δp of 1.2 bar and 3.0 bar
The first peak refers to the monomer, the second peak to an aggregated species.

The signal relative intensity of the monomer and the aggregate peak depends on the concentration method used. For the concentrates produced under a constant Δp of 3.0 bar, the aggregate peak at > 1000 nm hydrodynamic diameter significantly increased up to 44.5 % relative intensity while the monomer peak intensity decreased at the same time, contributing just 53.5 % of the total scattered light. For the concentrate from the optMeth the monomer peak shows a relative intensity of 87.2 % which is quite comparable to the value of the solution before concentration. For the aggregate peak the lowest relative intensity of 12.8 % was observed. Although reaching the upper limit of the measurement size range of the DLS system the intensity distribution confirms the results of turbidity measurements, LO and total peak area evaluation of the SE-chromatograms showing that the concentrates of the optMeth provide the most desirable quality with respect to aggregation.

Table III-5 summarizes the analytical data for turbidity at 350 nm, DLS relative intensity for the monomer and the aggregate peak, and the number of particles larger 1 μm for the above mentioned IgG4 (IgG A) in a citrate buffered system. In addition the data was collected for two IgG1 mAbs (IgG B and IgG C) in histidine buffer, indicating that the presented results are qualitatively transferable to other molecules in a different buffer system.

It is shown that the concentrated solutions of three different mAbs using the optMeth result in a reduced level of protein aggregates compared to the concentrates from the methods operating under constant pressure conditions. The analytical results for the concentrated solutions were compared at 90 mg/ml protein concentration to have comparable values, since the Δp 3.0 bar was not able to exceed this concentration.

mAb	Method	Turbidity at 350 nm [AU]	DLS relative intensity [%]		Number of particles per ml [> 1 µm]
			First peak [10 nm]	Second peak [> 1000 nm]	
IgG A	Before concentration	0.063 ± 0.010	98.83 ± 1.65	1.17 ± 1.65	$3.38 \times 10^4 \pm 305$
	Δp 1.2 bar	0.715 ± 0.010	81.30 ± 1.13	18.70 ± 1.13	$7.20 \times 10^6 \pm 55 \times 10^3$
	Δp 3.0 bar	0.935 ± 0.010	55.53 ± 3.49	44.47 ± 3.49	$7.90 \times 10^6 \pm 13 \times 10^3$
	optMeth	0.566 ± 0.030	87.17 ± 2.10	12.83 ± 2.10	$3.56 \times 10^6 \pm 22 \times 10^2$
IgG B	Before concentration	0.026 ± 0.010	100.00 ± 0.00	0.00 ± 0.00	$8.02 \times 10^3 \pm 100$
	Δp 1.2 bar	0.520 ± 0.060	75.43 ± 7.79	24.57 ± 7.79	$4.38 \times 10^6 \pm 20 \times 10^3$
	Δp 3.0 bar	0.881	51.40 ± 2.64	48.60 ± 2.64	$6.17 \times 10^6 \pm 40 \times 10^3$
	optMeth	0.409 ± 0.010	77.53 ± 1.75	20.17 ± 2.74	$2.09 \times 10^6 \pm 21 \times 10^3$
IgG C	Before concentration	0.029 ± 0.010	100.00 ± 0.00	0.00 ± 0.00	$9.16 \times 10^3 \pm 50$
	Δp 1.2 bar	0.454 ± 0.020	80.18 ± 2.79	19.93 ± 2.81	$14.88 \times 10^6 \pm 60 \times 10^3$
	Δp 3.0 bar	1.099 ± 0.050	70.53 ± 0.75	29.47 ± 0.75	$23.22 \times 10^6 \pm 58 \times 10^3$
	optMeth	0.393	94.53 ± 3.23	5.47 ± 3.23	$8.17 \times 10^6 \pm 22 \times 10^3$

Table III-5: Analytical data for three different mAbs (IgG A in citrate buffer, IgG B and IgG C in histidine buffer)
At 5 mg/ml (before concentration) and at 90 mg/ml derived from the indicated concentration methods; the mean values of three measurements are presented ± SD.

3.5 Secondary structure analysis

FT-IR spectroscopy was applied to elucidate if the protein exhibits changes in secondary structure due to the UF procedure. Therefore, the insoluble aggregates in the retentate were investigated, as well as the protein directly deposited on the surface of the membranes after UF concentration.

IgGs exhibit mainly β-sheet structure revealed by X-ray analysis (Costantino et al. 1997). MAbs show two characteristic bands in the second derivative FT-IR spectrum at around 1639 and 1690 cm^{-1} reflecting the presence of intramolecular ß-sheet structure (Chang et al. 2005; Cleland et al. 2001). Conformational changes are indicated by a shift to a strong temperature-induced frequency at 1615-1625 cm^{-1} and a concomitantly reduced intensity of the band at around 1639 cm^{-1} as well as at 1690 cm^{-1} (Matheus et al. 2006a; Pelton and McLean 2000). Hence, the second derivative spectra were truncated between 1700 and 1500 cm^{-1} to prospect for changes in secondary structure (Kendrick et al. 1996).

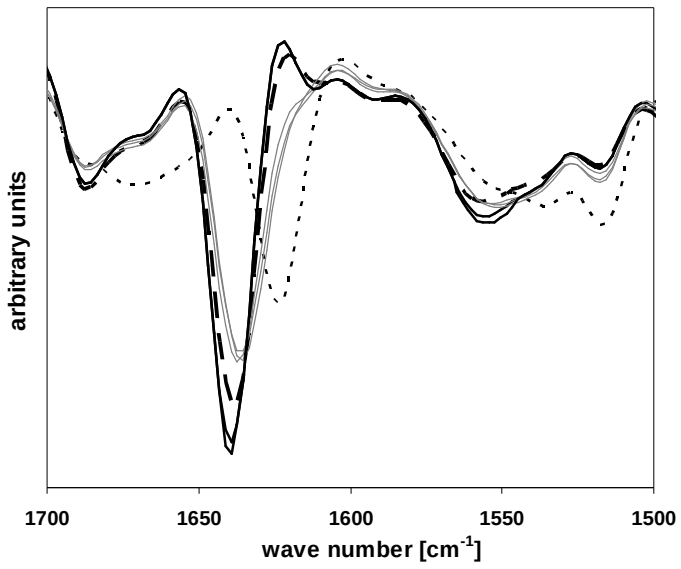

Figure III-16: Comparison of the second derivative FT-IR spectra
The native mAb in solution at 5 mg/ml and 90 mg/ml (black lines, almost perfectly overlaid), the protein adsorbed to the membrane (dashed black line), the separated insoluble aggregates from the Δp 3.0 bar-, Δp 1.2 bar-, and the optimized UF method (grey lines, almost perfectly overlaid) and the heat treated solution at 90 mg/ml (dotted line).

When the spectrum of the protein on the processed and washed hydrophilic cellulose based membrane was compared to the spectra of the protein in solution, only slight differences were observable (Figure III-16).

This reveals that the protein directly adsorbed to the membrane after processing almost remained in its native secondary conformation. By looking at the spectra of the separated insoluble aggregates from the retentate, the diminished bands at 1639 cm^{-1} and 1690 cm^{-1} as well as the shift of the band at 1639 cm^{-1} to a lower wave number revealed perturbation in secondary structure, i.e. loss in the proportion of ß-sheet motifs. This was shown to be much more pronounced by heating which is in accordance with current literature mentioned above.

The findings correspond to the work of Maruyama and coworkers who found that the simple adsorption to hydrophilic UF membranes induced only a slight perturbation in secondary structure of BSA (Maruyama et al. 2001b). Moreover, the aggregated protein was scratched from the gel layer near the membrane after concentrating the solution in a stirring cell. The sample exhibit significantly denatured protein investigated by FT-IR (Maruyama et al. 2001a).

It has to be pointed out that the investigated samples in this study showed no spectral differences depending on the applied UF method. The recorded spectra of the protein in solution at 5 mg/ml and at 90 mg/ml almost perfectly overlaid. Moreover, the different operational parameters applied during UF did not cause any spectral differences between the several insoluble aggregates removed from the retentate. All samples of the separated aggregates revealed the same spectral differences compared to the native protein in solution. However, the amount of the aggregates in the retentate during UF strongly depends on the applied flow and pressure conditions as shown before. Therefore, the increase of structurally altered insoluble aggregates during UF is not attributed to protein-membrane interactions but rather to the flow velocity during the tangential flow mode. The protein in solution is constantly moved over the membrane during TFF and the generated structurally perturbed aggregates are transported to the retentate adversely affecting the quality of the produced bulk.

3.6 Effect of bulk quality on the sterile filtration process

Sterile filtration in normal flow mode is mandatory for the formulated active pharmaceutical ingredient as well as during DSP to ensure the absence of particles, microorganisms and aggregates which can cause detrimental effects including loss of activity, altered half life or immunogenic reactions (Cleland et al. 1993).

Membrane fouling causing rapid filtrate flow decline and increased filtration time in microfiltration generally includes concentration polarization, adsorption of particles, pore blocking and deposition of particles on the membrane surfaces (Wang et al. 2007b). If concentrated solutions are sterile filtered the high viscosity plays an additional role in terms of filtrate flow decline (Green and Scheer 1998; Liu et al. 2005).

For the mAb solutions from the different concentration methods the filtrate flow rate was plotted over time (Figure III-17A). It is obvious that the concentrates of the optMeth showed an improved filtrate flow rate over time at a comparable protein concentration of 90 mg/ml and thus comparable viscosity. A linear correlation between filtrate flow rate and filtration volume was observed (Figure III-17B).

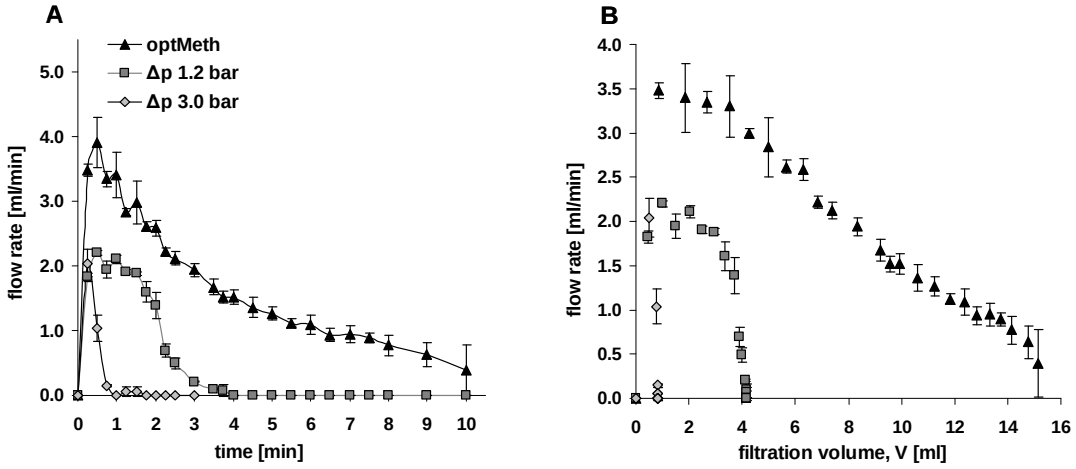

Figure III-17: Filtrate flow rate over time for concentrates at 90 mg/ml after UF
Solutions obtained from the optMeth and two other methods operating at constant Δp of 1.2 bar and 3.0 bar (A). Data plotted in accordance to the pore blockage model (B); experimental data is presented as mean values of three measurements ± SD.

This linear correlation is in accordance with a traditional pore blockage mechanism assuming that filtration flux decline is mainly related to the aggregate burden of the to be filtered solution (Hermia 1982; Ho and Zydney 2000).

The concentrates derived from constant pressure UF methods are more prone to pore blockage since these solutions have a higher level of insoluble protein aggregates. This is in agreement with Palacio et al. (2002) who found that pore blockage during microfiltration is directly related to the concentration of particles in solution.

Hence, to improve filtration flow and to reduce process time in sterile filtration operations, it is recommended to consider the optimal operating conditions during previously conducted UF.

4 Summary and conclusion

The influence of applied shear stress on permeate flux and aggregation during the UF concentration process was evaluated using an automated lab scale TFF system. It was demonstrated that this system equipped with a scalable flat sheet cassette adequately reflects process conditions in larger scale.

The studies presented in this chapter mainly revealed an increased level of large insoluble and structurally perturbed aggregates in the concentrated solutions. This increase is directly correlated to the applied shear stress during UF. Permeate flux decline was attributed to induced aggregates depositing on the membrane surface and causing pore clogging of the membrane device used. It was observed that a minimal wall shear stress has to be applied to ensure sufficient back transport of deposited solutes to the retentate. At the same time the wall shear stress has to be limited to avoid the generation of soluble and insoluble aggregates and their removal from the membrane device to the concentrated retentate, since these aggregates adversely affect bulk quality.

It was observed that permeate flux during UF strongly depends on the protein concentration in the retentate as well as on the applied pressure and flow conditions. By varying TMP and cross flow values systematically depending on the concentration in the retentate, an UF concentration method was developed particularly suitable for the production of highly concentrated mAb solutions up to 140 mg/ml. This optimized three stage process resulted in an improved permeate flux and a significantly reduced concentration time.

A 20 % reduction in process time was recognized when the optimized method is used compared to two UF methods operating at constant pressure and flow conditions.

Concomitantly, the concentrates generated by using this optimized UF method showed a reduced aggregate level compared to two other methods. This was observed for three different mAbs in two different buffer systems. The combination of SE-HPLC, DLS, LO and a filtration/ staining method allowed the characterization of a wide range of sizes of soluble and insoluble aggregates occurring during the UF concentration process. These techniques were used to evaluate the quality of the produced concentrates.

With regards to sterile filtration the optimized method showed an improved flow rate during filtration processing due to improved bulk quality in terms of aggregation. This is important because this essential final manufacturing step is already adversely affected by the high viscosity of the concentrated protein solution.

Finally, FT-IR spectroscopy revealed a perturbed secondary structure of the aggregates appearing during UF which was attributed to high flow and pressure values in tangential flow mode rather than to surface related unfolding. The protein adsorbed to the UF membrane remained nearly native independent of the applied flow and pressure conditions.

Chapter IV Effects of operational parameters during UF on the stability of highly concentrated mAb solutions

Abstract

Protein bulks have to show sufficient physical stability to minimize the risk of aggregation, since the opportunities to remove any process related impurity are limited to the final polishing during purification. Directly after UF concentrated IgG solutions of 90 mg/ml were stored at several conditions to investigate their physical stability depending on total protein concentration as well as on the UF protocol applied during processing. In general, the formation of differently sized aggregates was shown to be enhanced at a higher total protein concentration in the unformulated bulk. After 0.2 μm-filtration of the concentrated bulks no benefit was recognized regarding the formation of aggregates when the optimized method was used during UF. In general, 0.2 μm-filtration showed a significant influence on the level of soluble higher molecular weight species (HMWs) during storage at elevated temperatures. A reduced formation of the smaller HMWs was recognized in the presence of subvisible aggregates of up to 1-2 μm as well as those being larger than 1 μm in size. This was attributed to a repressed nucleation and subsequent growth of aggregated species which is a known mechanism of aggregate propagation in protein solutions. Moreover, a successive formation of visible precipitated aggregates was observed during storage at 2-8 °C when subvisible aggregates were already present. In general, the storage of the filtered solutions at 2-8 °C was found to be superior to storage in the frozen state regarding the level of soluble aggregates in the concentrated bulk. In addition, conformational stability was investigated using ATR FT-IR spectroscopy analysis. A consistently higher melting temperature (T_m) was found at a higher total protein concentration, however the concentrates generated by using the optimized method showed a consistently higher T_m value

compared to the concentrates derived from other UF protocols. Since aggregation was in general enhanced at a higher total protein concentration independent from the UF protocol used, aggregation at higher total protein concentrations seems to be rather based on homogeneous nucleation and growth than on aggregation based on perturbation in secondary structure.

1 Introduction

Currently, highly concentrated formulations of therapeutic mAbs can be considered as a trend in commercial manufacturing. Since the accessible volume for local s.c. application is 1-3 ml, mAb solutions at concentrations of at least 100 mg/ml are required (Harris et al. 2004; Shire et al. 2004) in order to achieve effective concentration levels in the blood of about 100-400 mg protein per administration (Dani et al. 2007). Following s.c. injection, most drugs pass through the interstitial matrix, traverse capillaries or lymphatics before they reach the vascular compartment (Bookbinder et al. 2006). The interstitial matrix is a complex three-dimensional structure where aggregated molecules can be retained and may increase the risk of immunogenicity (Schellekens 2005). Therefore, aggregation has to be particularly prevented for concentrated preparations since these solutions are intended to be subcutaneously administered. This is of special importance after the last concentration step of the purification process, since no instruments are available to further reduce the aggregate level in the formulated bulk.

Moreover, the stability of the intermediate pools at different stages of purification has to be evaluated considering protein aggregation. Due to high volumetric productivity of new cell line generations and optimized fermentation processes high product titer are achieved (Graumann and Premstaller 2006). This can result in large eluate volumes when high capacity resins are not available or suitable. The large pool volumes have to be handled by using the existing hard-piped manufacturing plants and vessels (Low et al. 2007). Therefore, the subsequent UF concentration is necessary to match the limited volume capacity of the existing plants by creating low volume units.

This chapter addresses the influence of applied operational parameters in tangential flow UF on the stability of highly concentrated API bulk during storage, since UF is the industry standard for concentration and diafiltration procedures in large scale purification processes. There are studies describing that large velocity gradients can deform or denature

the native structure of globular proteins resulting in a loss of activity or fragmentation of the covalent backbone (Charm and Lai 1971; Virkar et al. 1981; Wang et al. 2007a). Antigen-binding activity of a recombinant scFv antibody fragment was reduced in a buffer solution at a shear rate of 20 000/s (Harrison et al. 1998). Often, the processed solutions appear opalescent or precipitated after processing, although only a small amount of total protein loss was observed (Narendranathan and Dunnill 1982; Thomas et al. 1979). In contrast Jaspe and Hagen (2006) described more recently that even shear rates of 200 000/s did not result in any detectable destabilization of the protein regarding especially protein unfolding. Here, cytochrome C was used whose fluorescence increases sharply upon unfolding suitable to monitor conformational changes during the exposure to high shear.

As presented in chapter III, a three step process applying different flow and pressure conditions depending on the prevailing protein concentration in the retentate resulted in improved quality of the concentrates regarding aggregation. This was compared to two other UF methods operating under elevated constant flow and pressure during the concentration process. Therefore, the three differently processed concentrates were stored at 2-8 °C, at -20 °C and at elevated temperature in order to investigate the influence of operational conditions during UF on physical stability including aggregation and changes in secondary structure.

As described in chapter I, it is reported that aggregates already in small traces and without showing any conformational alterations can induce ongoing aggregation due to an nucleation and growth process (Cleland et al. 1993; Reithel 1964; Wood et al. 1999). Therefore, the filtered and unfiltered mAb solutions at 90 mg/ml derived from the different UF concentration methods were investigated regarding the effect of preformed aggregates and particles on stability during storage.

2 Materials and methods

2.1 Materials

A therapeutic mAb solution of a chimeric human Fc (IgG4)/ rat Fab antibody in histidine buffer at pH 5.5 was taken for the concentration experiments. The mAb was provided by

Roche Diagnostics GmbH (Penzberg, Germany). The solution of 5 mg/ml protein concentration was filtered through a 0.2 µm membrane filter (Sartorius, Goettingen, Germany) before UF processing. All chemicals and reagents used were at least analytical grade. Hydrochloric acid was taken from Merck KG (Darmstadt, Germany). L-histidine from Ajinomoto (Raleigh, USA) was used.

2.2 Methods

2.2.1 Ultrafiltration concentration procedure and storage

For the preparation of concentrated mAb solutions the automated TFF system ÄKTAcrossflow (GE Healthcare, Uppsala, Sweden) was used (Liten and Cohen 2007). The experiments were conducted by using the equipment and techniques as described in chapter III. Table IV-1 shows the applied UF concentration methods and the resulting operational conditions.

Method	c [mg/ml]	Δp [bar]	TMP [bar]	τ_w [Pa]	Qr [l/m²/h]
Δp 1.2 bar	5-90	1.2	0.60	216	310 [a]
Δp 3.0 bar	5-90	3.0	0.60	541	845[a]
optMeth	5-25	0.6	1.25	108	240
	25-50	1.2	0.85	216	450
	50-90	1.6	0.85	288	390

[a] Average calculated from the flow rate values (Qr) recorded during the whole process

Table IV-1: Overview of operating conditions of the different UF concentration methods
The indicated end concentrations (c) correspond to values before flushing the membrane.

The different concentration methods were run until a target concentration of about 90 mg/ml was reached, since the method applying a Δp of 3.0 bar is not applicable to exceed this concentration. Thus, solutions at comparable protein concentrations were obtained.

After the UF concentration up to 90 mg/ml, each concentrated pool was divided into two aliquots of an equal volume of 45 ml. One portion was filtered at a constant pressure of 1.0 bar through a Sartopore 2 XLG Disposable filter unit with a pore size of 0.8 and

0.2 µm and a filter area of 58 cm² (Sartorius, Goettingen, Germany). Both, the filtered and the unfiltered solutions were stored at 40 °C, 2-8 °C and -20 °C in sterile CRYO.S tubes (Greiner Bio-One, Frickenhausen, Germany). The frozen samples were stored over three months and were then thawed in a 25 °C tempered water bath. Afterwards, freezing and thawing was repeated two times to end up with three freeze and thaw cycles in total.

2.2.2 Concentration determination

Concentration was determined in the samples by using the photometric absorbance at 280 nm and 320 nm after buffer blank subtraction (UV-Vis spectrophotometer Evolution 500, Thermo Fisher Scientific, Waltham, USA). The absorbance at 320 nm was subtracted from the absorbance at 280 nm (UV 280-320) and this value was used to calculate the protein content according to the law of Lambert-Beer.

To determine the percent in soluble protein remaining in the filtered and unfiltered solutions during storage, the samples were centrifuged for 30 min at 10 000 x g (Heraeus Multifuge, Thermo Fisher Scientific, Waltham, USA) and the concentration was determined in the supernatant using UV 280-320 as described above. The percent soluble protein remaining was calculated by referring to the protein concentration of the respective sample before storage as 100 %.

2.2.3 Turbidity measurements

Turbidity was determined as photometric absorbance of the undiluted concentrates at 350 nm and 550 nm after buffer-blank subtraction (UV-Vis spectrophotometer Evolution 500, Thermo Fisher Scientific, Waltham, USA). The analysis was conducted as described in chapter III.

2.2.4 Size exclusion high pressure liquid chromatography

SE-HPLC analysis was conducted using a TSK 3000 SWXL column (Tosoh Biosep, Stuttgart, Germany) on a Summit HPLC-system (Dionex, Idstein, Germany). The elution peaks were monitored at 280 nm by the UV diode array detector UVD170U from Dionex (Idstein, Germany). Isocratic chromatography was conducted as described in chapter III. Integration procedure using the Chromeleon software (Dionex, Idstein, Germany) is shown exemplarily in Figure III-1 (see page 52). The percentage of higher molecular

weight species (HMWs) including dimers and larger soluble oligomers was determined as relative area (mAU·min) of the respective peaks referred to total area of all peaks including the monomer peak and the peak of the lower molecular weight species (LMWs). Total recovery was monitored throughout the analysis by comparing the total peak area of the respective sample to the total peak area of a control sample.

2.2.5 Light obscuration particle counting

LO was used to monitor the formation of particles in a range of 1-200 µm similar to the method <788> Particulate Matter of Injection in the United States Pharmacopoeia and the European Pharmacopoeia method 2.9.1 (EDQM 2001a; USPC 2002). The measurements were conducted using the particle counter SVSS-C (PAMAS Partikelmess- und Analysesysteme, Rutesheim, Germany) as described in chapter III.

2.2.6 Dynamic light scattering

The Zetasizer Nano S (Malvern Instruments, Worcestershire, UK) was used to monitor colloidal species in the size range of a hydrodynamic diameter between 1 nm and 6 µm. The scattering information is detected at an angle of 173 ° (Kaszuba and Connah 2006) operating with a 4 mW He-Ne-laser at 633 nm using the non-invasive back-scatter technique (NIBS). The samples were analyzed undiluted in a temperature controlled precision quartz cuvette (Hellma, Müllheim, Germany) at 25 °C. The size distribution by intensity was calculated from the time-dependent correlation function using the multiple narrow mode of the DTS software (Version 5.0, Malvern Instruments, Worcestershire, UK).

2.2.7 FT-IR spectroscopy

FT-IR spectra were recorded with the Tensor 27 (Bruker Optics, Ettlingen, Germany) applying the BioATR unit with a Silicium crystal (Bruker Optics, Ettlingen, Germany).

For each spectrum which was recorded from 850-4000 cm^{-1} a 120-scan interferogram was collected at a double sided acquisition mode with a resolution of 4 cm^{-1}. To monitor temperature induced conformational changes in secondary structure of the mAb spectral changes were followed from 25-90 °C at 90 mg/ml. 25 µl of the sample solution were applied into the unit and a temperature ramp from 25-60 °C and from 80-90 °C with a ΔT of 5 °C and from 60-80 °C with a ΔT of 2 °C were performed. The equilibrium time was

120 s at each temperature step. The respective temperature was adjusted by connecting the ATR cell to a thermostat (Haake DC30-K20, Thermo Scientific, Waltham, USA). To obtain the reference spectra of the buffer system used, the permeate of the UF concentration procedure was taken and the temperature ramps were performed as described before. The obtained buffer spectra were than subtracted to obtain the protein spectra.

The spectra were edited by a vector normalization. Afterwards, a second-derivative procedure was done to enhance the resolution, concomitantly preserving the band position (Pelton and McLean 2000). The second derivative was smoothed using a 13-point Savitsky-Golay smoothing function. For this, the OPUS software version 6.0 was used (Bruker Optics, Ettlingen, Germany).

3 Results and discussion

3.1 Aggregation behavior during storage

All samples were stored under quiescent conditions without shaking or stirring to reflect simple storage of the concentrates on-site. The unfiltered as well as the filtered API bulk was analyzed over time. Turbidity at 350 nm was measured to monitor especially the presence of smaller aggregates of up to 1-2 µm in size as detailed in chapter III. Figure IV-1 shows the difference in turbidity between the unfiltered and the filtered concentrates processed at indicated UF conditions (see Table III-1). The turbidity remains quite constant over 4 weeks at elevated temperature for all concentrates derived from the different UF methods used.

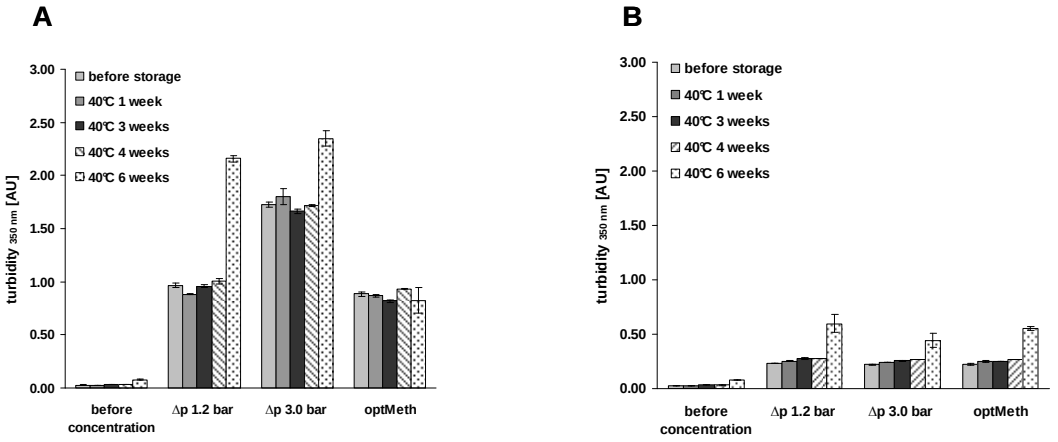

Figure IV-1: Turbidity at 350 nm during storage at 40 °C for mAb solutions before concentration (5 mg/ml) and after UF (90 mg/ml) by using different concentration methods
The data referring to the unfiltered solutions is shown on the left side (A) and the data referring to the filtered solutions is shown on the right side (B); mean values of three measurements are reported ± SD.

At every time, the unfiltered concentrates referring to the optMeth show the lowest turbidity values after UF processing and during storage (Figure IV-1A). After 6 weeks at 40 °C the turbidity of the samples referring to the Δp 1.2 bar and Δp 3.0 bar method increases sharply to > 2 AU, whereas the samples of the optimized method did not show this increase in turbidity.

Results from LO show the number of particles larger 1 µm per ml protein solution (Figure IV-2A). Again, the samples referring to the Δp 1.2 bar and Δp 3.0 bar method

showed a higher level of particles before and during storage, compared to the samples generated by using the optMeth. As observed for the turbidity measurements, the samples referring to the Δp 1.2 bar and Δp 3.0 bar method showed an increased level in particles larger 1 µm after 6 weeks at 40 °C. Whereas the samples of the optimized method did not. In general, the concentrates from the Δp 3.0 bar method showed the highest particle level and the highest turbidity values respectively.

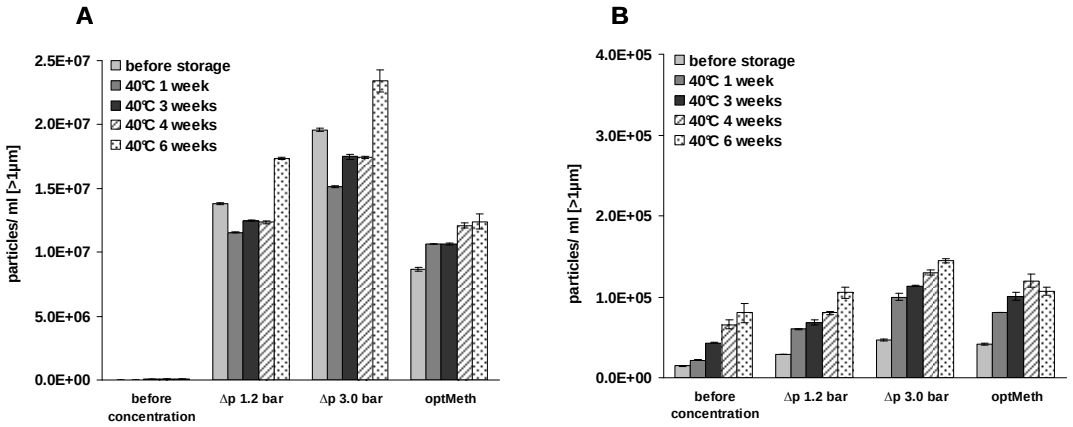

Figure IV-2: Particles per ml larger than 1 µm during storage at 40 °C for mAb solutions before concentration (5 mg/ml) and after UF (90 mg/ml) by using different concentration methods
The data referring to the unfiltered solutions is shown on the left side (A) and the data referring to the filtered solutions is shown on the right side (B); mean values of three measurements are reported ± SD.

Moreover, it was recognized that the quality of the produced concentrates considering the level of particles after 0.2 µm-filtration is comparable and independent of the applied operational parameters during UF. The turbidity values and particle numbers did not increase to the high levels observed before storage. This became obvious by comparing the turbidity data and number of particles during storage after filtration (Figure IV-1B and Figure IV-2B) to the respective data before filtration (Figure IV-1A and Figure IV-2A).

The yield after 0.8/ 0.2 µm-filtration of the concentrated solutions was determined. No significant differences were observed depending on the UF method used. The yield was calculated referring to the applied protein mass before conducting the filtration ($m_{\text{before filtr}}$) as 100 %. For each filtration experiment $m_{\text{before filtr}} \approx 4$ g was applied. Further, the protein mass after filtration was determined ($m_{\text{after filtr}}$). The measured concentration after filtration was therefore multiplied with the corresponding volume ($c_{\text{after filtr}} \times V_{\text{after filtr}}$).

Figure IV-3 shows the yield after filtration of the concentrated solutions, as well as for the solutions at 5 mg/ml protein concentration.

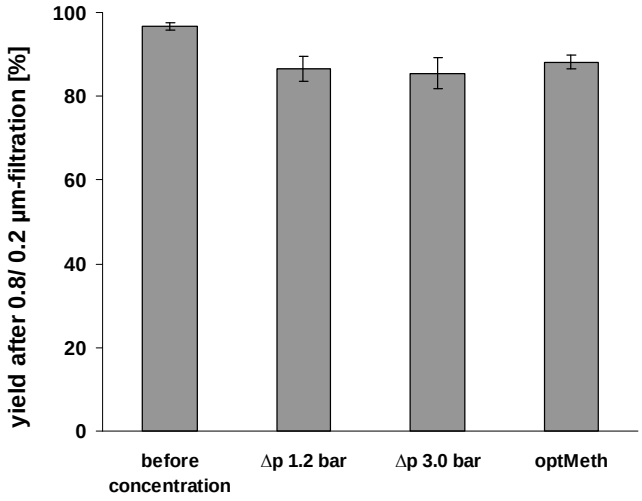

Figure IV-3: Yield after 0.8/ 0.2 µm-filtration
The 0.2 µm filtration was performed with the solutions at 5 mg/ml (before concentration) and at 90 mg/ml after UF applying three different methods (Δp 1.2 bar, Δp 3.0 bar and optMeth); mean values of three measurements are reported ± SD.

In general, all concentrated samples showed a lower yield of about 85-88 % after 0.8/ 0.2 µm-filtration, compared to the sample at 5 mg/ml. This is attributed to the higher viscosity of the concentrated samples contributing to an increased loss of protein on the filter and the filtration equipment.

Potential quality differences of the concentrated solutions due to different operational conditions during UF were further investigated during storage at -20 °C and 2-8 °C. The filtered solutions did not show any differences in turbidity during storage (Figure IV-4B). Neither an increase in turbidity after freezing and thawing, nor after storage at 2-8 °C was recognized. A slight increase in the number of particles larger 1 µm was only observed after 6 months at 2-8 °C for all filtered concentrates (Figure IV-5B).

As regards the unfiltered solutions before and after freezing and thawing, the concentrates derived from the optimized UF method revealed a slightly reduced turbidity as well as a slightly lower number of particles larger 1 µm compared to the solutions obtained from the two other UF methods (Figure IV-4A and Figure IV-5A).

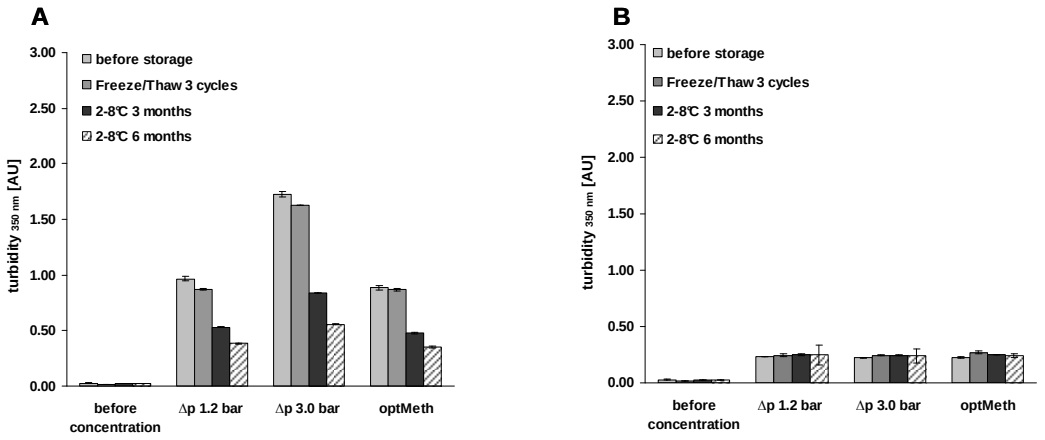

Figure IV-4: Turbidity at 350 nm during storage at -20 °C and 2-8 °C for mAb solutions before concentration (5 mg/ml) and after UF (90 mg/ml) by using different concentration methods

The data referring to the unfiltered solutions is shown on the left side (A) and the data referring to the filtered solutions is shown on the right side (B); mean values of three measurements are reported ± SD.

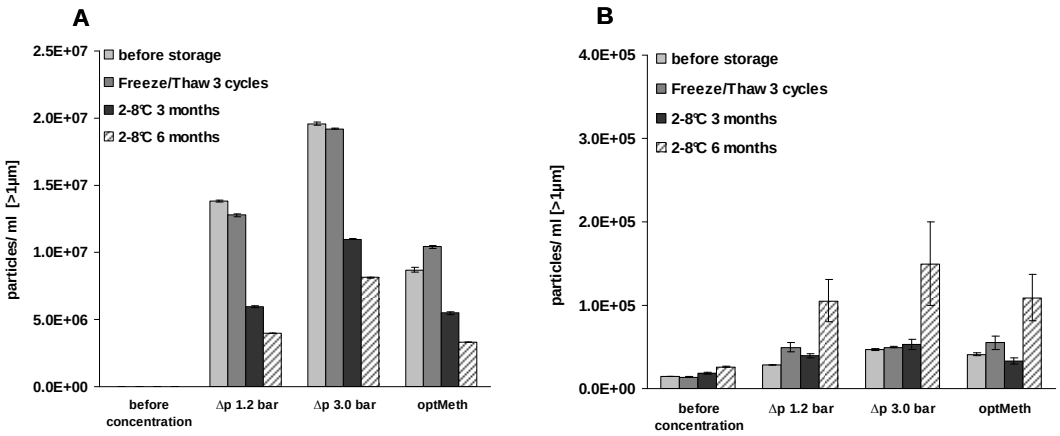

Figure IV-5: Particles per ml larger than 1 µm during storage at -20 °C and 2-8 °C for mAb solutions before concentration (5 mg/ml) and after UF (90 mg/ml) by using different concentration methods

The data referring to the unfiltered solutions is shown on the left side (A) and the data referring to the filtered solutions is shown on the right side (B); mean values of three measurements are reported ± SD.

Freezing and thawing did not result in significant differences regarding the turbidity and the particle burden of all unfiltered samples compared to the values before storage.

After storage at 2-8 °C over 3 months, all concentrates were less turbid and contained a lower number of particles larger 1 μm than before storage. After 3 months up to 6 months this reduction in the number of particles larger 1 μm detected by LO and the reduction of smaller particles of up to 1-2 μm in size detected by turbidity measurements continued. A significantly reduced total peak area of the SE-chromatograms was not observed which is often related to the formation of larger aggregates which are excluded by the SE-matrix and are therefore not detectable by this analytical method (see chapter III). However, precipitated protein which was visible by the unaided eye was observed during storage of these concentrated solutions at 2-8 °C.

Therefore, the concentration of the samples was determined by UV 280-320 after centrifugation for 30 min at 10 000 x g in order to determine the loss of soluble protein due to precipitation. It was assumed that the loss of differently sized proteinaceous particles detected by turbidity and LO measurements in the unfiltered solutions is caused by the formation of an insoluble precipitate during storage at 2-8 °C.

The analysis was done for the filtered as well as for the unfiltered samples, since the filtered solutions obtained from the several concentration methods did not show any difference during storage at -20 °C or 2-8 °C regarding turbidity and number of particles larger 1 μm (Figure IV-4B and Figure IV-5B). Moreover, only a marginally sedimented deposit was recognized on the bottom of the tubes.

A decrease in the percent soluble protein remaining with storage time was observed in the unfiltered concentrated solutions at 90 mg/ml during storage at 2-8 °C (Figure IV-6A). After 6 months, only about 80 % of soluble protein was found in solution. The decrease in the percent soluble protein remaining for the filtered concentrates stored at 2-8°C was only about 10 % after 6 months (Figure IV-6B).

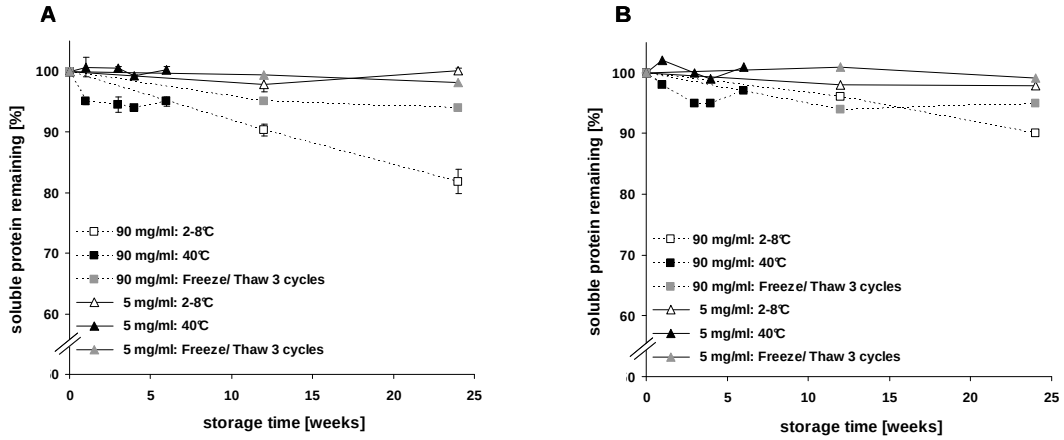

Figure IV-6: Percent soluble protein remaining in solution with storage time at 2-8 °C (plain symbols), 40 °C (black symbols) and after freezing and thawing in 3 cycles (grey symbols)
Analysis was done by UV 280-320 measurements after centrifugation for 10 min at 10 000 x g; the concentrates referring to the Δp 3.0 bar method were exemplarily analyzed; the data referring to the unfiltered solutions is shown on the left side (A) and the data referring to the filtered solutions is shown on the right side (B); only for figure (A) the mean values of three measurements are reported ± SD.

In general, a more pronounced decrease in percent soluble protein remaining after storage at 2-8 °C was observed at 90 mg/ml compared to solutions at 5 mg/ml. Freezing and thawing in three cycles did not result in this pronounced decrease of soluble protein, independent of protein concentration or filtration procedure conducted before storage. These results underline that the reduction of differently sized particles during storage at 2-8 °C over 6 months can be attributed to the formation and precipitation of much larger ones which are no longer detectable by turbidity measurements or LO.

As regards the percentage of soluble higher molecular weight species (HMWs) during storage at elevated temperature, the unfiltered solutions show no significant difference depending on the UF concentration method used, neither before nor after storage (Figure IV-7A). Moreover, the same trend is obvious for the filtered solutions (Figure IV-7B).

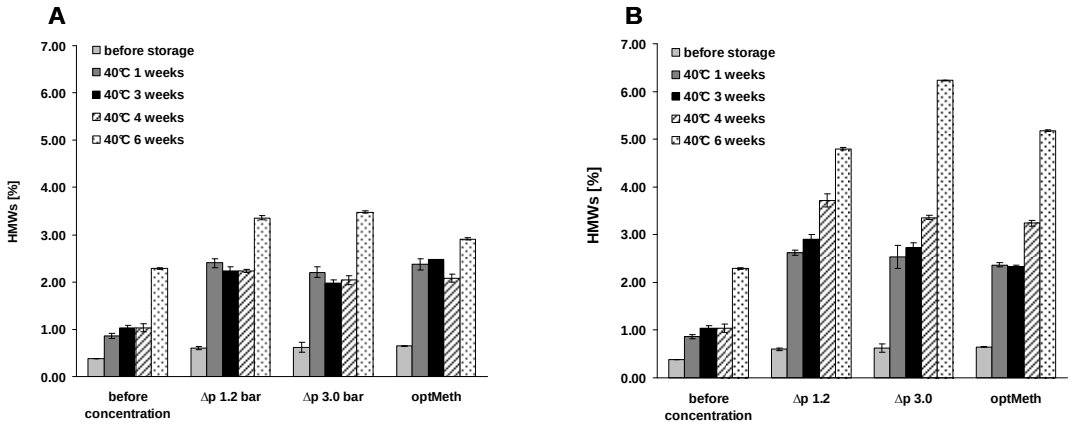

Figure IV-7: HMWs [%] during storage at 40 °C for mAb solutions before concentration (5 mg/ml) and after UF (90 mg/ml) by using different concentration methods

On the left side the unfiltered solutions (A) and on the right side the filtered solutions (B) are shown; mean values of three measurements are reported ± SD.

Only after 4 and 6 weeks at 40 °C the filtered solutions produced at a Δp of 3.0 bar revealed a significantly higher level of soluble aggregates than the concentrates derived from the optimized method and the Δp 1.2 bar method. In general, higher HMW levels were observed during storage of the filtered samples compared to the unfiltered ones. A possible explanation for this is discussed in section 3.2 of this chapter.

During storage at 2-8 °C and after freezing and thawing in three cycles all concentrates show a comparable quality regarding the HMW level independent of the UF method used (Figure IV-8A and Figure IV-8B). However, a slight increase in HMWs for all samples was observed over 3 and 6 months, especially in comparison to the samples at 5 mg/ml. Comparable HMW levels are observed for the filtered and unfiltered samples. Generally, it is observed that freezing and thawing at a high protein concentration of 90 mg/ml lead to much higher HMW level than storage at 2-8 °C. All concentrates show an increased level up to about 3 % HMWs after freezing and thawing in three cycles.

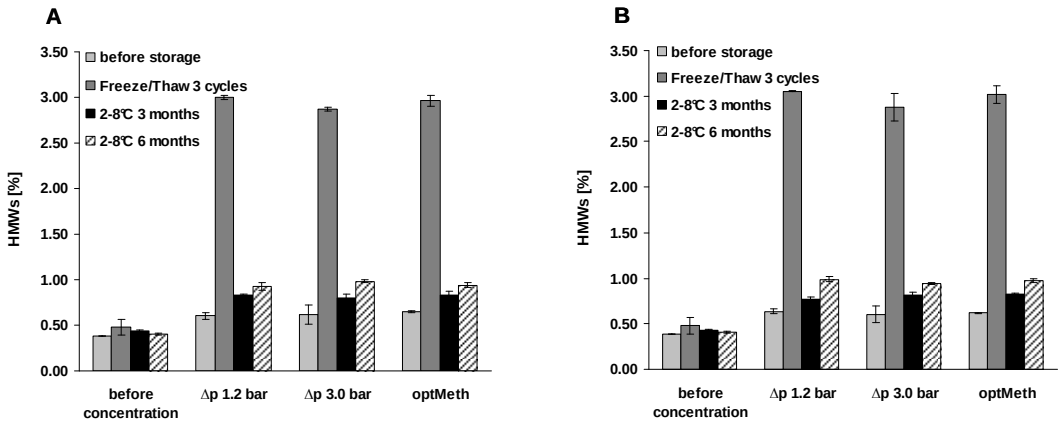

Figure IV-8: HMWs [%] during storage at -20 °C and 2-8 °C for mAb solutions before concentration (5 mg/ml) and after UF (90 mg/ml) by using different concentration methods
On the left side the unfiltered solutions (A) and on the right side the filtered solutions (B) are shown; mean values of three measurements are reported ± SD.

Freeze-thaw procedures are reported to cause partial unfolding of proteins leading to aggregation. This can be attributed to low temperature causing cold-denaturation (Privalov 1990), to pH changes due to buffer crystallization (Gomez et al. 2001; Pikal-Cleland and Carpenter 2001), to the exposure of protein molecules to the ice-liquid interface (Krielgaard et al. 1998; Sluzky et al. 1991), to different freezing and thawing rates (Cao et al. 2003) and to the container material, geometry and volume used (Kueltzo et al. 2008). Moreover, a higher protein concentration in aqueous solutions is suspected to increase the rate of aggregation (Zettlmeissl et al. 2002). During freezing, a local increase in protein concentration due to eutectic phase separation is observed which is expected to promote aggregation as well (Heller et al. 1997; Heller et al. 1999). However, it has been observed that increasing the concentration will reduce aggregation during freeze-thawing, due to the reduced fraction of protein molecules which is actually exposed to the ice interface (Treuheit et al. 2002; Zippelius 2002).

In the present study, a higher protein concentration of 90 mg/ml leads to a higher percentage of HMWs during storage compared to the 5 mg/ml solution (Figure IV-8). No changes in secondary structure determined with FT-IR in transmission mode were observed during storage independent of concentration or storage conditions (data not shown). For the storage of unformulated purification intermediates no excipients like sugars (Cleland et al. 2001; Kendrick et al. 1997), polyols, amino acids (Chen et al. 2003) or

surfactants (Chang et al. 1996) were applied which are known to protect the API against chemical and physical instability. Therefore, the most gentle storage condition has to be chosen to prevent especially the formation of soluble HMWs which are hardly removable at the end of the purification process. In this study, the storage at 2-8 °C was observed to be suitable to circumvent the formation of these aggregates in the concentrated protein solutions. However, the formation of larger insoluble aggregates and actually precipitated protein was observed under theses conditions.

3.2 Homogeneous nucleation and growth

Differences in the aggregation behavior due to the 0.2 µm-filtration procedure became obvious by looking concomitantly at the level of small soluble HMWs and the proteinaceous particles detectable by turbidity measurements and LO in the unfiltered and filtered concentrates during storage.

Regarding soluble aggregates, the filtered solutions showed a higher level of HMWs during storage at elevated temperature than the unfiltered ones (Figure IV-7). After 4 weeks at 40 °C all concentrated solutions revealed a level of 3.2-3.5 % HMWs in the filtered solutions and of only 2.0-2.2 % HMWs in the unfiltered solutions, analyzed with SE-HPLC. After 6 weeks at 40 °C, all concentrates generated by different UF methods showed 5-6.2 % HMWs in the filtered solutions and only 3-3.5 % HMWs in the unfiltered solutions.

By comparing concomitantly the level of larger aggregates in the unfiltered and filtered concentrates, all filtered ones showed a significantly reduced turbidity value at 350 nm over 6 weeks at 40 °C (Figure IV-1). Moreover, the level of particles larger 1 µm in the filtered solutions was inherently lower compared to the unfiltered ones during storage at elevated temperature over 6 weeks (Figure IV-2). Only the filtered solutions showed this reduced level of particles larger 1 µm as well as the lower turbidity values during storage, however a higher level of HMWs was obvious which was not recognized in the unfiltered solutions. Figure IV-9 shows the increase of HMWs and the turbidity values with storage time at 40 °C exemplarily for the concentrates derived from the Δp 3 bar method. After 3 weeks, the formation of HMWs is clearly increased when a lower turbidity and thus a lower number of particles of up to 1-2 µm is present in solution (Figure IV-9B).

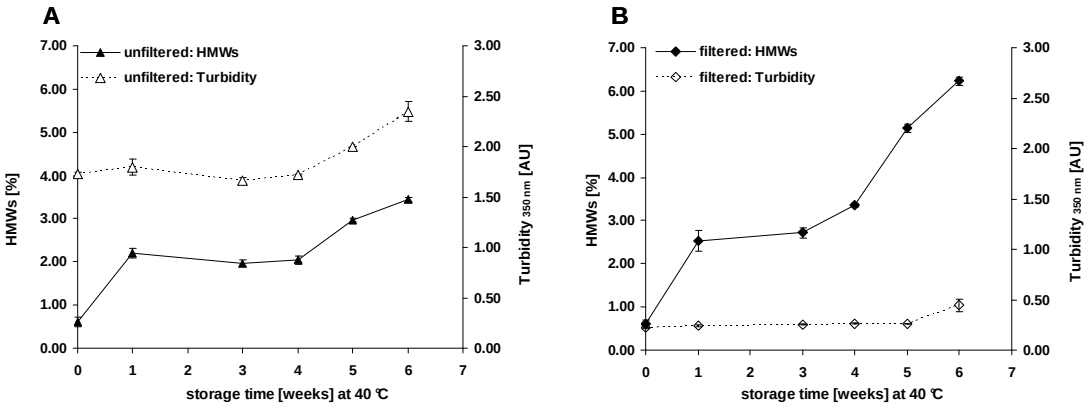

Figure IV-9: Percent HMWs and turbidity values with storage time at 40 °C depending on the filtration status of the concentrated solutions (90 mg/ml)
The data for the unfiltered (A) and filtered (B) concentrates derived from the Δp 3 bar method were taken; the data is a combination of Figure IV-1 and Figure IV-7.

After 6 weeks, the unfiltered solutions with a turbidity value of only 0.5 AU on average showed a significantly increased level of about 6.2 % HMWs compared to the filtered solutions containing only 3.5 % HMWs after 6 weeks.

This aggregation behavior during quiescent storage conditions can be explained by looking at aggregation as a nucleation and growth phenomenon (chapter I, section 3.4). Aggregation is propagated on the basis of the successive formation of larger aggregates from already existing smaller ones. These smaller ones which are called homogeneous nuclei, are reported to be created by spontaneous coalescence and are known to be therefore preferentially formed at a higher total protein concentration or at a higher temperature. After the formation of the nuclei and thus a new stable solid-liquid interface, aggregation is propagated on the basis of these nuclei which are growing into larger aggregates. Successively, much larger particles can be build up until their solubility is exceeded and the protein is precipitating. Conversely, the presence of already existing larger aggregates or particles should prevent the formation of the smaller ones, since a new solid-liquid interface is already build up and a stable species larger than the critical-sized nucleus is already present in solution.

In the here presented study, the formation of soluble aggregates was generally enhanced at a higher protein concentration or at a higher temperature which is in accordance with the presented theory. A filtered and nearly HMW free solution showed an increased level of up to 5-6 % HMWs after 6 weeks stored at elevated temperature as reported

above. In the presence of already existing large aggregates the formation of HMWs, the smallest aggregate species detected, was inhibited.

A quite similar level of HMWs was observed by comparing the unfiltered and the filtered concentrates stored at 2-8 °C (Figure IV-8). The HMW level of all concentrates stepped up from 0.6 % to only 1.0 % over 6 months. Concomitantly, a decrease in turbidity as well as in the number of particles larger 1 µm was recognized in the unfiltered concentrates (Figure IV-4A and Figure IV-5A). Moreover, the formation of visibly precipitated and therefore very large aggregates was recognized by a decrease in percent soluble protein remaining (Figure IV-6). This was more pronounced when the turbidity of the concentrates was already increased and particles larger 1 µm were already present in solution (unfiltered concentrates). Figure IV-10 shows the decrease in turbidity at 350 nm and the percent precipitated protein with storage time at 2-8 °C exemplarily for the concentrates derived from the UF method applying a Δp of 3 bar. The unfiltered solutions show a clear decrease in turbidity and concomitantly a more pronounced increase in precipitated and thus very large and visible aggregates compared to the filtered solutions.

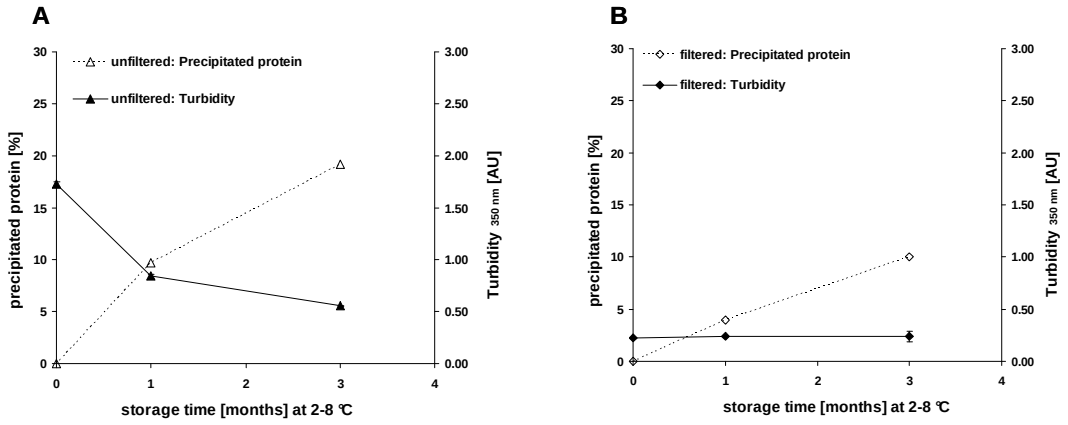

Figure IV-10: Turbidity values and percent precipitated protein with storage time at 2-8 °C depending on the filtration status of the concentrated solutions (90 mg/ml)
The data for the unfiltered (A) and filtered (B) concentrates derived from the Δp 3 bar method were taken; the data is a combination of Figure IV-4 and Figure IV-6.

Here, the formation of very large aggregates which are precipitating during storage is favored when smaller aggregates, detected by turbidity measurements and LO, are already present in solution. This is again in accordance with the already mentioned theory of homogeneous nucleation and growth detailing that the formation of a larger species is based

on the presence of already existing smaller ones. This process is presumably favored and therefore detectable at a lower temperature, since solubility inherently depends on the environmental temperature.

The assumed aggregation process in the concentrated solutions is illustrated schematically:

$$2\,N \leftrightarrow N_2 \qquad \text{(step 1)}$$

$$N_2 \xleftrightarrow{+nN} N_{2+n} \qquad \text{(step 2a)}$$

$$N_2 \xleftrightarrow{+nN_2} N_{2+n} \qquad \text{(step 2b)}$$

$$N_{2+n} \xrightarrow{+nN_x} N_m \qquad \text{(step 3)}$$

Here N refers to a native monomer forming at least a soluble dimer or oligomer N_2 preceding aggregation (step 1). These soluble aggregates detected by SE-HPLC represent the stable critical-sized nuclei. The schema suggests an equilibrium between the monomer and the soluble aggregates which are then forming larger aggregates. The soluble aggregates grow successively into larger ones (N_{2+n}), detected by turbidity measurement and LO, by incorporating further monomeric species N (step 2a) or soluble aggregates N_2 (step 2b). The aggregated species N_{2+n} can further grow into very large visible particles N_m which irreversibly precipitate by incorporating potentially all kinds of aggregates or monomeric molecules N_x (step 3).

To verify that larger aggregates are build up on the basis of already existing smaller ones, DLS analysis was performed to have an additional analytical method in place which is capable to detect aggregates in a size range which was not yet covered by the applied methods. LO is capable to detect particles of 1-200 µm whereas turbidity measurements at 350 nm are mainly suitable to recognize particles of up to 1-2 µm in size (see chapter III). The SE-column is capable for the separation of IgG monomers, dimers and oligomers up to about two-fold in hydrodynamic diameter which corresponds to about eight-fold in molecular weight (Ye 2006). Higher aggregates are usually excluded from the SE-column since the used SE-matrices commonly applied for the analysis of IgGs have a mean pore size of about 250 Å (Dolman and Thorpe 2002). Therefore, DLS in batch mode was used to detect the IgG monomer with a hydrodynamic diameter of about 10 nm (=100 Å) be-

side various aggregated species up to a hydrodynamic diameter of about 1 to 6 µm. In general, DLS is a sensitive method to detect aggregates even in small traces, since the total scattered light intensity is proportional to the size of the scattering particles (Kunitani et al. 1997).

After 6 weeks at 40 °C the DLS data revealed an additional aggregated species at about 100 nm mean hydrodynamic diameter in the unfiltered solutions derived from the Δp 1.2 bar and 3.0 bar method (Figure IV-11A and Figure IV-12A). This species is neither detectable by LO, nor by SE-HPLC.

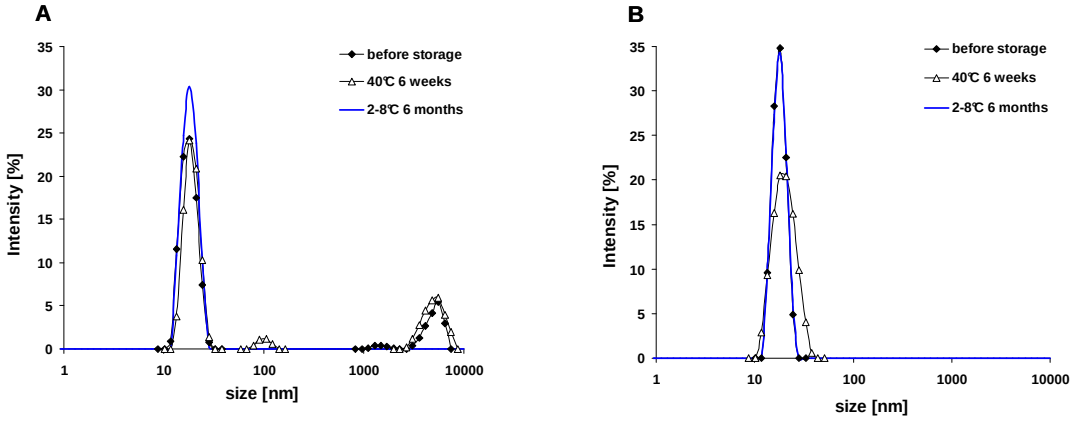

Figure IV-11: DLS size distribution by intensity for the concentrated solutions (90 mg/ml) derived from the Δp 1.2 bar UF method
Unfiltered solutions (A) and filtered solutions (B).

Moreover, the unfiltered concentrates derived from the UF method applying a Δp of 3.0 bar showed an increase in peak intensity of the aggregated species of about 1000 nm hydrodynamic diameter (Figure IV-12A). Both, aggregated species appearing at about 100 nm and 1000 nm in hydrodynamic diameter indicate that larger aggregates are formed over time in the unfiltered solutions at 40 °C. This was recognized by an increase in turbidity of these solutions after 6 weeks at elevated temperature (Figure IV-1A). Interestingly, the concentrates generated by using the optimized UF method did not show the aggregated species at around 100 nm hydrodynamic diameter (data not shown). Moreover, the turbidity of these samples was not increased after 6 weeks (Figure IV-1A).

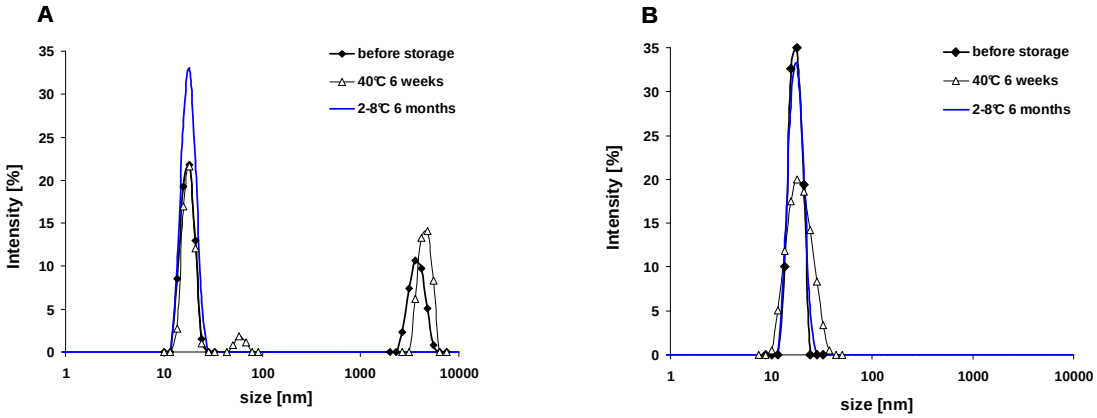

Figure IV-12: DLS size distribution by intensity for the concentrated solutions (90 mg/ml) derived from the Δp 3.0 bar UF method
Unfiltered solutions (A) and filtered solutions (B).

An aggregated species was not observed in the filtered solutions (Figure IV-11B and Figure IV-12B). No additional peak appeared beside the monomer peak during storage. However, the peak referring to the monomer is broadened. This is considered as an indication of the augmented formation of soluble aggregates smaller than an octamer which was already noticed by SE-HPLC (Figure IV-7B). Monomeric molecules and these soluble aggregates can not be resolved by DLS, since two species are only separated into two peaks if their hydrodynamic diameter differs at least by a factor of two (Demeester et al. 2005; Philo 2006).

By looking at the DLS size distribution by intensity of the unfiltered concentrates stored at 2-8 °C over 6 months the aggregate peak at about 1000 nm vanished (Figure IV-11A and Figure IV-12A). Moreover, the size distribution by intensity of the unfiltered concentrates after 6 months at 2-8°C is nearly equal to the filtered ones before storage (Figure IV-11B and Figure IV-12B), where the large aggregates were mechanically removed. This is considered therefore a further indication that much larger aggregates were build up during storage which are no longer detectable by DLS analysis. This formation of much larger visible particles was already recognized due to a decrease in the percent soluble protein remaining as reported before (Figure IV-6).

The filtered solutions do not show any alteration in the size distribution by intensity during storage at 2-8 °C which is consistent with the results obtained from SE-HPLC, since only a slight increase in soluble HMWs was recognized during storage (Figure IV-8B).

In summary it was shown that the level of existing aggregates has influence on the ongoing aggregate formation during quiescent storage of unformulated concentrated IgG solutions. In the presence of larger mainly subvisible aggregates, detected by turbidity measurements and LO, the formation of soluble HMWs was clearly reduced during storage at elevated temperature compared to a filtered bulk which was cleared from proteinaceous particles by 0.2-µm filtration. At 2-8 °C the formation of visible particles precipitating during storage was enhanced when subvisible aggregates were already present in the solution. Concomitantly, no further increase in soluble HMWs was detected, neither for the unfiltered, nor for the filtered solutions. Therefore, the highly concentrated purification intermediates have to be preferentially stored at 2-8 °C after 0.2 µm filtration, since the loss in soluble protein remaining and the formation of soluble HMWs was shown to be reduced.

3.3 Conformational stability

ATR FT-IR temperature ramps are known to be capable to evaluate the thermal stability of proteins. The protein melting temperature (T_m) which is defined as the temperature where equal amounts of native and denatured structure exist in equilibrium can be determined by monitoring the position and intensity of the amide I component frequencies as a function of temperature. In this study T_m was used to investigate if changes in conformational stability occur depending on the operational conditions used in UF, thus influencing aggregation during storage.

MAbs show two characteristic bands in the second derivative spectrum at around 1639 and 1690 cm^{-1} reflecting the presence of intramolecular ß-sheet (Chang et al. 2005; Cleland et al. 2001). Conformational changes are indicated by a reduced band at around 1639 cm^{-1} and a concomitantly arising strong temperature-induced band at 1615-1625 cm^{-1}. Moreover, a weak intensity peak at around 1690 cm^{-1} arises. All these spectral changes are assignable to the formation of intermolecular β-sheets which was fund to be mainly present in aggregated protein molecules (Pelton and McLean 2000). Figure IV-13A-C shows the second derivative spectra of the heated solutions at 90 mg/ml derived from the different UF methods. In the case of the used IgG, the band at 1637 cm^{-1} was found to strongly decrease and the band at 1624 cm^{-1} was found to strongly increase with higher temperature.

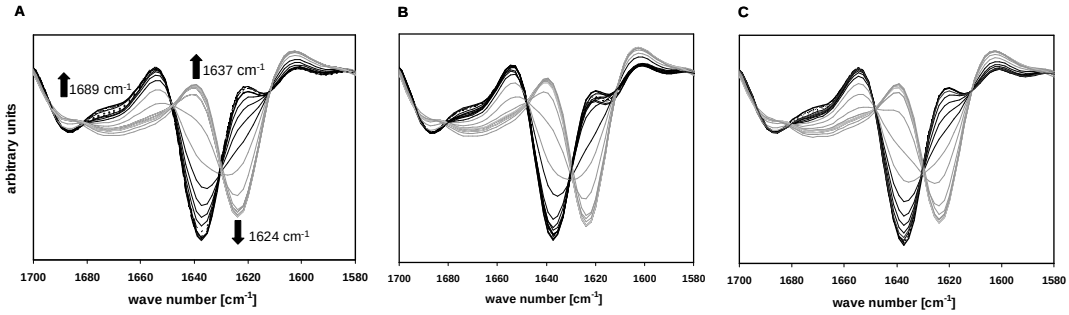

Figure IV-13: ATR FT-IR second derivative spectra of mAb solutions concentrated to 90 mg/ml by using different UF methods
Arrows mark the direction of spectral changes of the bands at 1637 cm^{-1} and 1624 cm^{-1} with increasing temperature from 25 (bolded black line) to 90 °C (bolded grey line); Δp 1.2 bar (A), Δp 3.0 bar (B) and optMeth (C).

Different methods can be in general applied to determine T_m of a protein from the FT-IR spectra. Based on direct plots of the relative intensity values of the decreasing native band and the increasing temperature induced band from the second derivative spectra, the mid-point of the thermal transition can be identified. For this, the inflection point of both curves can be determined which is described by Dong et al. (1997) for Factor XIII and by Kendrick et al. (1998b) for huIFN-γ. In addition, the intersection between the temperature-induced band and the disappearing frequency of the native state can be determined, as reported by Matheus et al. (2006a) for different proteins including an IgG1.

Figure IV-14 shows the changes in intensity in the second derivative spectra for the frequencies at 1637 cm^{-1} and 1624 cm^{-1} with increasing temperature up to 90 °C for the three concentrates generated by using different UF protocols. With increasing temperature a continuous increase in relative intensity of the native amide I band was observed which was accompanied by a continuous decrease in relative intensity at 1624 cm^{-1}. Both curves show a sigmoid shape with a clearly defined inflection point. The inflection point of the curves was calculated by using the Origin software (Origin 7.5 SR5, OriginLab Corporation, Northampton, USA) applying a sigmoid fit according to the Bolzmann equation (Markovic et al. 2007). Table IV-2 summarizes the determined melting temperatures based on the three different interpretation approaches described above.

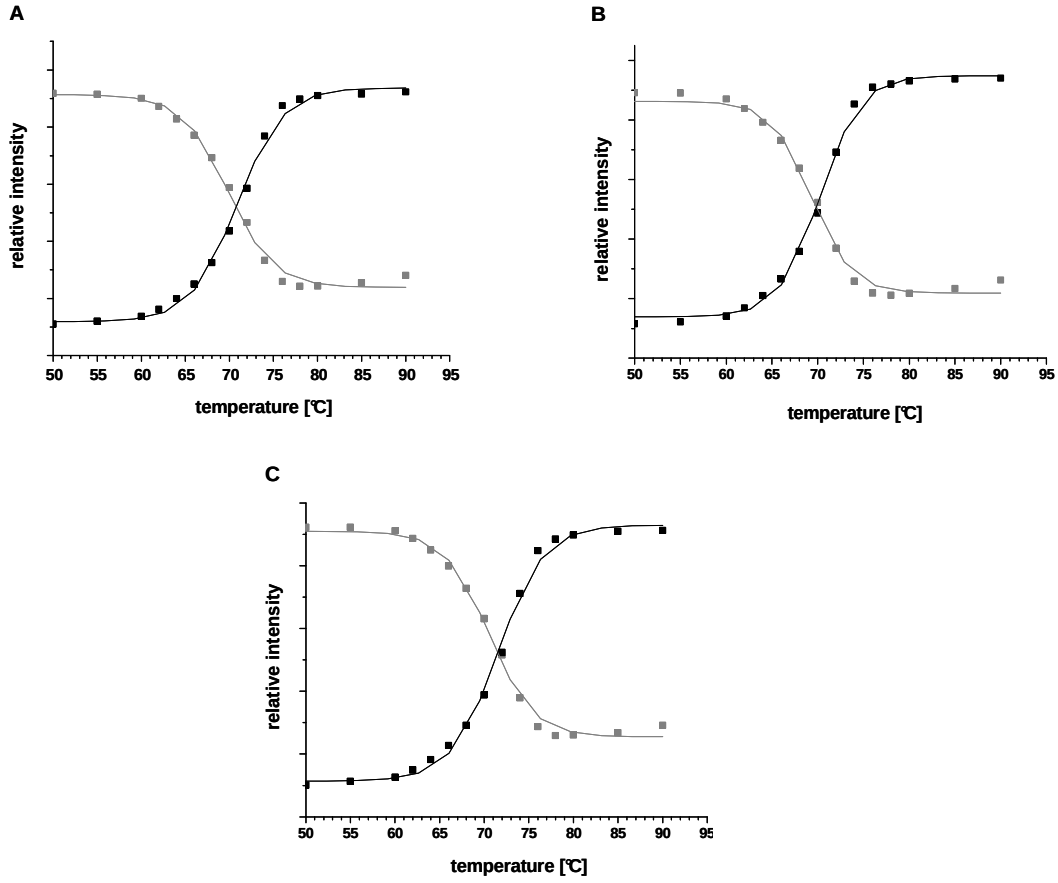

Figure IV-14: Changes in intensity in the ATR FT-IR second derivative spectra at 1637 cm^{-1} (black squares) and 1624 cm^{-1} (grey squares) during heating up to 90 °C of a 90 mg/ml mAb solution concentrated by using different UF methods

Δp 1.2 bar (A), Δp 3.0 bar (B) and optMeth (C); the respective sigmoid fit according to the Bolzmann equation is indicated by the solid line.

A T_m of around 70 °C was observed which correspond to the values for IgGs that have been reported in literature (Matheus et al. 2006a; Matheus et al. 2006b; Vermeer et al. 1998; Vermeer and Norde 2000). Considering the different interpretation approaches to determine T_m, quite similar values were obtained. In general, the values for T_m identified by using the inflection point of the decreasing band are always lower than the values based on the intensities of the increasing frequency. For both approaches, as well as for the interpretation by using the intersection between the denatured and native frequency, consistently higher values for T_m were identified for the concentrates generated by using the optimized UF method.

Method	Protein concentration	T_m (FT-IR) [°C]		
		Inflection point using sigmoid fit (Boltzmann equation)		Intersection between in- and decreasing band
		Increasing band at 1637 cm^{-1}	Decreasing band at 1624 cm^{-1}	
before UF	5 mg/ml	69.2 ± 0.2	69.6 ± 0.2	69.9
Δp 1.2 bar	90 mg/ml	70.9 ± 0.2	69.8 ± 0.2	71.2
Δp 3.0 bar	90 mg/ml	70.2 ± 0.1	69.4 ± 0.2	70.1
optMeth	90 mg/ml	71.5 ± 0.2	70.5 ± 0.2	71.9

Table IV-2: Melting temperature (T_m) for mAb solutions at 90 mg/ml determined from ATR FT-IR second derivative spectra by using three different interpretation approaches
Results of sigmoid fitting are listed with ± 1 standard error of the non-linear regression.

Concomitantly, a consistently higher T_m was recognized for the concentrated solutions at 90 mg/ml compared to the T_m values of the solutions at 5 mg/ml. This suggests that conformational stability regarding secondary structure is affected by the UF method used, but in general, a higher total protein concentration leads to an increase of the melting temperature as well. This is in accordance with current literature reporting that concentrated protein solutions are protected against conformational changes. The rate of denaturation of several proteins exposed to heat and ethanol has been found to be reduced in the presence of significant concentrations of up to 100 mg/ml of other heat stable proteins (Minton 2000; Minton et al. 1982). The addition of dextran at high concentrations stabilizes lysozyme and cytochrome C with respect to thermal denaturation (Sasahara et al. 2003). Matheus and coworkers (2006a) reported that an IgG1 formulation at 100 mg/ml showed nearly no difference in T_m when the pH was changed from 5 up to 8 although aggregation was clearly favored at pH 8.

An explanation is provided by the excluded volume theory arguing that in the presence of highly concentrated macromolecules the unfolding of proteins should be reduced due to facing a crowded or so-called volume-occupied system (Alford et al. 2008a; Hall and Minton 2003; Harn et al. 2007). Due to steric- and charge-based repulsion of the macromolecules, the protein molecules exclude volume to another thus resulting in an increase in free energy. As volume occupancy increases, compact protein conformations of the native state become increasingly energetically favored over extended conformations of

equal volume, present in the denatured state (Minton 1980). Therefore, the native conformation of a protein becomes more stable relative to any less compact denatured state.

It is concluded that the formation of aggregates in highly concentrated solutions is rather controlled by a homogeneous nucleation and growth process than by partially unfolded molecules, since the protein was shown to be in general protected against conformational changes at a higher total protein concentration. This is in accordance with the literature, since nucleation and growth phenomena were mainly recognized when the native conformation of the protein was preserved (see chapter I). The increase in T_m at a high protein concentration of 90 mg/ml did not result in a decreased formation of aggregates during storage below the melting temperature. Quite the contrary was recognized, since aggregation was enhanced with increasing total protein concentration in the solution. The applied UF method seems to significantly affect the conformational stability of the protein, but these results did not correspond to the aggregation behavior during performed stability studies. No significant differences regarding the level of several types of aggregates in the differently processed concentrates were observed during storage below T_m.

4 Summary and conclusion

In this chapter, the physical stability of highly concentrated IgG bulks derived from different UF methods was investigated. The three stage protocol using the optimized operational conditions presented in chapter III showed the lowest level of larger aggregates before and during storage at elevated temperature, at 2-8 °C and after freezing and thawing.

After 0.2 µm-filtration of the concentrates no differences regarding the level of larger subvisible protein aggregates detected by turbidity measurements and LO were observed depending on the UF method used. This was recognized during storage at elevated temperature, at 2-8 °C as well as after freezing and thawing in three cycles. Almost all proteinaceous particles were removed by filtration and did not reappear during storage. Therefore, the improved quality of the bulk derived from the optimized UF method regarding the level of proteinaceous particles is no longer relevant after the filtration of the concentrated bulk.

As regards soluble HMWs, no significant differences between the several unfiltered concentrates were observed neither before, nor after storage. Only after 6 weeks at 40 °C

the filtered concentrates revealed a significantly higher level of HMWs generated by using the Δ 3.0 bar method. In general, during freezing and thawing in three cycles a significantly increased level of HMWs was detected. Both, the filtered and unfiltered solutions at 90 mg/ml showed an increase in HMWs up to three times compared to the solutions at 5 mg/ml. Since the level of HMWs was quite stable at 1 % when the concentrates were stored at 2-8 °C, this is the recommended storage condition for the unformulated highly concentrated bulk material.

The filtered solutions stored at elevated temperature showed a higher level of soluble aggregates compared to the concentrates which remained unfiltered during storage. This was attributed to the already existing larger subvisible aggregates in the unfiltered solutions preventing the formation of the smaller soluble aggregate species in accordance with the theory of homogeneous nucleation and growth.

The secondary structure was found to be affected by the UF methods used. The concentrates generated by using the optimized method showed a consistently higher melting temperature which was evaluated by using three different interpretation approaches based on temperature dependent ATR FT-IR second derivative spectra analysis. Moreover, the highly concentrated protein solutions showed consistently higher T_m values compared to the solutions with a protein concentration of only 5 mg/ml. In contrast, aggregation during storage was in general enhanced at a higher total protein concentration, independent from the UF method used. Thus, aggregation during storage at higher total protein concentrations seems to be rather based on homogeneous nucleation and growth than on a perturbation in secondary structure. The preservation of the native conformation of the protein does not seem to be efficient enough to ensure the physical stability of the concentrated bulk. Physical stability encompasses in fact conformational and colloidal stability and the latter seems to be the more decisive factor regarding the storage stability of the highly concentrated solutions.

Chapter V Thermodynamic non-ideality during UF concentration of mAbs at the interface of DSP and final formulation

Abstract

The purified mAb bulk is generally obtained in a concentration requiring a subsequent UF concentration step prior to formulation especially for the supply of bulk material for highly concentrated mAb preparations up to 200 mg/ml.

It is known for a number of molecules that at high protein concentrations the molarity of the actually free diffusible buffer forming anions and cations changes during diafiltration. This thermodynamic non-ideality is based on electrostatic interactions of the solute and the protein at non isoelectric pH leading to unequal partitioning of charged solutes across the membrane. Due to this so-called Donnan-effect the buffer composition of different IgG solutions was shown to be significantly different before and after the UF concentration step having an impact on pH, conductivity and hence stability of the highly concentrated mAb bulk.

It has been found that by using the Donnan-effect theory the change in concentration of the buffer forming ions can be calculated prior to the UF filtration step, allowing for a "preventive" adjustment of the concentration of the ions in the solution before the UF process starts. The studies show that in the case of histidine a systematic and convenient add-on of this solute was successful in matching the predefined histidine molarities as well as pH of a highly concentrated bulk. Therefore, chemical and physical stability of the concentrated mAbs at 200 mg/ml were improved.

It has further been found that the systematic add-on in the case of histidine provides best results considering the formation of aggregates and particles during the UF concentra-

tion step as well as during storage. In comparison, the level of aggregates was clearly increased when the pH was adjusted closely to the IP of the mAb before starting the UF concentration in order to avoid the thermodynamic non-ideality during processing. Moreover, a reduction in concentration time and a higher permeate flux over time were observed for the solutions using the systematic add-on approach.

Finally, in the case of histidine, an add-on can contribute to a decrease in viscosity of the highly concentrated API bulk.

1 Introduction

After the final polishing step in a mAb purification process, the protein has usually to be diafiltrated into the required formulation buffer. Concomitantly, highly concentrated mAb formulations are favored today to provide both, low volume injections and efficient dosing for subcutaneous administration (Shire et al. 2004). UF is the industry standard for large-scale concentration and diafiltration processing. Since the appropriate formulation buffer ensures sufficient stability during the storage and shelf-life of the mostly liquid concentrates, it needs to be ensured that predefined conditions are present after the UF process. The pH, the conductivity and the concentration of the applied buffer components are known to have influence on the chemical and physical stability of the therapeutic protein (Daugherty and Mrsny 2006; Wang 2005; Wang et al. 2007a).

Concentration and diafiltration by using UF is based on the principle of a semi permeable membrane separating the protein (*P*) from diffusible water and solutes which can be either cationic (Cat^+) or anionic (An^-). In this system diluted solutions have to establish the same product of ion concentration and ion activity respectively on both sides of the membrane, the retentate side (*r*) and the permeate side (*p*) (Equation V-1). Moreover, electroneutrality is postulated having the same concentration of cations on both sides of the membrane (Equation V-2) and concomitantly the same concentration of anionic species on both sides (Equation V-3) (Martin et al. 1980):

$$\left[Cat^+\right]_p\left[An^-\right]_p = \left[Cat^+\right]_r\left[An^-\right]_r \qquad \text{Equation V-1}$$

$$\left[Cat^+\right]_p = \left[An^-\right]_p \qquad \text{Equation V-2}$$

$$\left[Cat^+\right]_r = \left[An^-\right]_r \qquad \text{Equation V-3}$$

By introducing a macromolecular polyion into the system which is retained by the membrane, e.g. a positively charged protein (P^+), this species disturbs the charge equilibrium on the retentate side shown in Equation V-3 (Martin et al. 1980) resulting in:

$$\left[Cat^+\right]_r \left[P^+\right]_r = \left[An^-\right]_r \qquad \text{Equation V-4}$$

To reestablish the equilibrium of charge, positively charged solutes are displaced to the permeate side while negatively charged solutes are accumulated on the retentate side. This is of special importance when the protein concentration increases. This can be underlined when Equation V-2 and Equation V-3 are inserted in Equation V-1 resulting in Equation V-5:

$$\frac{\left[Cat^+\right]_p}{\left[Cat^+\right]_r} = \sqrt{1+\frac{\left[P^+\right]_r}{\left[Cat^+\right]_r}} \qquad \text{Equation V-5}$$

Equation V-5 shows the ratio of the diffusible cationic solute concentrations on the permeate and the retentate side in equilibrium. When the charged protein [P^+] will be concentrated on the retentate side exceeding the solute concentration [Cat^+] by far, the concentration of the positively charged solute [Cat^+] on the permeate side is approximately the $\sqrt{\left[P^+\right]_r}$-fold of the concentration of the positively charged solute [Cat^+] on the retentate side.

This thermodynamic non-ideality results from intermolecular charge-charge based interactions between the macromolecular polyions and those of other macromolecular ions and charged solutes in its vicinity, affecting the partitioning of small solutes across the semi permeable membrane. This is termed the Donnan-effect which was first pointed out by Frederick G. Donnan in 1911 (Donnan 1911; Tanford 1967).

Stoner and coworkers related these facts in 2004 to the process development environment of therapeutic proteins showing that the Donnan-effect has an impact on the outcome of dialysis of Interleukin-1 receptor antagonist (IL-1ra), PEGylated soluble tumor necrosis factor receptor (PEG-sTNF-IR) and Fusion conjugate protein (AMG-719). The concentration of charged solutes encompassing chloride, histidine and acetate was monitored during dialysis of the different proteins at various protein concentrations (Stoner et al. 2004).

In the present study, thermodynamic non-ideality during UF concentration procedure of mAbs was investigated in buffer systems which are frequently applied at the interface of DSP and final formulation. The intention was to gain insight in the characteristics and

relevance of thermodynamic non-ideality during tangential UF processing of IgGs after final purification steps considering especially chemical and physical stability of API bulks. An automated TFF lab-scale system was used which has been shown to adequately reflect process conditions at manufacturing scale (see chapter III).

The pH and the conductivity were monitored during concentration experiments up to 200 mg/ml at a non isoelectric pH of about 5. Further, the concentration of histidine and sodium ions as well as of acetate and chloride ions during the UF concentration process of an IgG1 and an IgG4 were investigated. The characteristics oft the displacement and the accumulation respectively of cationic and anionic solutes during UF experiments was compared to different mathematical models based on protein-solute interaction and volume exclusion.

Based on this data, the extent of the displacement and accumulation of solutes is expected to be predictable before and during UF. This is of special importance for the production of highly concentrated solutions for sub-cutaneous use since the Donnan-effect is per definition pronounced with increasing protein concentrations and a pH further away from the IP of the protein. Following the concept of cGMP, predefined buffer conditions within defined specifications have to be present after a process step which can not be ensured at a high protein concentration as explained above. Thus, compared to processes at low protein concentrations, the buffer conditions have to be corrected afterwards to meet the specifications. This can be potentially relevant for the stability of the concentrated solutions, since it is assumed that the altered buffer composition during UF can affect the stability of the concentrated protein. Moreover, the inconvenient readjustment of pH in the highly concentrated bulks can result in an extreme high or low respectively local pH resulting in chemical or physical instability. Therefore, the stability of the IgG1 during and after UF was investigated for histidine as the buffer solute considering the influence of protein and solute concentration.

It is reported that the composition of the buffer potentially influences the viscosity of highly concentrated protein solutions, depending on type and amount of salts present (Kanai et al. 2008; Liu et al. 2005; Liu and Shire 2002). Thus, the effect of thermodynamic non-ideality of histidine during UF on the viscosity of the concentrated solutions was investigated.

2 Materials and methods

2.1 Materials

A therapeutic mAb solution of a chimeric human Fc (IgG1)/ mouse Fab antibody in 20 mM histidine buffer at pH 5.5 and a concentration of 50 mg/ml were taken for the concentration experiments in histidine buffer (IgG X). To obtain material containing a higher molarity of histidine, histidine base was added to the protein solution and the pH was titrated to 5.5 by using 0.1 M hydrochloric acid. To obtain solutions containing 20 mM and 45 mM acetate pH 5.0 respectively, the 20 mM histidine material was diafiltrated against the 10-fold volume of sodium acetate puffer pH 5.0 by using TFF.

A second therapeutic mAb solution of a chimeric human Fc (IgG4)/ mouse Fab antibody in 20 mM histidine buffer at pH 5.0 and a concentration of 20 mg/ml were taken for the experiments in histidine buffer (IgG Z). To generate material in different buffer system, the protein solution was diafiltrated as described before. Both mAbs were provided by Roche Diagnostics GmbH (Penzberg, Germany).

Before UF processing the solutions were diluted to 10 mg/ml protein concentration by using the suitable buffer and were filtered through a 0.22 μm membrane cartridge (Sartorius, Goettingen, Germany). All chemicals and reagents used were at least analytical grade. Hydrochloric acid, sodium hydroxide and sodium chloride were taken from Merck KG (Darmstadt, Germany). L-histidine from Ajinomoto (Raleigh, USA) was used. Acetic acid was taken from Fluka (Steinheim, Germany).

2.2 Methods

2.2.1 Ultrafiltration concentration procedure

For the preparation of concentrated mAb solutions the automated TFF system ÄKTAcrossflow (GE Healthcare, Uppsala, Sweden) was used (Liten and Cohen 2007). The optimized UF method (optMeth) as described in chapter III was used for all UF experiments up to 200 mg/ml protein concentration. The experiments were conducted by using the equipment and techniques as described in chapter III. After UF the concentrates were filtered at a constant pressure of 1.0 bar through a Sartopore 2 XLG Disposable filter unit

with a pore size of 0.8 and 0.2 µm and a filter area of 58 cm² (Sartorius, Goettingen, Germany). For stability studies, the filtered solutions were stored at 40 °C, 2-8 °C and -70 °C in 5 ml sterile CRYO.S tubes (Greiner Bio-One, Frickenhausen, Germany). The frozen samples were thawed in a 25 °C tempered water bath before analysis.

2.2.2 Concentration determination

The protein concentration was determined in the solutions by using the photometric absorbance at 280 nm and 320 nm after buffer blank subtraction (UV-Vis spectrophotometer Evolution 500, Thermo Fisher Scientific, Waltham, USA). The absorbance at 320 nm was subtracted from the absorbance at 280 nm and this value was used to calculate the protein content according to the law of Lambert-Beer.

2.2.3 Conductivity and pH monitoring

The pH was determined in the retentate by using the Microprocessor pH Meter pH 196 equipped with a pH single-rod measuring cell E50-1.5 from WTW (Weilheim, Germany). The conductivity was determined by using the ProfiLine Konduktumeter LF 197 equipped with a standard conductivity cell TetraCon 325 from WTW (Weilheim, Germany). All samples were tempered in a water bath to 25 °C before measuring pH and conductivity.

2.2.4 Size exclusion high pressure liquid chromatography

SE-HPLC analysis was conducted with a TSK 3000 SWXL column (Tosoh Biosep, Stuttgart, Germany) on a Summit HPLC-system (Dionex, Idstein, Germany). The elution peaks were monitored at 280 nm by the UV diode array detector UVD170U from Dionex (Idstein, Germany). Isocratic chromatography was conducted and evaluated as described in chapter III (see page 52).

2.2.5 Histidine quantification

The samples were diluted to about 100 µM histidine concentration with purified water (Milli-Q, Millipore, Billerica, USA). Afterwards, 500 µl diluted sample was mixed with 500 µl perchloric acid (5 %) (Fluka, Steinheim, Germany). After 10 min the sample was centrifuged at 25 °C with 13 000 rpm for 10 min (miniSpin, Eppendorf, Hamburg, Germany). 100 µl of the supernatant were injected on a MonoS 5/ 50 GL column (GE

Healthcare, Uppsala, Sweden). The CEX-chromatography was conducted on a Ultimate 3000 HPLC-system (Dionex, Idstein, Germany) at room temperature using a gradient elution applying two aqueous buffers composed of 50 mM acetate, pH 3.2 (buffer A) and 50 mM acetate, pH 3.2, 1 M sodium chloride (buffer B). A flow-rate of 1.0 ml/min was applied. Elution was monitored at 210 nm. At pH 3.2, histidine is greatly retained on the CEX resin due to its overall positive charge. Elution is achieved during the sodium chloride gradient due to charge shielding. The chromatograms were integrated manually by using the Chromeleon software (Dionex, Idstein, Germany). Figure V-1 shows a chromatogram exemplarily. To quantify the amount of histidine, the area (mAU ·min) of the defined peak was compared to a standard curve (r^2 = 0.9998).

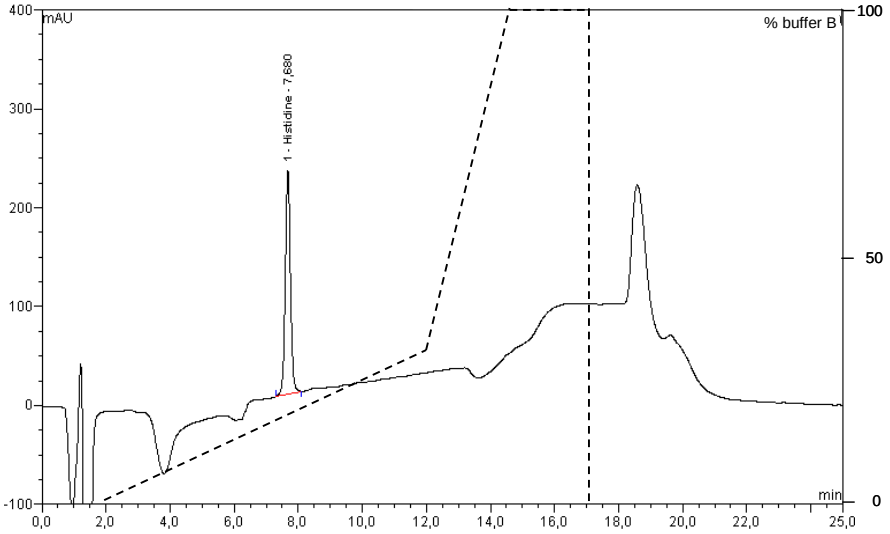

Figure V-1: CEX chromatogram of the histidine quantification method
UV signal at 210 nm (black line, left scale) and percentage of buffer B of the elution gradient (dotted black line, right scale) during chromatography.

2.2.6 Acetate quantification

The samples were diluted to about 25 mM acetate concentration with purified water (Milli-Q, Millipore, Billerica, USA). Afterwards, 500 µl diluted sample was mixed with 500 µl perchloric acid (5 %) (Fluka, Steinheim, Germany). After 10 min the sample was centrifuged at 25 °C with 13 000 rpm for 10 min (miniSpin, Eppendorf, Hamburg, Germany). 100 µl of the supernatant were injected to a LiChrosorb RP C18 4/ 250 column (Merck KG, Darmstadt, Germany). Chromatographic runs were conducted on a Ultimate 3000

HPLC-system (Dionex, Idstein, Germany) at room temperature using an isocratic elution over 15 min applying an aqueous buffer composed of 6 mM phosphoric acid (Fluka, Steinheim, Germany), pH 3 (Kordis-Krapez et al. 2001). Acetate as acidic acid is greatly retained on the C18 RP resin at the very low pH in the presence of perchloric acid. During elution with the aqueous phosphoric acid at pH 3, the acetic acid is partially deprotonated and thus removed from the column. After each sample run the column was washed with 3 ml acetonitrile (Merck KG, Darmstadt, Germany) to avoid sample carryover. A flow-rate of 1.0 ml/min was applied. Elution was monitored at 210 nm. The chromatograms were integrated manually by using the Chromeleon software (Dionex, Idstein, Germany). Figure V-2 shows a chromatogram exemplarily.

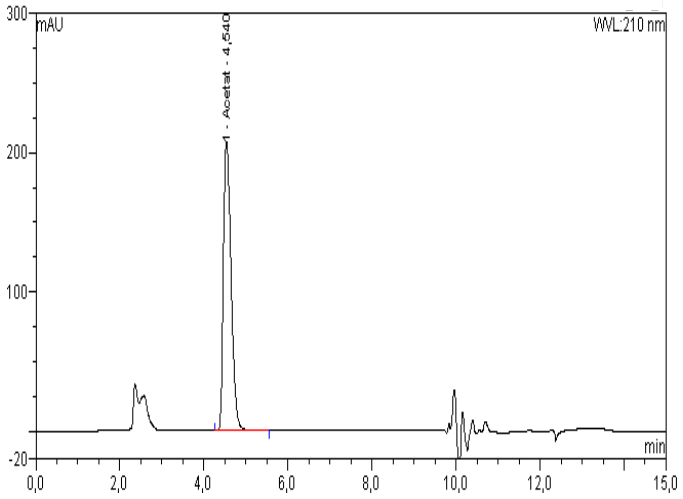

Figure V-2: Reversed phase chromatogram of the acetate quantification method
UV signal at 210 nm.

To quantify the amount of acetate the area (mAU·min) of the defined peak was compared to a standard curve ($r^2 = 0.9999$).

2.2.7 Chloride quantification

The samples were diluted 1:200 with purified water (Milli-Q, Millipore, Billerica, USA). 10 µl of the diluted sample was injected on an IonPac AS11-HC 2/250 column (Merck KG, Darmstadt, Germany). AEX-chromatography was conducted on an ICS 3000 Re-agent-Free Ion Chromatography system (Dionex, Idstein, Germany) at room temperature using a gradient elution over 30 min applying an aqueous solution up to 100 mM sodium

hydroxide. A flow-rate of 0.38 ml/min was applied. Detection was carried out on an ICS 3000 CD conductivity detector. The chromatograms were integrated manually by using the Chromeleon software (Dionex, Idstein, Germany). Figure V-3 shows a chromatogram exemplarily. To quantify the amount of chloride the area (mAU·min) of the defined peak was compared to a standard curve ($r^2 = 0.9963$).

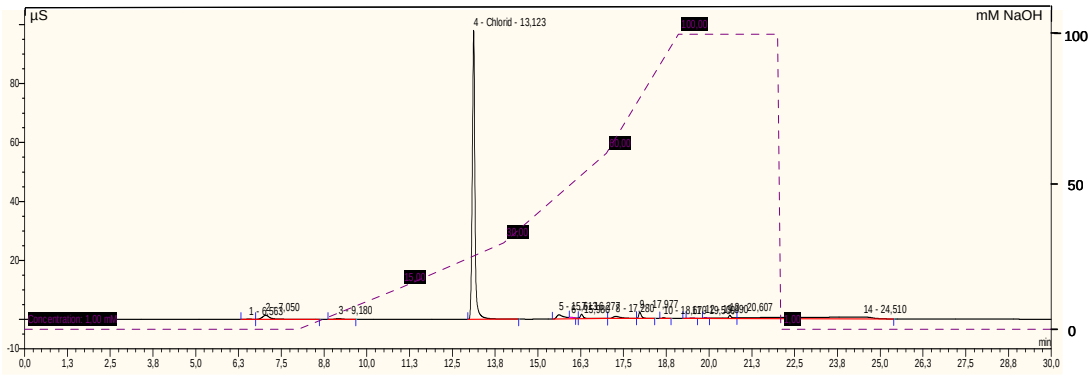

Figure V-3: AEX chromatogram of the chloride quantification method
Conductivity signal (black line, left scale) and concentration of NaOH [mM] in the elution gradient (black dotted line, right scale) during chromatography.

2.2.8 Sodium quantification

To quantify the amount of sodium ions, the samples were analyzed with the multi-sensor system BioProfile 100 plus (NOVA Biomedical, Waltham, USA). The method is based on potentiometry. The activity of the ions determines the voltage of the electrode. Sodium ions were quantified using a glass electrode at 25 °C after a two point calibration. Samples were diluted 1:1 with purified water (Milli-Q, Millipore, Billerica, USA) before measuring.

2.2.9 Turbidity measurement

Turbidity was determined as photometric absorbance of the undiluted concentrates at 350 nm after buffer-blank subtraction (UV-Vis spectrophotometer Evolution 500, Thermo Fisher Scientific, Waltham, USA). The samples were mixed before measuring in order to avoid a decrease in absorbance due to the settlement of large particles.

2.2.10 Light obscuration

LO was used to monitor the formation of particles in a range of 1-200 µm similar to the method <788> Particulate Matter of Injection in the United States Pharmacopoeia and the European Pharmacopoeia method 2.9.1 (EDQM 2001a; USPC 2002). The measurements were conducted using the particle counter SVSS-C (PAMAS Partikelmess- und Analysesysteme, Rutesheim, Germany) as described in chapter III and IV.

2.2.11 Isoelectric focusing

For isoelectric focusing (IEF) Servalyt Blank Precotes (125 mm x 125 mm x 300 µm) from Serva (Heidelberg, Germany) were used for horizontal flat bed electrophoresis. The blank ready to use gels were incubated for 45 min in Servalyt 3-10 buffer (Serva, Heidelberg, Germany) containing 2 % CHAPS and urea. Afterwards, the gels were dried in air for 20 min. The protein solutions were diluted to 1 mg/ml by using the appropriate bulk buffer. The amount of mAb per well was 6 µg per sample. As running buffer Servalyt 3-10 buffer was used. The IEF-markers 3-10 from Serva (Heidelberg, Germany) were used. Electrophoresis was performed at 500-2000 V over 2.5 hours. After fixation in 20 % trichloroacetic acid (Fluka, Steinheim, Germany) the washed gels were stained with Serva Blue W Coomassie dye (Serva, Heidelberg, Germany).

2.2.12 Papain ion exchange high pressure liquid chromatography

To quantify the extent of deamidated Fab fragments of IgG X analytical IEX chromatography after papain digestion was performed (papain IEX-HPLC). The samples were diluted to 1.0 mg/ml protein concentration containing 0.01 mg/ml papain (Roche Daignostics, Penzberg, Germany). Samples were incubated at 37 °C for 2 hours. Afterwards, 1 ml of the sample was applied to a sephadex G-25M PD-10 column (GE Healthcare, Uppsala, Sweden) and the buffer system was changed to 20 mM histidine, pH 5.5. 150 µl of the sample were loaded to a MonoS 5/50 GL column (GE Healthcare, Uppsala, Sweden). Chromatographic runs were conducted on a Ultimate 3000 HPLC-system (Dionex, Idstein, Germany) using a gradient elution over 45 min by applying an aqueous buffer composed of 50 mM 3-(N-morpholino) propanesulfonic acid (AppliChem, Darmstadt, Germany), pH 6.5 (buffer A) and a buffer composed of 50 mM 3-(N-morpholino) propanesulfonic acid and 1 M sodium acetate (Riedel-de-Haen, Seelze, Germany), pH 6.8

(buffer B). A flow-rate of 1.0 ml/min was applied. UV detection was carried out at 280 nm. The chromatograms were integrated manually by using the Chromeleon software (Dionex, Idstein, Germany). Peak characterization was performed on the basis of ESI-MS. This IgG1 is untypically complexly glycosylated in the antigen-binding region. Deamidated complex glycosylated Fab fragments with two and one N-acetyl-neuraminic acids (gFab_d_2SA and gFab_d_1SA) as well as deamidated non-glycosylated Fab fragments (Fab_d) were separated from the Fc-fragment and several glycosylated and non-glycosylated Fab fragments (gFab_2SA, gFab_1SA, gFab_0SA, gFab_hM, Fab). To quantify the overall extent of deamidated Fab-fragments the relative area (mAU·min) of the gFab_d_2SA-, the gFab_d_1SA- and the Fab_d peak referred to total area of all detected peaks in percent were summarized and presented as ∑Fab fragments_d [%]. Figure V-4 shows the IEX chromatogram exemplarily.

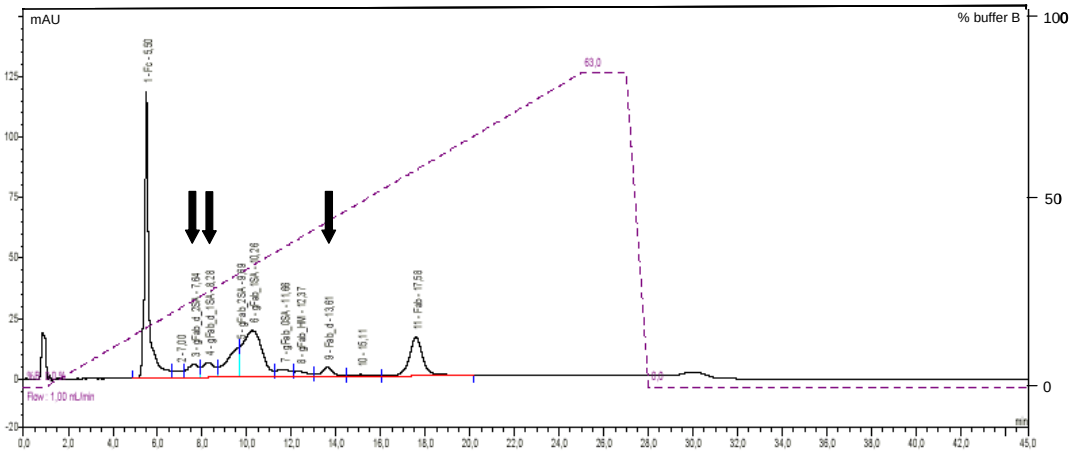

Figure V-4: IEX chromatogram of digested IgG X
UV signal at 280 nm (black line, left scale) and percentage of buffer B of the elution gradient (dotted black line, right scale) during chromatography. The species referring to ∑Fab fragments_d are arrow marked encompassing gFab_d_2SA, gFab_d_1SA and d_Fab (from left to right).

2.2.13 FT-IR spectroscopy

FT-IR spectra were recorded with the Tensor 27 (Bruker Optics, Ettlingen, Germany) applying the BioATR unit with a Silicium crystal. For each spectrum which was recorded from 850-4000 cm^{-1} a 120-scan interferogram was collected at a double sided acquisition mode with a resolution of 4 cm^{-1}. To monitor temperature induced conformational changes in secondary structure of the mAb, spectral changes were followed from 25-90 °C

at 90 mg/ml. 25 µl of the sample solution were applied into the unit and a temperature ramp from 25-60 °C and from 80-90 °C with a ΔT of 5 °C and from 60-80 °C with a ΔT of 2 °C was performed. The equilibrium time was 120 s at each temperature step. The respective temperature was adjusted by connecting the ATR cell to a thermostat (Haake DC30-K20, Thermo Scientific, Waltham, USA). To obtain the reference spectra of the buffer system used, the permeate of the UF concentration procedure was taken and the temperature ramps were performed as described before. The obtained buffer spectra were then subtracted to obtain the protein spectra.

The spectra were edited by a vector normalization. Afterwards, a second-derivative procedure was done to enhance the resolution, concomitantly preserving the band position (Pelton and McLean 2000). The second derivative was smoothed using a 13-point Savitsky-Golay smoothing function. For this, the OPUS software version 6.0 was used (Bruker Optics, Ettlingen, Germany).

2.2.14 Second derivative UV spectroscopy

Tertiary structure of the protein was examined by second derivative UV spectroscopy (2D-UV) using the Uvikon XL (Goebel Elektro, Ludwigshafen, Germany). The samples were diluted to a protein concentration of 1.0 mg/ml. Absorbance spectra from the near-UV region between 250-320 nm were collected at a scanning speed of 50 nm/min, a bandwidth of 1 nm and a scanning step interval of 0.5 nm. A second-derivative procedure was done to enhance the resolution, concomitantly preserving the band position (Pelton and McLean 2000). Therefore, the OPUS software was used (Bruker Optics, Ettlingen, Germany). The second derivative was smoothed applying a 13-point Savitsky-Golay smoothing function.

2.2.15 Viscosity measurement

To determine the viscosity of the concentrated mAb solutions the SV-10 vibro viscometer (AND, Tokyo, Japan) was used. Two gold-covered thin sensor plates are driven with electromagnetic force at the same frequency vibrating at constant sine-wave in reverse phase. The electromagnetic drive controls the vibration of the sensor plates to keep them in constant amplitude. The driving electric current which is the exciting force, will be detected as the magnitude of viscidity produced between the sensor plates and the sample fluid. The system was calibrated using water and praffinum liquidum in a two-point calibration.

Temperature was kept constant at 20 °C by using the water jacket AX-SV-37 (AND, Tokyo, Japan) which was connected to a Haake DC10 thermostat (Thermo Scientific, Waltham, USA). Measurements were carried out three times over 10 min using 10 ml sample solution. Every 30 s the viscosity was measured and results were calculated as mean value of three measurements.

2.2.16 Zeta potential measurement

To determine the charge of the protein at different pHs, electrophoretic mobility of the protein was determined by performing Laser-Doppler-Velocimetry using the Malvern Zetasizer Nano S (Malvern Instruments, Worcestershire, UK). The zeta potential ζ was calculated from the Henry's equation (Equation V-6) with assumption of uniform charge distribution (Henry 1931) by using the Malvern DTS software (Version 5.0, Malvern Instruments, Worcestershire, UK):

$$\mu_e = \frac{2\varepsilon k \xi}{3\eta} \qquad \text{Equation V-6}$$

Where μ_e is the electrophoretic mobility, ε is the dielectric constant of the solution, k_s is the model based constant with a value of 1.5 for a salt concentration higher than 1 mM (Faude et al. 2007), η is the viscosity of the solution and ζ is the zeta potential. For sample preparation the 5 mg/ml mAb solutions were dialyzed into 10 mM acetate buffer pH 5.0 and titrated to a pH of 2.0 afterwards by using 0.2 M hydrochloric acid. The samples were titrated with a 0.2 M sodium hydroxide solution from pH 2 to pH 12 by applying the titrator MPT2 (Malvern Instruments, Worcestershire, UK). The zeta potential was determined in 15 steps between pH 2 and 12 in a temperature controlled folded capillary cell (Malvern Instruments, Worcestershire, UK) at 25 °C.

2.2.17 Density determination

The density ϱ of the protein solutions was determined at every protein concentration. A pycnometer (Schott, Mainz, Germany) with a volume of 2.076 ml was filled with the sample solution previously tempered to 20 °C. The mass of the unfilled and filled pycnometer was determined by using an analytical balance (MC 210 S, Sartorius, Goettingen, Germany). The density was calculated according to the commonly known equation $\varrho = m/V$.

3 Results and discussion

3.1 Protein – solute interactions at the interface of mAb purification and final formulation

Mostly, IEX chromatography in product flow-through mode is the last chromatographic step in commercial purification processes of mAbs to remove mainly residual host cell DNA, endotoxins and retrovirus-like particles (see chapter I). Hence, the purified IEX pool is present in a phosphate or tris(hydroxymethyl)-aminomethan based buffer system at a concentration of approximately 10-20 mg/ml. Subsequently, the environmental conditions have to be changed to a buffer system ensuring stability during storage of the API during storage. Mostly, the pH has to be slightly acidic between 5 and 6 and a conductivity < 5 mS/cm is required (Daugherty and Mrsny 2006). Concomitantly, this buffer system is the basis buffer for formulation by using usually different stock solutions of excipients like surfactants and sugars to ensure a long shelf life. Therefore, the IEX pool is usually concentrated and diafiltrated into a suitable formulation buffer composition by applying UF to provide a defined composition of protein, buffer solutes, pH and conductivity.

3.1.1 Conductivity and pH shifts during UF

An IEX pool of IgG X was diafiltrated against 20 mM histidine buffer (pH 5.5; 1.6 mS/cm) applying a 1 to 10-fold diafiltration volume (DV) referred to the pool volume. Afterwards, the diafiltrated pool was concentrated up to 215 mg/ml. It was recognized that even after applying a 10-fold diafiltration volume the predefined conditions for the histidine buffer system concerning pH and conductivity were not stable after the concentration process had been started. Figure V-5 shows conductivity and pH during diafiltration and concentration of the IEX pool.

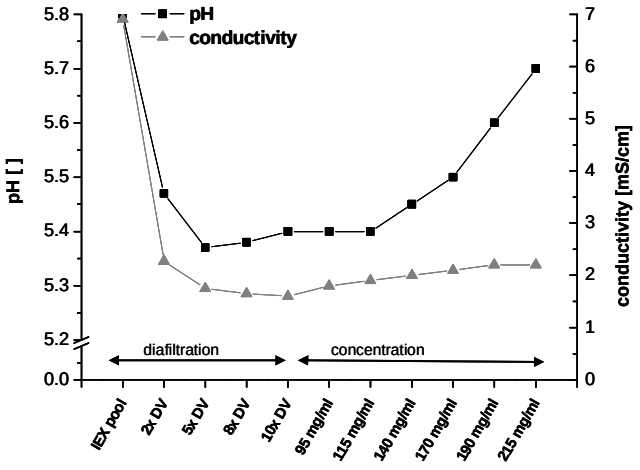

Figure V-5: Conductivity and pH during UF diafiltration and concentration of an IEX pool of IgG X
The IEX pool was diafiltrated applying a 1- to 10-fold diafiltration volume (DV) referred to the pool volume and afterwards concentrated up to 215 mg/ml.

After starting the concentration process the pH increases up to 5.7 and conductivity reaches 2.2 mS/cm at a protein concentration of 215 mg/ml in the retentate. Moreover, conductivity and pH were monitored solely during the UF concentration process of IgG X in 20 mM histidine buffer at pH 5.5 (Figure V-6).

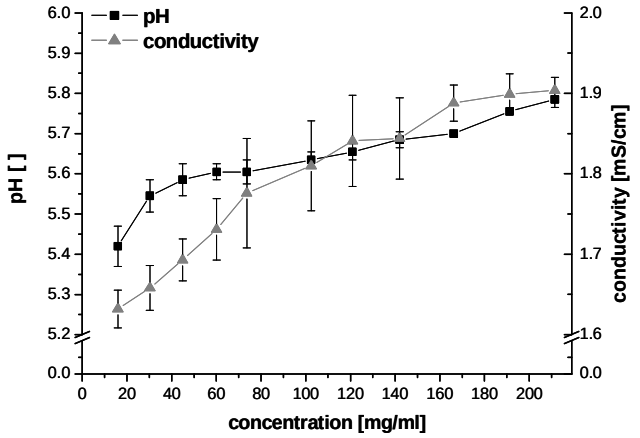

Figure V-6: Conductivity and pH during UF concentration of IgG X from 10 mg/ml to about 200 mg/ml protein concentration
In 20 mM histidine at pH 5.5; mean values of three measurements are reported ± SD.

With increased protein concentration an increase in conductivity and an increase in pH up to 5.8 were observed. Different observations were made considering the conductivity during UF concentration processes, if a second buffer system based on 20 mM acetate at pH 5 was used (Figure V-7A).

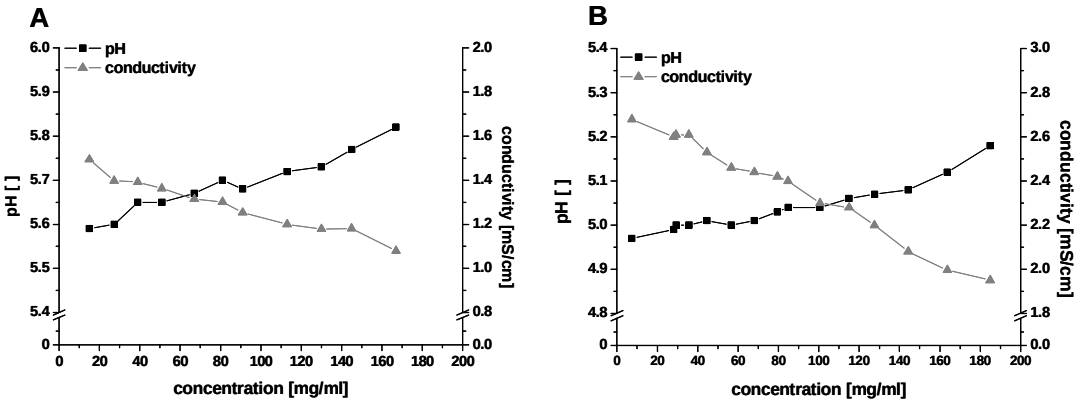

Figure V-7: Conductivity and pH during UF concentration from 10 mg/ml to about 200 mg/ml protein concentration
IgG X in 20 mM acetate at pH 5.5 (A) and in 45 mM acetate at pH 5.0.

During the UF process of IgG X in 20 mM acetate buffer, the pH increased up to 5.8 but the conductivity decreased with increasing protein concentration. At a higher acetate concentration of 45 mM at pH 5.0, essentially the same was obvious as for the 20 mM acetate solution referring to the trend of pH and conductivity during the concentration procedure (Figure V-7B).

It was actually expected that conductivity increases generally with protein concentration at a pH unequal to the IP of the protein (Figure V-6) due to higher charge density per volume in the concentrated solutions (Atchley and Nichols 1925). Since the presented conductivity trends during UF could not be solely attributed to the protein concentration, it was concluded that changes in the buffer system play a role in pH and conductivity shifts during UF. At the pH of about 5, histidine as a buffering agent is mainly positively charged since the imidazole side chain has a pK_a of 6.0 (Kuester and Thiel 2002). By comparison, acetic acid molecules with a pK_a of the carboxylic group of 4.7 (Kuester and Thiel 2002) exhibit dominantly a negative charge. Considering the Donnan-effect, positively charged protonated histidine ions should be displaced during UF since the IgG X is expected to appear mainly positively charged at a pH of 5. An IP > 9.5 was determined by

IEF of the IgG X (Figure V-8). As a consequence, the pH on the retentate side increases due to a loss of protons.

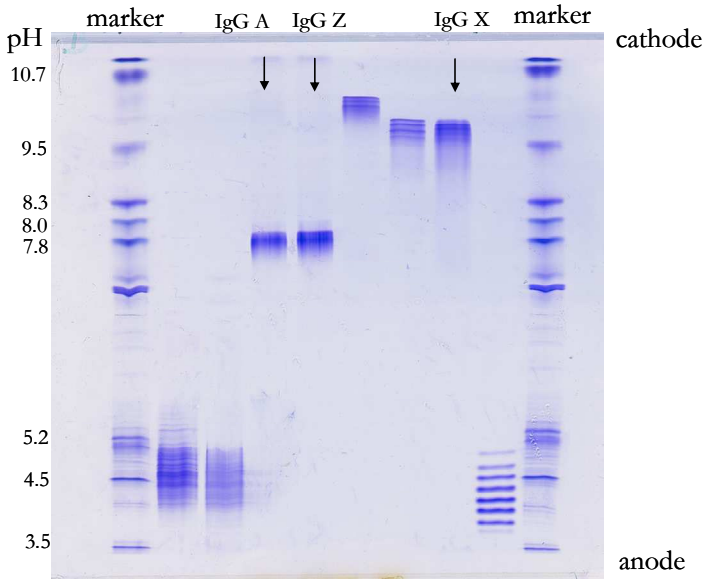

Figure V-8: IEF-gel image of different IgGs by using an immobilized pH gradient

Acetate ions should accumulate during UF at a pH of 5 referring to the Donnan-effect, since the cationic protein molecules interact with the anionic buffer species based on charge-charge interactions. Concomitantly, hydroxonium ions will be displaced to the permeate. Therefore, a decrease in conductivity and an increase in pH on the retentate side were observed during UF in an acetate buffered system at pH 5 (Figure V-7).

Conductivity and pH were expected to remain stable if UF experiments are conducted at a pH more closely to the IP of the protein. Figure V-9 shows that the conductivity of 1.8 mS/cm and the pH of 7.4 were not affected during UF processing up to 200 mg/ml protein concentration by using a buffer system containing 20 mM histidine at pH 7.4. At this pH the IgG carries positive as well as negative charge to nearly the same extent and the imidazole side chain of the histidine molecule is mainly unprotonated. Therefore, conductivity does not increase with a higher protein concentration during UF. Moreover, diffusible buffer ions do not accumulate in the retentate or are not displaced to the permeate to ensure electroneutrality on both sides of the membrane (Equation V-1 to V-3).

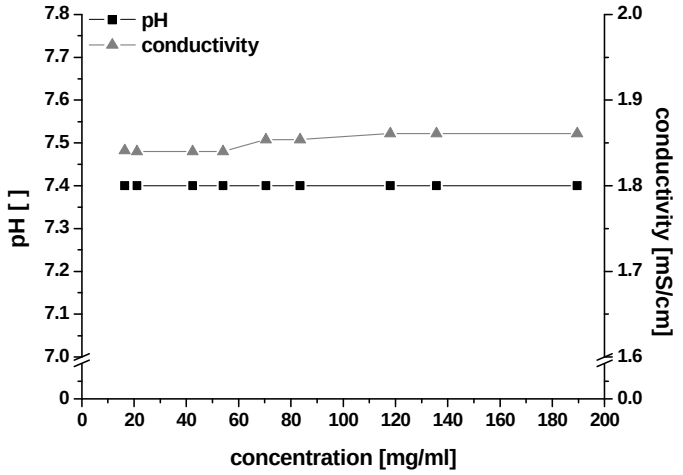

Figure V-9: Conductivity and pH during UF concentration of IgG X from 10 mg/ml to about 200 mg/ml protein concentration
UF was conducted in 20 mM histidine at pH 7.4.

3.1.2 Solute accumulation and displacement during UF

Molar concentration of the buffer solutes was determined to gain further insight into the root causes of pH and conductivity changes on the retentate side during UF (Figure V-10).

For a buffer system containing 20 mM histidine at pH 5.5 a steady decrease in histidine concentration was observed with increasing protein concentration. At a protein concentration > 200 mg/ml the histidine concentration decreased to < 10 mM.

If the pH was increased to 7.4, the loss of histidine during UF processing was reduced as expected. The mAb exhibits positive charge to a lesser extent than at a lower pH and histidine remains as an externally uncharged zwitterion at the pH above 6.0. Therefore, at a protein concentration of around 200 mg/ml the histidine concentration was nearly unaltered, decreasing only slightly from 19.2 ± 1.6 mM to 17.2 ± 0.21 mM histidine since the protein and the histidine molecule exhibit residual positive charge. Compared to the results of a histidine buffer system at pH 5 (Figure V-6) and pH 7.4 (Figure V-9) it is obvious that the pH increases only if protonated histidine is lost with increasing protein concentration during UF.

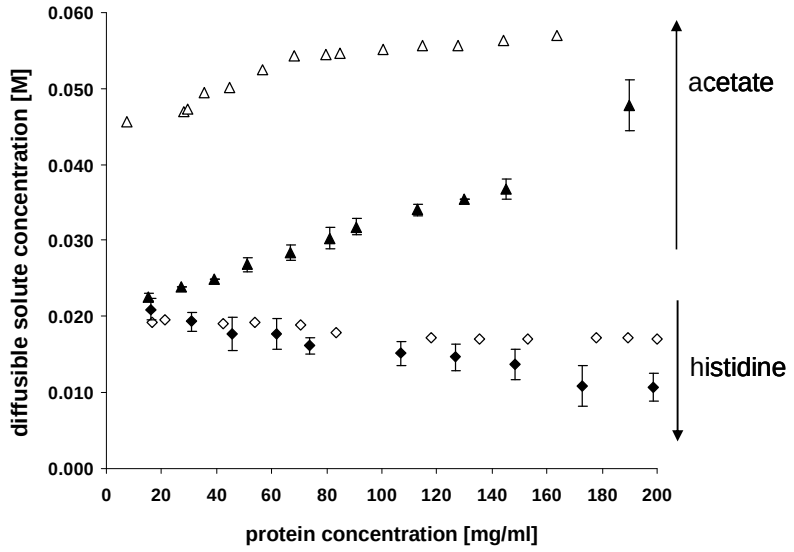

Figure V-10: Molar concentration of the diffusible solutes in the retentate during UF up to about 200 mg/ml IgG X concentration
The buffers were based on 20 mM histidine at pH 5.5 (black diamonds), 20 mM histidine at pH 7.4 (plain diamonds), 20 mM acetate at pH 5.5 (black triangles) and 45 mM acetate at pH 5.0 (plain triangles); experimental data is presented as mean values of three measurements ± SD.

When a 20 mM acetate based buffer at pH 5.5 was used, acetate was accumulated in the retentate during UF operations as expected by the Donnan-effect. Compared to the acetate molarity present in the solution before UF, the concentrated mAb at about 190 mg/ml showed an about 2-fold higher molarity of acetate. Therefore, conductivity decreased with increasing acetate molarity on the retentate side due to the accumulation of oppositely charged species which was shown for two different concentrations of acetate (Figure V-7).

The described results fit into the explanations presented above considering the pH and the conductivity characteristics during UF concentration processing using an acetate or histidine buffered system. During the UF concentration process of the mAb in two defined buffer systems ensuring stability of the API, a significant accumulation in the case of acetate, and a significant loss in the case of histidine was observed. The concentration of acetate nearly doubled and the concentration of histidine was reduced by half at a protein concentration of about 200 mg/ml. Both induced changes in conductivity and pH during the concentration process. Figure V-11 summarizes the effects.

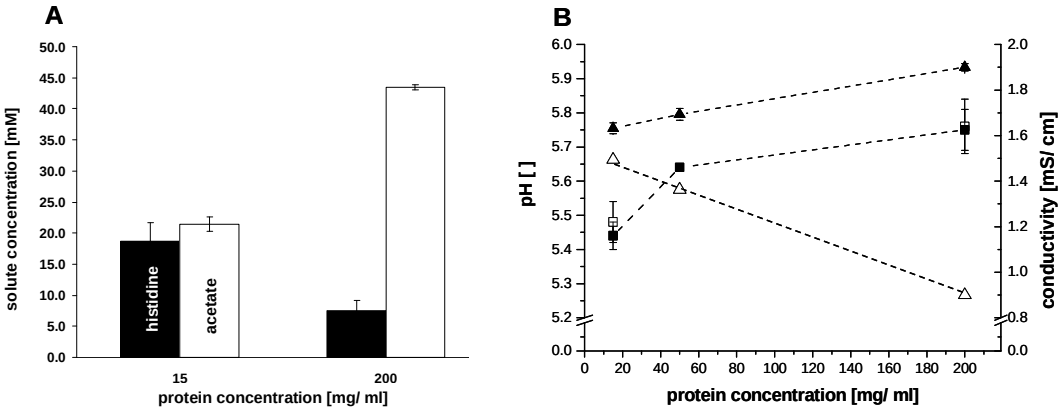

Figure V-11: Loss of histidine and accumulation of acetate during UF of IgG X
Molar concentration of histidine (black bars) and acetate (white bars) at 15 mg/ml and 200 mg/ml protein concentration (A); pH (squares) and conductivity (triangles) of solutions containing 20 mM histidine (black symbols) or 20 mM acetate (plain symbols) before the UF concentration starts (B); experimental data is presented as mean values of three measurements ± SD.

3.1.3 Protein-solute interactions during UF: The Donnan-model

The Donnan-equation describes the partitioning of the completely diffusible ion component of a totally dissociated electrolyte over the semi permeable membrane (Tanford 1967). Therefore, the solute concentration in the retentate was determined during UF experiments and compared to the theoretical values calculated by using the following Equations taken from Tanford (1967):

$$S^{+} = \frac{-zP + \sqrt{(zP)^2 + 4\left(\frac{S'}{\rho'}\left(\rho - \frac{P M_P}{1000}\right)\right)^2}}{2} \qquad \text{Equation V-7}$$

Equation V-7 describes the molar concentration in the retentate of positively charged solutes (S^+) being able to pass through the membrane. S^+ depends on the charge of the protein (z), the molar concentration (P) and the molecular weight (M_p) of the protein as well as on the density of the solution in the retentate (ϱ) and the permeate (ϱ'). S' is the theoretical molar concentration of the diffusible solute. Equation V-8 describes the molar concentration in the retentate of negatively charged solutes (S^-) being able to pass through the membrane.

$$S^{-} = \frac{z\,P + \sqrt{(z\,P)^2 + 4\left(\frac{S'}{\rho'}\left(\rho - \frac{P\,M_P}{1000}\right)\right)^2}}{2} \qquad \text{Equation V-8}$$

During the UF concentration process of IgG X in different buffer systems at pH 5.5, the concentration of positively and negatively charged buffer ions was determined. Since the protein is mainly positively charged at this pH, two cationic and two anionic solutes were used to characterize the displacement and the accumulation respectively in the retentate. Acetate and histidine at 20 mM were chosen as well as a buffer system containing sodium chloride. Sodium chloride was used since this salt is fully dissociated in aqueous solutions, providing cationic and anionic species independent of pH.

To test in particular the influence of the specific charge on the residual solute concentration, an alternative form of Equation V-7 and V-8 was used (Tanford 1967):

$$S = \frac{S'}{\rho'}\left(\rho - \frac{P\,M_P}{1000}\right) \qquad \text{Equation V-9}$$

Here, protein and solute charge (z) were set to zero. The molar concentration of the solute (S) in the retentate being able to pass through the membrane depends only on the density of the retentate (ρ) and the permeate (ρ') as well as on the molar concentration of the protein and the solute.

Moreover, experimental values were compared to a volume exclusion model assuming that the protein molecules occupy a significant volume in solution at high concentrations. During UF concentration the volume being available in the retentate is reduced for small solutes and solvents leading to unequal partitioning of small solutes on both sides of the semi permeable membrane (Stoner et al. 2004; Tanford 1967):

$$S = S'(1 - P\upsilon_p) \qquad \text{Equation V-10}$$

In this case the molar concentration of the solute (S) in the retentate is a linear function of the protein concentration (P), the molar concentration of the diffusible solute in the permeate (S') and the protein partial specific volume (υ_p). A value of 0.75 ml/g was used as protein partial specific volume, since mostly values between 0.7 and 0.8 ml/g are reported for different proteins including IgGs (Kratky et al. 1973; Lee and Timasheff 1974).

Figure V-12 shows the theoretical and experimental results of the molar concentration of histidine, sodium, acetate and chloride in the retentate during UF up to 200 mg/ml IgG X concentration.

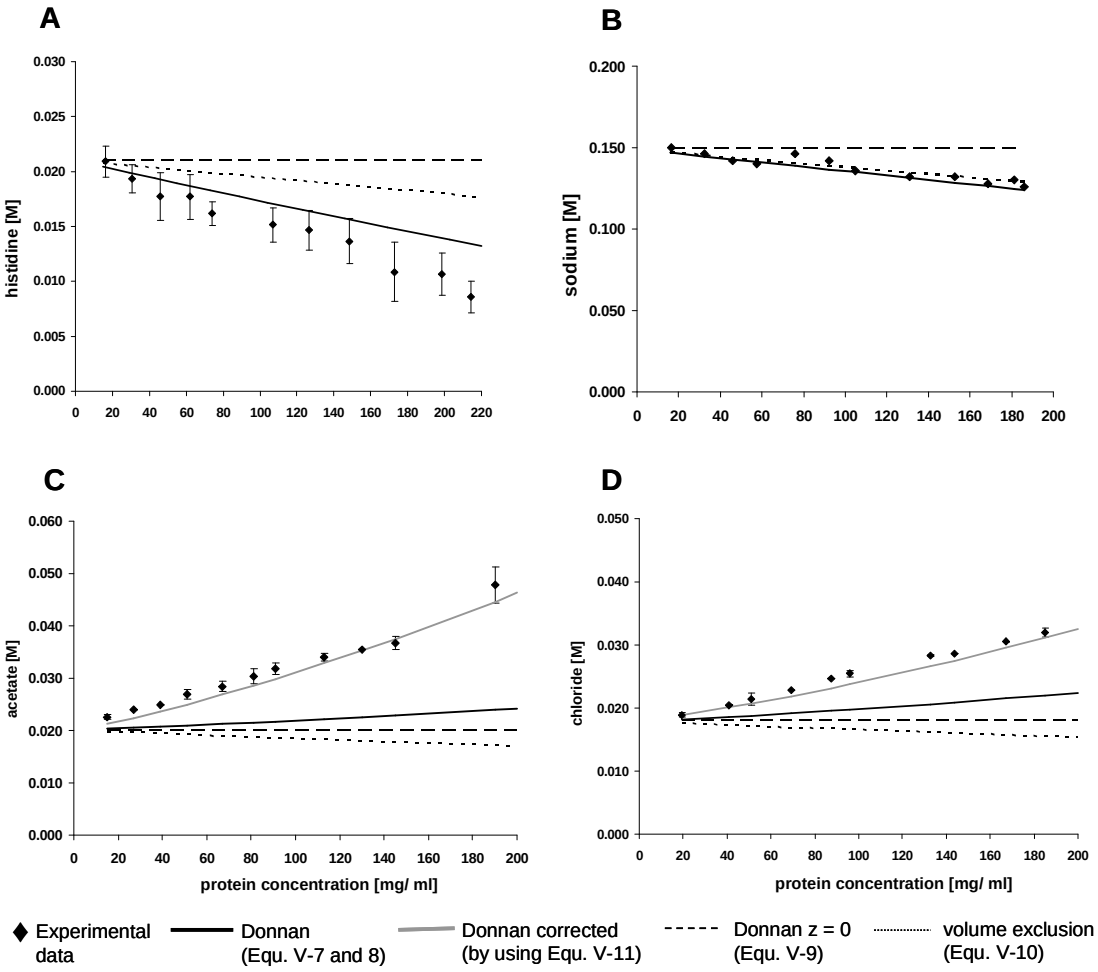

Figure V-12: Theoretical and experimental results of the molar concentration of histidine (A), sodium (B), acetate (C) and chloride (D) in the retentate during UF up to about 200 mg/ml IgG X concentration at pH 5.5
Experimental data is presented as mean values of three measurements ± SD.

For a buffer system containing 20 mM histidine a steady decrease in histidine concentration was observed with increasing protein concentration (Figure V-12A). It is obvious that the Donnan-equation is the most suitable model to adequately reflect the experimental data compared to the two other models. Since the Donnan-equation is the only model considering the protein charge, charge-charge interactions are considered to be the root cause of thermodynamic non-ideality during UF of the IgG in histidine buffer at pH 5.5.

By adding 150 mM sodium chloride to the mAb solution in a 5 mM histidine based buffer system, the molar concentration of sodium as a cation decreases as expected by the Donnan-equation (Figure V-12B). It has to be noted that under conditions of higher total

diffusible ion concentration, the Donnan-effect is suppressed. Equation V-5 shows that if total diffusible cation concentration is higher than the concentration of positively charged protein present in the retentate, the ratio between diffusible cationic solutes in the retentate and the permeate is 1 and therefore the solute concentration on both sides is equal. In our case the molar protein concentration is low compared to the sodium chloride molarity. This is due to the high molecular weight of 150 kDa of an IgG. The molar concentration of the IgG increased only from 0.1 mM to 1.2 mM during UF compared to a sodium chloride molarity of 150 mM. Thus, the Donnan-effect becomes more significant at low ionic strength and at high protein charge and concentration. Therefore, the two models which do not consider the protein charge gain in accuracy when 150 mM sodium chloride are added.

When a 20 mM acetate based buffer is used, acetate is accumulated in the retentate during UF operations as discussed before (Figure V-12C). At a pH of 5.5 acetate is present as both the anion and the acetic acid. It was determined that around 18 % of total acetate concentration [Ac^-] in the retentate is present as acetic acid [HAc] at a pH at 5.5 by using the Henderson-Hasselbalch equation (Harris 1995):

$$pH = pk_A + \log\frac{[Ac^-]}{[HAc]} \qquad \text{Equation V-11}$$

At a pH of 5.9 in the retentate which is the pH at 200 mg/ml protein concentration 7 % of acetic acid are present. Due to the increasing pH during the UF process the percentage of acetate increases and more acetate will actually be lost than calculated by using the Donnan-equation without considering the pH. Therefore, the theoretical diffusible solute concentration S' was corrected by using a factor considering the pH. The ratio between acetate and acetic acid was calculated at every pH measured in the retentate (see Figure V-7A) by using Equation V-11. The relative increase at every pH was used as the correction factor. Figure V-12C shows that by using the corrected values for S' (Donnan corrected, grey line) the Donnan-equation adequately reflects the experimentally determined values for the molar concentration of acetate in the retentate during UF.

By adding 20 mM sodium chloride to a 5 mM acetate based solution, chloride was accumulated during UF (Figure V-12D). The molar solute concentration for histidine, sodium and acetate were approximated by inserting the actual charge value of +9 mV of IgG X at a pH of 5.5 in Equation V-7 and Equation V-8 respectively. Generally, the over-

all protein charge was determined by zeta potential measurements. Figure V-13 shows the zeta potential characteristics depending on pH for three different IgGs.

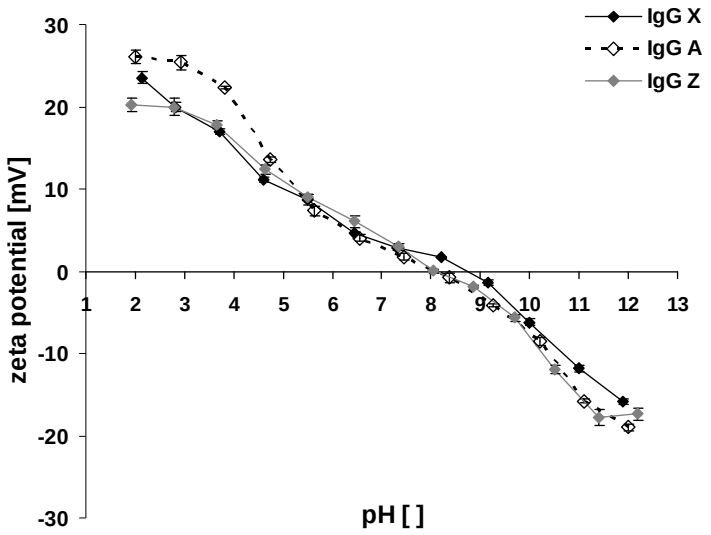

Figure V-13: Zeta potential titration curves of IgG X, IgG A and IgG Z
Experimental data is presented as mean values of three measurements ± SD.

In the case of chloride, the Donnan-effect approximation was not able to adequately reflect the experimentally determined molar concentrations of chloride during UF (Figure V-12D, Donnan, black line). Therefore, the determined charge was replaced in Equation V-8 by using the best fit charge of +18 mV (Figure V-12D, Donnan corrected, grey line), resulting in a representative approximation of the experimental values. Compared to the two other calculations neglecting the protein net charge, the corrected Donnan-equation is the only model to adequately reflect the experimental data.

Considering the results of histidine, sodium and acetate it is shown that a special emphasis is on the protein net charge since in all cases the volume exclusion model as well as the Donnan-model without considering protein charge ($z = 0$) are always inferior to display the experimental values. There are several possibilities to determine the protein valence depending on pH. Beside a calculation based on protein sequence, by combining the average pk_A values of all acidic and basic amino acid side chains, the experimental determination based on electrophoretic mobility is well known. Zeta potential measurement (Faude et al. 2007; Salinas et al. 2009) or isoelectric gel- and capillary electrophoresis (Winzor et al. 2004) are used. Since the protein valence depends not solely upon pH but also on the composition

of the buffer electrolytes, there is no reasonable alternative available to determine the actual charge of the protein. Due to that, the discrepancy between the actual values and the determined values of the molar solute concentration by using the Donnan-equation is particularly caused by the low precision in actual protein valence determination.

The importance of protein valence considering the Donnan-effect is underlined when the pH of the solution is adjusted more closely to the IP of the IgG. The Donnan-effect is then reduced and therefore the two other models which do not consider the charge gain in accuracy. This is shown in Figure V-14A for IgG Z in a histidine based buffer system at a pH of 7.4. In general, a pH more closely to the IP of the protein can be attributed to a suppression of the Donnan-effect (Figure V-14B). The z-values were taken from Figure V-13 (+3 mV at a pH of 7.4, +9 mV at pH 5.0 and +20 mV at pH 3.0 for IgG Z).

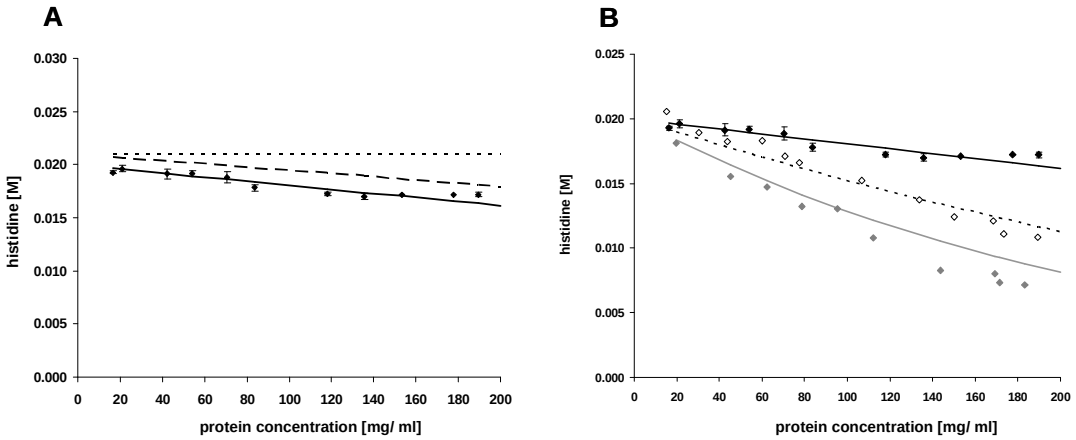

Figure V-14: Experimental and theoretical results of the molar concentration of histidine in the retentate during UF up to 200 mg/ml protein concentration
IgG Z at pH 7.4, figure description is equal to Figure IV-12 (A), IgG Z at pH 7.4 (black symbols), pH 5.0 (plain symbols) and pH 3.5 (grey symbols), symbols refer to the experimental data and the lines to the approximation using the Donnan-equation (Equation V-7).

Summarized, the experimentally determined quantities of two displaced cationic and two accumulated anionic diffusible solutes during the UF concentration process of two mAbs were compared to the calculated values using different model equations. During the UF of the two mAbs the Donnan-equation adequately reflects the experimental observations.

3.2 Prediction of the solute concentration during UF

It was shown that unequal partitioning of small solutes during mAb diafiltration and concentration operations can result in solute concentrations, pH- and conductivity values which are significantly different from those of the diafiltration buffer. Since this can potentially influence stability of the mAb and may result in deviations during DSP and final formulation, the accurate solute concentration should be present in the concentrated bulk material.

3.2.1 Application of the Donnan-equation

The Donnan-equation adequately reflects the displacement of histidine during UF concentration up to 200 mg/ml. Therefore, Equation V-7 was considered suitable to calculate the molar concentration of the diffusible solut ($S^{\wedge}$) which has to be present before starting the UF.

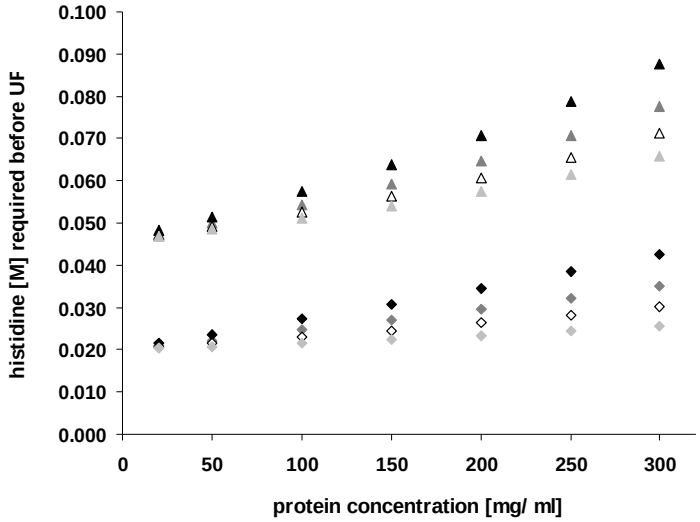

Figure V-15: Histidine molarities required before UF of IgG X to achieve 20 mM (diamonds) or 46 mM (triangles) histidine at a defined protein concentration
At pH 3.0 z = +17.8 mV (black), pH 5.5 z = +9 mV (grey), pH 7.0 z = +4 mV (white) and pH 9.0 z = 0 mV (light grey).

Figure V-15 pictures the required histidine molarity exemplarily which has to be available before starting the UF of the IgG X solution to end up with 20 mM or 46 mM histidine at different protein concentrations and pHs. The z-values at a given pH were taken from the zeta potential titration curves (Figure V-13). The required solute molarity to achieve

20 mM and 46 mM histidine at a protein concentration of 200 g/ml (pH of 5.5) was determined to 29 mM and 60 mM.

This was controlled experimentally by comparing UF runs conducted at 20 mM and 46 mM histidine, as well as at 29 mM and 60 mM histidine initially present. The histidine concentration was monitored during the UF concentration up to 200 mg/ml.

Moreover, the solute molarity required to achieve 20 mM histidine at 200 mg/ml protein concentration was calculated for IgG Z at pH 5.0. Here, a bulk having initially 31 mM histidine present is theoretically required (z = +11 mV).

The histidine concentration is quantitatively reflected by the Donnan-equation at any time during UF which was expected and reported before (Figure V-16).

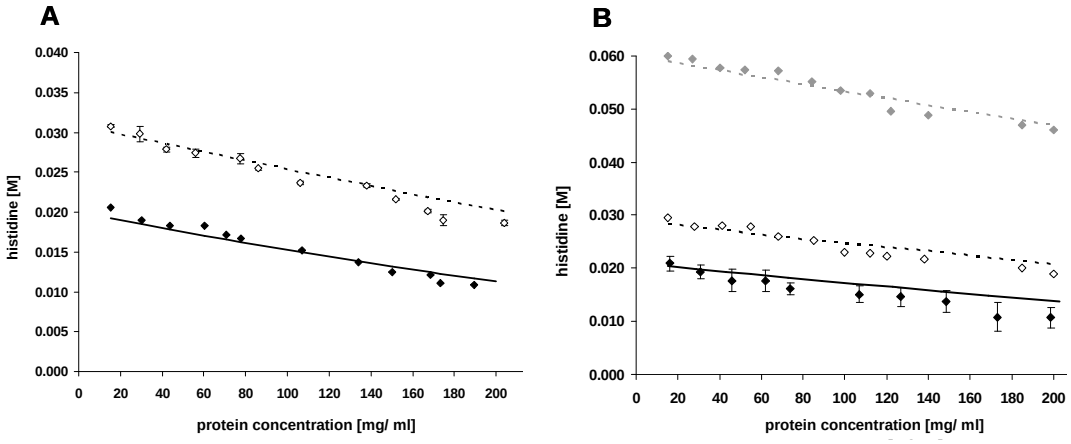

Figure V-16: Molar concentration of histidine during UF concentration operations
For IgG Z at pH 5.0 having 20 mM histidine (black diamonds) and 31 mM histidine initially present before UF (plain diamonds) (A) and for IgG X at pH 5.5 having 20 mM histidine (black diamonds), 29 mM histidine (unfilled diamonds) and 60 mM histidine (grey diamonds) initially present before UF (B); mean values of three measurements are presented with error bars ± SD; the lines represent the values theoretically predicted by using the Donnan-equation (Equation V-7).

The IgG Z solution at 200 mg/ml protein concentration showed only 11.6 ± 0.5 mM histidine when 20.4 ± 0.4 mM histidine were present before starting the UF. In comparison, 18.6 ± 0.5 mM histidine at 200 mg/ml protein concentration were found in the concentrates when 30.3 ± 0.7 mM histidine were initially present (Figure V-17A). The same was obvious for IgG X. By using the buffer system with the calculated higher solute concentration of 29 mM a concentration of 19 mM after UF was achieved (Figure V-17B). 47 mM histidine were found when 60 mM histidine were applied before starting the UF.

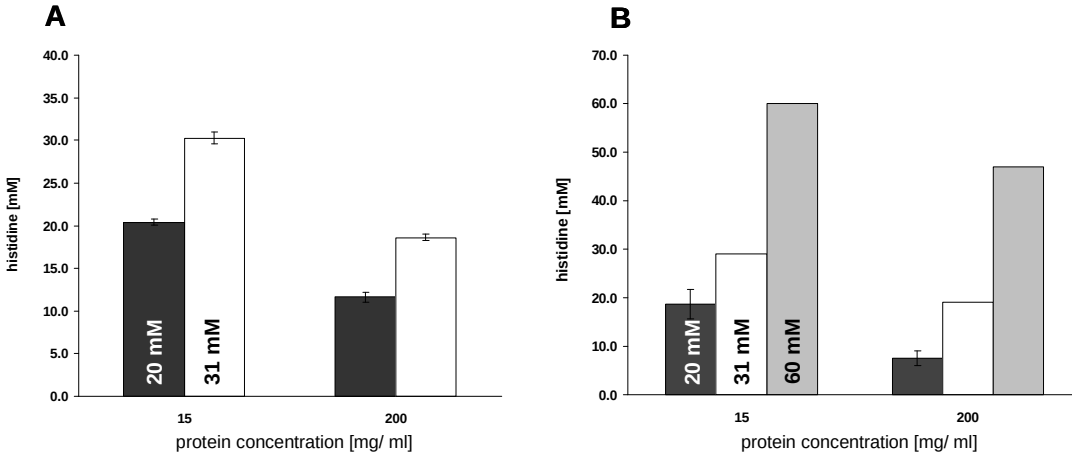

Figure V-17: Molar concentration of histidine before (at 15 mg/ml protein concentration) and after UF (at 200 mg/ml protein concentration)
For IgG Z pH 5.0 (A) and IgG X pH 5.5 (B); mean values of three measurements are presented with error bars ± SD.

In summary, the calculated higher histidine molarity before starting the UF concentration process can be predicted using the Donnan-equation resulting in the intended molarities of histidine in the concentrated bulks.

3.2.2 Consequences for pH and deamidation

The pH was stable during and after the UF when the predicted higher histidine molarity was applied before starting the UF concentration process.

Figure V-18 shows the pH during UF concentration of IgG X containing 20 mM and 29 mM histidine before processing. At a protein concentration of 200 mg/ml the pH was shifted from pH 5.4 to pH 5.8, if the histidine concentration was not increased to 29 mM histidine before starting the UF experiments. If the histidine concentration was increased to 29 mM, the pH was more stable during UF processing. The stable pH values can be potentially attributed to a lower buffer capacity at a lower buffer solute concentration. The buffer capacity describes the amount of acid or base needed to change the pH ± 1 (Harris 1995). At a higher concentration of the buffer component the capacity increases making the solution more resistant against pH changes.

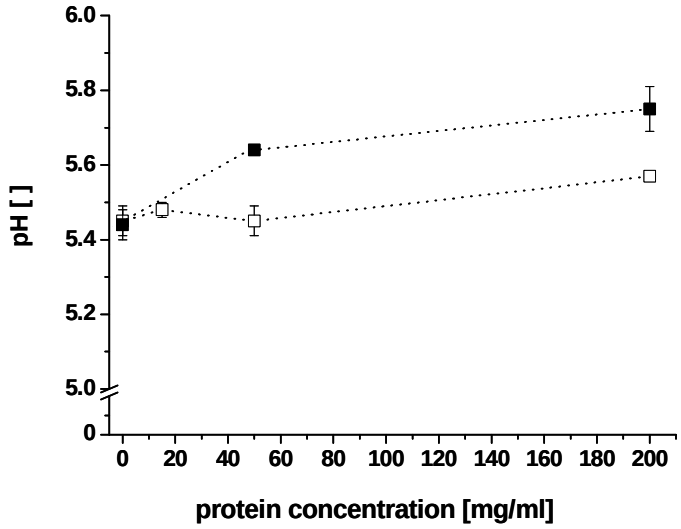

Figure V-18: pH during UF concentration of IgG X from 15 to 200 mg/ml
Solutions containing 20 mM histidine at pH 5.5 (black squares) and solutions containing 29 mM histidine at pH 5.5 (unfilled squares) before UF; mean values of three measurements are presented with error bars ± SD.

The pH of the solution is known to be important for protein stability. The side chain amide linkage in a glutamine or asparagine residue can be hydrolyzed to form a free carboxylic acid (Manning et al. 1989b). This deamidation is accelerated at more neutral or alkaline conditions and at increased temperature (Robinson and Rudd 1974; Robinson et al. 1973; Zheng and Janis 2006).

The introduced unfavorable negative charge in the deamidated molecule can cause structurally and biologically alterations encompassing a decrease in bioactivity, as well as alterations in pharmacokinetics (Huang et al. 2005). Particularly, the deamidation within the heavy or light chain of the Fab is of importance since the variable binding region can be affected (Tsai et al. 1993). Therefore, the effect of the histidine concentration and thus pH during UF on the deamidation of the Fabs was investigated by using analytical CEX chromatography after papain digestion. Papain is a thiol protease that cleaves IgG molecules at the heavy chain hinge region into one Fc and two identical Fab fragments (Smyth and Utsumi 1967). The digestion is useful to resolve inherent charge heterogeneity associated either with the Fab or the Fc fragment (Moorhouse et al. 1997). Figure V-19 shows the sum of deamidated Fab fragments for IgG X at 50 mg/ml and 200 mg/ml during storage at 40 °C.

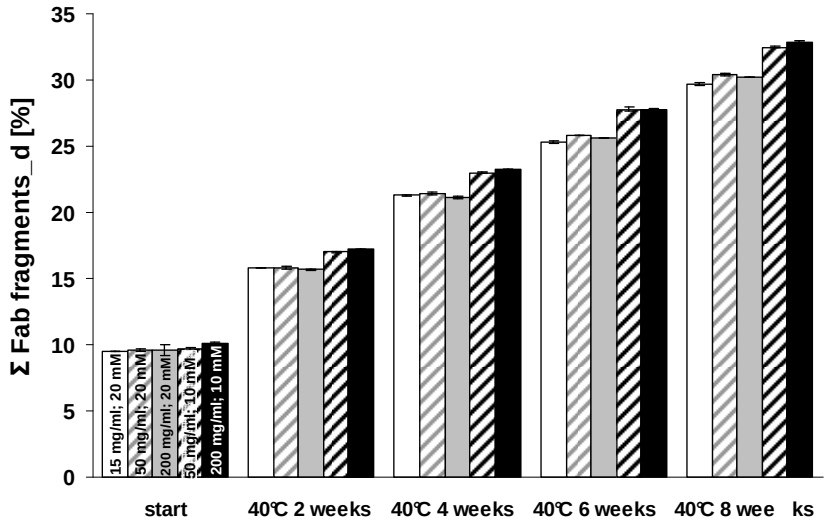

Figure V-19: Sum of deamidated Fab fragments of IgG X at 50 mg/ml (striped bars) and 200 mg/ml (solid bars) after UF and storage at 40 °C for 8 weeks
Samples containing 20 mM histidine (grey) and samples containing about 10 mM histidine (black) after UF; samples containing 15 mg/ml protein and 20 mM histidine are displayed as white bars; mean values of two measurements are presented ± SD.

In general, an increase in deamidated Fab fragments was observed for all samples during storage. Samples containing 20 mM histidine showed comparable values, independent of their protein concentration. At 50 and 200 mg/ml protein concentration, deamidation increased during storage over 8 weeks when only 10 mM histidine were present. During storage, an increase in deamidated Fab fragments of about 10 % was observed in relation to solutions having a higher amount of histidine present.

Since it was shown that the pH of the concentrated samples was increased when only 10 mM histidine were present in the solutions, it was assumed that the increased pH contributes to deamidation as well. Therefore, the pH of the samples at 50 mg/ml and 200 mg/ml protein concentration containing only 10 mM histidine were adjusted to pH 5.5 by using hydrochloric acid. Deamidation of the Fab fragments was monitored again over four weeks and the results at pH 5.5 were compared to those obtained before (Figure V-20). Again, an increase in deamidated Fab fragments of all samples was observed during storage. After two weeks a reduction of deamidated Fabs in the concentrated solutions containing 10 mM histidine at the lower pH was observed. After four weeks, all samples showed comparable results independent of pH. Therefore, it was concluded that both the pH and the histidine concentration have influence on the deamidation level of

the IgG. In summary, both concentrates at 50 mg/ml as well as at 200 mg/ml showed a higher level of deamidated Fab fragments during storage when the histidine concentration was not increased in the Donnan-manner before UF.

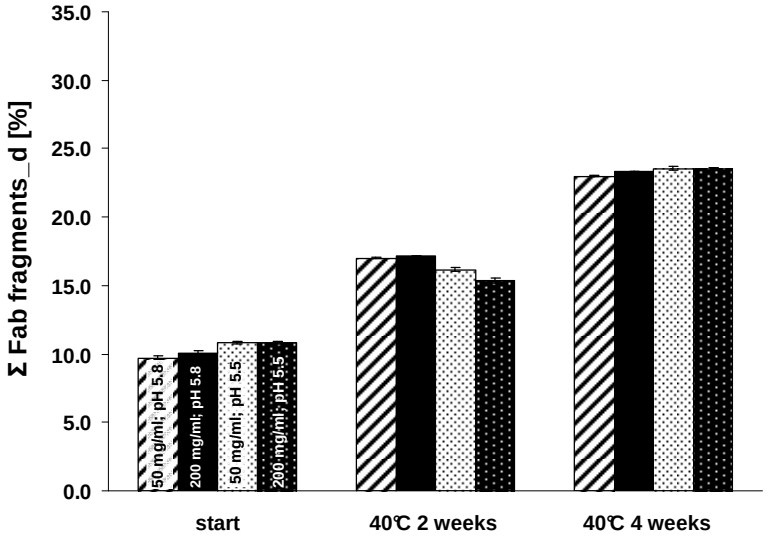

Figure V-20: Sum of deamidated Fab fragments of IgG X at 50 mg/ml (grey) and 200 mg/ml (black) after UF and storage at 40 °C for 4 weeks
All samples contain 10 mM histidine after UF; the samples had a pH of 5.8 (striped bars) and 5.5 (dotted bars); mean values of two measurements are presented ± SD.

3.2.3 Robustness of the Donnan-model

In order to confirm that the Donnan-model adequately reflects the experimental values concerning the loss of histidine during UF concentration, different membrane materials, UF systems and operational parameters were tested (Table V-1).

Histidine concentration [mM]	pH	UF membrane material - pore size	UF system	Δp [bar]
20	5.0	RC - 30 kDa	stirred cell	2.0
20	5.0	RC - 30 kDa	ÄKTAcrossflow TFF	0.8
20	5.0	RC - 30 kDa	ÄKTAcrossflow TFF	1.5
20	5.0	PES - 30 kDa	ÄKTAcrossflow TFF	1.5

Table V-1: Process conditions in confirmative experiments
Different UF systems, membranes and operational conditions were tested.

Different membrane materials are known to adsorb protein and solutes on the surface. Especially PES is known to adsorb protein to a higher extent than RC, due to enhanced hydrophobicity as reported in chapter I. Solutes can interplay with the membrane surface based on charge-charge interactions (Nystroem et al. 1989). As a consequence, the outcome of the Donnan-effect concerning the solute molarity in the concentrates can be potentially influenced by the choice of the membrane material.

Moreover, the UF system used as well as the operational parameters can influence the flow characteristics. Therefore, the solute molarity in the retentate during UF processes can be potentially affected. For lab-scale experiments, NFF as an orthogonal principle to TFF is used by applying stirred cells, operated under inert gas atmosphere. Here, the solute is forced to pass through the membrane by using pressurized gas up to 4 bar and a stirring procedure. The latter helps in addition to remove the deposited protein from the membrane surface. This can cause aggregation due to enlarged liquid-gas interface, resulting in pore narrowing, blockage and enhanced deposition of protein which can potentially influence the properties of the membrane.

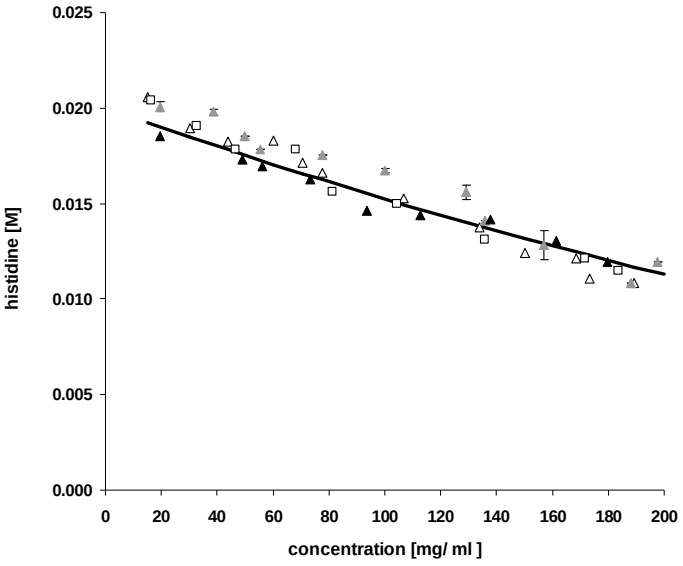

Figure V-21: Confirmation of the Donnan-model during UF concentration of IgG Z in 20 mM histidine buffer at pH 5.0 by applying different UF systems, membranes and operational conditions as described in Table V-1
Donnan fit (black line), experimental data from stirred cell experiment (grey triangles) and TFF experiments applying a RC membrane (unfilled triangles), a PES membrane (black triangles), a Δp of 0.8 bar (unfilled squares).

Figure V-21 shows the molar solute concentration of histidine during the UF experiments as described in Table V-1. Independent of the applied UF system, membrane material or operational conditions applied, the experimental data concerning the histidine molarity during UF is adequately reflected by using the Donnan-equation as described before.

3.3 Evaluation of different approaches to achieve predefined solute concentrations in highly concentrated mAb solutions

In general, different approaches are possible to end up with the predefined solute concentration and thus pH in the highly concentrated end product. On the one hand the Donnan-equation can be used to predict the solute molarity needed, as shown before. On the other hand the UF process can be conducted at a pH more closely to the IP of the protein, since the Donnan-effect is suppressed as shown in Figure V-14B. In this case, the pH has to be readjusted after UF processing. In addition, the histidine molarity and the pH can generally be adjusted in the concentrated solutions after UF. All three approaches were tested concerning the physical stability of the mAb. Aggregation was examined during the UF concentration process and after readjustment of the pH by using different analytical techniques. Moreover, the stability of the concentrated API during storage was evaluated depending on the molar concentration of histidine and the protein concentration in the bulk.

3.3.1 Effect on stability during UF processing

IgG Z at a concentration of 20 mg/ml was ultrafiltrated up to 200 mg/ml. Buffer systems based on histidine were applied. On the one hand, experiments were conducted in a 31 mM histidine buffer pH 5.0. On the other hand UF was performed in a 20 mM histidine buffer at pH 7.4. Results were compared to experiments conducted in a buffer system containing 20 mM histidine at pH 5.0.

Figure V-22 shows the results for LO (A) and turbidity measurements at 350 nm (B). It was observed that the particle formation during UF was enhanced at pH 7.4. In the course of UF particles larger 1 μm were formed up to a number of $8x10^6$ and the turbidity increased from 0.1 to 1.6 AU. The formation of particles and the turbidity were clearly reduced at pH 5.0. The higher turbidity and the higher number of particles at pH 7.4 can be attributed to the reduced electrostatic repulsion between the protein molecules enhanc-

ing self-association, since the pH is closer to the IP of the IgG Z which was determined to be around 8 (Figure V-8 and Figure V-13).

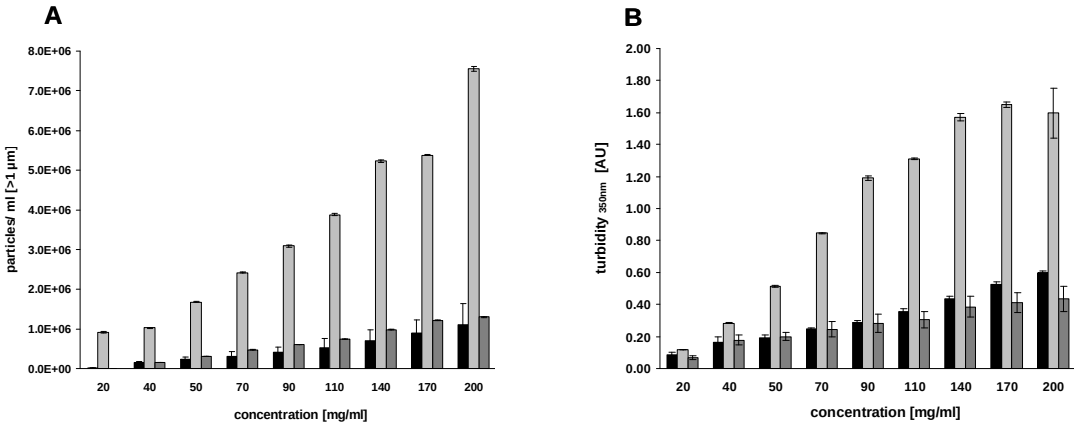

Figure V-22: Particles per ml larger 1 µm (A) and turbidity at 350 nm (B) during UF concentration of IgG Z
In 20 mM histidine pH 5.0 (black), in 20 mM histidine pH 7.4 (light grey) and in 31 mM histidine pH 5.0 (dark grey); results are presented as mean values of three measurements ± SD.

The massive formation of proteinaceous particles in the retentate at pH 7.4 was clearly visible during and after UF processing. Figure V-23 shows a picture of the concentrated solutions at 200 mg/ml directly after processing.

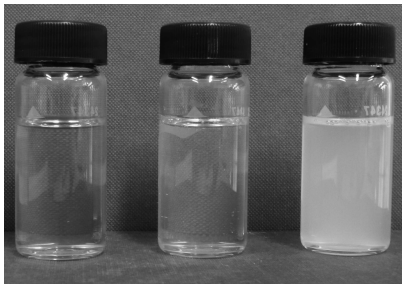

Figure V-23: Visual inspection of the concentrated IgG Z after UF (200 mg/ml)
In 20 mM histidine pH 5.0 (left), in 31 mM histidine pH 5.0 (middle) and in 20 mM histidine pH 7.4 (right).

At a pH equal to the IP of the protein, the overall charge of the protein is nearly zero resulting in a more compact packing of the molecules on the UF membrane than under electrostatic repulsion (Nakatsuka and Michaels 1992). Therefore, the permeate flux at pH 7.4 was significantly reduced during processing compared to the experiments conducted at

pH 5.0. Figure V-24 visualizes the permeate flux during UF experiments at pH 7.4 and pH 5.0. Moreover, the process time was more than doubled, increasing from 120 min to 300 min when a pH of 7.4 was adjusted before the UF started. It was observed that the addition of histidine up to 31 mM did not result in any changes concerning permeate flux or process time compared to experiments conducted in 20 mM histidine at pH 5.0.

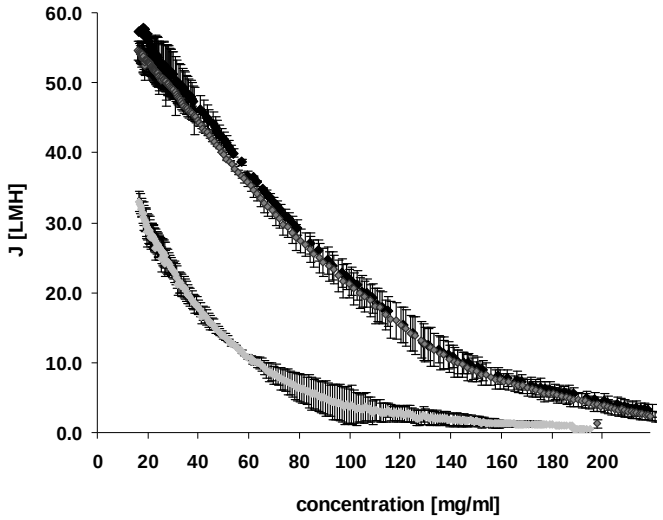

Figure V-24: Permeate flux (J) versus concentration of IgG Z during UF
In 20 mM histidine pH 5.0 (black), in 31 mM histidine pH 5.0 (dark grey) and in 20 mM histidine pH 7.4 (light grey); results are presented as mean values of three UF runs ± SD.

After UF, the concentrates were readjusted to a pH of 5.0 by adding 0.5 M hydrochloric acid (HCl). This was only necessary for the solutions which were concentrated at pH 7.4 as well as for the solutions processed at 20 mM histidine pH 5.0 due to the pH shift.

Starting conditions	pH before UF	pH after UF	pH end product
20 mM histidine pH 5.0	4.97 ± 0.04	5.40 ± 0.06	4.90 ± 0.14
31 mM histidine pH 5.0	5.07 ± 0.04	5.20 ± 0.05	5.20 ± 0.05*
20 mM histidine pH 7.4	7.37 ± 0.06	7.47 ± 0.05	4.81 ± 0.22

* No pH adjustment was done (pH after UF = pH end product)

Table V-2: pH before UF, after UF and for the end-product after readjustment
0.5 M hydrochloric acid was taken to readjust the end product to pH 5; mean values of three measurements are presented ± SD.

The experiments conducted at 31 mM histidine pH 5.0 did not show a pH shift as reported before. Table V-2 summarizes the pH values before UF, after UF and after readjustment to pH 5.0.

Particle measurements, turbidity at 350 nm and SE-HPLC were performed to monitor the induction of aggregates due to the addition of hydrochloric acid.

Figure V-25 shows the results for the IgG solutions before UF, after UF and for the pH adjusted end products by using 0.5 M hydrochloric acid.

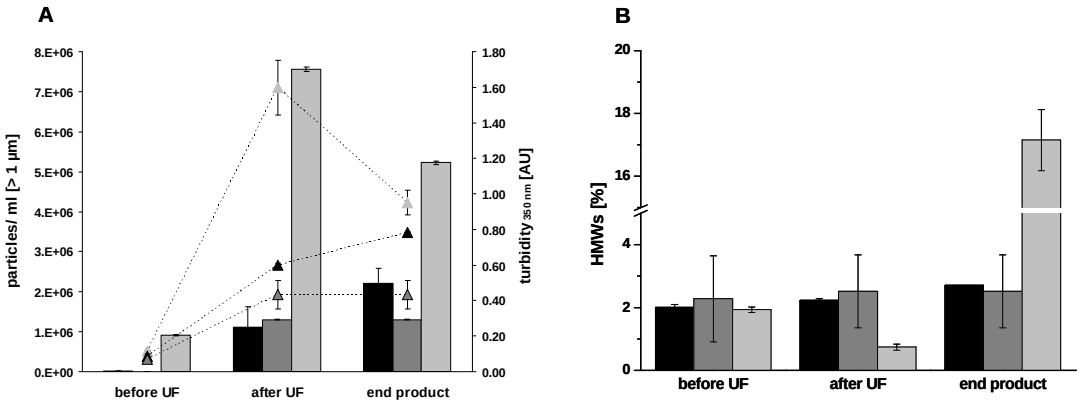

Figure V-25: Aggregation of IgG Z before UF, after UF and in the final end product after pH readjustment using 0.5 M hydrochloric acid: 20 mM histidine pH 5.0 (black), 31 mM histidine pH 5.0 (dark grey) and 20 mM histidine pH 7.4 (light grey)
Particles per ml larger 1 µm (bars), turbidity at 350 nm (triangles) (A) and percentage of HMWs (B); mean values of three measurements are presented ± SD.

For the pH adjusted end product an induction of particles larger 1 µm and an increase in turbidity were observed for the solutions concentrated in 20 mM histidine at pH 5.0 (Figure V-25A). A slight induction of HMWs from 2.23 % to 2.71 % was recognized (Figure V-25B). For the solution containing 31 mM histidine at pH 5.0 before UF, the number of particles per ml larger than 1 µm, the turbidity values and the percentage of HMWs remained constant since no hydrochloric acid was needed due to an unaltered pH during UF. The solutions concentrated at a pH more closely to the IP of the protein showed a highly increased number of particles directly after UF, since colloidal stability is compromized under these conditions as explained before. In addition, a decreased level of HMWs directly after UF processing was recognized. However, after readjusting the pH from 7.4 to pH 5.0 the percentage in HMWs stepped up from 0.74 % to 17.15 % by using 0.5 M HCl. Concomitantly, the number of particles larger 1 µm and the turbidity values decreased. Due to

the lower pH the electrostatic repulsion between the protein molecules increases resulting in a dissociation of the reversible large aggregate particles. Nevertheless, the number of particles and the turbidity values remained much higher compared to the two other end products.

Due to the massive induction of HMWs by adding 0.5 M HCl to the concentrates after UF at pH 7.4, the pH readjustment was conducted using 0.02 M and 0.1 M HCl. It was expected that the addition of a lower molar acid concentration results in reduced aggregation, since the local concentration of acid is much lower. Figure V-26 shows the results referring to the induction of oligomers and dimers as well as the sum of HMWs induced by adding HCl of different molar concentrations.

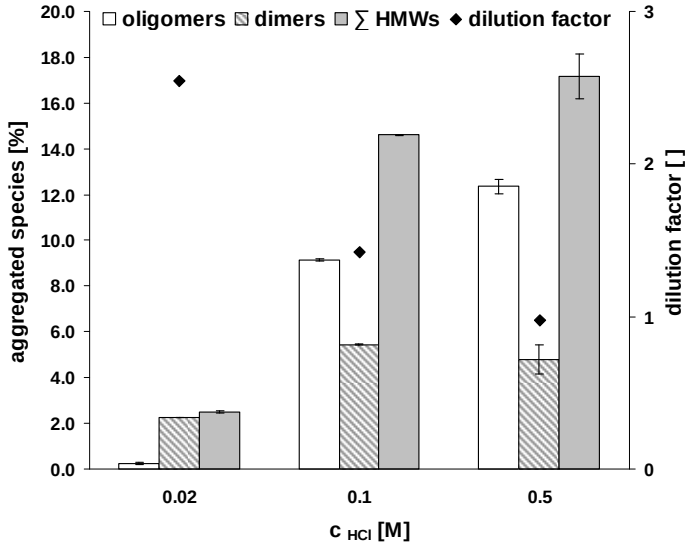

Figure V-26: Percentage of aggregated species of IgG Z and the dilution factor resulting from the addition of 0.02-0.5 M hydrochloric acid (HCl)
IgG Z at 200 mg/ml in 20 mM histidine pH 7.4 after pH correction to pH 5.0 with 0.02-0.5 M HCl; mean values of three measurements are presented ± SD.

It was observed that the percentage of dimers as well as of oligomers increases with the molar concentration of the hydrochloric acid added. This was prevented by using the 0.02 M HCl. However, the addition of a diluted HCl resulted in a massive dilution of the concentrated protein bulk ending up with about a third in protein concentration after pH readjustment. This is in direct opposite to the intention of the UF process to provide highly concentrated immunoglobulin solutions.

Summarized, the add-on of histidine to 31 mM is the approach of choice to circumvent the induction of aggregates since no addition of acid is necessary after UF due to stable pH

conditions during the concentration process. Further, this strategy is the only way to provide the predefined histidine concentration and pH values in the concentrated bulk without a readjusting procedure which is accompanied by a dilution of the concentrates.

3.3.2 Effect on stability during storage

With the systematic add-on to 29 mM histidine before UF the desired 20 mM histidine at 200 mg/ml protein concentration was achieved in the case of IgG X. If the Donnan-effect is not considered during UF operations the concentrated solutions at 200 mg/ml had only 7.4 ± 1.6 mM histidine remaining as reported before (Figure V-16B).

To evaluate the impact of histidine concentration on storage stability of concentrated solutions after UF, stability was investigated at 10 and 20 mM histidine concentration. Protein concentrations of 15, 50 and 200 mg/ml were applied. Accelerated storage at 40 °C over 8 weeks and real time studies were conducted at 2-8 °C (4 °C) and -70 °C over 6 months. Table V-3 provides an overview of the experiments including the analytical methods used to investigate the stability of IgG X.

IgG X [mg/ml]	Histidine [mM]	Sample description	Analytical methods
15	20	15/20 mM	SE-HPLC, LO, UV $_{350\ nm}$, DLS
50	20	50/20 mM	
200	20	200/20 mM	2D UV, ATR FT-IR
50	10	50/10 mM	
200	10	200/10 mM	

Table V-3: Overview of experiments addressing the storage stability at 40 °C over 8 weeks and at 2-8 °C and -70 °C over 6 months

The formation of soluble HMWs during accelerated stability studies depends on both, protein concentration and histidine molarity (Figure V-27A). A slight increase in HMWs at 50 mg/ml protein concentration was recognized compared to the 15 mg/ml samples at comparable histidine concentrations (20 mM). At 200 mg/ml the samples showed a significant increase in soluble aggregates during storage compared to the 15 mg/ml and 50 mg/ml samples at comparable histidine concentrations (20 mM).

The addition of histidine revealed no effect concerning the formation of aggregates at 50 mg/ml protein concentration. At a protein concentration of 200 mg/ml the solutions

containing 20 mM showed a significantly lower level of HMWs compared to the solutions containing only 10 mM histidine. A difference in the HMW level of 1.8 % after 8 weeks was recognized. During real time storage a slight increase in soluble aggregates was recognized depending on the protein concentration (Figure V-27B).

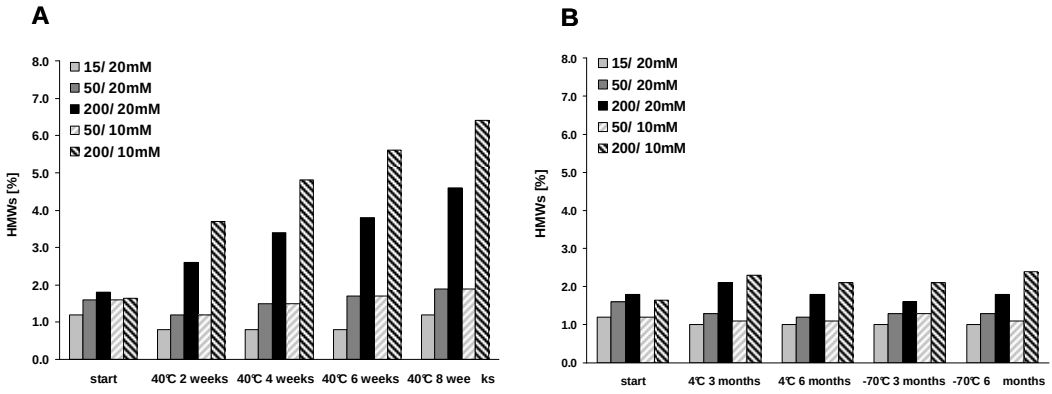

Figure V-27: Formation of soluble aggregates during storage of IgG X solutions determined by SE-HPLC
At 40 °C over 8 weeks (A) and at 2-8 °C and -70 °C over 6 months (B).

Again, at 200 mg/ml a higher level of HMWs was observed compared to the solutions at 15 mg/ml and 50 mg/ml protein concentration. The increase in histidine from 10 mM to 20 mM reduces the formation of HMWs only slightly. After 6 months at -70 °C the samples containing a higher molarity of histidine showed 1.8 % HMWs compared to the samples containing only 10 mM, having 2.6 % HMWs. After 6 months at 4 °C, the samples containing 20 mM histidine showed 1.8 % HMWs compared to the samples containing only 10 mM, having 2.2 % HMWs.

Regarding the formation of particles, it was observed that a higher protein concentration leads to a higher number of particles during storage at 40 °C and 4 °C (Figure V-28A and B). The addition of histidine leads to a reduction in the number of particles larger 1 μm only at a protein concentration of 200 mg/ml during accelerated as well as real time stability studies.

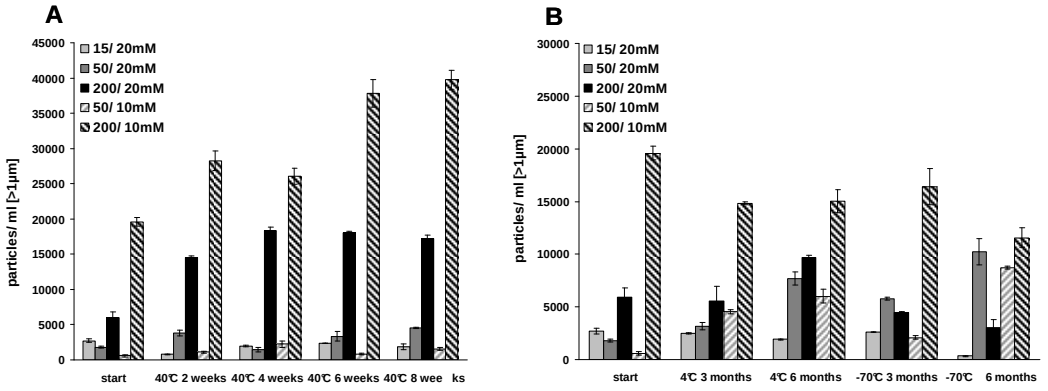

Figure V-28: Formation of particles per ml larger than 1 µm during storage of IgG X solutions determined by SE-HPLC
At 40 °C over 8 weeks (A) and at 4 °C and -70 °C over 6 months (B); mean values of three measurements are presented ± SD.

As regards turbidity, measured at 350 nm it was observed that a higher protein concentration leads to higher turbidity values (Figure V-29).

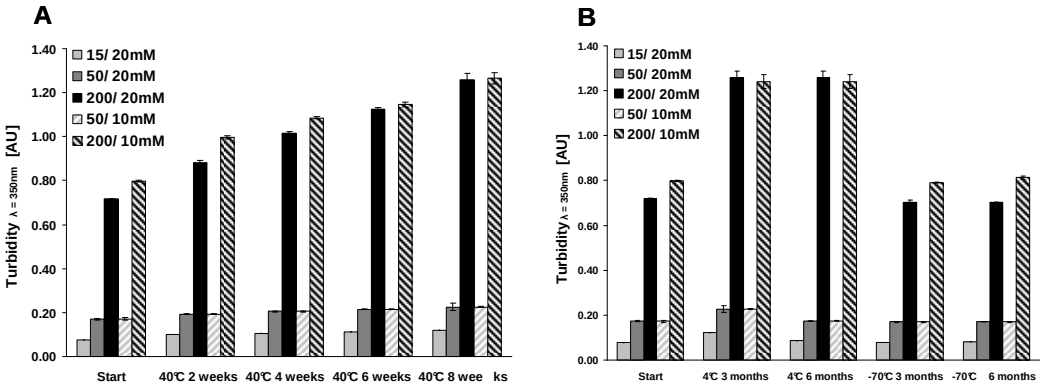

Figure V-29: Turbidity at 350 nm during storage of IgG X solutions
At 40 °C over 8 weeks (A) and at 4 °C and -70 °C over 6 months (B); mean values of three measurements are presented ± SD.

In general, a higher molecular density and higher number of particles result in an increase in UV absorbance at all wave lengths due to scattering effects (Eberlein et al. 1994). The addition of histidine at 50 mg/ml and 200 mg/ml protein concentration did not result in a decrease in turbidity. The samples at 200 mg/ml protein concentration showed only a neglectable decrease in turbidity at 350 nm when the histidine concentration was increased from

10 mM to 20 mM. This was found during accelerated stability as well as during real time studies.

Proteins are known to be more susceptible to aggregation in the more extensively unfolded intermediate state or the completely unfolded state, since hydrophobic residues are presented to the aqueous environment as reported in chapter I. Since it was recognized that IgG X was more prone to aggregation depending on protein concentration and histidine molarity at pH 5.5, conformational stability was investigated. Therefore, FT-IR and 2D-UV analysis were performed to examine secondary and tertiary structure respectively.

ATR FT-IR was used to determine the melting temperature (T_m) at 5, 50 or 200 mg/ml protein concentration and 10 mM or 20 mM histidine molarity according to Table V-3. Conformational changes in secondary structure were recognized by a temperature induced band at 1621 cm^{-1} and a concomitantly diminished band at 1637 cm^{-1}. A weak intensity peak at and 1690 cm^{-1} was detected as well with increased temperature. Figure V-30A shows the second derivative spectra of the tempered solution containing 50 mg/ml protein and 10 mM histidine exemplarily.

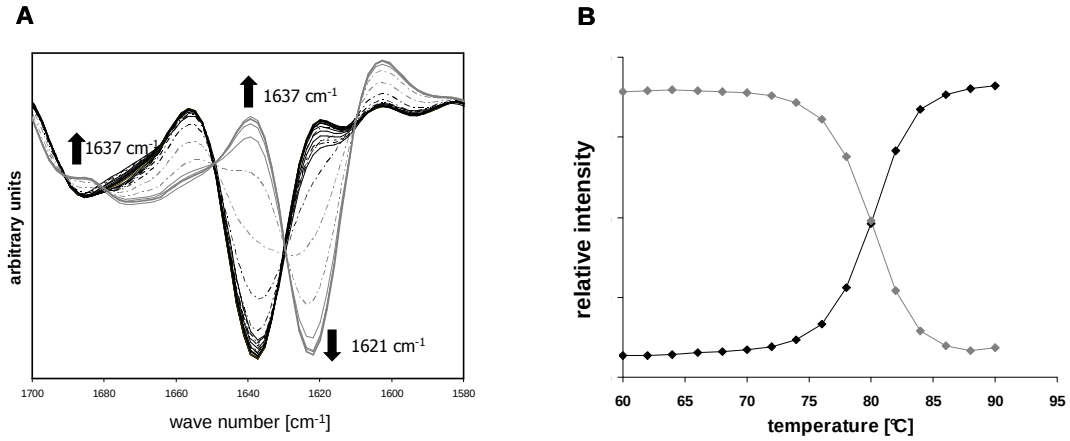

Figure V-30: The 50g/ml IgG X solution containing 10 mM histidine was heated from 25 to 90 °C

Arrows mark the direction of the spectral changes of the bands at 1637 cm^{-1}, 1621 cm-1 and 1690 cm^{-1} in the ATR FT-IR second derivative spectra during heating from 25 (black) to 90 °C (grey) (A) and changes in the intensity in the second derivative spectra at 1637 cm^{-1} (black) and 1621 cm^{-1} (grey) during heating (B).

T_m was determined based on direct plots of the intensity values of the decreasing native band at 1637 cm^{-1} and the increasing temperature induced band at 1621 cm^{-1} as the midpoint of

the thermal transition. Figure V-30B shows the changes in intensity of the two bands for the sample at 50 mg/ml protein concentration containing 10 mM histidine exemplarily.

Table V-4 summarizes the values for T_m. As described in chapter IV, three different approaches were applied to identify T_m using the inflection point as well as the intersection of the intensity curves of the second derivative ATR spectra. No significant differences for T_m were observed depending on protein concentration or histidine molarity. A value of about 80 °C was determined for IgG X at pH 5.5 up to a protein concentration of 200 mg/ml in the presence of 10 and 20 mM histidine.

Protein concentration [mg/ml]	Histidine molarity [mM]	Sample	T_m (FT-IR) [°C]		
			Inflection point using sigmoid fit (Bolzmann equation)		Intersection of in- and decreasing band
			Increasing band at 1637 cm^{-1}	Decreasing band at 1621 cm^{-1}	
15 mg/ml	20 mM	15/ 20 mM	80.3 ± 0.1	80.2 ± 0.2	80.0
50 mg/ml	20 mM	50/ 20 mM	79.9 ± 0.2	79.6 ± 0.2	78.8
200 mg/ml	20 mM	200/ 20 mM	80.2 ± 0.2	80.1 ± 0.2	79.5
50 mg/ml	10 mM	50/ 10 mM	80.3 ± 0.1	80.3 ± 0.1	79.0
200 mg/ml	10 mM	200/ 10 mM	80.1 ± 0.2	80.1 ± 0.1	79.0

Table V-4: Denaturation temperature (T_m) for IgG X solutions at 200 mg/ml determined from ATR FT-IR second derivative spectra by using three different interpretation approaches as described in chapter IV
Results of sigmoid fitting are listed with ± standard error of the non-linear regression.

Information about tertiary structure was collected by using 2D-UV analysis. The broad protein absorbance peak between 240 and 300 nm is composed of overlapping spectra arising from the absorbance of phenylalanine (245-270 nm), tyrosine (265-285 nm) and tryptophan (265-295 nm) residues (Ichikawa and Terada 1979). Calculating the derivative of the absorbance spectrum enhances the resolution and is useful to deconvolute the complex multi-spectrum of zero order (Grum et al. 1972; Ichikawa and Terada 1977; Lange and Balny 2002). In the second derivative of the spectrum, the absorbance referring to the residues is resolved as minima in the region of 245-270 nm for phenylalanine, 265-285 nm for tyrosine and 265-295 nm for tryptophan.

Shifts in the derivative peak positions were shown to arise from changes in the polarity of the local environment of the chromophores with a shift to shorter wave lengths indicating an increase in environment polarity (Mach and Middaugh 1994). This is the case when the residues are no longer buried in an apolar region within the protein but located on the surface of the more or less unfolded molecule. Moreover, total spectral shifts have been observed due to transition from the folded state to the unfolded state (Kueltzo 2005; Kueltzo et al. 2003). The peak intensity also provides useful information about protein conformation (Ragone et al. 1984). In this study, the second derivative spectrum of the IgG X showed a blue shift between 280 and 300 nm when a solution at 15 mg/ml was incubated in 4 M guanidine hydrochloride or heated to 80 °C for 10 min. Concomitantly, the intensity of the band at 285 nm, 289 nm and 292 nm was decreased compared to untreated samples (Figure V-31).

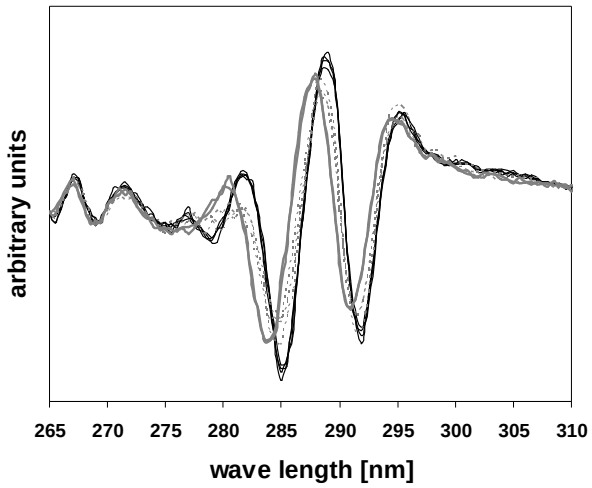

Figure V-31: 2D-UV spectrum of IgG X at pH 5.5.
Native solution (black lines), incubated at 80 °C for 10 min (grey dotted lines) and incubated in 4 M guanidine hydrochloride for 10 min (grey lines).

Therefore, the second derivative spectra of the samples at different protein and histidine concentrations were monitored at 270-300 nm. Figure V-32 visualizes the 2D-UV spectra of the samples directly recorded after UF and stored for 2 and 8 weeks at 40 °C. Under accelerated storage conditions no spectral differences were recognized in the 2D-UV spectra, neither after 2 weeks, nor after 8 weeks. Tertiary structure seems to be unaffected at pH 5.5 independent from the protein or histidine concentration in the samples.

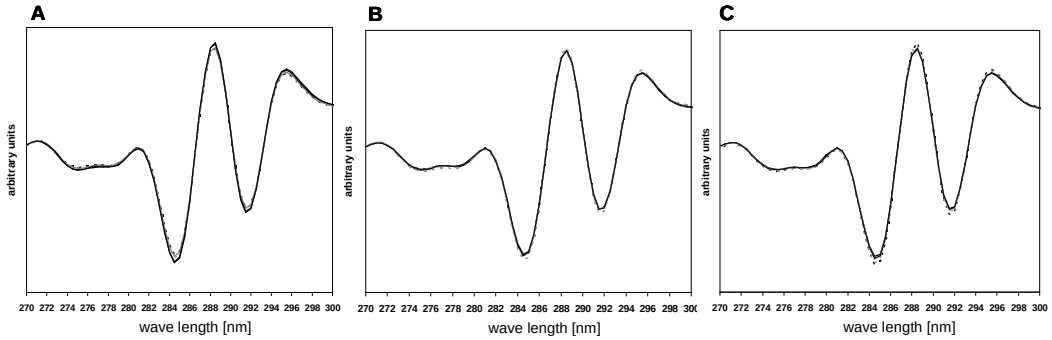

Figure V-32: 2D-UV spectra of IgG X at different protein and histidine concentrations (in accordance with Table V-3) during storage
After UF (A), after 2 weeks at 40 °C (B), after 8 weeks at 40 °C (C); all spectra of the different samples almost perfectly overlaid.

Amino acids as cosolvents are known to increase the conformational stability of the protein. Therefore, it was actually assumed that the conformational stability should increase with increased histidine concentration, since amino acids as cosolvents are known to be excluded from the surface of the protein, leading to preferential hydration of the protein (Cleland et al. 1993; Timasheff 1993). An increase in surface tension of water is assumed to be the root cause of the exclusion mechanism (Arakawa and Timasheff 1983; Timasheff 1992). As a consequence of the increased surface tension per molecule in the unfolded state, the compact native state is thermodynamically favored due to a reduced free energy of the system at minimized protein surface.

Since neither a decrease in T_m, nor changes in tertiary structure were observed with decreased histidine concentration, it is assumed that the protein is more prone to native self-association at a lower concentration of histidine rather than to aggregation based on conformational changes.

At high protein concentrations the molecules exclude volume to another, based on steric- and charge-charge repulsion, resulting in an increase of the total free energy of the system (Minton 2000). Since the formed aggregates exclude less volume compared to the monomeric molecules, the aggregated species is thermodynamically favored due to a reduced surface. This provides a non-specific force for macromolecular compaction and association in crowded solutions (Minton 1980; Zimmerman and Minton 1993).

The tendency to form native aggregates minimizing the protein surface of the system was shown to be reduced when the histidine concentration is increased in a concentrated protein solution. Due to shielding of attractive charge-charge interactions the volume ex-

clusion between the IgG molecules is potentially reduced resulting in a decrease of the total free energy of the system. Therefore, association is no longer that pronounced in order to minimize accessible surface. Alford et al. (2008b) reported an enhanced aggregation in concentrated rhIL-1ra solutions (200 mg/ml) at low ionic strength presumably due to a reduced screening of the attractive interactions. In our study the IgG solutions containing 20 mM histidine showed a two fold higher conductivity than the samples with only 10 mM histidine (Figure V-33).

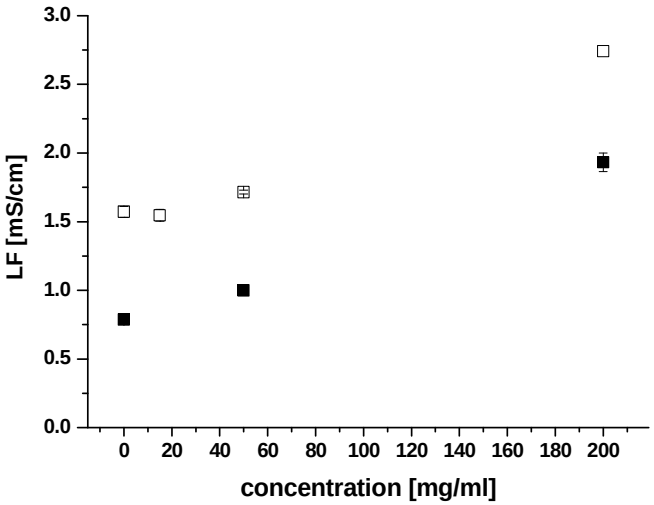

Figure V-33: Conductivity of IgG X solutions at pH 5.5
Solutions contain 20 mM histidine (black squares) and 10 mM histidine (plain squares).

Alford et al. (2008b) refer to cation-π interactions between monomers as a possible origin of attractive interactions that can contribute to aggregate formation (Raibekas et al. 2005; Woods 2004). Cation-π interactions can be qualitatively described by an electrostatic model, although dispersion forces and polarizability are additionally involved (Dougherty 1996). The aromatic side chains of the amino acid residues of phenylalanine, tryptophan and tyrosine are able to attract cations due to their significant quadrupole moment (Bohorquez et al. 2003). While phenylalanine is mostly completely buried in the interior of the protein, indolyl and hydroxyphenyl moieties of tryptophan and tyrosine are possibly displayed on the surface (Lucas et al. 2006). Thus, these residues are able to interact with a cationic solute like histidine reducing attractive interactions between the protein molecules and therefore aggregation. It is reported that an IgG was protected against aggregation at a

concentration of 100 mg/ml when histidine as a buffering component was applied. Both liquid and lyophilized formulations in the presence of mannitol, glycine, glutamic acid and polysorbate showed a reduced formation of soluble aggregates when histidine was added (Chen et al. 2003). When the concentration of histidine was nearly doubled from 10 to 25 mM the formation of aggregates was reduced by 50 %.

In contrast, there are several cases in literature, where aggregation formation was increased with increasing ionic strength. Especially at non isoelectric pH it is reported that electrostatic repulsion is reduced due to increasing salt concentration leading to aggregation. This was shown to be the root cause for aggregation of an IgG revealing an enhanced self-association at high ionic strength (Moore et al. 1999).

3.4 Effect of solute concentration on the viscosity of concentrated mAb solutions

It is known that the viscosity of a macromolecular system depends on the concentration, shape, and molecular weight of the dispersed molecules and the viscosity of the dispersion medium. The viscosity of an aqueous protein solution is reported to increases with increasing protein concentration (Ross and Minton 1977; Shire et al. 2004). Both mAbs, IgG X and IgG Z, showed an increase in viscosity during UF concentration up to 200 mg/ml (Figure V-34). The IgG X solutions revealed an increase in viscosity up to 13.8 mPas when the protein was concentrated to 200 mg/ml. For IgG Z an increase in viscosity was recognized up to 27.4 mPas at a protein concentration of 200 mg/ml.

This increased viscosity can introduce several challenges during manufacturing, filling and administration to the patient. Filtration and pumping operations can become infeasible with increasing protein concentration and the time required for filtration operations increases due to pore blocking of the filtration device. In the case of pumping, an introduction of heat to the product bulk due to increased resistance of the viscous solution can compromize product quality (Harris et al. 2004).

Beside the protein concentration, the viscosity of the solution depends on the extent of molecular interactions. Ionic strength influences protein solution viscosities by modulating the electrostatic contribution to the intermolecular potential. Shire and coworkers detail an analysis of a mAb at 100 mg/ml that reversibly self-associates leading to solutions

of higher viscosity in comparison to two non-associating molecules (Harris et al. 2004; Liu et al. 2005).

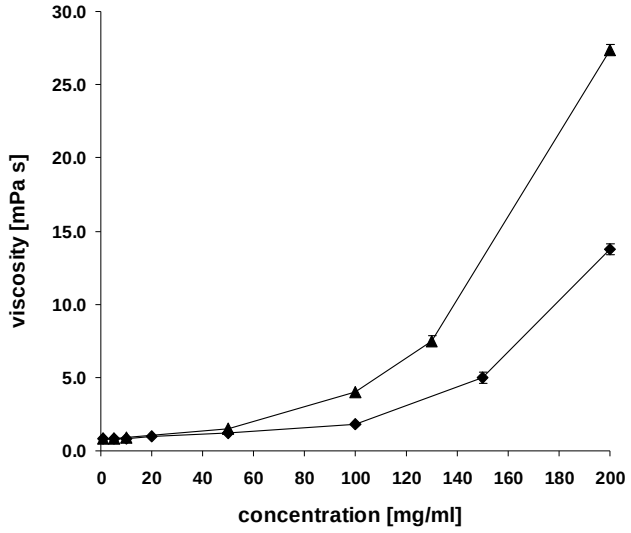

Figure V-34: Viscosity of the two mAbs as a function of protein concentration
IgG X (diamonds) and IgG Z (triangles) concentrated in 20 mM histidine buffer at pH 5.5 and 5.0; mean values of three measurements are presented ± SD.

It was observed that the highest viscosity appeared near the IP at low ionic strength. Moreover, the addition of sodium chloride at this pH led to a decrease in self-association and viscosity. Kanai et al. (2008) showed that in this case the Fab part of the molecule was the primary site mediating self-association. Since the addition of salts is reported to reduce the viscosity of the concentrated solutions it was expected that the use of a higher molarity of histidine respectively histidine hydrochloride should end up in a reduced viscosity as well (Figure V-35).

It was found that an increase in concentration of the buffer solute at a pH of around 5 was effective in reducing the viscosity of both mAb solutions at 130 and 180 mg/ml. At a protein concentration of 180 mg/ml of IgG Z the viscosity was reduced by about 33 % from 27.4 mPas to 18.4 mPas when the histidine concentration was increased from 10 mM to 30 mM. For IgG X a reduction in viscosity from 13.8 mM to 7.4 mPas was recognized when the histidine molarity was increased to 40 mM. In general, no further significant decrease in viscosity was detected when a concentration of about 40 mM histidine was reached.

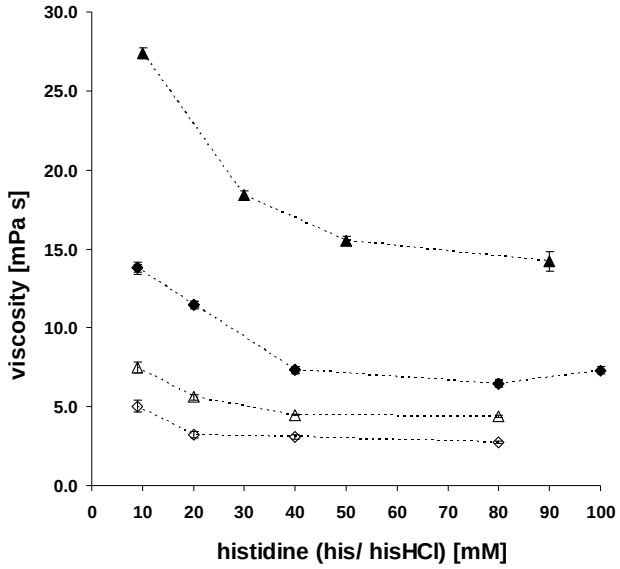

Figure V-35: Viscosity of two mAbs as a function of histidine/ histidine HCl molarity
IgG X at a concentration of 180 mg/ml, pH 5.5 (black diamonds), IgG X at a concentration of 130 mg/ml, pH 5.5 (white diamonds), IgG Z at a concentration of 180 mg/ml, pH 5.0 (black triangles) and IgG Z at a concentration of 130 mg/ml, pH 5.0 (white triangles); mean values of three measurements are presented ± SD.

Salinas at al. (2009) described that the addition of only 2 mM NaCl resulted in an approximately three fold decrease in the viscosity of a mAb at 80 mg/ml. Therefore, the effect of added sodium chloride on viscosity was compared to the effect of added histidine/ histidine hydrochloride. Moreover, the actual viscosity of the concentrated solutions after UF was determined containing 10 mM and 20 mM histidine. (Figure V-36).

A decrease in viscosity of the concentrated solutions was observable with increased molarity of both, sodium chloride and histidine. In comparison, the addition of sodium chloride results in slightly higher viscosity values when more than 20 mM salt were added. Chen et al. (2003) observed as well that an increase in histidine molarity was able to decrease the viscosity of an IgG. In our case increasing the histidine molarity from 10 to 20 mM was successful in decreasing the viscosity from 20 to about 15 mPas. The addition of 60 mM histidine resulted in a viscosity of < 10 mPas. The concentrates having 20 mM histidine present after UF revealed a decrease in viscosity from 27.4 mPas to 24.9 mPas compared to the solution having only 10 mM histidine present after UF.

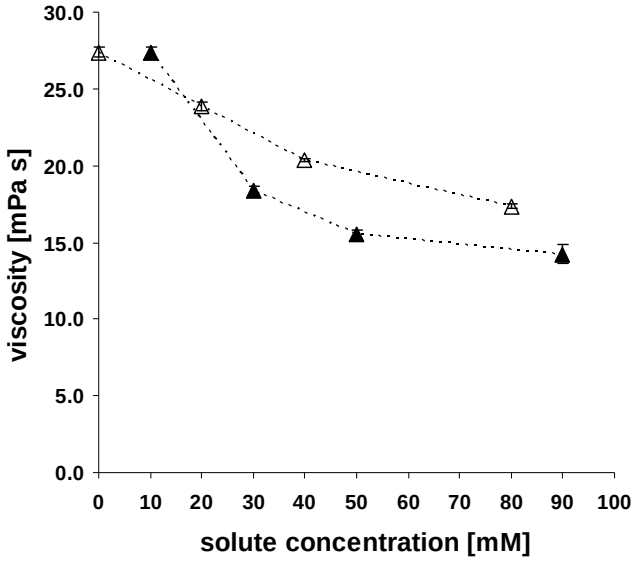

Figure V-36: Viscosity of IgG Z at 180 mg/ml, pH 5.0 as a function of buffer solute molarity
Addition of sodium chloride (white triangles) and addition of histidine/ histidine hydrochloride (black triangles); mean values of three measurements are presented ± SD.

4 Summary and conclusion

At the interface of downstream processing and final formulation of highly concentrated mAbs up to 200 mg/ml a significant deviation in solute concentration, pH and conductivity was observed with increased protein concentration during UF. During the concentration process of two IgGs the loss of histidine and the accumulation of acetate respectively were monitored and attributed to thermodynamic non-ideality. Electrostatic interaction between the protein and the buffer solutes at the non-isoelectric pH were identified to be the root cause of this phenomenon which is especially pronounced at high protein concentrations. The Donnan-equation was shown to be a feasible model to adequately reflect the experimentally determined molarities of cationic and anionic buffer solutes during UF processing of mAbs.

Therefore, the Donnan-equation was successfully used to predict the histidine molarity required before UF in order to achieve the desired concentration of 20 mM after UF and to avoid concomitantly an increase in pH during UF. It was shown that this approach was able to circumvent pH corrections in the final concentrated solutions and contributed thus to a reduced level of aggregates in the bulk solutions at 200 mg/ml. In addition, a

higher protein concentration was achieved, since the dilution of the bulk by the pH-corrective solution was avoided. Moreover, an improved chemical stability considering Fab deamidation at high protein concentrations was observed which was again related to stable pH conditions and an increased histidine molarity during UF processing.

In the case of histidine, it was shown that the loss of this buffer solute during UF can affect the physical stability of an IgG1 in solution. The add-on of histidine contributed to a reduced level of HMWs and proteinaceous particles especially at an IgG concentration of 200 mg/ml.

In addition, the add-on of histidine can contribute to a decrease in viscosity which is strongly increased at high protein concentrations.

Chapter VI Investigation of heterogeneous nucleation dependent aggregation of mAbs during purification

Abstract

The downstream process of biotechnologically produced proteins comprises in general at least one chromatographic step to ensure the removal of aggregated species. However, rate and onset of aggregation are usually not predictable and aggregation occurs also after the aggregate competent step. This is reported to depend on environmental conditions encompassing the contact to different surfaces and the presence of exogenous particles of divers materials which are currently under discussion to induce protein aggregation via a heterogeneous nucleation controlled mechanism.

In this study protein aggregation was examined in the course of the purification process, since the protein is exposed here to numerous surfaces which are moreover a potential source of shed and abraded particles. Thus, IgG aggregation was investigated in the presence of three different chromatographic matrices based on glass, agarose and polymethacrylate. Adsorption of the IgG and its aggregates to the micro- and nano-sized particles was evaluated at different pH values and the formation of differently sized aggregates was monitored over time. Conformational stability of the IgG was investigated by (ATR) FT-IR and UV spectroscopy.

Moreover, a typical process related impurity, indigenous proteins expressed by the applied host cell, was investigated considering the potential to induce aggregation of an IgG. Therefore, purified host cell proteins (HCPs) from a CHO master cell, usually applied to produce IgGs, were characterized considering their molecular weight and IP and

IgG aggregation was monitored in the presence of these HCP species under different environmental conditions.

1 Introduction

Aggregation of therapeutic proteins can potentially occur during all stages of the lifetime of a protein, including refolding, purification, storage, shipping and delivery to the patient.

The purification process offers various capabilities to decrease the level of proteinaceous aggregates. Usually, the intermediate purification steps are dedicated to remove higher molecular weight species (HMWs) beside other undesired product variants (Kelley et al. 2008b). CEX, HIC, reversed phase chromatography and hydroxyl apatite have been shown to offer sufficient capability concerning the removal of mAb aggregates (see chapter I). Mostly, CEX in binding mode is used in cGMP purification processes and soluble aggregates are separated from the desired product species during washing or gradient elution using sodium chloride (Fahrner et al. 2001; Kelley et al. 2008a). The removal performance is highly governed by pH and counter ion concentration of the load, wash and elution solutions used. In general, the removal of HMWs, encompassing soluble dimers and oligomers, can be challenging if their level exceed a few percent in product mass (Karlsson et al. 1998; Williams and Frasca 2001).

The capability to remove aggregates after the dedicated chromatographic steps is limited to larger insoluble aggregates and particles which can be usually addressed by micro filtration (Chi et al. 2005b; Sifton 2002). This constraint is relevant for purification intermediates as well as for fully purified material or formulated bulks, since aggregation behavior including onset, rate and morphology of the aggregated state is usually not predictable. Hence, the environmental conditions as well as the mechanisms leading to aggregation phenomena need to be elucidated to prevent the protein from aggregation. Protein aggregation is known to depend on environmental conditions such as temperature, storage period, pH and the presence or absence of solutes and stabilizing excipients (Carpenter et al. 1999; Chi et al. 2003b; Manning et al. 1995; Manning et al. 1989b; Wang 1999; Wang 2005). Moreover, the induction of protein aggregates was observed in the presence of exogenous micro- and nano-sized particles of different materials. Nano-sized silica particles (Chi et al. 2005b), silicone oil droplets (Jones et al. 2005; Thirumangalathu et al. 2009),

teflon beads (Sluzky et al. 1991), as well as micro-particles out of stainless steel (Bee et al. 2009a) or tungsten (Bee et al. 2009b; Jiang et al. 2009) are reported to cause protein aggregation.

In general, the adsorption of protein molecules to interfaces and solid surfaces is known to potentially induce aggregation. The adsorption process is mostly driven by either hydrophobic interactions or electrostatic interactions between the surface and the protein (Norde 1995; Norde and Lyklema 1978). As a consequence of the surface contact, partial unfolding of the protein molecules may occur, and these structurally perturbed molecules are reported to be precursors for aggregation (Dong et al. 1995; Fink 1998; Fink et al. 1994; Kendrick et al. 1998a).

In the presence of the nano- and micro-sized solid particles, as reported above, partial unfolding of the protein molecules was hardly recognized, although the formation of aggregates was clearly enhanced and the monomer population was depleted. It is discussed in current literature that aggregation is inherently a nucleation and growth phenomenon, where molecules have to accumulate, eventually exceed their solubility and can actually precipitate (Chi et al. 2005a). Stable assembly of the molecules into a so-called critical-sized nucleus and further its growth into larger aggregates is not possible until an energy barrier is overcome which results from the free energy required to build a new solid-liquid interface (Debenedetti 1996). Existing particles in solution can serve as so-called heterogeneous nuclei facilitating the accumulation of the protein molecules and thus their aggregation. Heterogeneous nucleation dependent aggregation can be potentially prevented, if the protein is hindered to adsorb to the particle surface. This was shown for hydrophilic glass particles and silicon oil droplets by adding surfactant to the protein solutions (Chi et al. 2005b; Thirumangalathu et al. 2009).

In general, the protein is exposed to numerous surfaces during all stages of the manufacturing process, as well as during storage, and particles can be shed or abraded from all of them and thus potentially enter the protein bulk solutions. As regards the purification process, the protein is exposed to large surfaces during preparative chromatography and various filtration steps. Moreover, particles from the packed chromatographic bed may be introduced into the eluate serving as heterogeneous nuclei. Usually, the micro-sized chromatographic beads are retained in the packed column by a frit out of metal, glass of plastic. However, grinding of the beads can potentially occur due to high pressure caused by the compression via drag forces exerted by fluid flow through the bed especially at large scale

(Tran et al. 2007). Thus, small fragments of different matrix materials can potentially pass through the frit and may enter the purified protein bulk. Mostly, matrices based on glass, polysaccharides or the synthetic polymer polymethacrylate are usually applied in cGMP purification processes of therapeutic mAbs (Fahrner et al. 2001; Fahrner et al. 1999; Hahn et al. 2003).

Beside these already mentioned particles which can be shed or abraded from the bio-processing equipment, containers or closures, foreign proteinaceous species are suspected to induce heterogeneous nucleation dependent aggregation of the therapeutic protein (Arakawa et al. 2006). The coding gen-sequence of mAbs is usually expressed in mammalian host cells, e.g. CHO cells (Prouty et al. 1975). Therefore, process related impurities such as indigenous proteins expressed by the host cell (called host cell proteins: HCPs), DNA or cellular components are present in the harvested cell culture fluid as well as in the purification intermediates and can potentially facilitate aggregation of the therapeutic protein.

In this study, aggregation of an IgG was investigated in the course of protein purification. Interaction of the protein with various marketed chromatographic resins which are commonly applied in cGMP purification processes of mAbs, were investigated. The potential induction of aggregates was monitored by SE-HPLC and turbidity measurements. Potential heterogeneous nucleation dependent aggregation was studied in the presence of nano- and micro-sized chromatographic particles as well as HCPs from CHO cells.

2 Materials and methods

2.1 Materials

A completely purified bulk of a chimeric human Fc (IgG4)/ rat Fab antibody in histidine buffer pH 6.0 was taken for the experiments. The mAb was provided by Roche Diagnostics GmbH (Penzberg, Germany). Aliquots were dialyzed into 100 mM acetate pH 3.0, 100 mM acetate pH 5.0 and 200 mM tris(hydroxymethyl)-aminomethan pH 7.5. Afterwards, the solutions were filtered by using a Sterivex-GV 0.22 µm filter (Millipore, Billerica, USA).

Porous chromatographic beads of different matrix materials were applied. Controlled pored glass (CPG 700) particles from Millipore (Billerica, USA), sepharose (cross-linked agarose) beads from GE Healthcare (Uppsala, Sweden) and polymethacrylate based media (Toyopearl HW-65M, Tosoh Bioscience, Stuttgart, Germany) were used. Moreover, the corresponding functionalized Protein A affinity and IEX resins were obtained from Millipore (ProSep vA ultra), GE Healthcare (MabSelect) and Tosoh (Toyo CM 65M and Toyo Q 65M).

A CHO master cell usually applied to produce IgG and identical to the CHO master cell (Roche Diagnostics GmbH, Penzberg, Germany), except the gene encoding the therapeutic protein ("null" CHO cell), was fermented under typical expression conditions (Rathore et al. 2003) to obtain host cell proteins (HCPs). The HCPs were purified from the filtered harvested cell culture fluid by using ammonium sulfate precipitation. Therefore, 2.6 mol ammonium sulfate per liter culture fluid were added and the precipitate was collected by filtration (Sartopure PP2 20, Sartorius, Goettingen, Germany). The precipitate was then removed from the filter by washing with phosphate buffer pH 7.2 containing 20 mM sodium phosphate and 150 mM sodium chloride. The solution was afterwards concentrated and diafiltrated in this phosphate buffer to get rid of the ammonium sulfate applying a 5 kDa UF membrane (Hydrosart, Sartorius, Goettingen, Germany). This HCP standard solution was then stored at -70 °C. Before performing the seeding experiments, the thawed HCP standard solution (HCP concentration about 10 mg/ml) was diluted 1:10 with acetate buffer pH 5.0 and was filtered by using a 0.2 µm Sterivex-GV filter (Millipore, Billerica, USA). The concentration of CHO HCP in solution was determined by an in-house enzyme-linked immunosorbent assay (ELISA) (Roche Diagnostics GmbH, Penzberg, Germany) as required by the ICH guideline Q6B (ICH 1999a) and is in general described elsewhere (Champion et al. 2005; Eaton 1995).

All chemicals and reagents used were at least analytical grade. Acetic acid was taken from Fluka (Steinheim, Germany), citric acid, hydrochloric acid, sodium hydroxide, ammonium sulfate and sodium chloride were taken from Merck KG (Darmstadt, Germany), tris(hydroxymethyl)-aminomethan was taken from Angus (Ibbenbueren, Germany). L-histidine from Ajinomoto (Raleigh, USA) was used.

2.2 Adsorption experiments

Adsorption of the mAb to the different chromatographic surfaces was investigated at different pH by incubating a defined surface of the beads with a defined protein mass. Therefore, the bead slurry was suspended and mixed with purified and 0.2 µm filtered water (Milli-Q, Millipore, Billerica, USA). The beads were collected by vacuum filtration (0.22 µm cellulose filter discs, Sartorius, Goettingen, Germany) and were afterwards rinsed with purified and 0.2 µm filtered water (Milli-Q, Millipore, Billerica, USA). Subsequently, the beads were dried at 40 °C and a defined mass was weighed representing a defined surface as determined by BET gas adsorption experiments. Therefore, about 0.2 g of each bead matrix were mixed in sterile 5 ml CRYO.S tubes (Greiner Bio-One, Frickenhausen, Germany) with about 5 ml of an IgG solution (5 mg/ml) at pH 3.0, pH 5.0 and pH 7.5. The samples were incubated without head space on the rotary mixer RM5 (Froebel, Lindau, Germany) at 35 rpm for 12 hours at room temperature. The samples were then centrifuged for 10 min at 10 000 x g to separate the beads from the protein solution. The amount of IgG adsorbed to the respective surface was determined by subtracting the amount of the protein determined in the supernatant from the amount of protein initially present before incubation. Adsorption to the tubes used was found to be neglectable, since < 1 % of total protein were adsorbed to the tubes after incubation for 12 hours at pH 3.0, pH 5.0 and pH 7.5.

Adsorption isotherms were determined by preparing samples containing 5 m² CPG surface and various concentrations of the IgG between 0.2 and 6.0 mg/ml at pH 5.0 and pH 7.5. Again the bead matrix was mixed in sterile 5 ml CRYO.S tubes (Greiner Bio-One, Frickenhausen, Germany) with about 5 ml of the respective IgG solution (5 mg/ml). The samples were incubated over 12 hours as described before and were centrifuged for 10 min at 10 000 x g to separate the beads from the protein solution and to determine the protein concentration in the supernatant. The amount of protein adsorbed was determined by subtracting the amount of the protein determined in the supernatant from the amount of protein initially present before incubation.

To look at preferential adsorption of HMWs on the CPG surface, IgG solutions at pH 5.0 containing 3.2 %, 5.7 % and 6.8 % HMWs were incubated with 0.1-10 m² CPG surface. The bead matrix was mixed in sterile 4 ml CRYO.S tubes (Greiner Bio-One, Frickenhausen, Germany) with about 4 ml of the respective IgG solution (about

5 mg/ml). The samples were incubated over 12 hours as described before and were centrifuged for 10 min at 10 000 x g to separate the beads from the protein solution and to determine the protein concentration in the supernatant. In addition, the supernatant was analyzed by SE-HPLC. The amount of adsorbed HMWs and monomers in percent was determined by subtracting the amount of HMWs determined in the supernatant from the amount of HMWs initially present before incubation.

2.3 Seeding experiments

Chromatographic beads were suspended in water and were sonicated to obtain nano-sized seeds. Therefore, the Sonoplus Ultrasonic Homogenizer (Bandelin Electronic, Berlin, Germany) at a processing frequency of 20 kHz over 3x10 min using the 3 mm microtip sonotrode was applied. After 20 min hold time the very large particles remaining in solution sedimented and the size distribution by intensity of the sonicated particles in the supernatant was recorded by using laser diffraction. The fragmented suspended particles after 10 min and 30 min sonication time were washed with purified and 0.2 µm filtered water (Milli-Q, Millipore, Billerica, USA) and dried in air at 35 °C. 50, 100, 150 and 200 m^2 bead surface per gram protein were seeded into IgG solutions at pH 5.0, at pH 5.0 with 150 mM sodium chloride and at pH 7.5 with an initial protein concentration of 6 mg/ml (total protein: about 30 mg) and 6 % HMWs. The samples were incubated over one week without head space on the rotary mixer RM5 (Froebel, Lindau, Germany) at 35 rpm at room temperature. At each time point, the samples were centrifuged for 10 min at 10 000 x g to separate the beads from the protein solution. Protein concentration determination, turbidity measurements and SE-HPLC analysis were performed with the supernatant of the centrifuged samples.

To investigate the effect of HCP on aggregation, IgG solutions at pH 3.0, at pH 5.0, at pH 5.0 with 10, 100, 150 and 250 mM sodium chloride and at pH 7.5 with an initial protein concentration of about 5 mg/ml (about 20 mg total protein) were spiked with 0 ng, 500 ng and 1000 ng HCP per mg IgG by using the diluted HCP standard solution. The samples were incubated at room temperature and at 40 °C in sterile 4 ml CRYO.S tubes (Greiner Bio-One, Frickenhausen, Germany) without head space on the rotary mixer RM5 (Froebel, Lindau, Germany) at 35 rpm. Aggregate formation was monitored by SE-HPLC and turbidity measurements in the HCP-spiked and unspiked solutions.

2.4 Concentration determination

Concentration was determined by using the photometric absorbance at 280 nm and 320 nm after buffer blank subtraction (UV-Vis spectrophotometer Evolution 500, Thermo Fisher Scientific, Waltham, USA). The absorbance at 320 nm was subtracted from the absorbance at 280 nm (UV 280-320) and this value was used to calculate the protein content according to the law of Lambert-Beer.

2.5 Turbidity measurements

The turbidity of the seeded solutions was determined after centrifugation as the photometric absorbance at 350 nm after buffer-blank subtraction (UV-Vis spectrophotometer Evolution 500, Thermo Fisher Scientific, Waltham, USA).

2.6 Size exclusion high pressure liquid chromatography

SE-HPLC analysis was conducted with a TSK 3000 SWXL column (Tosoh Biosep, Stuttgart, Germany) on a Summit HPLC-system (Dionex, Idstein, Germany). The elution peaks were monitored at 280 nm by the UV diode array detector UVD170U from Dionex (Idstein, Germany). Isocratic chromatography was conducted as described in chapter III. The chromatograms were integrated manually by using the Chromeleon software (Dionex, Idstein, Germany). This is shown exemplarily in Figure III-1 (see page 52). The percentage of higher molecular weight species (HMWs) including dimers and larger soluble oligomers was determined as relative area (mAU·min) of the respective peaks referred to total area of all peaks including the monomer peak and the peak of the lower molecular weight species (LMWs).

2.7 FT-IR spectroscopy

Both, the CPG and the ProSep vA ultra particles were incubated at room temperature for 12 hours with a 6 mg/ml solution of IgG in acetate buffer at pH 5.0. The solutions showed a level of 1.5 % HMWs determined by SE-HPLC before incubation. Incubation was conducted in saturation mode. After centrifugation for 10 min at 10 000 x g, the particles were washed two times with 2 ml acetate buffer pH 5 since nearly no protein was de-

tectable in the washing solution by using UV 280-320. FT-IR spectra of the adsorbed protein were recorded with the Tensor 27 (Bruker Optics, Ettlingen, Germany) by applying the slurry directly on the Germanium crystal of the MIRacle attenuated total reflection (ATR) cell to investigate the secondary structure of the protein on the chromatographic particles. The AquaSpec transmission cell was used to investigate the protein secondary structure after desorption from the particles. Therefore, the particles were incubated in 200 mM tris buffer pH 9.0 to remove the protein from CPG and in 100 mM acetate buffer pH 3.0 to remove the protein from ProSep vA ultra. Incubation time was 12 hours.

For each spectrum which was recorded from 850-4000 cm^{-1} a 120-scan interferogram was collected at a double sided acquisition mode with a resolution of 4 cm^{-1}. The reference spectrum of the respective buffer and the respective wetted particles was subtracted to obtain the protein spectrum. The spectra were edited by a vector normalization followed by the generation of the second derivative smoothed using a 13-point Savitsky-Golay smoothing function applying the OPUS 6.0 software (Bruker Optics, Ettlingen, Germany). Moreover, the absorption spectra recorded in ATR mode were corrected concerning band intensity and band position to allow the comparison to spectra recorded in transmission mode. Therefore, the extended ATR-correction of the software OPUS 6.0 (Bruker Optics, Ettlingen, Germany) according to Fringeli (1992) was used to overcome wave number dependent anomalous dispersion (Goldberg and Chaffotte 2005; Grdadolnik 2002).

2.8 Second derivative UV spectroscopy

Tertiary structure of the protein in solution was examined by 2D-UV spectroscopy using the Uvikon XL (Goebel Elektro, Ludwigshafen, Germany). The protein was desorbed from the chromatographic surfaces by using a buffer at pH 9.0 to desorb the protein from the CPG particles and by using a buffer at pH 3.0 to remove the protein from ProSep vA ultra. Afterwards, the samples were diluted to a protein concentration of 1.0 mg/ml. Absorbance spectra from the near-UV region between 250-320 nm were collected at a scanning speed of 50 nm/min, a bandwidth of 1 nm and a scanning step interval of 0.5 nm. The OPUS software (Bruker Optics, Ettlingen, Germany) was used to enhance the resolution, concomitantly preserving the band position. The second derivative was smoothed applying a 13-point Savitsky-Golay smoothing function.

2.9 Laser diffraction

Particle size distribution by intensity of the chromatographic particles was determined by using the Horiba LA-950 (Retsch, Haan, Germany) equipped with two laser light sources at 650 and 405 nm and 23 wide angle detectors. The particles were suspended in purified and 0.2 µm filtered water (Milli-Q, Millipore, Billerica, USA) using the low volume cuvette LA-950. A sample refractive index of 1.51 for the glass particles, of 1.54 for the sepharose beads and of 1.49 for the polymethacrylate beads were applied. A refractive index of 1.33 for water was used. Based on the Mie-Scattering theory a particle size over a range of 0.01-3000 µm can be determined from the recorded intensity and angle of the scattered light using the LA-950 software (Retsch, Haan, Germany).

2.10 BET gas adsorption

Multipoint (10 measurement points) Brunauer-Emmett-Teller (BET) specific surface area of the chromatographic beads was determined at 77 K with the TriStar II 3020 (Micromeritics, Mönchengladbach, Germany). Nitrogen was used as an adsorbate. For each measurement at least 0.2 g of the chromatographic beads were applied. Before measuring, the samples were stored under vacuum at 45 °C for 24 hours. A relative gas pressure (p/p_0) of 0.06-0.30 was applied.

2.11 Scanning electron microscopy

Scanning electron microscopy (SEM) was carried out using the JSM-6500F (Joel, Eching, Germany). The beads were dried in a VO 200 vacuum chamber (Memmert, Schwabach, Germany) and coated with a fine carbon layer before starting the surface morphology analysis.

2.12 Zeta potential measurements

To determine the charge of the protein, the HCP and the sonicated nano-sized CPG 700 at different pH, electrophoretic mobility of the proteins and the CPG 700 particles were determined by performing Laser-Doppler-Velocimetry using the Malvern Zetasizer

Nano S (Malvern Instruments, Worcestershire, UK). The zeta potential ζ was calculated from the Henry's equation (Henry 1931) with assumption of uniform charge distribution by using the Malvern DTS software (Version 5.0, Malvern Instruments, Worcestershire, UK) (see Equation V-6). For sample preparation a 5 mg/ml mAb solution and a 5 mg/ml HCP standard solution were dialyzed into 10 mM acetate buffer pH 5.0 and were titrated to a pH of 2.0 afterwards by using 0.2 M hydrochloric acid. The CPG 700 particles were suspended in the same buffer system and the pH was adjusted to 2.0. All samples were titrated with a 0.2 M sodium hydroxide solution from pH 2 to pH 12 by applying the titrator MPT2 (Malvern Instruments, Worcestershire, UK). The zeta potential was determined in 15 steps between pH 2 and pH 12 in a temperature controlled folded capillary cell (Malvern Instruments, Worcestershire, UK) at 25 °C.

2.13 Sodium dodecyl sulfate-polyacrylamide gel electrophoresis

Non-reducing sodium dodecyl sulfate-polyacrylamide gel electrophoresis (SDS-PAGE) was performed by using the Novex mini-Cell system (Invitrogen, Karlsruhe, Germany) equipped with 4-20 % tris-glycine gels. The protein solutions were diluted to 1 mg/ml by using the appropriate bulk buffer. Subsequently, the samples were diluted 1:1 with tris-glycine SDS sample buffer containing 2 % SDS (Invitrogen, Karlsruhe, Germany) and denatured at 70 °C for 10 minutes. The amount of IgG per well was 2 µg per sample. As running buffer tris-glycine SDS running buffer (Invitrogen, Karlsruhe, Germany) was used. Electrophoresis was performed at 200 V. As molecular weight standard the Mark12 from Invitrogen (Karlsruhe, Germany) was applied. The gels were stained with silver by using the Silver Xpress Staining Kit according to the Kit manual (Invitrogen, Karlsruhe, Germany).

2.14 Two-dimensional-gel electrophoresis

Two-dimensional-gel electrophoresis (2D-gel electrophoresis) of the HCP standard solution was performed after sample preparation with the Perfect-FOCUS Kit (Calbiochem, San Diego, USA). The precipitated protein pellet was resolved in 200 µl buffer (containing 8 M urea, 2% CHAPS, 0.002% bromphenol blue, 20 mM DTT and 0.5 % IPG buffer). Both, isoelectric focusing (IEF) and SDS-PAGE were performed by using the ZOOM

Benchtop System (Invitrogen, Karlsruhe, Germany). For IEF, 7 cm buffer hydrated IPG strips with a non-linear pH gradient from 3-10 were applied. Focusing was carried out at 175-2000 V for 2 hours. Afterwards, the proteins in the IPG strips were denatured and reduced for 15 min by incubating the strips in equilibration buffer containing 2 % SDS and 1 % DTT. Afterwards, the strips were incubated in equilibration buffer containing 2.5 % iodoacetamide for 15 min to alkylate the proteins.

The IPG strips were than placed on top of the SDS gel (4-12% tris-glycine gels) and sealed onto the gel. SDS-PAGE was performed by using the MES SDS running buffer. The gels were run at 100-200 V for about 2 hours. As molecular weight standard the Mark12 from Invitrogen (Karlsruhe, Germany) was applied. The gels were stained with silver by using the Silver Xpress Staining Kit according to the Kit manual (Invitrogen, Karlsruhe, Germany).

3 Results and discussion

3.1 Characterization of chromatographic surfaces

In general, the matrix material of the chromatographic solid phase, the particle- and the pore diameter have impact on the mechanical and physical stability of the beads, the resolution and selectivity and the accessible surface and hence binding capacity (Boschetti 1994; Jungbauer 2005).

On the one hand, one is usually interested in applying a high flow velocity of the mobile phase to decrease cycle time during chromatography. Therefore, the bead matrix has to be rigid enough to circumvent sorbent shrinkage and high back-pressure. On the other hand, a high binding capacity is desired which is usually achieved by applying highly porous materials (LeVan et al. 1997; Yao and Lenhoff 2006). Moreover, these porous materials also show a good mass transfer characteristic reducing, among other parameters, peak dispersion and band spreading (Van Deemter et al. 1956).

The features of the matrices are mutually exclusive to some extent, since porous materials like sepharose can have good mass transfer characteristics but low equilibrium capacity due to limited surface area and can not be operated at very high flow velocities due to their porosity and hence softness. Rigid and hence less porous materials like glass are more mechanically stable but concomitantly they can show increased mass transfer resistance and a reduced accessible surface (Hahn et al. 2003). Moreover, smaller beads are applied to increase the number of plates and hence the separation capacity. Concomitantly, this requires more rigid matrices since smaller beads lead to increased back-pressure which can be easily overcome by using a more rigid material.

The matrices out of CPG, sepharose and polymethacrylate were investigated by SEM at 400-10 000 times magnification (Figure VI-1A-C). The shape of the sepharose and polymethacrylate beads is perfectly spherical whereas the CPG particles are fragmented pieces which are irregularly shaped with sharp edges. The surface of all matrix materials is highly porous. The pore-size estimated from the SEM pictures at 10 000 times magnification is around 1000 Å, as pictured in A2 which refers to the CPG surface.

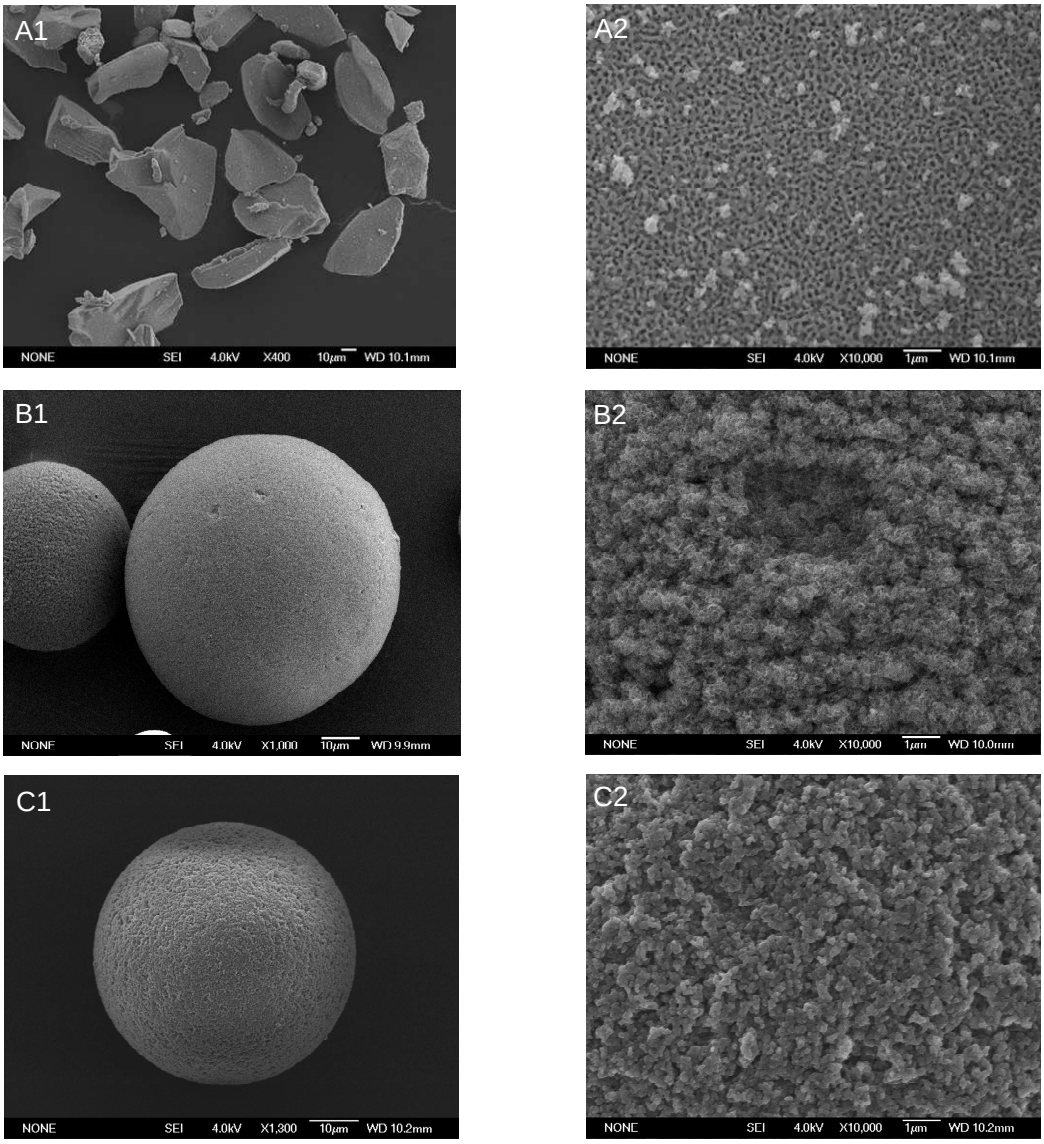

Figure VI-1: SEM pictures of chromatographic surfaces at 400-1000x (left) and at 10 000x (right) magnification
Pictures of CPG (A), sepharose (B) and polymethacrylate (C) beads.

The CPG surface shows a very uniform porous structure which can be explained by the production procedure. Porous glass is obtained by polycondensation of sodium silicate usually under mild acidic conditions (Tarutani 1984). After the formation of an aqueous silica gel the surface area, porous volume and pore size of the final solid particles can be precisely controlled by time, temperature, pH and added electrolytes (Iler 1979; Von Vansant et al. 1995). Therefore, CPG was initially applied in liquid chromatography and here

especially in gel permeation chromatography due to extremely sharp pore-size distributions (Haller 1965).

Polysaccharide networks as present in agarose gels are often cross-linked with divinyl sulphone to improve the mechanical stability of the material (Andersson et al. 1998; Porath et al. 1975). Thus, the surface pore-structure is more irregularly formed as observed in picture B2 compared to the CPG surface.

A quite similar irregular sponge-like surface structure as recognized for the agarose beads was observed for the polyacrylamide beads at 10 000 times magnification (picture C2). Polyacrylamide cross-linked with methylene-bisacrylamide is well known to result in low and defined exclusion limits and thus in a fine pored and dense material (Boschetti 1994; Gressel and Robards 1975). Therefore, this material is essentially used for gel filtration chromatography.

The pore size values of the different matrices determined by mercury porosimetry were collected from the literature provided by the respective manufacturers. Table VI-1 shows the reported values. All matrices show a pore diameter between 560 and 1000 Å. Therefore, the structure can be described as macro-porous according to the IUPAC classification of pores (Everett 1972). Since IgG monomers have a hydrodynamic diameter of about 100 Å (see chapter III) their diffusion into the pores of the beads is not limited by the size and therefore the inner surface is in all cases accessible for the adsorption of an IgG. Moreover, most soluble aggregates separated by SE-HPLC are expected to enter the inner surface as well, since an octamer shows only a doubled hydrodynamic diameter of about 200 Å referred to the hydrodynamic diameter of the monomer (see chapter IV). This is expected to be still small enough to enter the inner surface of all three chromatographic matrices.

Regarding the size of the chromatographic particles, the CPG fragments show a mean particle diameter of about 125 µm, whereas the sepharose and the polymethacrylate beads are smaller. These particles show a mean particle diameter of 85 µm and 72 µm respectively determined by laser diffraction (Table VI-1).

Matrix material	Mean particle diameter [µm]	Multipoint BET specific surface area ± SD [m²/g]	Pore diameter* [Å]
Controlled pored glass (CPG)	125 ± 60	35.99 ± 3.52	700
Sepharose	85 ± 37	89.41 ± 2.34	560
Polymethacrylate	72 ± 19	12.33 ± 0.26	1000

* Determined by mercury porosimetry. Values were taken from the material description of CPG 700 (www.millipore.com), MabSelect (www.gehealthcare.com) and Toyopearl HW-65M (www.tosoh.com).

Table VI-1: Mean particle diameter determined by laser diffraction and BET specific surface area of the chromatographic beads
Results are presented as mean values of three measurements ± SD.

The specific surface area of the CPG particles was determined to 36 m²/g while the value for the sepharose beads was much higher showing a specific area of 89 m²/g. The polymethacrylate beads exhibit the lowest specific surface area of 12 m²/g as a consequence of their large pore size. These beads are more porous compared to the other two matrices, since their accessible surface is much lower and their pore size is much larger. The sepharose beads can be considered as the densest ones, since their accessible surface is much higher and their pore size is smaller compared to the other matrices.

3.2 Adsorption to porous chromatographic matrices

About 0.2 g of the unfunctionalized chromatographic matrices based on CPG, sepharose and polymethacrylate were incubated with the IgG solutions at pH 3.0, pH 5.0 and pH 7.5. The mass of protein adsorbed to the chromatographic surface was referred to the mass of protein initially present as 100 %. Moreover, this value was divided by the surface area which was incubated with the protein solution, to compare the efficacy of the different matrices (per m²) in adsorbing the IgG. In addition, the commonly applied functionalized beads of the different matrices were incubated as well and adsorption efficacy was compared to the unfunctionalized surfaces. This was done to evaluate unspecific adsorption to the bead matrix.

3.2.1 MAb adsorption

The CPG matrix shows the highest adsorption at pH 5.0, while the adsorption of the IgG is reduced at a lower pH of 3.0 and at a higher pH of 7.5 (Figure VI-2).

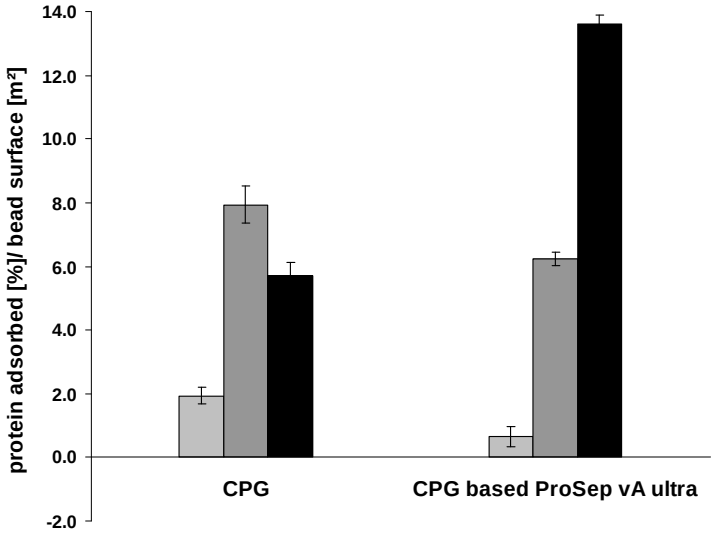

Figure VI-2: Adsorption of IgG to CPG based matrices at pH 3.0, pH 5.0, pH 7.5
Percent protein mass adsorbed per square meter matrix; protein mass initially present in solution was about 25 mg (initial concentration = 5 mg/ml, volume = 5 ml); adsorption at pH 3.0 (light grey), at pH 5.0 (dark grey) and at pH 7.5 (black); results are presented as mean values of three measurements ± SD.

In comparison, the ProSep vA ultra medium shows the highest adsorption of the IgG at pH 7.5. ProSep vA ultra is a functionalized CPG material having a Protein A affinity ligand coupled to its surface. The adsorption of mAbs to the Protein A ligand usually increases with pH and shows a maximum at a pH > 5 (see chapter I). At a pH of 5.0 adsorption of the IgG to CPG was observed to be comparable to the functionalized Protein A gel. Thus, the IgG is considered to be mainly unspecifically adsorbed to the glass matrix at this pH.

Adsorption to sepharose beads was found to be negligible. Almost no IgG adsorbs to the sepharose surface at a pH between 3.0 and 7.5 (Figure VI-3). In comparison, MabSelect which is a Protein A affinity resin as well, but based on sepharose, shows again a pH dependent adsorption as expected. The higher the pH, the more IgG is bound to the resin. At a pH of 7.5 the highest amount of IgG was adsorbed per square meter gel. In general, the overall capacity to adsorb the mAb on the surface is reduced compared to the CPG based MabSelect and the unfunctionalized CPG.

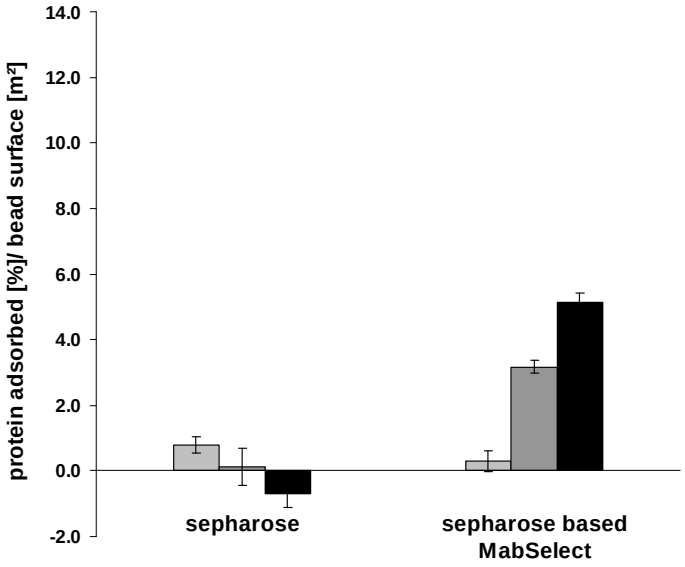

Figure VI-3: Adsorption of IgG to sepharose matrices at pH 3.0, pH 5.0, pH 7.5
Percent protein mass adsorbed per square meter matrix; protein mass initially present in solution was about 25 mg (initial concentration = 5 mg/ml, volume = 5 ml); adsorption at pH 3.0 (light grey), at pH 5.0 (dark grey) and at pH 7.5 (black); results are presented as mean values of three measurements ± SD.

Adsorption of the IgG to the unfunctionalized polymethacrylate beads was observed to be negligible as well. Almost no protein was lost on the surface during incubation at pH 3.0, 5.0 and 7.5 (Figure VI-4).

Moreover, the weak CEX resin having a carboxy-methyl (CM) functionalization on the surface adsorbs the IgG at pH 3.0 and 5.0 as expected, since the protein is predominantly positively charged at these pH values. Adsorption capacity is in general clearly reduced compared to the affinity matrices based on CPG and sepharose presented above. At pH 7.5 almost no protein adsorbs to the resin, since the net charge of the protein is strongly reduced at a pH closely to the IP of the protein. The strong IEX resin based on sepharose, exhibiting a quaternary ammonium function (Q) on the surface, shows no adsorption of the IgG at a pH between 3.0 and 7.5, since the protein is here predominantly positively charged.

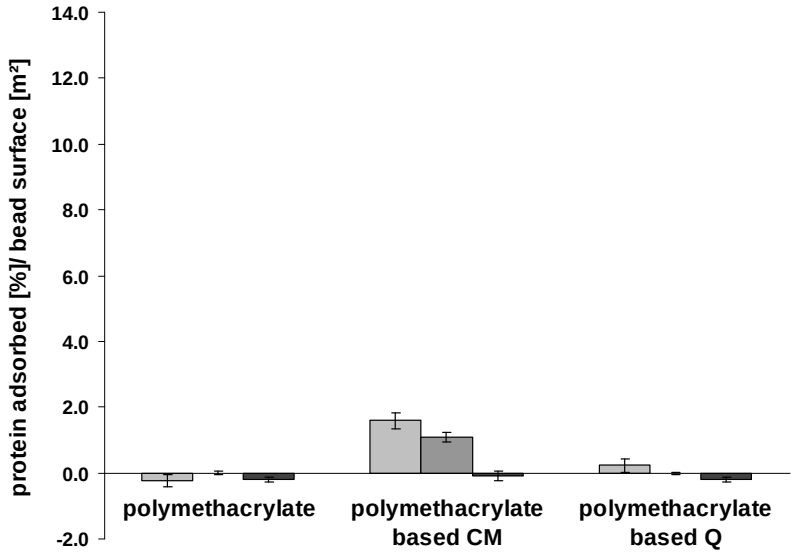

Figure VI-4: Adsorption of IgG to polymethacrylate matrices at pH 3.0, pH 5.0, pH 7.5
Percent protein mass adsorbed per square meter matrix; protein mass initially present in solution was about 25 mg (initial concentration = 5 mg/ml, volume = 5 ml); adsorption at pH 3.0 (light grey), at pH 5.0 (dark grey) and at pH 7.5 (black); results are presented as mean values of three measurements ± SD.

In summary, the unfunctionalized CPG matrix shows the highest adsorption capacity of the IgG. This is especially pronounced at pH 5.0 while unfunctionalized sepharose and polymethacrylate beads did not show any noteworthy adsorption capacity, neither at acidic pH, nor at a more neutral pH.

3.2.2 Aggregate adsorption

Before and after incubation of the IgG solution with the different chromatographic surfaces at pH 3.0, pH 5.0 and pH 7.5, the solutions were analyzed by SE-HPLC. It was observed that after incubation with the unfunctionalized CPG surface at pH 5.0 and 7.5 the solution was almost fully cleared from soluble aggregates (Figure VI-5A). At pH 3.0 a reduction from 3 % to about 2 % HMWs in solution was recognized after incubation with the CPG matrix.

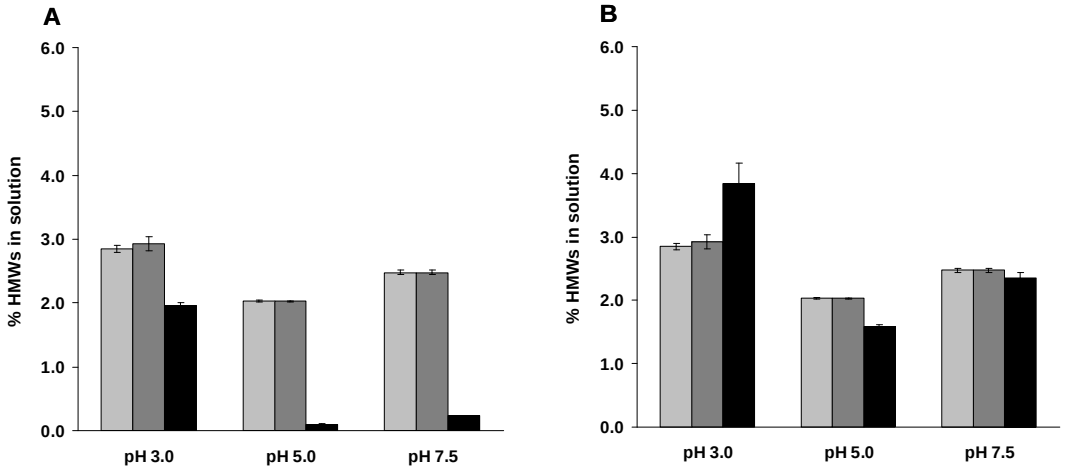

Figure VI-5: Percent HMWs in solution with and without contact to the CPG surface (A) and the functionalized Prosep vA ultra surface (B)
Percent HMWs in solution determined by SE-HPLC before incubation (light grey), after incubation without contact to the chromatographic surface (dark grey) and after incubation with the chromatographic surface (black); for each sample about 25 mg IgG were incubated with about 10 m² of the respective chromatographic surface; results are presented as mean values of three measurements ± SD.

The reduction of HMWs was not observed after incubation with the functionalized ProSep vA ultra resin (Figure VI-5B). Only at pH 5.0 the HMW level dropped from about 2 % to 1.5 %. At pH 7.5 no significant removal of HMWs was detected. At pH 3.0 an increase in HMWs was observed after incubation if the functionalized surface was present.

When sepharose beads were incubated with the IgG solution at the three different pH conditions almost no adsorption of HMWs was detectable (Figure VI-6A). Again, at pH 3.0 an increase in HMWs was observed after incubation with the unfunctionalized beads. At pH 3.0 and pH 5.0 almost no decrease in the level of HMWs was detected when the solution was incubated with the functionalized MabSelect resin (Figure VI-6B). Only at pH 7.5 a decrease in HMWs was detected.

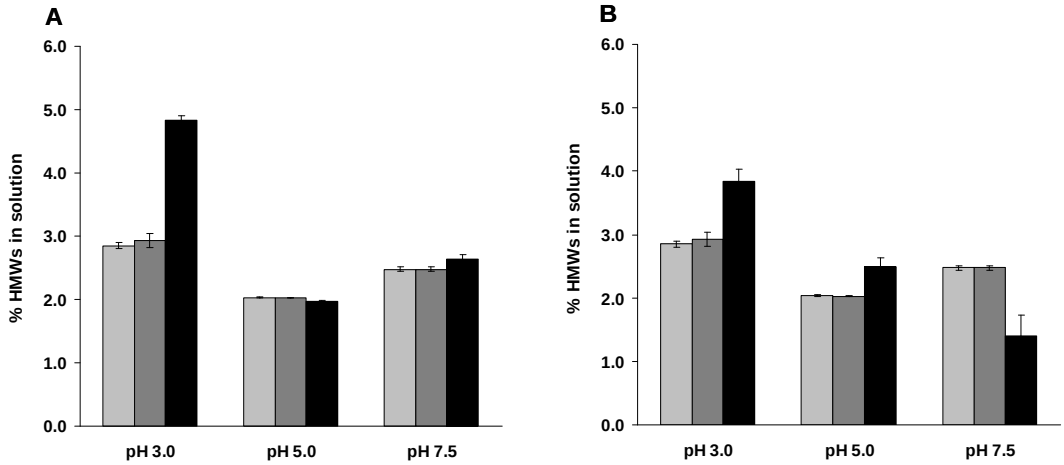

Figure VI-6: Percent HMWs in solution with and without contact to the sepharose surface (A) and the MabSelect surface (B)
Percent HMWs in solution determined by SE-HPLC before incubation (light grey), after incubation without contact to the chromatographic surface (dark grey) and after incubation with the chromatographic surface (black); for each sample about 25 mg IgG were incubated with about 25 m² of the respective chromatographic surface; results are presented as mean values of three measurements ± SD.

3.2.3 Characteristics of mAb adsorption to CPG

The incubation studies clearly showed that unfunctionalized porous CPG surfaces are capable to adsorb IgG molecules as well as their soluble aggregates. Figure VI-7 shows the amount of IgG adsorbed to the CPG particles after 12 h incubation at pH 5.0 versus the concentration of protein remaining in the solution. This adsorption isotherm shows a sharp initial slope which was attributed to a strong binding affinity of the protein to the porous surface at this pH (Figure VI-7B). Complete saturation of the surface was reached at a relatively low protein concentration. Maximum adsorption was reached at about 2.0 mg IgG per square meter CPG.

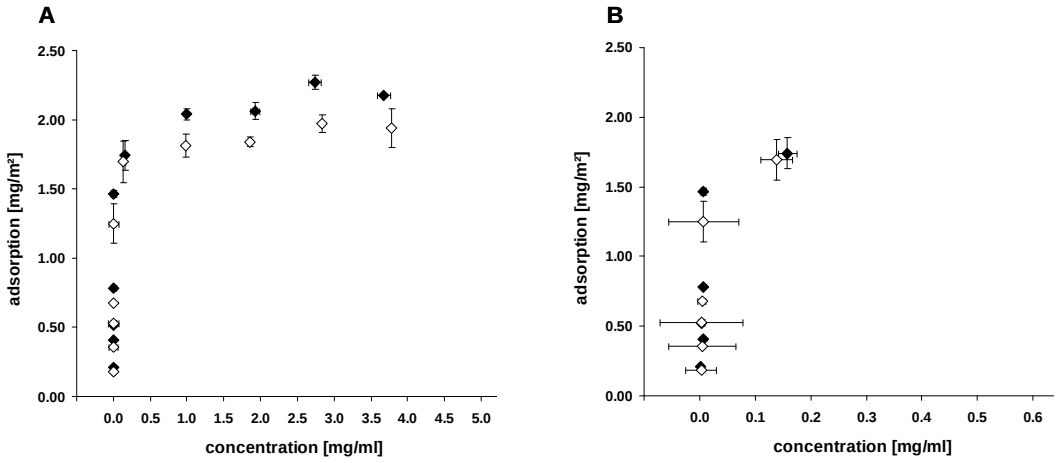

Figure VI-7: Adsorption and desorption isotherm of IgG on CPG particles
Adsorption studies were done at pH 5.0 (black diamonds), desorption studies at pH 3.0 (white diamonds); (B) is a zoom of (A); results are presented as mean values of three measurements ± SD.

Figure VI-8 shows the adsorption isotherm at pH 7.5. At this pH the binding affinity of the mAb to the CPG surface was found to be reduced since the adsorption isotherm was much flatter (Figure VI-8B) compared to the one determined at pH 5.0. Maximum adsorption was already reached at about 1.0 mg IgG per square meter CPG.

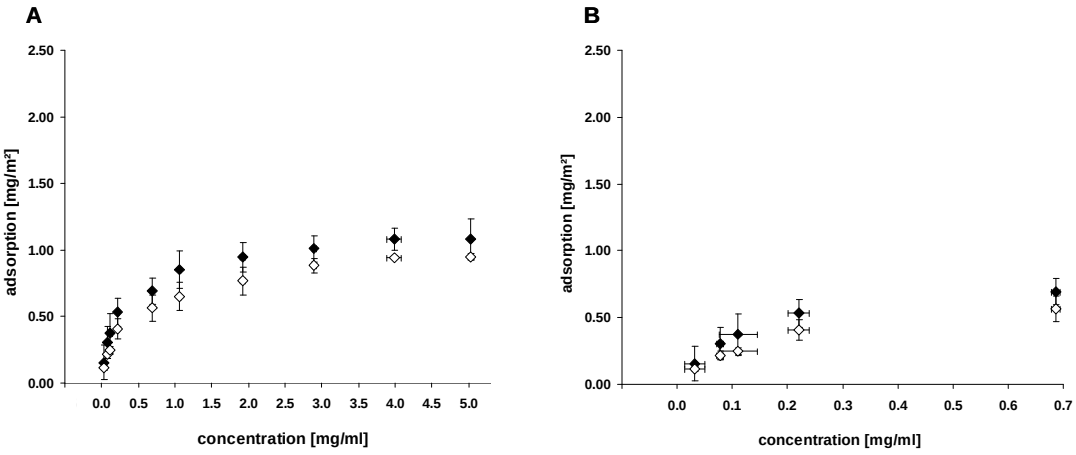

Figure VI-8: Adsorption and desorption isotherm of IgG on CPG particles
Adsorption studies were done at pH 7.5 (black diamonds), desorption studies at pH 3.0 (white diamonds); (B) is a zoom of (A); results are presented as mean values of three measurements ± SD.

Quantitative desorption was only possible, when the protein loaded CPG particles were incubated in a buffer solution at pH 3.0 (Figure VI-7 and Figure VI-8). Adsorption of protein to silica surfaces is in general reported to be reversible under defined conditions. On the one hand, harsh chemical solvents like chloroform, methanol or isopropanol are capable to desorb the protein from the glass surface (Manning et al. 1989a; Stankovic et al. 1990). On the other hand, chaotropic salts are reported to be suitable for protein desorption (Mecs et al. 1984), beside the option of changing the pH (Edy et al. 1976).

Adsorption of the IgG to the CPG particles was in general found to be pH dependent. Maximum adsorption was observed at pH 5.0 (Figure VI-9). In the presence of 150 mM sodium chloride (NaCl) at pH 5.0 a slight decrease in IgG adsorption was observed.

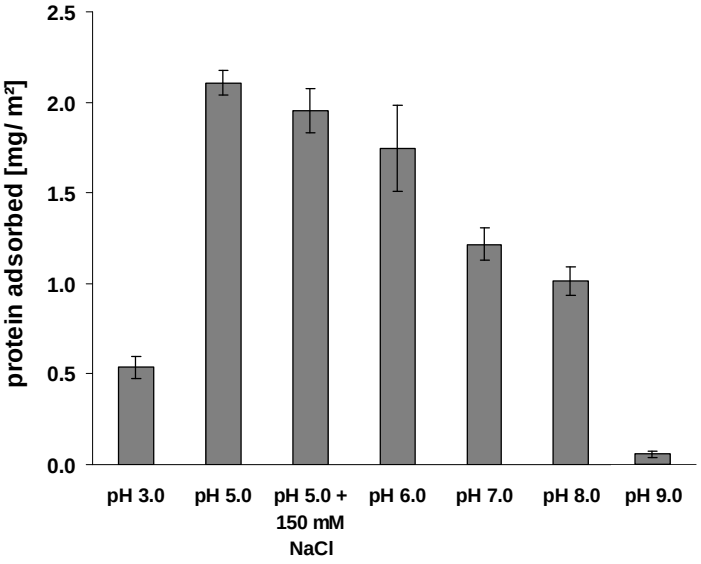

Figure VI-9: Adsorption of IgG on CPG particles at different pHs
Experiments were carried out in the saturation regime at a soluble protein concentration of 2 mg/ml or higher; results are presented as mean values of three measurements ± SD.

A significant decrease in IgG adsorption to the CPG surface was observed when the pH was raised above the IP of the protein which was determined to 8.0 by using zeta potential measurements (Figure VI-10). At a pH of 9.0 only 0.05 mg protein were found to adsorb per square meter CPG.

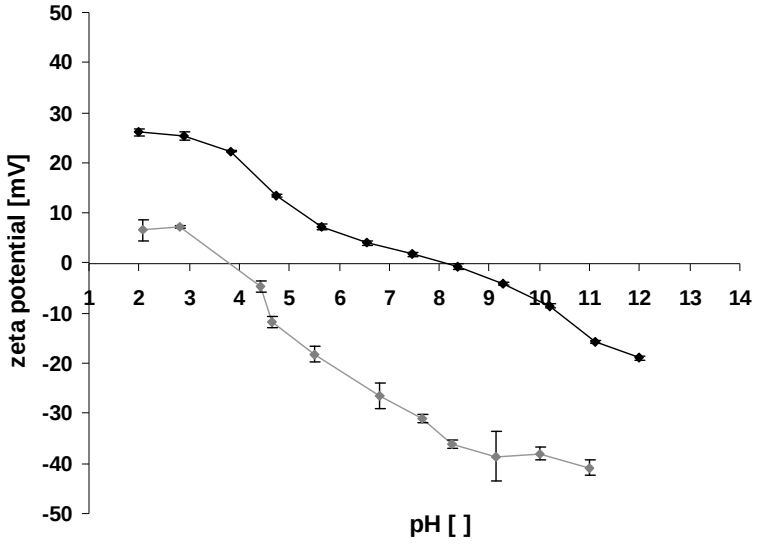

Figure VI-10: Zeta potential titration curves of the IgG (black) and the nano-sized CPG particles (grey)
Experimental data is presented as mean values of three measurements ± SD.

Beside the zeta potential of the IgG, the zeta potential of the nano-sized CPG particles was determined at different pH values (Figure VI-10). The surface charge of the nano-sized CPG was found to depend on pH. The IP of these glass particles was determined to be 4.0. At a pH above 4 the surface charge of the CPG changes from positive to negative whereas the overall charge of the IgG remains positive at a pH below 8.0. Therefore, the adsorption of IgG to the CPG surfaces is considered to be strongly driven by electrostatic interactions, reaching the maximum at pH 5 when the protein and the CPG particles have an oppositely charged surface.

Above pH 4 the residual unreacted surface hydroxyl groups left over from polymerization (called silanols) exist in ionized form (SiO^-) (Behrens and Grier 2001; Tarutani 1984) attracting any positively charged species by electrostatic forces (Nawrocki 1997; Rezwan et al. 2005).

Moreover, hydrophobic siloxane sites are located on the glass surface (Ghose et al. 2004) ready for interaction with other hydrophobic surfaces. In aqueous solutions of proteins the various non-polar amino acid residues will tend to be buried in the interior of the molecule, thus shielded from water (Norde 1986). However, apolar parts of the protein may become exposed to the sorbent surface which are therefore shielded from water as well. Moreover, a fraction of the hydrophobic residues can be exposed to the aqueous

environment due to geometrical restrictions as reported for albumin (Riddiford and Jennings 1966). Therefore, the more lipophilic isopropanol is more effective in the removal of residual protein from an underivatized silica surface compared to methanol or ethanol (Reifsnyder et al. 1996) showing that hydrophobic interactions are involved in the adsorption of protein on glass surfaces.

A third mode of interaction with silica is hydrogen bonding. However, in an aqueous mobile phase hydrogen bonding between an amino group and the silanol group is considered to be unlikely, since both moieties will be hydrated with water molecules (Nawrocki 1997).

Sulkowski et al. (1987) showed that the simultaneous suppression of both electrostatic and hydrophobic interactions are necessary to prevent binding between a protein and a glass based surface. Figure VI-9 shows that at the isolelectric pH of 8.0 of the IgG, the amount of protein adsorbed was still approximately half of that at optimal binding pH of 5.0. This suggests that the adsorption of the IgG to the CPG surface is based on both, electrostatic and hydrophobic interaction.

3.2.4 Preferential adsorption of aggregates to CPG

Soluble mAb aggregates were shown to adsorb to the CPG surface. Especially at pH 5.0 the addition of 10 m² CPG resulted in a drop of HMWs from about 2.0 % to 0.1 % (Figure VI-5A). To further investigate the capability of the undrivatized CPG surface to adsorb HMWs and to evaluate the concomitant loss of the monomer on the added surface, protein solutions containing different levels of HMWs (6.8 %, 5.7 % and 3.2 %) were incubated with different surface areas of CPG (0.1 m² to 10 m²) at pH 5.0. The percentage of monomer and HMWs in solution was determined in the supernatant after incubation with the CPG particles by using SE-HPLC. Figure VI-11 shows that the addition of about 3 m² CPG surface (about 150 m² per gram protein) results in a nearly HMW free solution. After incubation, a monomer level of about 99 % was achieved independently of the initial level of HMWs present before incubation.

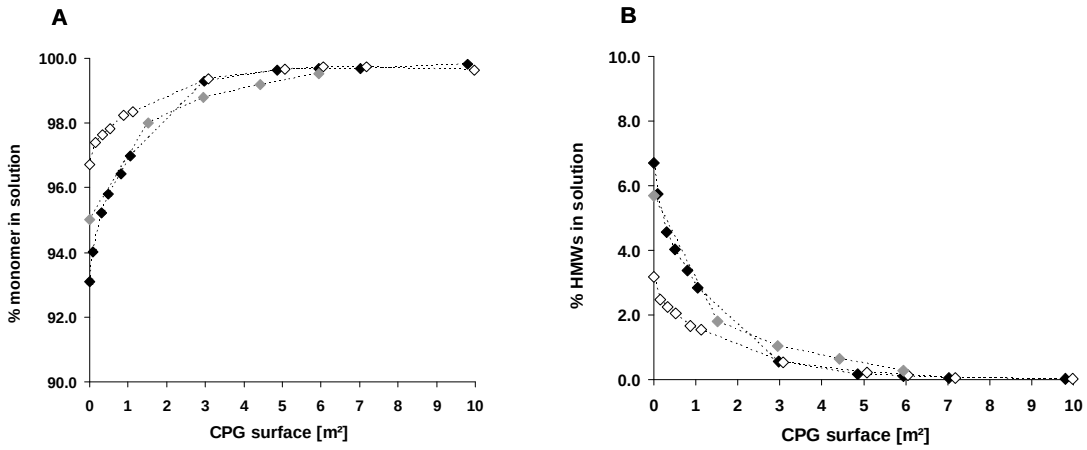

Figure VI-11: Percent monomer (A) and percent HMWs (B) in solution after contact to a defined CPG surface area at pH 5.0
About 20 mg IgG (c = 5 mg/ml) with an initial level of 3.2 % (white diamonds), 5.7 % (grey diamonds) and 6.8 % (black diamonds) of HMWs were incubated with up to 10 m² of CPG.

To evaluate the loss of the IgG monomer and the HMWs on the CPG particles the amount of the respective protein species being adsorbed to the CPG surface was calculated. Therefore, the amount of monomer and HMWs remaining in solution after incubation with the CPG particles were subtracted from the amount of monomer and HMWs initially present in solution. The amount of total protein (encompassing monomer, HMWs and LMWs) initially present in solution was about 20 mg. Figure VI-12 shows that the amount of adsorbed monomer increases linearly with increased CPG surface area present in solution. By adding 10 m² of CPG nearly 100 % (20 mg) of the IgG initially present in solution are bound to the CPG particles. This was already identified as the maximum adsorption of 2.0 mg IgG per m² CPG (Figure VI-7). However, about 95 % of the HMWs initially present in solution were found to adsorb to the CPG surface when only 3 m² are present in solution. Concomitantly, 4 mg of the monomer (about 20 % initially present in solution) are lost on the CPG surface. Thus, it is concluded that soluble aggregates are preferentially adsorbed to the CPG particles since nearly total HMW adsorption was already recognized at a significant smaller surface area compared to total monomer adsorption.

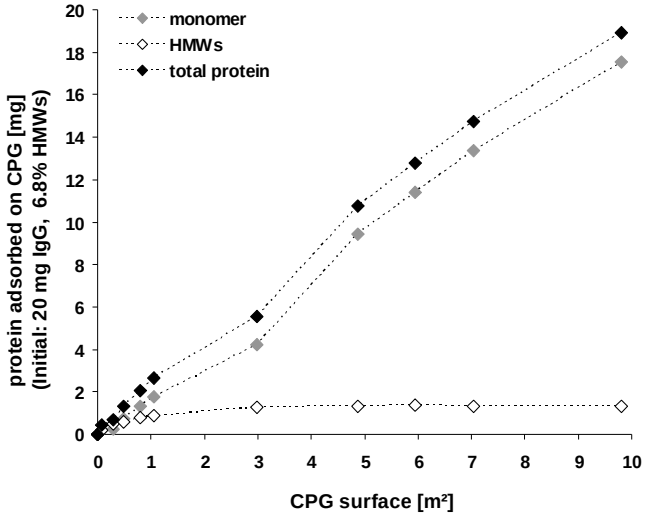

Figure VI-12: Milligram of protein adsorbed to a defined CPG surface area at pH 5.0
About 20 mg IgG (c = 5 mg/ml) with an initial level of 6.8 % HMWs were incubated with up to 10 m² of CPG; the protein concentration was determined by using UV 280-320 measurements and the percentage of the monomer and the HMWs was determined by using SE-HPLC.

Figure VI-13 shows the percent of monomer and HMWs adsorbed to the CPG surface area per gram protein which was initially present before incubation.

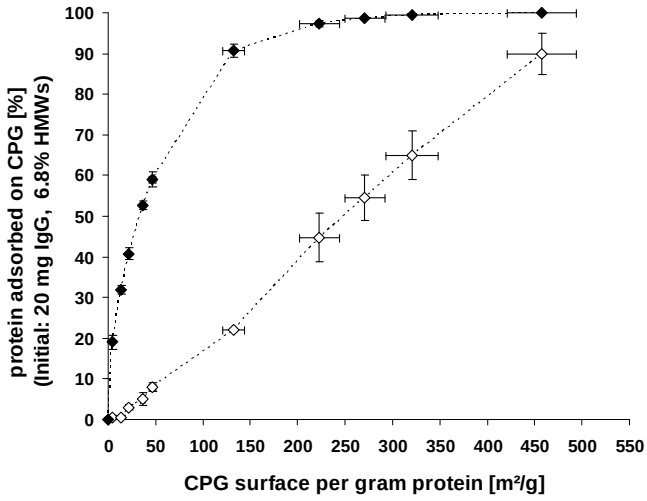

Figure VI-13: Percent of IgG monomer (white) and HMWs (black) adsorbed to CPG
20 mg IgG containing 6.8 % HMWs were initially present before incubation with 0.1-10 m² CPG; experimental data is presented as mean values of three measurements ± SD.

Here, the adsorption of HMWs is again clearly favored over the adsorption of the monomer, since the slope of the corresponding curve is much steeper for the HMWs than for the monomer. Figure VI-14 shows the corresponding SE-chromatograms of the analyzed supernatants after incubation with the CPG surface.

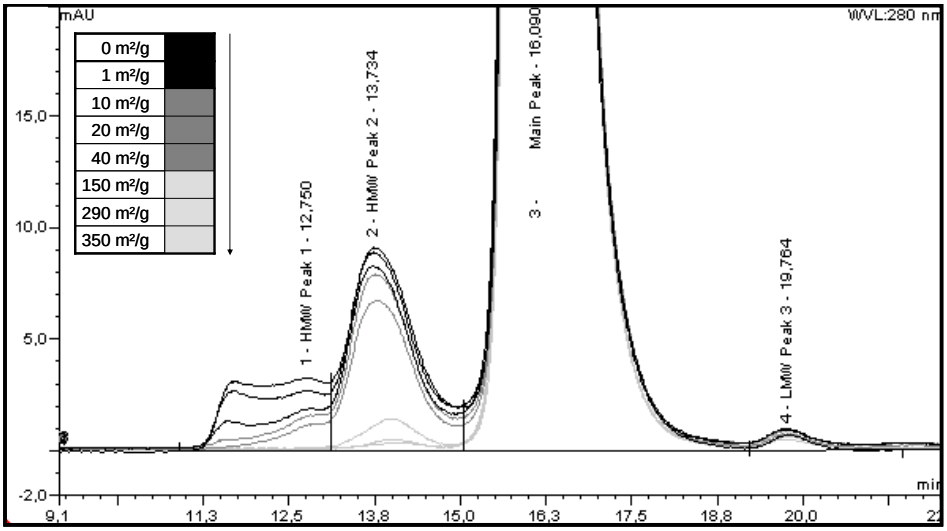

Figure VI-14: SE-chromatograms of the IgG solutions after incubation with up to 350 m² surface area of CPG per gram protein
20 mg IgG containing 6.8 % HMWs were initially present before incubation with CPG (black profile); decreasing UV-signal with increasing CPG surface is indicated by changing the colour from black to light grey.

It is observed that the signal of both, HMW species represented as HMW peak 1 and HMW peak 2 is decreasing with increasing CPG surface area present during incubation. In first line, the amount of the HMW peak 1 which is considered to be the oligomeric species decreases with increasing CPG surface area. Between 40 and 150 m² CPG per gram protein, the oligomers are completely removed. Only a reduced amount of the HMW peak 2 species which is considered to be the dimer with a retention time of 13.73 min, was found in the solution after incubation. The CPG surface area present during incubation has no effect on the amount of the LMWs remaining in solution. Thus, it can be concluded that larger soluble aggregates are preferentially adsorbed to the CPG particles. Moreover, dimers are prone to adsorb to this surface. The monomeric species is in addition able to adsorb to CPG but to a much lesser extent. The surface area of CPG available per gram protein can be used to control the amount of aggregated and monomeric species remaining after simple batch incubation. A surface area of 100-150 m² per gram protein is suit-

able to remove nearly 80-90 % of soluble aggregates from an IgG solution at pH 5.0, having concomitantly 80-85 % monomeric IgG remaining in solution. For a solution containing 20 mg IgG and 6.8 % HMWs the addition of 0.1 g CPG (3 m^2) is sufficient to obtain a solution of 99 % monomer determined by SE-HPLC by loosing concomitantly about 20 % of total monmeric protein.

3.3 Effect of contact to chromatographic surfaces on mAb aggregation

Interfacial adsorption can result in physical instability potentially encompassing the formation of structural altered molecules (Mollmann et al. 2005; Sluzky et al. 1991; Tzannis et al. 1997) which are considered as precursors for aggregation (Kendrick et al. 1998a). Moreover, a rapid loss of active soluble protein in solution is reported in the presence of nano- and micro-sized seeds potentially serving as heterogeneous nuclei facilitating protein aggregation as reported before (see chapter I, section 3.4). In this case, the protein adsorbs to the surface, but unfolding does not seem to be involved in this aggregation phenomenon, since alterations in secondary or tertiary structure were hardly ever detectable (Bee et al. 2009a; Bee et al. 2009b; Chi et al. 2005b; Sluzky et al. 1991; Tyagi et al. 2008).

Therefore, in this study the IgG solutions were incubated with different surface areas of nano- and micro-sized CPG particles over one week to investigate the effect of added CPG particles on IgG aggregation. Solutions at pH 5 were applied where the IgG showed the most pronounced adsorption to CPG. In addition, the experiments were conducted at pH 5 with 150 mM sodium chloride (NaCl) and at pH 7.5, since the protein was shown to adsorb to a lesser extent under these conditions. Protein concentration and aggregation in the supernatant were monitored over incubation time. Finally, the conformation of the protein was investigated before, during and after adsorption to the surface.

3.3.1 Seeding and aggregation

To obtain nano-sized particles, the commercially available CPG particles were sonicated in water. After sedimentation of the residual large particles, the size distribution in the supernatant was investigated by laser diffraction. Figure VI-15 shows the size distribution by intensity before and after sonication. Before sonication the CPG particles showed a mean particle diameter of about 125 μm. A decrease in particle size was observed with

sonication time. After 10 min sonication, particles of about 10 µm and smaller were generated.

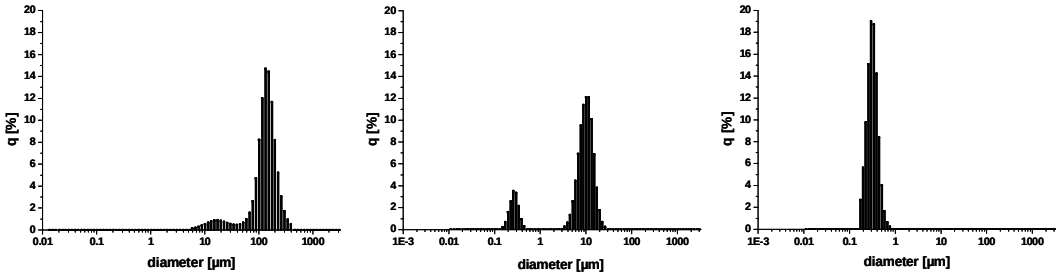

Figure VI-15: Size distribution by intensity [q] of the CPG particles
CPG particles before sonication (left), after 10 min sonication (middle) and after 30 min sonication (right).

After 30 min a mean particle diameter of about 290 ± 88 nm (n = 3) was determined. The particles after 10 min and 30 min sonication were used for the seeding experiments. IgG solutions (about 6 mg/ml) were incubated with 0-200 m² CPG surface per gram protein over one week without headspace on a rotary mixer. The protein was shown to strongly adsorb to the CPG surface at pH 5.0 as reported before (Figure VI-16A).

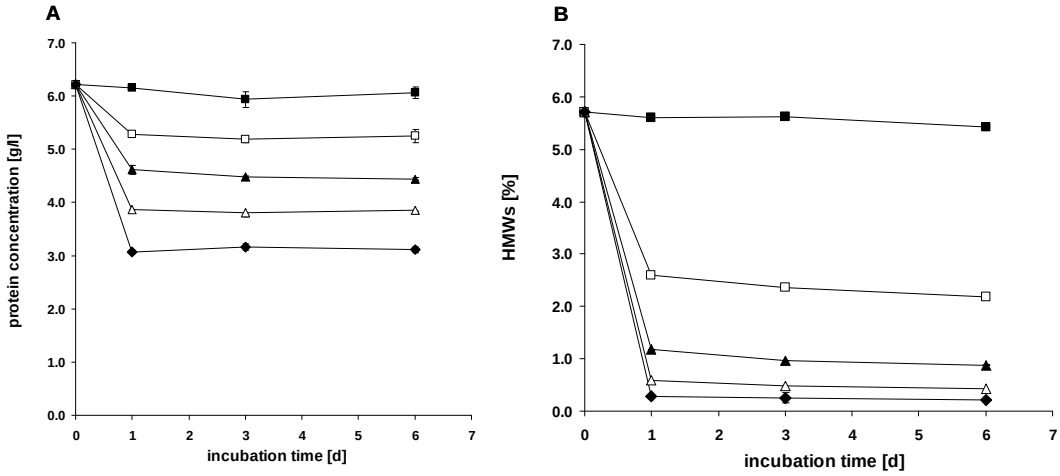

Figure VI-16: Incubation of IgG at pH 5.0 over 6 days after seeding with CPG particles
Concentration of soluble IgG remaining in solution (A) and percentage of HMWs remaining in solution (B); a defined surface area per gram protein was seeded: 0 m²/g (black squares), 50 m²/g (white squares), 100 m²/g (black triangles), 150 m²/g (plain triangles), 200 m²/g (black diamonds); experimental data is presented as mean values of three measurements ± SD.

The extent of adsorption clearly depends on the surface area of CPG seeded into the solutions. An initial decrease in protein concentration was observed in the supernatant after one day incubation. This initial protein loss was proportional to the present surface in solution. The higher the surface area added, the more protein was lost on the CPG particles. After this initial adsorption the protein concentration remains constant during incubation independent of the initially added surface. No protein loss due to further adsorption or the formation of insoluble aggregates was observed during 6 days.

Moreover, the level of HMWs determined by SE-HPLC decreased with increasing CPG surface area as reported before (Figure VI-16B). After one day incubation, no further decrease in the level of soluble aggregates was detectable over 6 days. Moreover, no increase of HMWs in the supernatant was recognized. Thus, it can be concluded that neither desorption of initially bound aggregates, nor an additional formation of aggregates during incubation took place.

The same experiments were conducted at pH 5.0 using a buffer which contains 150 mM NaCl (Figure VI-17).

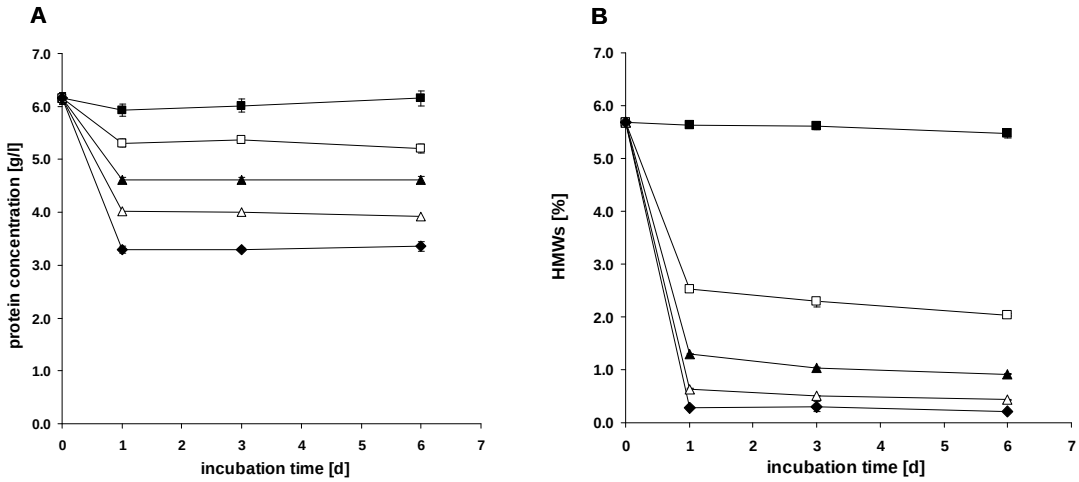

Figure VI-17: Incubation of IgG at pH 5.0 and 150 mM NaCl over 6 days after seeding with CPG particles
Concentration of soluble IgG remaining in solution (A) and percentage of HMWs remaining in solution (B); a defined surface area per gram protein was seeded: 0 m^2/g (black squares), 50 m^2/g (white squares), 100 m^2/g (black triangles), 150 m^2/g (plain triangles), 200 m^2/g (black diamonds); experimental data is presented as mean values of three measurements ± SD.

Initially, the protein loss was again proportional to the surface area present (Figure VI-17A). Beyond one day incubation, no further adsorption of protein was observed over 5 days.

In addition, the HMW level was observed to decrease again with provided CPG area during one day incubation (Figure VI-17B). Further incubation showed no effect on the HMW level in the solutions. Compared to the experiments conducted without adding 150 mM NaCl, the adsorption of the IgG was in general slightly reduced, as reported before. Moreover, the adsorption of HMWs under these conditions can be considered as similar compared to the values obtained at pH 5.0 without using salt.

Furthermore, the seeding experiments were conducted at pH 7.5 (Figure VI-18).

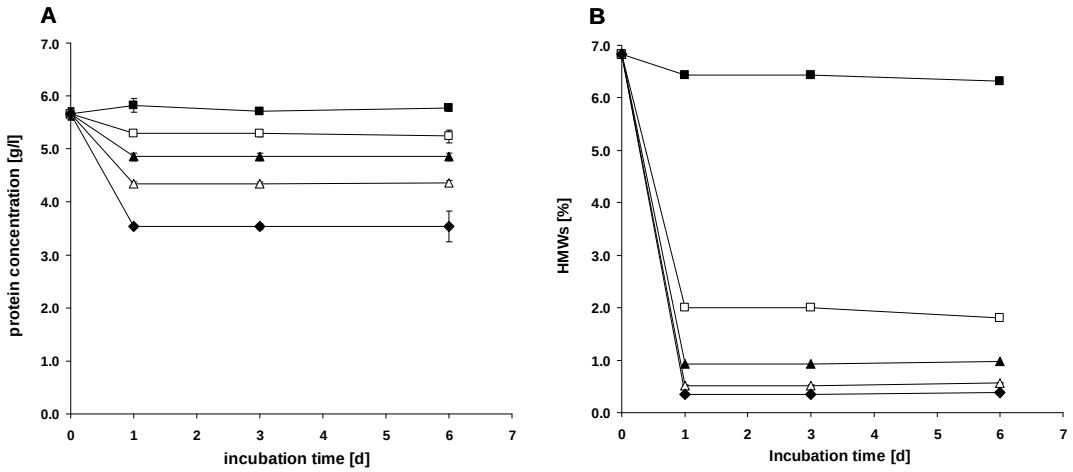

Figure VI-18: Incubation of IgG at pH 7.5 over 6 days after seeding with CPG particles
Concentration of soluble IgG remaining in solution (A) and percentage of HMWs remaining in solution (B); a defined surface area per gram protein was seeded: 0 m^2/g (black squares), 50 m^2/g (white squares), 100 m^2/g (black triangles), 150 m^2/g (plain triangles), 200 m^2/g (black diamonds); experimental data is presented as mean values of three measurements ± SD.

The adsorption of soluble IgG is reduced at this pH as expected and explained above. Once more, an increase in the CPG surface area results in a decrease in soluble protein remaining in solution. After one day incubation, maximal adsorption was observed and no further loss of protein was recognized during the following days (Figure VI-18A). A decrease in HMWs was detected with increasing surface area seeded into the solutions (Figure VI-18B). The adsorption of the soluble aggregates is complete after one day and remains constant over the following 5 days.

In general, the adsorption of the soluble aggregates was enhanced at this pH compared to the incubation experiments at pH 5. After one day, the level of HMWs was decreased from 6.5 % to 2.0 % by adding 50 m² CPG per gram protein at pH 7.5. In comparison, a reduction in HMWs from 5.6 % to 2.5 % was recognized having again 50 m² CPG per gram IgG at pH 5.0.

This can be potentially attributed to a reduction in the electrostatic interactions between the protein and the CPG surface at pH 7.5 leading to a generally reduced adsorption of the monomeric IgG. Concomitantly, hydrophobic interactions between the protein and the CPG surface are more pronounced. Since aggregated species are assumed to be more hydrophobic than the monomers, this can result in facilitated adsorption of the aggregates at this pH, since CPG possesses both, hydrophobic as well as charged functions as reported before. It is reported that both, hydrophobic and charged regions, are present on the surface of a protein, potentially mediating the assembly of the molecules to form aggregates (Chiti et al. 2002; Valerio et al. 2005). Differences between the monomeric species and the aggregated form of a protein regarding surface charge and hydrophobicity are considered to be the principle of separation on a charged chromatographic surface. The selectivity of an ion exchange media to separate aggregates is augmented with elevated hydrophobicity. It was shown that aggregate removal was facilitated on charged-hydrophobic mixed mode surfaces (Gagnon 2009a), better than on exclusively hydrophobic (Lu et al. 2009) or exclusively charged surfaces (Yigzaw et al. 2009). These mixed mode media exploit the relatively constant hydrophobicity of a phenyl group in combination with a positively charged quaternary amine or a pyridyl nitrogen ligand (Huse et al. 2002).

Under all presented conditions, the adsorption of the IgG and the adsorption of the soluble aggregates increased with increasing CPG surface area. The molecules seem to be strongly and irreversibly adsorbed to the CPG material under these conditions. Neither the protein concentration, nor the level of HMWs in the supernatant changed during further incubation. Hence, the seeding of different surface areas did not result in an increase in soluble aggregates. Moreover, no precipitation of protein over time was recognized, since the concentration of the soluble IgG in the supernatant did not decrease after initial adsorption to the CPG particles during incubation over 5 days (Figure VI-16A, Figure VI-17A and Figure VI-18A). Turbidity at 350 nm was found to decrease with increasing CPG surface area present in solution and did not change significantly during further incubation over 5 days, too (Figure VI-19).

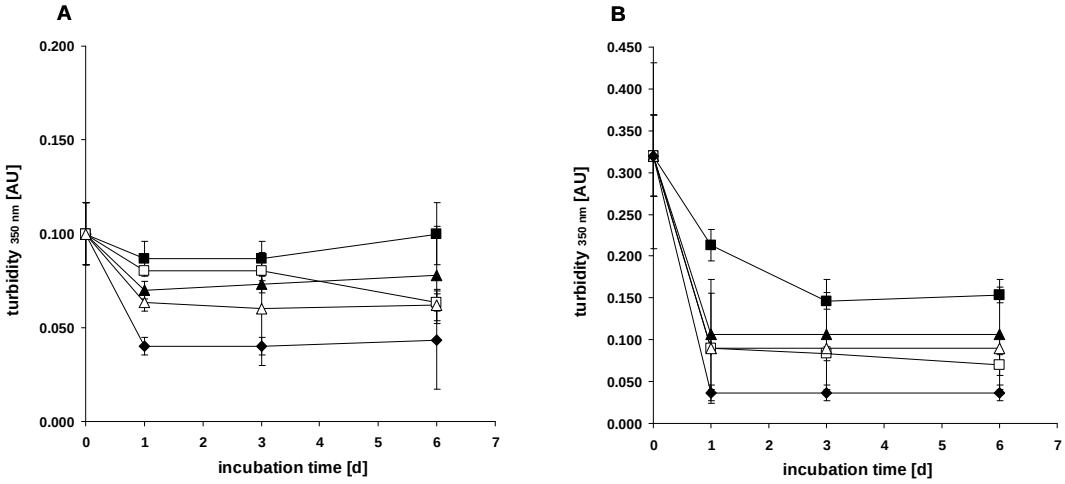

Figure VI-19: Turbidity at 350 nm during incubation of IgG over 6 days after seeding with CPG particles
At pH 5.0 (A) and at pH 7.5 (B); a defined surface area per gram protein was seeded: 0 m²/g (black squares), 50 m²/g (white squares), 100 m²/g (black triangles), 150 m²/g (plain triangles), 200 m²/g (black diamonds); experimental data is presented as mean values of three measurements ± SD.

Since an increase in turbidity can be attributed to an increased number of larger protein aggregates of up to 1-2 µm in size (Mahler et al. 2005) the decrease in turbidity with increasing CPG surface area present is considered to be the consequence of the initial adsorption of these aggregates to the CPG surface. The IgG solutions seeded with CPG particles did not show an induction of aggregates monitored by turbidity measurements during incubation over 6 days, neither at pH 5.0, nor at pH 7.5. It has to be stated that the centrifugation procedure conducted to separate the seeded CPG particles from the protein solution can potentially remove or dissolve larger aggregates.

3.3.2 Conformational stability

Secondary structure of the IgG was investigated by using FT-IR spectroscopy. It was possible to obtain the spectrum of the protein directly attached to the surface of the CPG and the ProSep vA ultra particles at pH 5.0 by using the ATR technique. At pH 5.0 a sufficient adsorption of protein to both surfaces allowed to record the spectra. The protein covered chromatographic particles were washed two times with buffer at pH 5.0 until the washing solution was almost cleared from protein. Afterwards, the in buffer suspended particles were directly applied to the crystal of the ATR cell. The spectrum of the directly adsorbed

protein was compared to the spectrum of a protein sample which had no contact to the surface before (Figure VI-20).

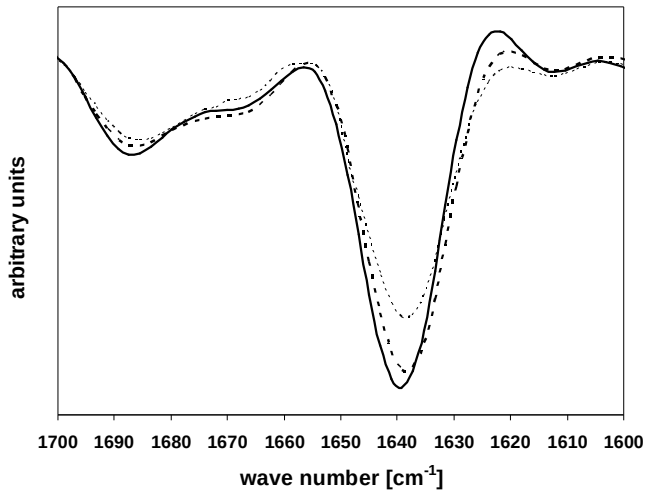

Figure VI-20: Second derivative ATR FT-IR spectra of the IgG at pH 5.0
On CPG (bolded dashed line), on ProSep vA ultra (dotted line) and without contact to the chromatographic surface (solid line).

In general, differences in the second derivative spectra of the three samples were observed. The amid I band at a wave number of 1639 cm^{-1} in the native solution (without contact to the chromatographic surface) was slightly shifted to a lower wave number at 1637 cm^{-1} when the IgG was directly adsorbed to the CPG surface. This shift was recognized as well when the IgG was bound to ProSep vA ultra. Moreover, a loss in intensity of the shifted amid I frequency at 1639 cm^{-1} was observed, when the protein was adsorbed to both surfaces. In addition, the band at a wave number of 1687 cm^{-1} showed an increased intensity in the second derivative spectrum when the protein was adsorbed to the surfaces.

The described spectral changes in the amid I region were assigned to the formation of intermolecular ß-sheet structure (Chang et al. 2005; Cleland et al. 2001). A shift of the band at 1640 cm^{-1} to a lower wave number and a concomitantly reduced intensity of this band, as well as a weak intensity peak at 1690 cm^{-1} were related to changes in the secondary structure elements of IgGs before (Matheus et al. 2006a; Pelton and McLean 2000).

Interestingly, the protein attached to ProSep vA ultra being predominantly adsorbed via the Protein A ligand, seems to exhibit stronger alterations in secondary structure compared to the protein adsorbed to the CPG surface.

After desorption from the surfaces, the transmission spectrum of the protein in solution was recorded. Desorption from CPG was achieved by using a buffer at pH 9.0 and by using a buffer at pH 3.0 to remove the protein from ProSep vA ultra (Figure VI-21A).

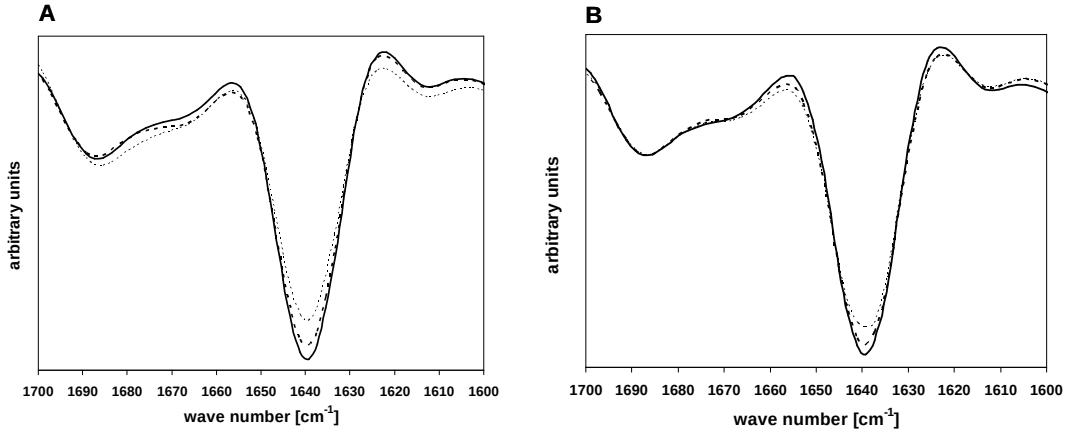

Figure VI-21: Second derivative FT-IR spectra of the IgG
After desorption at pH 9.0 from CPG (bolded dashed line), at pH 3.0 from ProSep vA ultra (dotted line) and without contact to the chromatographic surface at pH 5.0 (solid line) (A); after incubation without contact to the beads at pH 9.0 (bolded dashed line), at pH 3.0 (dotted line) and at pH 5.0 (solid line).

When the protein was desorbed from both surfaces only a decrease of the band at 1639 cm^{-1} was observed. The decrease of the band was more pronounced for the protein which was desorbed from ProSep vA ultra at pH 3.0 compared to the protein which was desorbed from CPG at pH 9.0. The desorption experiments had to be conducted using a buffer at pH 9.0 in the case of CPG and a buffer at pH 3.0 in the case of the Protein A medium to ensure sufficient removal of the protein. Figure VI-21B shows the spectra obtained from the protein which was solely incubated at pH 3.0 and at pH 9.0 without having contact to the chromatographic surfaces before. Again, the decrease of the band at 1639 cm^{-1} was more pronounced for the sample at pH 3.0 compared to the sample at pH 9.0. Thus, the potential conformational changes are rather ascribed to the buffer conditions used than to the previous contact to the chromatographic beads.

Potential changes in tertiary structure were monitored by using 2D-UV spectroscopy. The spectra of the desorbed protein were recorded and compared to those of a solution which was not exposed to the surfaces before. Moreover, the spectra were compared to structurally altered IgG molecules as a positive control. Therefore, the protein was incu-

bated for 2 hours at 80 °C and for 10 min in 6 M guanidine hydrochloride. Figure VI-22 summarizes all the recorded spectra.

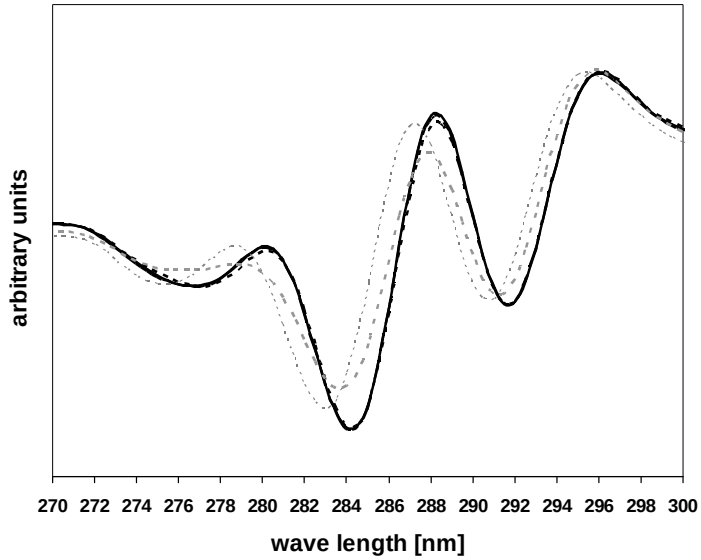

Figure VI-22: 2D-UV spectra of the IgG in solution
Desorbed from CPG at pH 9.0 (black dashed line), from ProSep vA ultra at pH 3.0 (black dotted line) and without contact to the chromatographic surface at pH 5.0, pH 3.0 and pH 9.0 (black solid line); IgG at pH 5.0 incubated at 80 °C (dashed grey line) and in 6 M guanidinium hydrochloride (dotted grey line).

No differences between the spectra of the desorbed protein and the protein which had no contact to the surface before were observed, since all spectra almost perfectly overlaid. The protein which was exposed to heat and guanidine hydrochloride showed a shift to lower wave lengths as expected (see chapter IV).

After incubation with the beads, the protein remaining in the liquid supernatants after centrifugation was analyzed with FT-IR in transmission mode. The spectra in the amide I region were compared to the spectra of the protein which had no contact to the surface before. No differences were observed since all recorded spectra of the IgG in solution almost perfectly overlaid (Figure VI-23).

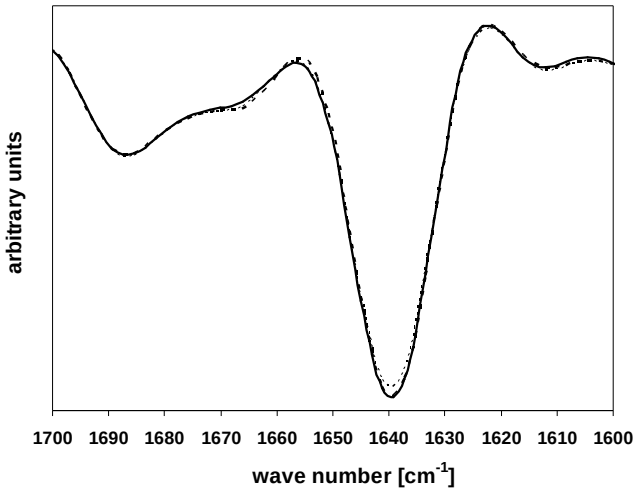

Figure VI-23: Second derivative FT-IR spectra of the IgG
After contact to CPG (bolded dashed line), to ProSep vA ultra (dotted line) and without contact to the chromatographic surface (solid line).

Summarizing, it can be concluded that the exposure of the IgG to CPG or CPG based Protein A particles did not result in detectable conformational alterations of the protein molecules as regards secondary and tertiary structure.

3.4 Effect of host cell proteins on mAb aggregation

As reported before, heterogeneous nucleation induced aggregation of proteins may not solely be induced by exogenous particles shed or abraded from several kinds of surfaces to which the protein solution is exposed during bioprocessing or storage. Indigenous protein species like host cell proteins (HCPs) present in solution are also suspected to induce aggregation of the mAb. The HCPs, a typical process related impurity, have to be removed during the purification process of therapeutically used recombinantly derived proteins. Multiple separation steps have to be performed, since HCPs are a complex mixture of numerous proteins with divers physicochemical properties regarding IP and molecular weight (Jin et al. 2010; Rathore et al. 2003). The abundance and diversity of HCPs in the harvested product pool have been shown to depend on the protein of interest, the host organism and the cell culture and harvest conditions (Eaton 1995).

In this study, the HCPs purified from a "null" CHO in-house master cell were characterized and the potential of this HCP composition to induce mAb aggregation was in-

vestigated afterwards by performing spiking experiments at different pHs and buffer conditions.

3.4.1 Host cell proteins from CHO cell culture

The pattern of the HCP composition was analyzed by 2D-gel electrophoresis to resolve the complex protein mixture in charge (IEF) and size (SDS-PAGE). The protein properties molecular weight and IP can be obtained by this method. Figure VI-24 shows a 2D-gel image of the HCPs isolated from the "null" CHO cell culture harvest.

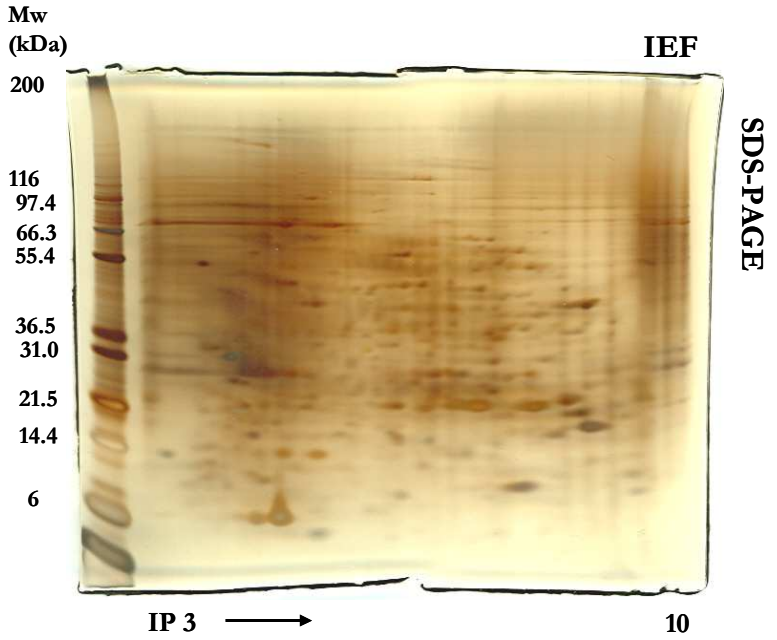

Figure VI-24: 2D-gel image of HCPs from the HCP standard solution derived from a purified "null" CHO cell mock culture harvest
First dimension: IEF pH 3-10 (horizontal); second dimension: SDS-PAGE (vertical).

An uneven distribution of protein species was observed across the molecular weight (Mw) and IP range investigated. A bias towards the lower to mid molecular weight proteins (< 70 kDa) was recognized. It has to be stated that the 2D-gels were operated under reducing and denaturing conditions which dissociate disulfide bonds and protein complexes. Thus, the HCP standard may additionally contain protein species of higher molecular weight. Considering the IP of the proteins, divers species distributed over the acidic as well as the basic region were recognized. No major population located either in the acidic or

the basic region was identified. The abundance (spot volume) was shown to differ among the detected species (spots). Some big spots are obvious suggesting that a set of abundant proteins constitute a major portion of all HCPs in the harvested cell culture fluid. The reported pattern of HCP distribution in the used CHO cell culture fluid is somehow different from the pattern observed in other studies, where a bias of CHO dedicated extracellular HCPs towards acidic proteins has been shown (Jin et al. 2010; Wimmer et al. 1994). However, intracellular HCPs are reported to be more uniformly distributed over a pH range of 3-10 (Krawitz et al. 2006). Both, intracellular as well as extracellular HCPs are a subset of the total CHO cell proteome. The secreted as well as the intracellular proteome of a specific cell may bias towards species with various properties and each contains in general thousands of different proteins. Moreover, lyzed and healthy cells can differ significantly in their expressed proteome since they are in a very different physiological state (Jin et al. 2010). Furthermore, the harvested cell culture fluid can contain much more different protein species if the cells were destructed. Since engineered mammalian host cells are able to secrete the target protein of interest into the cell culture fluid, the cell membrane is usually not disrupted deliberately to harvest the protein. However, it is known that death and disruption of the cells always occur during cultivation and harvesting and thus protein species which are normally not secreted into the fermentation broth may be released. Thus, the present population of HCPs is considered a representative mixture of HCPs derived from CHO cell culture which may occur in the harvested cell culture fluid and in the purification intermediates.

In addition, the HCP standard solution was investigated by zeta potential measurements at pH 2-12 to determine the average IP of all HCPs present in solution. Figure VI-25 shows that an IP of about 4.5 was determined for the HCP composition present in the standard solution. Since the charge of a protein depends not only on the environmental pH but also on buffer electrolyte composition this method potentially allows for a more representative analysis of the proteins in solution compared to isoelectric gel electrophoresis (Winzor 2005). Moreover, the average IP of all HCPs accounts for the abundance of individual protein species with a defined IP. Thus, it is concluded that the major fraction of the HCPs in the standard solutions are proteins with an IP in the acidic region.

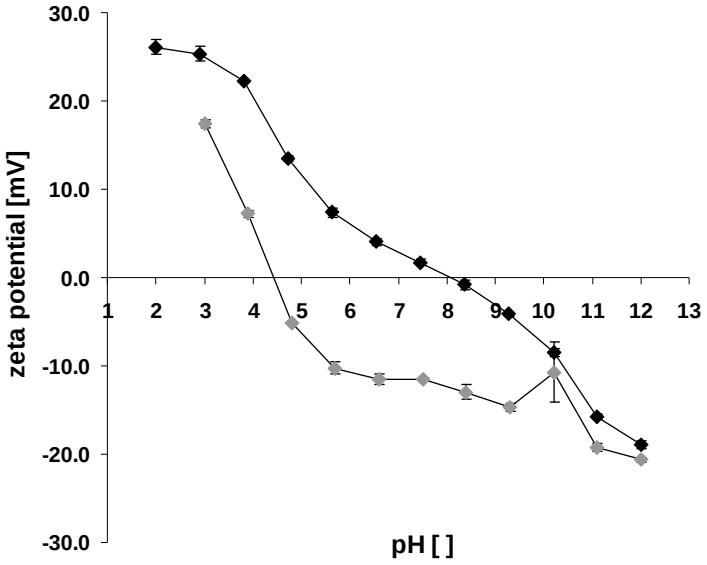

Figure VI-25: Zeta potential titration curves of the IgG (black) and the HCP standard solution derived from a purified "null" CHO cell mock culture harvest (grey)
Experimental data is presented as mean values of three measurements ± SD.

Figure VI-25 also reveals the property differences between this defined HCP population and the IgG used in this study. Most IgGs are basic with an IP in the range of 8 and 9 (see in addition chapter V: Figure V-8 and Figure V-13V), as observed here. Thus, interactions between the HCPs and an IgG based on charge-charge interactions may potentially occur leading to aggregation. At a pH above 4.5 the surface charge of the major HCP fraction changes from positive to negative whereas the overall charge of the IgG remains positive at a pH below 8. Therefore, charge-charge based interactions of several HCP species and the IgG are considered to reach the maximum at a pH between 5 and 6 when both exhibit an oppositely charged surface.

3.4.2 Seeding and aggregation

Spiking experiments were conducted at pH 3.0, pH 5.0 and pH 7.5 covering both, the pH region of potential charge-charge based interaction (pH 5.0 and pH 7.5) and charge-charge based repulsion (pH 3.0) of the major fraction of HCPs and the IgG. 500 ng and 1000 ng HCP (derived from the HCP standard solution) per mg IgG (= 2.5 µg/ml HCP and 5 µg/ml HCP) were spiked into the solutions and the samples were incubated on a rotary mixer at room temperature and at 40 °C. This HCP is considered representative for Pro-

tein A and CEX purification intermediates. Results were compared to samples which were incubated without adding HCP standard solution (0 ng/mg HCP). Figure VI-26 shows the level of HMWs and LMWs in solution monitored with SE-HPLC during storage at 40 °C.

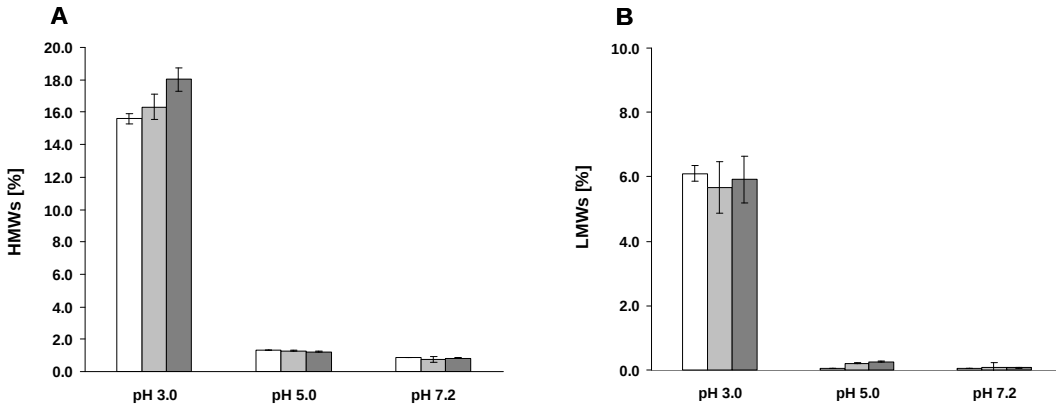

Figure VI-26: Percent HMWs (A) and LMWs (B) in solution determined with SE-HPLC
Incubation at room temperature for 24 hours after spiking with 0 ng/mg HCP (white), 500 ng/mg HCP (light grey) and 1000 ng/mg HCP (dark grey); for each sample about 20 mg IgG were applied; results are presented as mean values of three measurements ± SD.

Differences in the level of HMWs considering the pH of the solutions were observed. At pH 3.0, the HMW level stepped up to about 16 % compared to solutions at pH 5.0 and pH 7.5 showing a HMW level below 2 %. A slight induction of HMWs in the presence of HCPs was only observed at pH 3.0. The percentage of LMWs was recognized to depend on the pH of the solutions as well (Figure VI-26B). At pH 3.0 an increase in LMWs up to about 6 % was observed. In general, the HCP concentrations applied in the experiments were sufficiently low enough to be not detectable by the SE-HPLC method used. This was evaluated by diluting the HCP standard solution with buffer and injecting 200 ng of HCP into the SE-column. This amount of HCP is about two times higher than the amount of HCP injected to the SE-column when the 1000 ng/mg HCP samples are analyzed. No peak was detected in the SE-chromatogram when this buffer diluted solution was analyzed.

During storage at 40 °C a slight increase in the level of HMWs of the HCP spiked solutions at pH 3.0 was recognized compared to the unspiked solutions after two weeks (Figure VI-27A). However, after four weeks no differences in the HMW level between the HCP spiked and unspiked solutions were observed. At pH 5.0 and pH 7.5 no differences

in the percentage of HMWs of the spiked and unspiked solutions were recognized over two weeks. However, the LMW level at pH 5.0 of about 0.2 % stepped up to 2 % after two weeks when 500 ng/mg HCP were present (Figure VI-27B). In the presence of 1000 ng/mg HCP the percentage of LMWs further increased up to 3 %. This increase in LMWs at pH 5.0 in the presence of HCPs further proceeded over time.

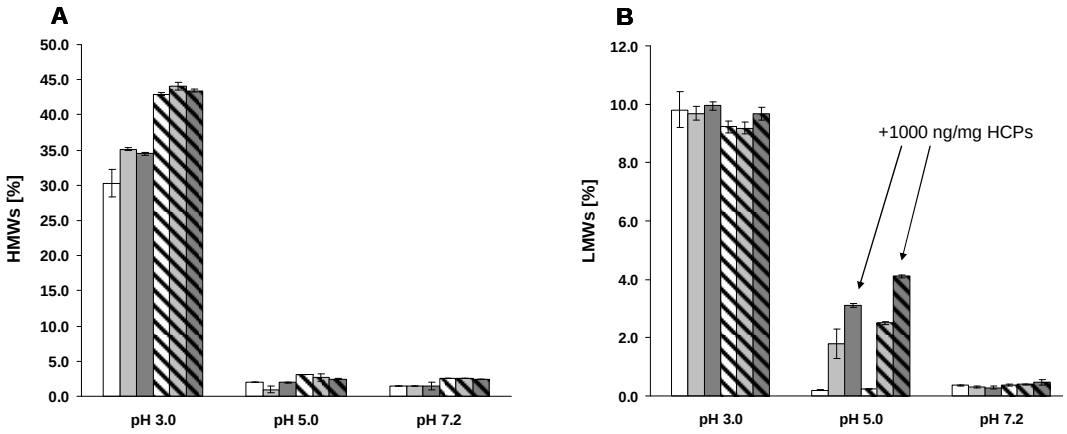

Figure VI-27: Percent HMWs (A) and LMWs (B) in solution determined with SE-HPLC
Incubation at 40 °C for two week (solid bars) and four weeks (striped bars) after spiking with 0 ng/mg HCP (white), 500 ng/mg HCP (light grey) and 1000 ng/mg HCP (dark grey); for each sample about 20 mg IgG were applied; results are presented as mean values of three measurements ± SD.

By looking at the incubated samples at pH 7.5, no increase in HMWs or LMWs was recognized in the presence of 500 ng/mg or 1000 ng/mg HCP in comparison to the unspiked samples.

Degradation of full-length antibodies can be the consequence of multiple causes encompassing physical, chemical and biological ones. Cleavage in the flexure point between the Fc and the Fv domain (hinge region), clippings in the sequence in general or breakage of disulfide bonds are known to result in fragmented molecules of different size and amino acid sequence. A variety of processing conditions is known to potentially accelerate mAb fragmentation, such as thermal treatment (Harrison et al. 1998; Liu et al. 2006), radiation treatment (Caballero et al. 2004), exposure to light (Kerwin and Remmele 2007; Qi et al. 2008) or basic or acidic treatment (Daugherty and Mrsny 2006; Gaza-Bulseco and Liu 2008; Usami et al. 1996). In this study, the degradation of the IgG was in fact enhanced at pH 3.0. However, an increase in fragments was solely observed at pH 5.0 when the HCP

standard solution was added. It is known that IgG degradation moreover occurs in the presence of proteolytic enzymes, whose activity can be controlled by temperature, pH or specific inhibitors and substrates (Robert et al. 2009). Papain and pepsin are the most prominent ones which are well known to cleave peptide bonds in the hinge and hinge proximal region of the C_{H2} domain of IgG. Since a variety of proteases are expressed during cultivation of CHO cell lines which were shown to lead to degradation of the recombinant protein (Busby et al. 2000; Robert et al. 2009; Sandberg et al. 2006), it was concluded that the HCP standard solution used contains at least one proteolytic protein species resulting in IgG degradation at pH 5.0.

SDS-PAGE of the solutions containing 1000 ng/mg HCP after storage for four weeks at 40 °C revealed that actually at pH 5.0 (lane 6) additional bands below 30 kDa appeared in the gel which were not observed in the absence of the spiked HCP standard (lane 5) (Figure VI-28A).

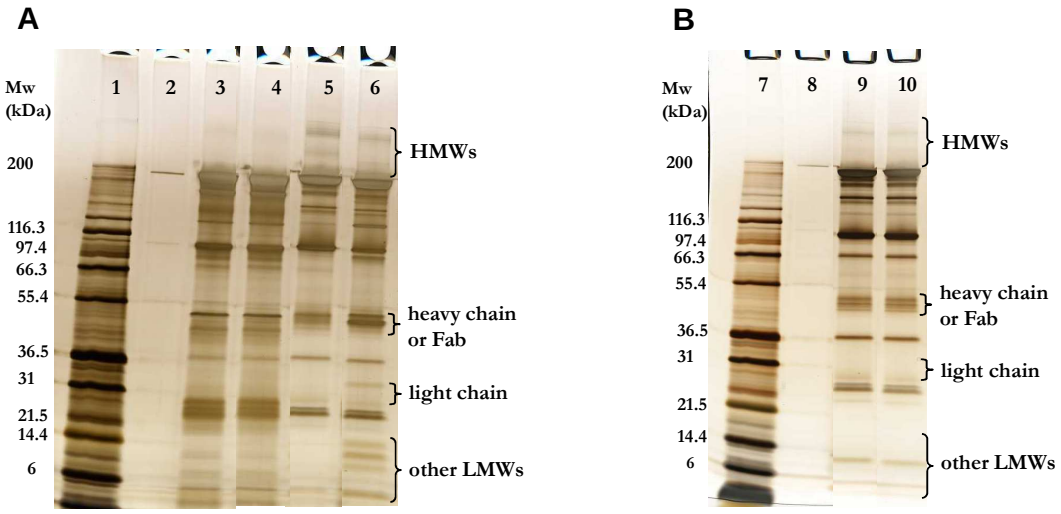

Figure VI-28: SDS-PAGE silver stained gels of non-reduced IgG samples at pH 3.0 and pH 5.0 (A) and pH 7.5 (B) after incubation with 0 ng/mg and 1000 ng/mg HCP at 40 °C for four weeks
Lane 1 and 7: molecular weight (Mw) standard; lane 2 and 8: buffer; lane 3: IgG at pH 3.0; lane 4: IgG + 1000 ng/mg at pH 3.0; lane 5: IgG at pH 5.0; lane 6: IgG + 1000 ng/mg at pH 5.0; lane 9: IgG at pH 7.5; lane 10: IgG + 1000 ng/mg at pH 7.5.

Moreover, the bands at about 50 kDa which can be assigned to IgG heavy chain or Fab fragments (Mahler et al. 2009) showed an increase in intensity solely in the presence of HCP. The samples containing 1000 ng/mg HCP during storage at pH 3.0 and pH 7.5 did

not show any significant differences in the band composition compared to the unspiked ones (Figure VI-28B). The bands which are assignable to the HMWs showed a decreased intensity for the samples at pH 5.0 containing 1000 ng/mg HCPs, suggesting that HMWs were also degraded in the presence of the proteolytic proteins (Figure VI-28A).

Beside the analysis of soluble aggregates detected by SE-HPLC, the HCP spiked and unspiked samples were investigated by turbidity measurements. Figure VI-29 shows that an induction of larger aggregates can be solely attributed to the environmental pH, since turbidity was shown to generally increase with increasing pH of the solutions. Incubation of the spiked solutions did not reveal any significant difference in turbidity depending on the HCP level, neither at room temperature, nor at 40 °C.

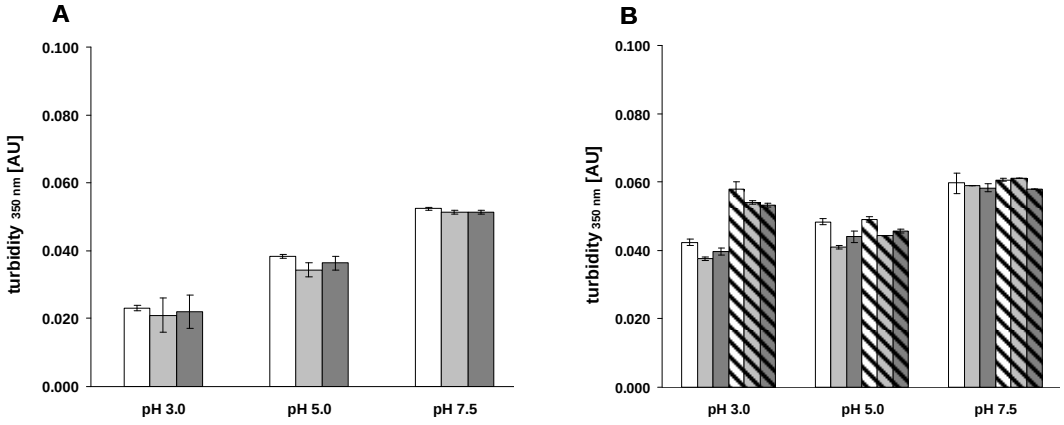

Figure VI-29: Turbidity at 350 nm during storage at room temperature (A) and storage at 40 °C (B)
Incubation at room temperature for 24 hours (A) and at 40 °C for two week (solid bars) and four weeks (striped bars) (B) after spiking with 0 ng/mg HCP (white), 500 ng/mg HCP (light grey) and 1000 ng/mg HCP (dark grey); for each sample about 20 mg IgG were applied; results are presented as mean values of three measurements ± SD.

The potential induction of aggregates in the presence of HCPs derived from CHO cells was moreover investigated in acetate buffer containing 10-250 mM sodium chloride at pH 5.0. It was expected that the level of aggregates may increase in the presence of salt and the addition of HCP may further promote the propensity of the IgG to aggregate. Figure VI-30A shows that the increasing molarity of NaCl at pH 5.0 results in an induction of HMWs determined by SE-HPLC after storage at 40 °C. This was expected, since it is known that repulsive electrostatic interactions between the protein molecules at non

isoelectric pH are reduced leading to self-association (Chi et al. 2003b; Przybycien and Bailey 1989). The presence of HCPs in solution results in a decrease of the HMW level which was further pronounced with a higher salt molarity. The decrease in HMWs in the presence of HCP was already visible after 24 hours at room temperature (data not shown). Concomitantly, the level of LMWs increased in addition with increasing salt concentration (Figure VI-30B). The level of LMWs increased in addition with the concentration of HCPs and with storage time.

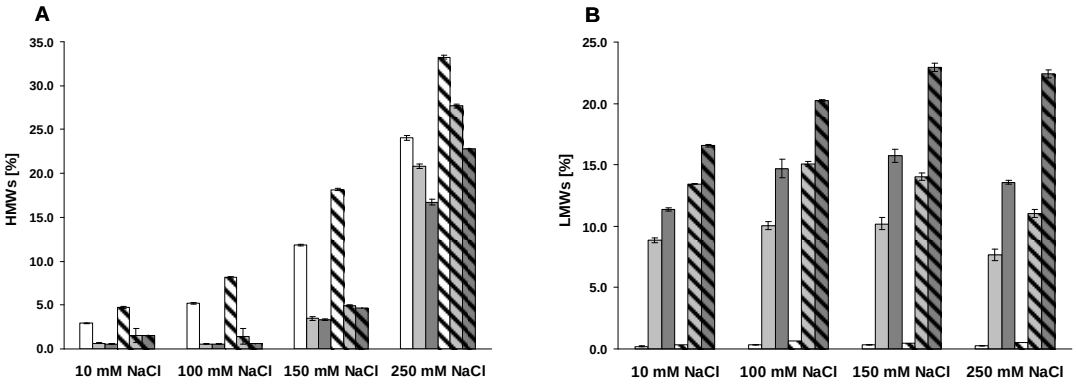

Figure VI-30: Percent HMWs (A) and LMWs (B) in solution determined with SE-HPLC
Incubation at 40 °C for two week (solid bars) and four weeks (striped bars) after spiking with 0 ng/mg HCP (white), 500 ng/mg HCP (light grey) and 1000 ng/mg HCP (dark grey); for each sample about 20 mg IgG were applied; results are presented as mean values of three measurements ± SD.

SDS-PAGE gels showed additional bands in the region of < 31 kDa in molecular weight which appeared only in the presence of HCPs (lane 7-8) (Figure VI-31). The number of bands which are assignable to small fragments of about 10-20 kDa increased with higher molarity of salt. Moreover, the intensity of the bands in the region of 50 kDa increased in the samples containing 1000 ng/mg HCP. The increased propensity of the IgG to form HMWs with increasing NaCl concentration was no longer obvious when 1000 ng/mg HCP were present in solution. The formation of differently sized fragments and the absence of HMWs during incubation with HCPs were assigned to a proteolytic activity at pH 5.0 of the HCPs being clearly enhanced in the presence of salt. Thus, it was concluded that potential formation of HMWs induced by HCPs does not appear under the selected conditions or was not detectable due to the proteolytic activity of at least one HCP species in the standard solution used.

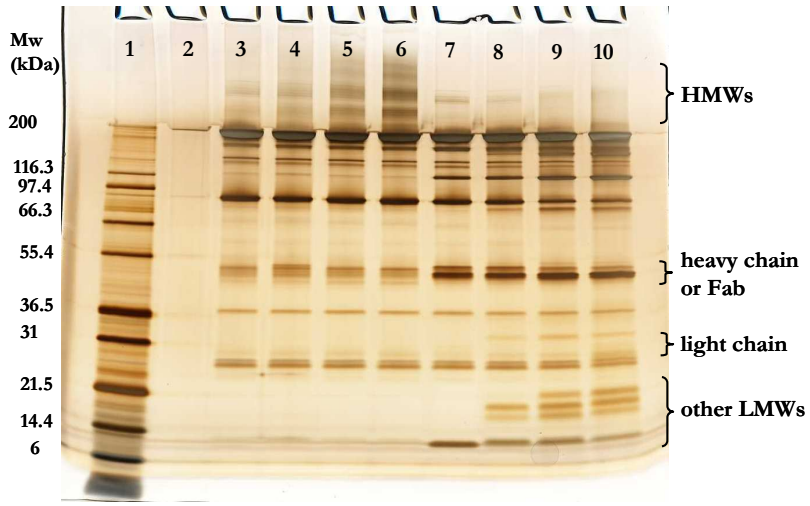

Figure VI-31: SDS-PAGE silver stained gels of non-reduced IgG samples at pH 5.0 after incubation with 0 ng/mg and 1000 ng/mg HCP at 40 °C for four weeks
Lane 1: molecular weight (Mw) standard; lane 2: buffer; lane 3: IgG in 10 mM NaCl; lane 4: IgG in 100 mM NaCl; lane 5: IgG in 150 mM NaCl; lane 6: IgG in 250 mM NaCl; lane 7: IgG + 1000 ng/mg HCP in 10 mM NaCl; lane 8: IgG + 1000 ng/mg HCP in 100 mM NaCl; lane 9: IgG + 1000 ng/mg HCP in 150 mM NaCl; lane 10: IgG + 1000 ng/mg HCP in 250 mM NaCl.

Finally, turbidity measurements were conducted during storage at 40 °C (Figure VI-32). Turbidity did not increase in general with higher salt concentration. All samples which were not spiked with HCPs revealed a turbidity value of about 0.05 AU after storage for two weeks. In the presence of HCPs the turbidity increased after two weeks in a buffer containing 10 mM and 100 mM salt. Turbidity increased further with incubation time. After four weeks, turbidity values were found to step up from 0.05 AU to 0.23 AU in the presence of 500 ng/mg HCP and to 0.56 AU in the presence of 1000 ng/mg in the buffer containing 10 mM NaCl. A level of 0.78 AU was found after four weeks in 100 mM NaCl when 1000 ng/mg HCP were present in solution. At higher salt molarities exceeding 100 mM this strong increase in turbidity during storage in the presence of HCPs was no longer observable. This was once more assigned to the proteolytic activity of the HCPs, which was shown to be enhanced at a higher salt concentration. During storage over four weeks in 250 mM salt, almost no differences in turbidity between the HCP spiked and unspiked samples were identified.

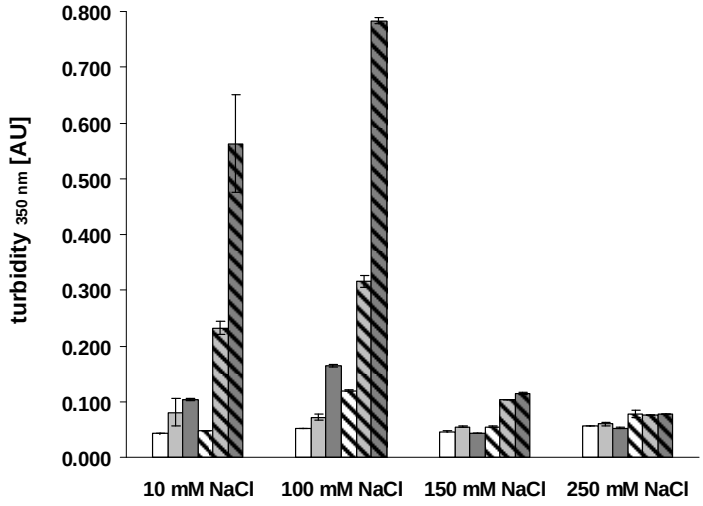

Figure VI-32: Turbidity at 350 nm during storage at 40 °C
Incubation for two weeks (solid bars) and four week (striped bars) after spiking with 0 ng/mg HCP (white), 500 ng/mg HCP (light grey) and 1000 ng/mg HCP (dark grey); for each sample about 20 mg IgG were applied; results are presented as mean values of three measurements ± SD.

In summary, HCPs from CHO cells were only partly involved in the formation of IgG aggregates. Solely at pH 3.0 an increase in the formation of aggregates monitored by SE-HPLC and turbidity measurements was observed due to the presence of 500 ng/mg and 1000 ng/mg HCP. At pH 5.0 an increase in turbidity due to the presence of HCPs was recognized in a buffer containing 10-100 mM salt. Both pH 3.0 and pH 5.0 with 10-150 mM NaCl were shown to be the conditions reducing protease activity. In general, the spiking material applied in this study was shown to contain at least one proteolytic HCP species which was involved in the degradation of the IgG.

4 Summary and conclusion

It was shown that unfunctionalized macro-porous matrices adsorb soluble IgG molecules from liquid bulks. Especially, the surface of controlled pored glass (CPG) which is a commonly applied matrix material in Protein A chromatography, was shown to strongly adsorb the protein at different buffer conditions. A maximum adsorption of 2 mg IgG per m^2 CPG was observed at pH 5.0. The main driving forces for IgG adsorption to the CPG surface was found to be based on electrostatic and hydrophobic interactions between the

protein and the CPG. However, adsorption of protein molecules to interfaces and solid surfaces is in general reported to cause aggregation potentially entailed by conformational changes in secondary or tertiary structure, no induction of soluble IgG aggregates was observed after contact to the CPG surface in a pH range of 3.0 to 7.5. Moreover, CPG particles were shown to preferentially adsorb soluble aggregates, encompassing dimers as well as oligomeric species. 3 m² of CPG (about 0.1 g) were found to be sufficient to adsorb nearly 95 % of the HMWs from a solution containing about 5 mg/ml IgG including 6.8 % HMWs before incubation. Concomitantly, 20 % (about 4 mg) of total protein in solution was lost on the surface. In general, a surface area of 100-150 m² per gram IgG in solution is suitable to remove nearly 80-90 % of soluble aggregates from an IgG solution at pH 5.0, having concomitantly 80-85 % monomeric IgG remaining in solution.

Soluble aggregates were shown to irreversibly bind to the CPG surface at pH 5.0 and pH 7.5 over 6 days. Furthermore, no induction of HMWs was recognized due to the exposure of the IgG to the glass based surface. Here, exogenous micro- as well as nano-sized particles were shown to be capable to adsorb monomeric as well as aggregated IgG species. However, an additional formation of aggregates potentially expected to occur via a heterogeneous nucleation dependent mechanism was not observed. After initial adsorption of monomeric and aggregated species no further loss of soluble protein was observed. Moreover, neither induction of larger aggregates monitored by turbidity measurements, nor precipitated protein was recognized.

The protein being adsorbed to the porous material was shown to be only slightly perturbed with regards to secondary structure monitored by ATR FT-IR. The protein in the supernatant remaining in solution after incubation with the CPG based surface did not show any spectral differences compared to the native protein, with regards to secondary structure (FT-IR spectroscopy) as well as tertiary structure (UV spectroscopy).

Since the rate and onset of aggregation are usually not predictable and a limited removal capacity of soluble aggregates is only possible during the purification process, it is considered useful to have additional capacity in place to reduce the aggregate level especially at the interface to final formulation or directly prior to or during parenteral administration. The application of unfunctionalized CPG particles is considered suitable to remove soluble aggregates from process intermediates as well as from fully purified bulks or formulated material. CPG is known to be a rigid material showing high chemical inertness. The material is reported to withstand heat sterilization and cleaning with hot nitric acid

(Schnabel and Langer 1991). Thus, actually the application in combination with prefilled devices is possible to remove aggregates potentially formed during storage prior to parenteral administration. During purification processes or at the interface to final formulation, the unfunctionalized porous matrix can be simply added to the liquid protein solution in batch mode. After incubation, the aggregate-loaded particles can be removed from the bulk solution by centrifugation and micro-filtration.

As regards IgG aggregation induced by HCPs derived from a CHO cell were shown to be only partially involved in IgG aggregation. It was assumed, that IgG aggregation may be induced in the presence of HCPs at pH 5-6 were attractive electrostatic interaction between the major HCP fraction and the IgG were expected. However, at pH 3.0 a slight increase in the formation of aggregates monitored by SE-HPLC and turbidity measurements was observed due to the presence of 500 ng/mg and 1000 ng/mg HCP. At pH 5.0 an increase in turbidity due to the presence of HCPs was recognized in a buffer containing 10-100 mM salt. In general, the spiking material applied in this study was shown to contain at least one proteolytic HCP species which was involved in the degradation of the monomeric as well as the aggregated IgG.

For further investigations regarding the potential induction of IgG aggregates due to the presence of HCPs, it is recommended to suppress the proteolytic activity of the spiking material. Proteolytic enzymes are organized in type, clan and family depending on which amino acid is envolved in the catalytic site, e.g. serine-, cystein or aspartic proteases are known (Barrett et al. 2004). Moreover, if a metal ion is required as co-factor the enzyme is identified as a metallo-protease. The different types of proteases have specific inhibitors, like aprotinin, pepstatin or EDTA which are detailed elsewhere (Barrett et al. 2004; Cordoba et al. 2005; Robert et al. 2009) and compositions of them are considered useful to be tested in future experiments to control degradation of the IgG caused by the proteases.

Chapter VII Final summary of the thesis

Monoclonal antibodies represent one of the fastest growing segments in biotechnology and due to enormous progress in recombinant DNA technology a large number of pharmaceutically relevant peptides and proteins became accessible as therapeutic products. Although, the structure of IgGs is well known, all recombinant derived molecules of this class have unique sources of heterogeneity due to different structure and glycosylation, heterologous expression systems and impurity profiles, processing conditions and degradation processes. Thus, during the development of each new therapeutic candidate all characteristics of the molecule have to be elucidated considering their effect on potency, stability or immunogenicity. Since substantial progress was made in all fields of therapeutic mAb generation, encompassing cell culture, purification, analytic and formulation development, this triumphal procession of mAbs as treatments for numerous human diseases in the last decades was possible. A crucial problem of protein based biopharmaceuticals is still their stability, since proteins are inherently prone to degradation. Factors influencing protein stability are of special importance during formulation development to ensure long-term stability of the formulated drug product. However, the integrity of the molecule is of utmost importance during all stages of bioprocessing and the focus of this thesis was to gain more insight in mainly physical instability occurring during the purification process of therapeutic mAbs and at its interface to final formulation. The evaluation of critical factors leading to aggregation as well as the development of strategies to improve the quality of the purified bulk was focused.

Chapter I provides an introduction into the field of therapeutic antibodies especially focusing on purification techniques being applicable at lab scale as well as at manufacturing scale. An overview encompassing different chromatographic principles, as well as several filtration techniques is given. Applied manufacturing strategies and their influence on protein aggregation were presented and a general overview on different factors leading to pro-

tein aggregation was summarized. Conformational and colloidal aspects, as well as concentration and nucleation dependent aggregation were accounted for.

The main objectives of the present work are detailed in chapter II.

In chapter III the effect of operational parameters during tangential UF was evaluated regarding their potential to adversely affect the physical stability of concentrated IgGs in the retentate. The influence of flow and pressure conditions as well as of the protein concentration during processing was examined. A previously described correlation between shear stress and applied pressure and flow conditions showed that wall shear stress has to be limited to avoid an increased level of mainly insoluble and structurally perturbed aggregates in the concentrated bulk. Concomitantly, a minimal shear stress was shown to be necessary to ensure sufficient back transport of deposited solutes from the membrane into the retentate leading to sufficient permeate flux over time.

In general, permeate flux was recognized to strongly decrease with increasing protein concentration. Therefore, a systematic variation of process conditions was performed at different protein concentrations in the retentate. It was shown that the defined variation of retentate flow and TMP during the process was successful in achieving a high end-concentration exceeding 100 mg/ml. Additionally, a 20 % reduction in process time was recognized when this optimized method was used in comparison to two UF methods operating at constant pressure and flow conditions. Concomitantly, a decreased level of conformationally altered aggregates in the concentrated solutions was shown for three different mAbs.

Finally, the operational parameters applied during UF were shown to impact subsequent processing steps. The concentrates derived from the optimized UF method showed an improved flow rate during sterile filtration processing due to improved bulk quality in terms of aggregation. This is important because this essential final manufacturing step is already adversely affected by the high viscosity of the concentrated protein solution.

Chapter IV deals with the stability of highly concentrated IgG solutions generated by applying different UF methods. A reduced level of insoluble aggregates before and during storage of the concentrated solutions was recognized when the optimized UF method was applied. These aggregates were completely removed by 0.22 μm filtration and did not re-

appear during storage. A significant reduction of the HMW level was not that pronounced when the optimized method was used. Interestingly, filtration of the concentrated solutions was observed to facilitate the formation of soluble aggregates during storage. In the presence of large particulate aggregates the formation of HMWs was repressed. The protein aggregation behavior in highly concentrated solutions was shown to be rather controlled by a homogeneous nucleation and growth process than by partially unfolded molecules, since the protein was recognized to be in general protected against conformational changes at a higher total protein concentration. The increase in the melting temperature (T_m) at a high protein concentration of 90 mg/ml did not result in a decreased formation of aggregates during storage below T_m. The applied UF method seemed to significantly affect the conformational stability of the protein, however these results did not correspond to the aggregation behavior during stability studies, since no significant differences regarding the level of several types of aggregates in the differently processed concentrates were observed during storage below T_m. In general, storage at 2-8 °C was clearly shown to be the best choice for unformulated highly concentrated IgG solutions to circumvent the formation of aggregates.

At the interface of downstream processing and final formulation of highly concentrated mAb solutions a significant deviation in solute concentration, pH and conductivity was observed with increasing protein concentration during UF processing (chapter V). It was known from current literature that during dialysis of non-IgG proteins the concentration of the diffusible buffer forming solutes changes on the retentate side compared to the permeate side. This thermodynamic non-ideality, based on electrostatic interactions of the solutes and the protein at non isoelectric pH leads to unequal partitioning of charged solutes across the membrane. The so-called Donnan-effect was investigated and evaluated for two different IgGs during the UF concentration process adequately reflecting process conditions at manufacturing scale. It was shown that post-diafiltration as well as post-concentration assays of 200 mg/ml IgG revealed up to 50 % lower molar histidine concentrations than those of the diafiltration buffer. Deviations were also observed when the IgG was dialyzed and concentrated in an acetate buffered environment. Here, up to 100 % higher molar acetate concentrations were found. The Donnan-equation was shown to adequately reflect the partitioning characteristics of the small solutes during UF of IgGs depending mainly on protein charge

and concentration. The partitioning behavior was successfully correlated to pH and conductivity characteristics observed during UF processing.

Since it was known, that pH as well as the solute composition and concentration of the buffer system are important factors to provide sufficient stability of the protein in solution, the relevance of the altered solution conditions as a consequence of the UF processing was evaluated. It was shown, that chemical and physical stability of the concentrated bulk were compromized in the case of a histidine buffer at a protein concentration of 200 mg/ml. Moreover, pH corrections in the concentrated solutions were observed to contribute to an increased level of differently sized aggregates. Therefore, the Donnan-equation was applied for the feasible prediction of the molar histidine concentration required before UF in order to achieve the desired molarities after UF and to circumvent concomitantly deviations in pH. An increase in the histidine molarity to 31 mM before UF as predicted by the Donnan-equation was suitable to end up with 20 mM histidine at pH 5 after UF up to 200 mg/ml IgG concentration. It was shown that this feasible approach led to a reduced level of protein aggregates as well as of deamidated Fab fragments in the concentrated bulk solutions. Moreover, an improved chemical and physical stability of the concentrated protein was recognized during storage which was related again to the higher histidine molarity and the stable pH conditions during and after UF.

In addition, the add-on of histidine before UF contributed to a decrease in viscosity of the concentrated protein solutions. This is of special interest since a higher viscosity of the solutions can introduce divers issues during manufacturing, filling and administration to the patient.

In chapter VI the potential role of exogenous impurities on the physical stability of mAb purification intermediates was investigated. An IgG was shown to strongly adsorb to an unfunctionalized chromatographic matrix based on controlled pored glass (CPG). The main driving forces for adsorption were found to be based on electrostatic and hydrophobic interactions between the CPG surface and the protein molecules. No induction of protein aggregates at different buffer conditions was recognized, however the adsorption of protein molecules to surfaces is generally known to facilitate their aggregation. ATR FT-IR spectroscopy was successfully used to access the secondary structure of the IgG directly adsorbed to the CPG surface and the exposure to CPG particles did not result in detectable conformational alterations of the protein molecules as regards secondary and tertiary

structure (UV-spectroscopy). Furthermore, no induction of aggregates was observed when micro- and nano-sized particles were incubated with IgG solutions for one week. After initial adsorption of monomeric and aggregated species no further loss of soluble monomeric protein was observed. However, an additional formation of aggregates potentially expected due to a heterogeneous nucleation dependent mechanism was not recognized.

Since the CPG matrix was shown to have the potential to irreversibly adsorb protein aggregates it was assumed to utilize the particles specifically to reduce the aggregate level of IgG solutions. It was recognized that soluble aggregates, encompassing dimers and oligomers, were favorably adsorbed to the CPG surface. After incubation of the glass surfaces with the IgG solution at pH 5, the aggregate loaded CPG particles were removed by simple centrifugation and nearly 80-90 % of the soluble aggregates were cleared from the protein bulk, when 100-150 m^2 CPG per gram protein were applied. Concomitantly, about 80-85 % of the monomer remained in solution. In spite of this unavoidable loss of monomeric protein, the quite simple procedure of incubation and the removal of the aggregate-loaded surface provides for convenient capacity for aggregate clearance during purification processing, storage or prior to parenteral administration.

In the course of evaluating the potential role of exogenous impurities on the stability of mAbs, a typical process related impurity, the indigenous proteins expressed by the recombinant host cells, was chosen. Purified host cell proteins (HCPs) derived from a specific CHO master cell were shown to be a complex mixture of numerous proteins with divers physicochemical properties regarding IP and molecular weight. This specific HCP composition was shown to be partly involved in the formation of IgG aggregates under specific conditions. Unfortunately, the HCPs applied were shown to encompass at least one proteolytic species which was shown to be involved in the degradation of the IgG monomer as well as its aggregates. For further investigations regarding the potential induction of IgG aggregates due to the presence of HCPs, it is recommended to suppress the proteolytic activity of the HCP material by applying specific protease inhibitors.

Chapter VIII Addendum

1 List of abbreviations

Δp	Pressure drop
ADCC	Antibody dependent cytotoxicity
AEX	Anion exchange chromatography
API	Active pharmaceutical ingredient
ATR	Attenuated total reflection
BHK	Baby hamster kidney
BSA	Bovine serum albumin
CCL	Continuous cell line
CDC	Complement dependent cytotoxicity
CEX	Cation exchange chromatography
cGMP	Current good manufacturing practice
CHO	Chinese hamster ovary
ConcF	Concentration factor
DLS	Dynamic light scattering
DSP	Downstream processing
FT-IR	Fourier transformed infrared spectroscopy
HCP	Host cell protein
HIC	Hydrophobic interaction chromatography
HMWs	Higher molecular weight species
IEF	Isoelectric focusing
IEX	Ion-exchange chromatography
IgG	Immunoglobulin G
IP	Isoelectric point
J	Permeate flux
kDa	Kilodalton
LMWs	Lower molecular weight species

LO	Light obscuration
mAb	Monoclonal antibody
NFF	Normal flow filtration
NMWC	Normal molecular weight cut-off
NWF	Normalized water flow
Mw	Molecular weight
PES	Polyethersulfone
PS	Polysulfone
Q	Feed flow rate
Q_r	Retentate flow rate
RC	Regenerated cellulose
Re	Reynolds number
Rpm	Rounds per minute
SD	Standard deviation
SDS-PAGE	Sodium dodecyl sulfate-polyacrylamide gel electrophoresis
SE-HPLC	Size exclusion high pressure liquid chromatography
SEM	Scanning electron microscopy
TFF	Tangential flow filtration
T_m	Melting temperature
TMP	Transmembrane pressure
UF	Ultrafiltration

2 List of figures

3 List of tables

4 Curriculum vitae

Eva Rosenberg

Personal details

Date of birth:	January 29th, 1978
Place of birth:	Stuttgart, Germany
Nationality:	German
Qualification for university entrance:	Graduation with "allgemeine Hochschulreife", Immanuel-Kant-Gymnasium, Leinfelden, 1997

Academic Education

05/2009 to present	Group leader at Roche Diagnostics GmbH, Penzberg, Germany Pharma Biotech Development Recovery and DSP
05/2006-04/2009	PhD-Thesis at the Department of Pharmacy, Pharmaceutical Technology and Biopharmaceutics, Ludwig-Maximilians-University Munich (supervisor: Prof. Dr. Gerhard Winter) in a research cooperation with Roche Diagnostics GmbH, Penzberg, Germany Pharma Biotech Development Recovery and DSP
02/2006-04/2006	Internship at Roche Diagnostics GmbH, Penzberg, Germany
12/2005	Licence to practice as pharmacist
05/2005-10/2005	Internship at Roche Diagnostics GmbH, Penzberg, Germany
11/2004-04/2005	Internship in public pharmacy, Kloster-Apotheke, Munich, Germany
10/2000-07/2004	Study of Pharmacy at the Ludwig-Maximilians-University, Munich

5 Presentations and publications associated with this thesis

Articles

E. Rosenberg, S. Hepbildikler, W. Kuhne, G. Winter
Ultrafiltration concentration of monoclonal antibody solutions: Development of an optimized method minimizing aggregation, J. Mem. Sci., 342 (2009) 50.

R. Falkenstein, S. Hepbildikler, W. Kuhne, T. Lemm, H. Rogl, E. Rosenberg, G. Winter, F. Zettl, R. Zippelius, Approaches in DSP to face aggregation: Influence by process control, in: H.-C. Mahler and W. Jiskoot (Eds.), Analysis of aggregates and particles in protein pharmaceuticals, John Wiley & Sons, Hoboken, in preparation.

Patent applications

WO2009/010269
S. Hepbildikler, W. Kuhne, E. Rosenberg, G. Winter
Variable tangential flow filtration

WO2009/068282
E. Rosenberg, S. Hepbildikler, W. Kuhne, G. Winter
Immunoglobulin aggregates

Submitted
E. Rosenberg, S. Hepbildikler, W. Kuhne, G. Winter
Pre-filtration adjustment of buffer solutes

Poster presentations

E. Rosenberg, K. Heinrich, S. Hepbildikler, W. Kuhne, J. Burg, G. Winter
Optimization of TFF in DSP for highly concentrated mAb intermediate solutions with respect to aggregation, Colorado Protein Stability Conference, Breckenridge, CO, USA, July, 19th-21st 2007.

E. Rosenberg, K. Heinrich, S. Hepbildikler, W. Kuhne, G. Winter
The influence of shear stress and preformed soluble aggregates in TFF on the aggregation in highly concentrated mAb intermediate solutions in DSP, 6th World Meeting on Pharmaceutics, Biopharmaceutics and Pharmaceutical Technology, Barcelona, Spain, April, 6th-10th 2008.

E. Rosenberg, S. Hepbildikler, W. Kuhne, G. Winter
Highly concentrated mAb solutions at the interface of DSP and final formulation, Evolution by Innovation, PR&D Asilomar GNE, Asilomar, CA, USA, July, 22nd-25th September, 2009.

6 References

Advant, S.J., Braswell, E.H., Kumar, C.V., Kalonia, D.S., The effect of pH and temperature on the self association of recombinant human interleukin-2 as studied by equilibrium sedimentation, Pharm. Res., 12 (1995) 637.

Aggarwal, S., What is fueling the biotech engine 2008, Nat. Biotechnol., 27 (2009) 987.

Ahrer, K., Buchacher, A., Iberer, G., Josic, D., Jungbauer, A., Analysis of aggregates of human immunoglobulin G using size-exclusion chromatography, static and dynamic light scattering, J. Chromatogr. A, 1009 (2003) 89.

Ahrer, K., Buchacher, A., Iberer, G., Jungbauer, A., Effects of ultra-/diafiltration conditions on present aggregates in human immunoglobulin G preparations, J. Membr. Sci., 274 (2006) 108.

Aimar, P., Howell, J.A., Turner, M., Effects of concentration boundary layer development on the flux limitations in ultrafiltration, Chem. Eng. Res. Des., 67 (1989) 255.

Alford, J.R., Kendrick, B.S., Carpenter, J.F., Randolph, T.W., High concentration formulations of recombinant human interleukin-1 receptor antagonist: II. aggregation kinetics, J. Pharm. Sci., 97 (2008a) 3005.

Alford, J.R., Kwok, S.C., Roberts, J.N., Wuttke, D.S., Kendrick, B.S., Carpenter, J.F., Randolph, T.W., High concentration formulations of recombinant human interleukin-1 receptor antagonist: I. physical characterization, J. Pharm. Sci., 97 (2008b) 3035.

Andersson, M., Ramberg, M., Johansson, B.-L., The influence of the degree of cross-linking, type of ligand and support on the chemical stability of chromatography media intended for protein purification, Process Biochemistry, 33 (1998) 47.

Andrews, J.M., Roberts, C.J., A Lumry-Eyring nucleated polymerization model of protein aggregation kinetics: Aggregation with pre-equilibrated unfolding, J. Phys. Chem. B, 111 (2007) 7897.

Andya, J.D., Hsu, C.C., Shire, S.J., Mechanisms of aggregate formation and carbohydrate excipient stabilization of lyophilized humanized monoclonal antibody formulations, AAPS J., 5 (2005) 1.

Ansaldi, D., Lester, P., Separation of protein monomer from aggregates by use of ion-exchange chromatography, EP1500661 A1, 2005.

Apfel, R.E., The role of impurities in cavitation: Threshold determination, J. Acoust. Soc. Am., 48 (1970) 1179.

Arakawa, T., Philo, J.S., Ejima, D., Tsumoto, K., Arisaka, F., Aggregation analysis of therapeutic proteins (part 1), Bio Process Int., 4 (2006) 32.

Arakawa, T., Philo, J.S., Tsumoto, K., Yumioka, R., Ejima, D., Elution of antibodies from a Protein A column by aqueous arginine solutions, Prot. Expr. Pur., 36 (2004) 244.

Arakawa, T., Timasheff, S.N., Preferential interactions of proteins with salts in concentrated solutions, Biochemistry, 21 (1982) 6545.

Arakawa, T., Timasheff, S.N., Preferential interactions of proteins with solvent components in aqueous amino acid solutions, Arch. Biochem. Biophys., 224 (1983) 169.

Arakawa, T., Timasheff, S.N., Mechanism of protein salting in and salting out by divalent cation salts: Balance between hydration and salt binding, Biochemistry, 23 (1984) 5912.

Ariza, M.J., Cañas, A., Benavente, J., Electrokinetic and electrochemical characterizations of porous membranes, Colloids Surf. A, 189 (2001) 247.

Atchley, D.W., Nichols, E.G., The influence of protein concentration on the conductivity of human serum, J. Biol. Chem., 65 (1925) 729.

Bacchin, P., Aimar, P., Critical fouling conditions induced by colloidal surface interaction: From causes to consequences, Desalination, 175 (2005) 21.

Bam, N.B., Cleland, J.L., Yang, J., Manning, M.C., Carpenter, J.F., Kelley, R.F., Randolph, T.W., Tween protects recombinant human growth hormone against agitation-induced damage via hydrophobic interactions, J. Pharm. Sci., 87 (1998) 1554.

Barrett, A.J., Woessner, F.J., Rawlings, N.D., Handbook of proteolytic enzymes, Academic Press, Lodon, 2004, pp. 2368.

Bee, J.S., Chiu, D., Sawicki, S., Stevenson, J.L., Chatterjee, K., Freund, E., Carpenter, J.F., Randolph, T.W., Monoclonal antibody interactions with micro- and nanoparticles: Adsorption, aggregation, and accelerated stress studies, J. Pharm. Sci. (2009a) in press.

Bee, J.S., Nelson, S.A., Freund, E., Carpenter, J.F., Randolph, T.W., Precipitation of a monoclonal antibody by soluble tungsten, J. Pharm. Sci. (2009b) in press.

Bee, J.S., Stevenson, J.L., Mehta, B., Svitel, J., Pollastrini, J., Platz, R., Freund, E., Carpenter, J.F., Randolph, T.W., Response of a concentrated monoclonal antibody formulation to high shear, Biotechnol. Bioeng. (2009c) in press.

Behrens, S.H., Grier, D.G., The charge of glass and silica surfaces, J. Chem. Phys., 115 (2001) 6716.

Belfort, G., Davis, R.H., Zydney, A.L., The behavior of suspensions and macromolecular solutions in crossflow microfiltration, J. Membr. Sci., 96 (1994) 1.

Benavente, J., Jonsson, G., Effect of adsorbed protein on the hydraulic permeability, membrane and streaming potential values measured across a microporous membrane, Colloids Surf. A, 138 (1998) 255.

Birch, J.R., Racher, A.J., Antibody production, Adv. Drug Deliv. Rev., 58 (2006) 671.

Blackwell, H.R., Contrast thresholds of the human eye, J. Opt. Soc. Am., 36 (1946) 624.

Bohorquez, H.J., Obregon, M., Cardenas, C., Llanos, E., Suarez, C., Villaveces, J.L., Patarroyo, M.E., Electronic energy and multipolar moments characterize amino acid side chains into chemically related groups, J. Phys. Chem. A, 107 (2003) 10090.

Bookbinder, L.H., Hofer, A., Haller, M.F., Zepeda, M.L., Keller, G.-A., Lim, J.E., Edgington, T.S., Shepard, H.M., Patton, J.S., Frost, G.I., A recombinant human enzyme for enhanced interstitial transport of therapeutics, J. Contr. Rel., 114 (2006) 230.

Boschetti, E., Advanced sorbents for preparative protein separation purposes, J. Chromatogr. A, 658 (1994) 207.

Boschetti, E., Jungbauer, A., Separation of antibodies by liquid chromatography, in: Ahuja, S. (Ed.), Handbook of bioseparations, Academic Press, San Diego, CA, 2000, pp. 535.

Brange, J., Physical stability of proteins, in: Frokjaer, S., Hovgaards, L. (Ed.), Pharmaceutical formulation development of peptides and proteins, Taylor and Francis, London, 2000, pp. 89-112.

Brorson, K., Krejci, S., Lee, K., Hamilton, E., Stein, K., Xu, Y., Bracketed generic inactivation of rodent retroviruses by low pH treatment for monoclonal antibodies and recombinant proteins, Biotechnol. Bioeng., 82 (2003) 321.

Burton, D.R., Immunoglobulin G: Functional sites, Mol. Immunol., 22 (1985) 161.

Busby, W.H., Nam, T.-J., Moralez, A., Smith, C., Jennings, M., Clemmons, D.R., The complement component C1s Is the protease that accounts for cleavage of insulin-like growth factor-binding protein-5 in fibroblast medium, J. Biol. Chem., 275 (2000) 37638.

Caballero, I., Altanes, S., Castillo, A., Deridder, V., Gomez, T., Miralles, Y., Naydenov, V., Prieto, E., Tilquin, B., Radiosensitivity study of freezedried antibodies to gamma irradiation, Ame. Pharm. Rev., 7 (2004) 40.

Cao, E., Chen, Y., Cui, Z., Foster, P.R., Effect of freezing and thawing rates on denaturation of proteins in aqueous solutions, Biotechnol. Bioeng., 82 (2003) 684.

Capelle, M.A.H., Gurny, R., Arvinte, T., High throughput screening of protein formulation stability: Practical considerations, Eur. J. Pharm. Biopharm., 65 (2007) 131.

Carpenter, J.F., Kendrick, B.S., Chang, B.S., Manning, M.C., Randolph, T.W., Inhibition of stress-induced aggregation of protein therapeutics, Meth. Enzymol., 309 (1999) 236.

Carpenter, J.F., Randolph, T.W., Jiskoot, W., Crommelin, D.J.A., Middaugh, C.R., Winter, G., Fan, Y.-X., Kirshner, S., Verthelyi, D., Kozlowski, S., Clouse, K.A., Swann, P.G., Rosenberg, A.S., Cherney, B., Overlooking subvisible particles in therapeutic protein products: Gaps that may compromise product quality, J. Pharm. Sci., 98 (2009) 1201.

Center for Biologics Evaluation and Research (CBER), Points to consider in the characterization of cell lines used to produce biologicals, http://www.fda.gov/cber/cberftp.html, 1993.

Center for Biologics Evaluation and Research (CBER), Points to consider in the manufacture and testing of monoclonal antibody products for human use, http://www.fda.gov/cber/cberftp.html, 1997.

Chadd, H.E., Chamow, S.M., Therapeutic antibody expression technology, Curr. Opinion Biotech., 12 (2001) 188.

Champion, K., Madder, H., Dougherty, J., Shacter, E., Defining you product profile and maintaining control over it, Part 2, Bio Process Int., 3 (2005) 53.

Chan, R., Fouling mechanisms in the membrane filtration of single and binary protein solutions, School of Chemical Engineering and Industrial Chemistry, The University of New South Wales, Sydney, 2002, pp. 290.

Chandavarkar, A.S., Dynamics of fouling of microporous membranes by proteins, Department of Chemical Engineering, Massachusetts Institute of Technology, Cambridge, MA, 1990, pp. 284.

Chang, B.S., Kendrick, B.S., Carpenter, J.F., Surface-induced denaturation of proteins during freezing and its inhibition by surfactants, J. Pharm. Sci., 85 (1996) 1325.

Chang, L.L., Shepherd, D., Sun, J., Ouellette, D., Grant, K.L., Tang, X.C., Pikal, M.J., Mechanism of protein stabilization by sugars during freeze-drying and storage: Native structure preservation, specific interaction, and/or immobilization in a glassy matrix, J. Pharm. Sci., 94 (2005) 1427.

Charm, S.E., Lai, C.J., Comparison of ultrafiltration systems for concentration of biologicals, Biotechnol. Bioeng., 13 (1971) 185.

Chen, B., Bautista, R., Yu, K., Zapata, G.A., Mulkerrin, M.G., Chamow, S.M., Influence of histidine on the stability and physical properties of a fully human antibody in aqueous and solid forms, Pharm. Res., 20 (2003) 1952.

Cheryan, M., Ultrafiltration and microfiltration handbook, CRC Press, Boca Raton, FL, 1998, pp. 539.

Chi, E.Y., Kendrick, B.S., Carpenter, J.F., Theodore W. Randolph, Population balance modeling of aggregation kinetics of recombinant human interleukin-1 receptor antagonist, J. Pharm. Sci., 94 (2005a) 2735.

Chi, E.Y., Krishnan, S., Kendrick, B.S., Chang, B.S., Carpenter, J.F., Randolph, T.W., Roles of conformational stability and colloidal stability in the aggregation of recombinant human granulocyte colony-stimulating factor, Protein Sci., 12 (2003a) 903.

Chi, E.Y., Krishnan, S., Randolph, T.W., Carpenter, J.F., Physical stability of proteins in aqueous solution: Mechanism and driving forces in nonnative protein aggregation, Pharm. Res., 20 (2003b) 1325.

Chi, E.Y., Weickmann, J., Carpenter, J.F., Manning, M.C., Randolph, T.W., Heterogeneous nucleation-controlled particulate formation of recombinant human platelet-activating factor acetylhydrolase in pharmaceutical formulation, J. Pharm. Sci., 94 (2005b) 256.

Chiti, F., Taddei, N., Baroni, F., Capanni, C., Stefani, M., Ramponi, G., Dobson, C.M., Kinetic partitioning of protein folding and aggregation, Nat. Struct. Mol. Biol., 9 (2002) 137.

Clarke, A.R., Waltho, J.P., Protein folding pathways and intermediates, Curr. Opinion Biotech., 8 (1997) 400.

Cleland, J.L., Lam, X., Kendrick, B., Yang, J., Yang, T.-H., Overcashier, D., Brooks, D., Hsu, C.C., Carpenter, J.F., A specific molar ratio of stabilizer to protein is required for storage stability of a lyophilized monoclonal antibody, J. Pharm. Sci., 90 (2001) 310.

Cleland, J.L., Powell, M.F., Shire, S.J., The development of stable protein formulations: A close look at protein aggregation, deamidation, and oxidation, Crit. Rev. Ther. Drug Carr. Syst., 10 (1993) 307.

Commitee for Proprietary Medicinical Products, Position statement on DNA and HCP impurities, routine testing versus validation studies, http://www.emea.eu.int/, 1997.

Commitee for Proprietary Medicinical Products, Position statement on the use of tumourigenic cells of human origin for the production of biological and biotechnological medicinical products, http://www.emea.eu.int/, 2001.

Cordoba, A.J., Shyong, B.-J., Breen, D., Harris, R.J., Non-enzymatic hinge region fragmentation of antibodies in solution, J. Chromatogr. B, 818 (2005) 115.

Costantino, H.R., Andya, J.D., Shire, S.J., Hsu, C.C., Fourier-transform infrared spectroscopic analysis of the secondary structure of recombinant humanized immunoglobulin G, Pharm. Sci., 3 (1997) 121.

Cromwell, M., Hilario, E., Jacobson, F., Protein aggregation and bioprocessing, AAPS J., 8 (2006) 572.

Cuatrecasas, P., Anfinsen, C.B., Affinity chromatography, in: Jakoby, W.B. (Ed.), Enzyme purification and related techniques, Academic Press, London, 1971, pp. 345-378.

Curtis, S., Lee, K., Blank, G.S., Brorson, K., Xu, Y., Generic/ matrix evaluation of SV40 clearance by anion exchange chromatography in flow-through mode, Biotechnol. Bioeng., 84 (2003) 179.

Damodaran, S., Kinsella, J., The effects of neutral salts on the stability of macromolecules. A new approach using a protein-ligand binding system, J. Biol. Chem., 256 (1981) 3394.

Dani, B., Platz, R., Tzannis, S.T., High concentration formulation feasibility of human immunoglubulin G for subcutaneous administration, J. Pharm. Sci., 96 (2007) 1504.

Daugherty, A.L., Mrsny, R.J., Formulation and delivery issues for monoclonal antibody therapeutics, Adv. Drug Deliv. Rev., 58 (2006) 686.

Davis, R.H., Leighton, D.T., Shear-induced transport of a particle layer along a porous wall, Chem. Eng. Sci., 42 (1987) 275.

Deanin, R.D., Polymer structure, properties and applications, Chaners Books, Boston, MA, 1972, pp. 496.

Debenedetti, P.G., Metastable liquids: Concepts and principles, Princeton University Press, Princeton, NJ, 1996, pp. 400.

Demeester, J., De Smedt, S.S., Sanders, N.N., Haustraete, J., Light scattering, in: Jiskoot, W., Crommelin, D. (Ed.), Methods for structural analysis of protein pharmaceuticals, AAPS Press, Arlington, VA, 2005, pp. 245-275.

Dill, K.A., Shortle, D., Denatured states of proteins, Ann. Rev. Biochem., 60 (1991) 795.

Dobson, C.M., Unfolded proteins, compact states and molten globules, Curr. Opin. Struct. Biol., 2 (1992) 6.

Dolman, C., Thorpe, R., Analysis and purification of IgG using size-exclusion high performance liquid chromatography, in: Walker, J.M. (Ed.), The Protein Protocols Handbook, Humana Press, Tatowa, NJ, 2002, pp. 995-997.

Donahue, R., Kessler, S., Bodine, D., McDonagh, K., Dunbar, C., Goodman, S., Agricola, B., Byrne, E., Raffeld, M., Moen, R., Helper virus induced T cell lymphoma in nonhuman primates after retroviral mediated gene transfer, J. Exp. Med., 176 (1992) 1125.

Donaldson, T.L., Boonstra, E.F., Hammond, J.M., Kinetics of protein denaturation at gas-liquid interfaces, J. Colloid. Interf. Sci, 74 (1980) 441.

Dong, A., Kendrick, B., Kreilgard, L., Matsuura, J., Manning, M.C., Carpenter, J.F., Spectroscopic study of secondary structure and thermal denaturation of recombinant human Factor XIII in aqueous solution, Arch. Biochem. Biophys., 347 (1997) 213.

Dong, A., Prestrelski, S.J., Allison, S.D., Carpenter, J.F., Infrared spectroscopic studies of lyophilization- and temperature-induced protein aggregation, J. Pharm. Sci., 84 (1995) 415.

Donnan, F.G., Theorie der Membrangleichgewichte und Membranpotentiale bei Vorhandensein von nicht dialysierenden Elektrolyten, Z. Elektrochemie, 17 (1911) 572.

Dougherty, D.A., Cation-pi interactions in chemistry and biology: A new view of benzene phenylalanine, tyrosine and tryptophan, Science, 271 (1996) 163.

Eaton, L.C., Host cell contaminant protein assay for recombinant biopharmaceuticals, Journal of Chromatography A, 705 (1995) 105.

Eberlein, G.A., Stratton, P.R., Wang, Y.J., Stability of rhbFGF as determined by UV spectroscopic measurements of turbidity, J. Pharm Sci. Technol., 48 (1994) 224.

Edy, V.G., Braude, I.A., De Clercq, E., Billiau, A., De Somer, P., Purification of interferon by adsorption chromatography on controlled pore glass, J. Gen. Virol., 33 (1976) 517.

Ejima, D., Tsumoto, K., Fukada, H., Yumioka, R., Nagase, K., Arakawa, T., Philo, J.S., Effects of acid exposure on the conformation, stability, and aggregation of monoclonal antibodies, Proteins, 66 (2006) 941.

Ejima, D., Yumioka, R., Tsumoto, K., Arakawa, T., Effective elution of antibodies by arginine and arginine derivatives in affinity column chromatography, Anal. Biochem., 345 (2005) 250.

European Directorate for the Quality of Medicine, Partikelkontamination - Nichtsichtbare Partikel, in: European Directorate for the Quality of Medicine (Ed.), European Pharmacopoeia, Deutscher Apotheker Verlag/ Govi-Verlag, Stuttgart/ Eschborn, 2001a, pp. 140-141.

European Directorate for the Quality of Medicine, Partikelkontamination - Sichtbare Partikel, in: European Directorate for the Quality of Medicine (Ed.), European Pharmacopoeia, Deutscher Apotheker Verlag/ Govi Verlag, Stuttgat/ Eschborn, 2001b, pp. 141-141.

Everett, D.H., Chairman, Commission on Colloid and Surface Chemistry (1969-1972), Manual of symbol and terminology for physicochemical quantities and units: Appendix for definitions, terminology and symbols in colloid and surface chemistry, part I (adopted by the IUPAC Council at Washington, DC), Pure Appl. Chem., 31 (1972) 579.

Fahrner, R.L., Knudsen, H.L., Basey, C.D., Galan, W., Feuerhelm, D., Vanderlaan, M., Blank, G.S., Industrial purification of pharmaceutical antibodies: Development, operation, and validation of chromatography processes, Biotechnol. Gen. Eng. Rev., 18 (2001) 301.

Fahrner, R.L., Whitney, D.H., Vanderlaan, M., Blank, G.S., Performance comparison of Protein A affinity-chromatography sorbents for purifying recombinant monoclonal antibodies, Biotechnol. Appl. Biochem., 30 (1999) 121.

Fane, A.G., Fell, C.J.D., Suki, A., The effect of pH and ionic environment on the ultrafiltration of protein solutions with retentive membranes, J. Membr. Sci., 16 (1983) 195.

Faude, A., Zacher, D., Müller, E., Böttinger, H., Fast determination of conditions for maximum dynamic capacity in cation-exchange chromatography of human monoclonal antibodies, J. Chromatogr. A, 1161 (2007) 29.

Ferrara, C., Brünker, P., Suter, T., Moser, S., Püntener, U., Umaña, P., Modulation of therapeutic antibody effector functions by glycosylation engineering: Influence of Golgi enzyme localization domain and co-expression of heterologous beta1, 4-N-acetylglucosaminyltransferase III and Golgi alpha-mannosidase II, Biotechnol. Bioeng., 93 (2006) 851.

Ferrone, F.A., Ivanova, M., Jasuja, R., Heterogeneous nucleation and crowding in sickle hemoglobin: An analytic approach, Biophys. J., 82 (2002) 399.

Field, R.W., Wu, D., Howell, J.A., Gupta, B.B., Critical flux concept for microfiltration fouling, J. Membr. Sci., 100 (1995) 259.

Fink, A.L., Compact intermediate states in protein folding, Ann. Rev. Biophys. Biomol. Struct., 24 (1995) 495.

Fink, A.L., Protein aggregation: Folding aggregates, inclusion bodies and amyloid, Folding and Design, 3 (1998) R9.

Fink, A.L., Calciano, L.J., Goto, Y., Kurotsu, T., Palleros, D.R., Classification of Acid Denaturation of Proteins: Intermediates and Unfolded States, Biochemistry, 33 (1994) 12504.

Fradin, B., Field, R.W., Crossflow microfiltration of magnesium hydroxide suspensions: determination of critical fluxes, measurement and modelling of fouling., Sep. Purif. Technol., 16 (1999) 25.

Fringeli, U.P., In situ infrared attenuated total reflection membrane spectroscopyl, in: Mirabella, F.M. (Ed.), Internal reflection spectroscopy: Theory and applications, Vol. 15, CRC Press, Boca Raton, FL, 1992, pp. 255-325.

Gagnon, P., Polishing methods for monoclonal IgG purification, in: Shukla, A.A., Etzel, M.R., Gadam, S. (Ed.), Process scale bioseparation for the biopharmaceutical industry, CRC Press, Boca Raton, FL, 2007, pp. 491-505.

Gagnon, P., IgG aggregate removal by charged-hydrophobic mixed mode chromatography, Curr. Pharm. Biotechnol., 10 (2009a) 434.

Gagnon, P., Monoclonal antibody purification with hydroxyapatite, New Biotechnol., 25 (2009b) 287.

Gaza-Bulseco, G., Liu, H., Fragmentation of a recombinant monoclonal antibody at various pH, Pharm. Res., 25 (2008) 1881.

Geiger, T., Clarke, S., Deamidation, isomerization, and racemization at asparaginyl and aspartyl residues in peptides. Succinimide-linked reactions that contribute to protein degradation, J. Biol. Chem., 262 (1987) 785.

Gelderman, K.A., Tomlinson, S., Ross, G.D., Gorter, A., Complement function in mAb-mediated cancer immunotherapy, Trends. Immunol., 25 (2004) 158.

Gerhart, P.M., Gross, R.J., Hochstein, J.I., Viscous flow in pipes, in: Munson, B.R., Young, D.F., Okiishi, T.H. (Ed.), Fundamentals of fluid mechanics, Addison-Wesley, Reading, MA, 1993, pp. 461-581.

Gésan-Guiziou, G., Boyaval, E., Daufin, G., Critical stability conditions in crossflow microfiltration of skimmed milk: Transition to irreversible deposition, J. Membr. Sci., 158 (1999) 211.

Ghose, S., McNerney, T.M., Hubbard, B.R., Preparative protein purification on underivatized silica, Biotechnol. Bioeng., 87 (2004) 413.

Giovannini, R., Freitag, R., Comparison of different types of ceramic hydroxyapatite for the chromatographic separation of plasmid DNA and a recombinant anti-Rhesus D antibody, Bioseparation, 9 (2001) 359.

Goldberg, M.E., Chaffotte, A.F., Undistorted structural analysis of soluble proteins by attenuated total reflectance infrared spectroscopy, Protein Sci., 14 (2005) 2781.

Gomez, G., Pikal, M.J., Rodriguez-Hornedo, N., Effect of initial buffer composition on pH changes during far-from-equilibrium freezing of sodium phosphate buffer solutions, Pharm. Res., 18 (2001) 90.

Gomme, P.T., Prakash, M., Hunt, B., Stokes, N., Cleary, P., Tatford, O.C., Bertolini, J., Effect of lobe pumping on human albumin: Development of a lobe pump simulator using smoothed particle hydrodynamics, Biotechnol. Appl. Biochem., 43 (2006) 113.

Goolcharran, C., Khossravi, M., Borchardt, R.T., Chemical pathways of peptide and protein degradation, in: Frokjaer, S., Hovgaards, L. (Ed.), Pharmaceutical formulation development of peptides and proteins, Taylor and Francis, London, 2000, pp. 70-88.

Graumann, K., Premstaller, A., Manufacturing of recombinant therapeutic proteins in microbial systems, Biotechnol. J., 1 (2006) 164.

Grdadolnik, J., An attenuated total reflection infrared spectroscopy of water solutions, Int. J. Vibr. Spectr., 6 (2002) 2.

Green, H., Scheer, L.A., Sizing mocroporous membrane filter systems, in: Meltzer, T.H., Jornitz, M.W. (Ed.), Filtration in the biopharmaceutical industry, Marcel Dekker, New York, NY, 1998, pp. 373-418.

Gressel, J., Robards, A.W., Polyacrylamide gel structure resolved?, J. Chromatogr. A, 114 (1975) 455.

Grillo, A.O., Edwards, K.T.-L., Kashi, R.S., Shipley, K.M., Hu, L., Besman, M.J., Middaugh, C.R., Conformational origin of the aggregation of recombinant human factor VIII, Biochemistry, 40 (2001) 586.

Grum, F., Paine, D., Zoeller, L., Derivative absorption and emission spectrophotometry, Appl. Opt., 11 (1972) 93.

Guerrier, L., Flayeux, I., Boschetti, E., A dual-mode approach to the selective separation of antibodies and their fragments, J. Chromatogr. B, 755 (2001) 37.

Guse, A.H., Milton, A.D., Schulze-Koops, H., Müller, B., Roth, E., Simmer, B., Wächter, H., Weiss, E., Emmrich, F., Purification and analytical characterization of an anti-CD4 monoclonal antibody for human therapy, J. Chromatogr. A, 661 (1994) 13.

Hahn, R., Schlegel, R., Jungbauer, A., Comparison of Protein A affinity sorbents, J. Chromatogr. B, 790 (2003) 35.

Hall, D., Minton, A.P., Macromolecular crowding: Qualitative and semiquantitative successes, quantitative challenges, Biochim. Biophys. Acta, 1649 (2003) 127.

Haller, W., Chromatography on glass of controlled pore size, Nature, 206 (1965) 693.

Hammond, P.M., Philip, K.A., Hinton, R.J., Jack, G.W., Recombinant Protein A from Escherichia coli, Ann. NY Acad. Sci., 613 (1990) 863.

Harn, N., Allan, C., Oliver, C., Middaugh, C.R., Highly concentrated monoclonal antibody solutions: Direct analysis of physical structure and thermal stability, J. Pharm. Sci., 96 (2007) 532.

Harper, J.D., Lansbury, P.T., Models of amyloid seeding in Alzheimers´s disease and scrapie: Mechanistic truths and physiological consequences of the time-dependent solubility of amyloid proteins, Ann. Rev. Biochem., 66 (1997) 385.

Harris, D.C., Quantitative chemical analysis, W.H. Freemann, New York, NY, 1995, pp. 1778.

Harris, R.J., Shire, S.J., Winter, C., Commercial manufacturing scale formulation and analytical characterization of therapeutic recombinant antibodies, Drug Dev. Res., 61 (2004) 137.

Harrison, J.S., Gill, A., Hoare, M., Stability of a single-chain Fv antibody fragment when exposed to a high shear environment combined with air-liquid interfaces, Biotechnol. Bioeng., 59 (1998) 517.

Hawe, A., Friess, W., Development of HSA-free formulations for a hydrophobic cytokine with improved stability, Eur. J. Pharm. Biopharm., 68 (2008) 169.

Heller, M.C., Carpenter, J.F., Randolph, T.W., Manipulation of lyophilization-induced phase separation: Implications for pharmaceutical proteins, Biotechnol. Progr., 13 (1997) 590.

Heller, M.C., Carpenter, J.F., Randolph, T.W., Protein formulation and lyophilization cycle design: Prevention of damage due to freeze-concentration induced phase separation, Biotechnol. Bioeng., 63 (1999) 166.

Henry, D.C., The cataphoresis of suspended particles (part I): The equation of cataphoresis, Proc. Royal Soc. London Ser. A, 133 (1931) 106.

Henson, A.F., Mitchell, J.R., Mussellwhite, P.R., The surface coagulation of proteins during shaking, J. Colloid. Interf. Sci, 32 (1970) 162.

Herb, L., Raghunath, B., Ultrafiltration process design and implementation, in: Shukla, A.A., Etzel, M.R., Gadam, S. (Ed.), Process scale bioseparation for the biopharmaceutical industry, CRC Press, Boca Raton, FL, 2007, pp. 297-332.

Hermia, J., Constant pressure blocking filtration laws - application to power-law non-Newtonian fluids, Trans. Inst. Chem. Eng., 60 (1982) 183.

Hessell, A.J., Hangartner, L., Hunter, M., Havenith, C.E.G., Beurskens, F.J., Bakker, J.M., Lanigan, C.M.S., Landucci, G., Forthal, D.N., Parren, P.W.H.I., Marx, P.A., Burton, D.R., Fc receptor but not complement binding is important in antibody protection against HIV, Nat. Biotechnol., 449 (2007) 101.

Ho, C.-C., Zydney, A.L., A combined pore blockage and cake filtration model for protein fouling during microfiltration, J. Colloid. Interf. Sci, 232 (2000) 389.

Hoogenboom, H.R., Selecting and screening recombinant antibody libraries, Nat. Biotechnol., 23 (2005) 1105.

Howell, J.A., Velicangil, O., Theoretical considerations of membrane fouling and its treatment with immobilized enzymes for protein ultrafiltration, J. Appl. Polym. Sci., 27 (1982) 21.

Huang, L., Lu, J., Wroblewski, V.J., Beals, J.M., Riggin, R.M., In vivo deamidation characterization of monoclonal antibody by LC/MS/MS, Anal. Chem., 77 (2005) 1432.

Huisman, I.H., Pradanos, P., Hernandez, A., The effect of protein-protein and protein-membrane interactions on membrane fouling in ultrafiltration, J. Membr. Sci., 179 (2000) 79.

Huse, K., Böhme, H.-J., Scholz, G.H., Purification of antibodies by affinity chromatography, J. Biochem. Biophys. Meth., 51 (2002) 217.

Hwang, W.Y.K., Foote, J., Immunogenicity of engineered antibodies, Methods, 36 (2005) 3.

Ichikawa, T., Terada, H., Second derivative spectrophotometry as an effective tool for examining phenylalanine residues in proteins, Biochim. Biophys. Acta, 494 (1977) 267.

Ichikawa, T., Terada, H., Estimation of state and amount of phenylalanine residues in proteins by second derivative spectrophotometry, Biochim. Biophys. Acta, 580 (1979) 120.

Iler, R.K., The chemistry of silica, Wiley, New York, NY, 1979, pp. 896.

International Conference on Harmonization of Technical Requirements for Registration of Pharmaceuticals for Human Use, ICH specifications: Test procedures and acceptance criteria for biotechnological/ biological product (Q6B), www.ich.org, 1999a.

International Conference on Harmonization of Technical Requirements for Registration of Pharmaceuticals for Human Use, Viral safety evaluation of biotechnology products derived from cell lines of human or animal origin (Q5A R1), http://www.ich.org, 1999b.

Israelachvili, J., Wennerstrom, H., Role of hydration and water structure in biological and colloidal interactions, Nature, 379 (1996) 219.

Jaspe, J., Hagen, S.J., Do proteins molecules unfold in a simple shear flow?, Biophys. J., 91 (2006) 3415.

Jiang, Y., Nashed-Samuel, Y., Li, C., Liu, W., Pollastrini, J., Mallard, D., Wen, Z.-Q., Fujimori, K., Pallitto, M., Donahue, L., Chu, G., Torraca, G., Vance, A., Mire-Sluis, T., Freund, E., Davis, J., Narhi, L., Tungsten-induced protein aggregation: Solution behavior, J. Pharm. Sci., 98 (2009) 4695.

Jin, M., Szapiel, N., Zhang, Jennifer , Hickey, J., Ghose, S., Profiling of host cell proteins by two-dimensional difference gel electrophoresis: Implications for downstream process development, Biotechnol. Bioeng., 105 (2010) 306.

Jones, L.S., Kaufmann, A., Middaugh, C.R., Silicone oil induced aggregation of proteins, J. Pharm. Sci., 94 (2005) 918.

Jungbauer, A., Chromatographic media for bioseparation, J. Chromatogr. A, 1065 (2005) 3.

Kanai, S., Liu, J., Patapoff, T.W., Shire, S.J., Reversible self-association of a concentrated monoclonal antibody solution mediated by Fab-Fab interaction that impacts solution viscosity, J. Pharm. Sci., 97 (2008) 4219.

Karlsson, E., Ryden, L., Brewer, J., Ion-exchange chromatography, in: Janson, J.-C., Ryden, L. (Ed.), Protein purification: Principles, high resolution methods, and applications, Wiley, New York, NY, 1998, pp. 145-205.

Kaszuba, M., Connah, M., T., Protein and nanoparticle characterization using light scattering techniques, Part. Part. Syst. Char., 23 (2006) 193.

Kelley, B.D., Switzer, M., Bastek, P., Kramarczyk, J.F., Molnar, K., Yu, T., Coffman, J., High-throughput screening of chromatographic separations: IV. Ion-exchange, Biotechnol. Bioeng., 100 (2008a) 950.

Kelley, B.D., Tobler, S.A., Brown, P., Coffman, J.L., Godavarti, R., Iskra, T., Switzer, M., Vunnum, S., Weak partitioning chromatography for anion exchange purification of monoclonal antibodies, Biotechnol. Bioeng., 101 (2008b) 553.

Kelly, S.T., Zydney, A.L., Mechanisms for BSA fouling during microfiltration, J. Membr. Sci., 107 (1995) 115.

Kendrick, B.S., Carpenter, J.F., Cleland, J.L., Randolph, T.W., A transient expansion of the native state precedes aggregation of recombinant human interferon-gamma, PNAS, 95 (1998a) 14142.

Kendrick, B.S., Chang, B.S., Arakawa, T., Peterson, B., Randolph, T.W., Manning, M.C., Carpenter, J.F., Preferential exclusion of sucrose from recombinant interleukin-1 receptor antagonist: Role in restricted conformational mobility and compaction of native state, PNAS, 94 (1997) 11917.

Kendrick, B.S., Cleland, J.L., Lam, X., Nguyen, T., Randolph, T.W., Manning, M.C., Carpenter, J.F., Aggregation of recombinant human Interferon gamma: Kinetics and structural transitions, J. Pharm. Sci., 87 (1998b) 1069.

Kendrick, B.S., Dong, A., Allison, S.D., Manning, M.C., Carpenter, J.F., Quantitation of the area of overlap between second-derivative amide I infrared spectra to determine the structural similarity of a protein in different states, J. Pharm. Sci., 85 (1996) 155.

Kerwin, B.A., Remmele, R.L.J., Protect from light: Photodegradation and protein biologics, J. Pharm. Sci., 96 (2007) 1468.

Khazaeli, M.B., Conry, R.M., LoBuglio, A.F., Human immune response to monoclonal antibodies, J. Immunother., 15 (1994) 42.

Kiefhaber, T., Rudolph, R., Kohler, H.-H., Buchner, J., Protein aggregation in vitro and in vivo: A quantitative model of the kinetic competition between folding and aggregation, Nat. Biotechnol., 9 (1991) 825.

Kiese, S., Papppenberger, A., Friess, W., Mahler, H.-C., Shaken, not stirred: Mechanical stress testing of an IgG1 antibody, J. Pharm. Sci., 97 (2008) 4347.

Kim, D., Yu, M.-H., Folding pathway of human alpha(1)-antitrypsin: Characterization of an intermediate that is active but prone to aggregation, Biochem. Biophys. Res. Commun., 226 (1996) 378.

Kim, K.J., Fane, A.G., Fell, C.J.D., Joy, D.C., Fouling mechanisms of membranes during protein ultrafiltration, J. Membr. Sci., 68 (1992) 79.

Koehler, G., Milstein, C., Continuous cultures of fused cells secreting antibody of predefined specificity, Nature, 256 (1975) 495.

Koehler, J.A., Ulbricht, M., Belfort, G., Intermolecular forces between proteins and polymer films with relevance to filtration, Langmuir, 13 (1997) 4162.

Kordis-Krapez, M., Abram, V., Kac, M., Ferjancic, S., Determination of organic acids in white wines by RP-HPLC, Food Technol. Biotechnol., 39 (2001) 93.

Kratky, O., Leopold, H., Stabinger, H., The determination of the partial specific volume of proteins by the mechanical oscillator technique, in: Hirs, C.H.W., Timasheff, S.N. (Ed.), Meth. Enzymol., Academic Press, London, 1973, pp. 98-110.

Krawitz, D.C., Forrest, W., Moreno, G.T., Kittleson, J., Champion, K.M., Proteomic studies support the use of multi-product immunoassays to monitor host cell protein impurities, PROTEOMICS, 6 (2006) 94.

Krielgaard, L., Jones, L.S., Randolph, T.W., Frokjaer, S., Flink, J.M., Manning, M.C., Carpenter, J.F., Effect of tween 20 on freeze-thawing- and agitation-induced aggregation of recombinant human factor XIII, J. Pharm. Sci., 87 (1998) 1593.

Krishnan, S., Chi, E.Y., Webb, J.N., Chang, B.S., Shan, D., Goldenberg, M., Manning, M.C., Randolph, T.W., Carpenter, J.F., Aggregation of granulocyte colony stimulating factor under physiological conditions: Characterization and thermodynamic inhibition, Biochemistry, 41 (2002) 6422.

Krishnan, S., Chi, E.Y., Wood, S.J., Kendrick, B.S., Li, C., Garzon-Rodriguez, W., Wypych, J., Randolph, T.W., Narhi, L.O., Biere, A.L., Citron, M., Carpenter, J.F., Oxidative dimer formation is the critical rate-limiting step for Parkinson's disease alpha-synuclein fibrillogenesis, Biochemistry, 42 (2003) 829.

Kueltzo, L.A., Ultraviolet absorption spectroscopy, in: Jiskoot, W., Crommelin, D. (Ed.), Methods for structural analysis of protein pharmaceuticals, AAPS press, Arlington, VA, 2005, pp. 1-27.

Kueltzo, L.A., Ersoy, B., Ralston, J.P., Middaugh, C.R., Derivative absorbance spectroscopy and protein phase diagrams as tools for comprehensive protein characterization: A bGCSF case study, J. Pharm. Sci., 92 (2003) 1805.

Kueltzo, L.A., Wang, W., Randolph, T.W., Carpenter, J.F., Effects of solution conditions, processing parameters, and container materials on aggregation of a monoclonal antibody during freeze-thawing, J. Pharm. Sci., 97 (2008) 1801.

Kuester, W.F., Thiel, A., Rechentafeln für die chemische Analytik, De Gruyter, New York, NY, 2002, pp. 393.

Kunitani, M., Wolfe, S., Rana, S., Apicella, C., Levi, V., Dollinger, G., Classical light scattering quantitation of protein aggregates: Off-line spectroscopy versus HPLC detection, J. of Pharm. Biomed. Anal., 16 (1997) 573.

Lange, R., Balny, C., UV-visible derivative spectroscopy under high pressure, Biochim. Biophys. Acta, 1595 (2002) 80.

Langone, J.J., Protein A of Staphylococcus aureus and related immunoglobulin receptors produced by streptococci and pneumonococci, Adv. Immunol., 32 (1982) 157.

Lee, J.C., Timasheff, S.N., Partial specific volumes and interactions with solvent components of proteins in guanidine hydrochloride, Biochemistry, 13 (1974) 257.

LeVan, M.D., Carta, G., Yon, C.M., Chapter 16, in: Perry, R.H., Green, D.W. (Ed.), Perry's Chemical Engineers' Handbook, McGraw-Hill, New York, NY, 1997.

Li, B., Flores, J., Corvari, V., A simple method for the detection of insoluble aggregates in protein formulations, J. Pharm. Sci., 96 (2007) 1840.

Li, H., Fane, A.G., Coster, H.G.L., Vigneswaran, S., Direct observation of particle deposition on the membrane surface during crossflow microfiltration, J. Membr. Sci., 149 (1998a) 83.

Li, Q., MacDonald, S., Bienek, C., Foster, P.R., MacLeod, A.J., Design of a UV-C irradiation process for the inactivation of viruses in protein solutions, Biologicals, 33 (2005) 101.

Li, R., Dowd, V., Stewart, D.J., Burton, S.J., Lowe, C.R., Design, synthesis, and application of a Protein A mimetic, Nat. Biotechnol., 16 (1998b) 190.

Li, Y., Weiss, W.F., Roberts, C.J., Characterization of high-molecular-weight nonnative aggregates and aggregation kinetics by size exclusion chromatography with inline multi-angle laser light scattering, J. Pharm. Sci. (2009) in press.

Lieber, M.M., Benveniste, R.E., Livingston, D.M., Todaro, G.J., Mammalian cells in culture frequently release type C viruses, Science, 182 (1973) 56.

Lindmark, R., Movitz, J., Sjoequist, J.S., Extracellular Protein A from a methicillin-resistant strain of Staphylococcus aureus, Eur. J. Biochem., 74 (1977) 623.

Liten, A., Cohen, D., Simultaneous processing with ÄKTA™ systems reduces overall process time and protects proteins, Bio Process Int., 5 (2007) 80.

Liu, H., Gaza-Bulseco, G., Sun, J., Characterization of the stability of a fully human monoclonal IgG after prolonged incubation at elevated temperature, J. Chromatogr. B, 837 (2006) 35.

Liu, J., Nguyen, M.D.H., Andya, J.D., Shire, S.J., Reversible self-association increases the viscosity of a concentrated monoclonal antibody in aqueous solution, J. Pharm. Sci., 94 (2005) 1928.

Liu, J., Shire, S.J., Reduced-viscosity concentrated protein formulations, PCT WO 2002030463, 2002.

Low, D., O'Leary, R., Pujar, N.S., Future of antibody purification, J. Chromatogr. B, 848 (2007) 48.

Lu, Y., Williamson, B., Gillespie, R., Recent advancement in application of hydrophobic interaction chromatography for aggregate removal in industrial purification process, Curr. Pharm. Biotechnol., 10 (2009) 427.

Lucas, L.H., Ersoy, B.A., Kueltzo, L.A., Joshi, S.B., Brandau, D.T., Thyagarajapuram, N., Peek, L.J., Middaugh, C.R., Probing protein structure and dynamics by sec-

ond-derivative ultraviolet absorption analysis of cation-p interactions, Protein Sci., 15 (2006) 2228.

Lumry, R., Eyring, H., Conformation changes of proteins, J. Phys. Chem., 58 (1954) 110.

Luo, G.X., Kohlstaedt, L.A., Charles, C.H., Gorfain, E., Morantte, I., Williams, J.H., Fang, F., Humanization of an anti-ICAM-1 antibody with over 50-fold affinity and functional improvement, J. Immunol. Meth., 275 (2003) 31.

Luo, R., Waghmare, R., Krishnan, M., Adams, C., Poon, E., Kahn, D., High-concentration UF/DF of a monoclonal antibody. Strategy for optimization and scale-up, Bio Process Int., 4 (2006) 44.

Mach, H., Middaugh, C.R., Simultaneous monitoring of the environment of Tryptophan, Tyrosine, and Phenylalanine residues in proteins by near-ultraviolet second-derivative spectroscopy, Anal. Biochem., 222 (1994) 323.

Madaeni, S.S., Fane, A.G., Wiley, D.E., Factors influencing critical flux in membrane filtration of activated sludge, J. Chem. Technol. Biotechnol., 74 (1999) 539.

Maenttaeri, M., Pihlajamäki, A., Nystroem, M., Effect of pH on hydrophilicity and charge and their effect on the filtration efficiency of NF membranes at different pH, J. Membr. Sci., 280 (2006) 311.

Mahler, H.-C., Friess, W., Grauschopf, U., Kiese, S., Protein aggregation: Pathways, induction factors and analysis, J. Pharm. Sci., 98 (2009) 2909.

Mahler, H.-C., Müller, R., Friess, W., Delille, A., Matheus, S., Induction and analysis of aggregates in a liquid IgG1-antibody formulation, Eur. J. Pharm. Biopharm., 59 (2005) 407.

Manning, J.N., Sullivan, G.S., Davis, P.F., Reversed-phase liquid chromatography of elastin peptides, J. Chromatogr. B, 487 (1989a) 41.

Manning, M.C., Matsuura, J.E., Kendrick, B.S., Meyer, J.D., Dormish, J.J., Vrkljan, M., Ruth, J.R., Carpenter, J.F., Sheftert, E., Approaches for increasing the solution stability of proteins, Biotechnol. Bioeng., 48 (1995) 506.

Manning, M.C., Patel, K., Borchardt, R.T., Stability of protein pharmaceuticals, Pharm. Res., 6 (1989b) 903.

Markovic, D., Pröll, S., Bubenzer, C., Scheer, H., Myoglobin with chlorophyllous chromophores: Influence on protein stability, Biochim. Biophys. Acta, 1767 (2007) 897.

Marques, B.F., Roush, D.J., Göklen, K.E., Virus filtration of high-concentration monoclonal antibody solutions, Biotechnol. Progr., 25 (2009) 483.

Martin, A.N., Swarbick, J., Cammarata, A., Physikalische Pharmazie, Wissenschaftliche Verlagsgesellschaft, Stuttgart, 1980, pp. 631.

Maruyama, T., Katoh, S., Nakajima, M., Nabetani, H., Mechanism of bovine serum albumin aggregation during ultrafiltration, Biotechnol. Bioeng., 75 (2001a) 233.

Maruyama, T., Katoh, S., Nakajima, M., Nabetani, H., Abbott, T.P., Shono, A., Satoh, K., FT-IR analysis of BSA fouled on ultrafiltration and microfiltration membranes, J. Membr. Sci., 192 (2001b) 201.

Matheus, S., Friess, W., Mahler, H.-C., FTIR and nDSC as analytical tools for high-concentration protein formulations, Pharm. Res., 23 (2006a) 1350.

Matheus, S., Mahler, H.-C., Friess, W., A critical evaluation of Tm(FTIR) measurements of high-concentration IgG1 antibody formulations as a formulation development tool, Pharm. Res., 23 (2006b) 1617.

McDonald, P., Victa, C., Carter-Franklin, J.N., Fahrner, R.L., Selective antibody precipitation using polyelectrolytes: A novel approach to the purification of monoclonal antibodies, Biotechnol. Bioeng., 102 (2009) 1141.

Mecs, I., Chin, D., Fox, F., Krim, M., Purification of human leukocyte interferon alpha by carboxymethyl controlled pore glass bead chromatography, Arch. Virol., 81 (1984) 303.

Meireles, M., Aimar, P., Sanchez, V., Albumin denaturation during ultrafiltration: Effects of operating conditions and consequences on membrane fouling, Biotechnol. Bioeng., 38 (1991) 528.

Militello, V., Casarino, C., Emanuele, A., Giostra, A., Pullara, F., Leone, M., Aggregation kinetics of bovine serum albumin studied by FTIR spectroscopy and light scattering, Biophysical Chemistry, 107 (2004) 175.

Minton, A.P., Excluded volume as a determination of protein structure and stability, Biophys. J., 32 (1980) 77.

Minton, A.P., Molecular crowding: Analysis of effects of high concentrations of inert cosolutes on biochemical equilibria and rates in terms of volume exclusion, in: Ackers, G.K., Johnson, M.L. (Ed.), Energetics of Biological Macromolecules part B, Academic Press, London, 1998, pp. 127-149.

Minton, A.P., Implications of macromolecular crowding for protein assembly, Curr. Opin. Struct. Biol., 10 (2000) 34.

Minton, A.P., Influence of macromolecular crowding upon the stability and state of association of proteins: Predictions and observations, J. Pharm. Sci., 94 (2005) 1668.

Minton, K.W., Karmin, P., Hahn, G.M., Minton, A.P., Nonspecific stabilization of stress-susceptible proteins by stress-resistant proteins: A model for the biological role of heat shock proteins, PNAS, 79 (1982) 7107.

Mirchev, R., Ferrone, F.A., The structural link between polymerization and sickle cell disease, J. Mol. Biol., 265 (1997) 475.

Mollmann, S.H., Bukrinsky, J.T., Frokjaer, S., Elofsson, U., Adsorption of human insulin and AspB28 insulin on a PTFE-like surface, J. Colloid. Interf. Sci, 286 (2005) 28.

Mondor, M., Ippersiel, D., Lamarche, F., Boye, J.I., Effect of electro-acidification treatment and ionic environment on soy protein extract particle size distribution and ultrafiltration permeate flux, J. Membr. Sci., 231 (2004) 169.

Moore, J.M.R., Patapoff, T.W., Cromwell, M.E.M., Kinetics and thermodynamics of dimer formation and dissociation for a recombinant humanized monoclonal antibody to vascular endothelial growth factor, Biochemistry, 38 (1999) 13960.

Moorhouse, K.G., Nashabeh, W., Deveney, J., Bjork, N.S., Mulkerrin, M.G., Ryskamp, T., Validation of an HPLC method for the analysis of the charge heterogeneity of the recombinant monoclonal antibody IDEC-C2B8 after papain digestion, J. of Pharm. Biomed. Anal., 16 (1997) 593.

Mulkerrin, M.G., Wetzel, R., pH dependence of the reversible and irreversible thermal denaturation of gamma interferons, Biochemistry, 28 (2002) 6556.

Nakatsuka, S., Michaels, A.S., Transport and separation of proteins by ultrafiltration through sorptive and non-sorptive membranes, J. Membr. Sci., 69 (1992) 189.

Narendranathan, T.J., Dunnill, P., The effect of shear on globular proteins during ultrafiltration: Studies of alcohol dehydrogenase, Biotechnol. Bioeng., 24 (1982) 2103.

Nawrocki, J., The silanol group and its role in liquid chromatography, J. Chromatogr. A, 779 (1997) 29.

Nielsen, L., Khurana, R., Coats, A., Frokjaer, S., Brange, J., Vyas, S., Uversky, V.N., Fink, A.L., Effect of environmental factors on the kinetics of insulin fibril formation: Elucidation of the molecular mechanism, Biochemistry, 40 (2001) 6036.

Nissim, A., Chernajovsky, Y., Historical development of monoclonal antibody therapeutics, in: Nissim, A., Chernajovsky, Y. (Ed.), Therapeutic antibodies, Springer, Berlin, 2008, pp. 3-18.

Niwa, R., Sakurada, M., Kobayashi, Y., Uehara, A., Matsushima, K., Ueda, R., Nakamura, K., Shitara, K., Enhanced natural killer cell binding and activation by low-fucose IgG1 antibody results in potent antibody-dependent cellular cytotoxicity induction at lower antigen density, Clin. Canc. Res., 11 (2005) 2327.

Norde, W., Adsorption of proteins from solution at the solid-liquid interface, Adv. Colloid Interface Sci., 25 (1986) 267.

Norde, W., Adsorption of proteins at solid-liquid interfaces, Cells and Materials, 5 (1995) 97.

Norde, W., Lyklema, J., The adsorption of human plasma albumin and bovine pancreas ribonuclease at negatively charged polystyrene surfaces: IV. The charge distribution in the adsorbed state, J. Colloid. Interf. Sci, 66 (1978) 285.

Nystroem, M., Lindstroem, M., Matthiasson, E., Streaming potential as a tool in the characterization of ultrafiltration membranes, Colloids Surf., 36 (1989) 297.

Palacio, L., Calvo, J.I., Pradanos, P., Hernandez, A., Vaisanen, P., Nystrom, M., Contact angles and external protein adsorption onto UF membranes, J. Membr. Sci., 152 (1999) 189.

Palacio, L., Ho, C.-C., Zydney, A.L., Application of a pore-blockage - Cake-filtration model to protein fouling during microfiltration, Biotechnol. Bioeng., 79 (2002) 260.

Palecek, S.P., Mochizuki, S., Zydney, A.L., Effect of ionic environment on BSA filtration and the properties of BSA deposits, Desalination, 90 (1993) 147.

Palecek, S.P., Zydney, A.L., Intermolecular electrostatic interactions and their effect on flux and protein deposition during protein filtration, Biotechnol. Progr., 10 (1994) 207.

Patton, W.F., Lim, M.J., Shepro, D., Protein detection using reversible metal chelate stains, in: Walker, J.M. (Ed.), Methods in molecular biology, 112, Humana Press, Clifton, NJ, 1999, pp. 331-339.

Pavlou, A.K., Reichert, J.M., Recombinant protein therapeutics - success rates, market trends and values to 2010, Nat. Biotechnol., 22 (2004) 1513.

Pelton, J.T., McLean, L.R., Spectroscopic methods for analysis of protein secondary structure, Anal. Biochem., 277 (2000) 167.

Philo, J.S., Is any measurement method optimal for all aggregate sizes and types?, AAPS J., 8 (2006) 564.

Piggee, C., Therapeutic antibodies coming through the pipeline, Anal. Chem., 80 (2008) 2305.

Pikal-Cleland, K.A., Carpenter, J.F., Lyophilization-induced protein denaturation in phosphate buffer systems: Monomeric and tetrameric beta-galactosidase, J. Pharm. Sci., 90 (2001) 1255.

Porath, J., Janson, J.C., Laas, T., Agar derivatives for chromatography, electrophoresis and gel-bound enzymes: Rigid agarose gels cross-linked with divinyl sulphone, J. Chromatogr. A, 103 (1975) 49.

Porter, M.C., Concentration polarization with membrane ultrafiltration, Ind. Eng. Chem. Res. Dev., 11 (1972) 234.

Powers, E.T., Powers, D.L., The kinetics of nucelated polymerization at high concentrations: Amyloid fibril formation near and above the supercritical concentration, Biophys. J., 91 (2006) 122.

Pradanos, P., Hernandez, A., Calvo, J.I., Tejerina, F., Mechanisms of protein fouling in cross-flow UF through an asymmetric inorganic membrane, J. Membr. Sci., 114 (1996) 115.

Privalov, P.L., Cold denaturation of protein, Crit. Rev. Biochem. Mol. Biol., 25 (1990) 281.

Prouty, W.F., Karnovsky, M.J., Goldberg, A.L., Degradation of abnormal proteins in Escherichia coli. Formation of protein inclusions in cells exposed to amino acid analogs, J. Biol. Chem., 250 (1975) 1112.

Przybycien, T.M., Bailey, J.E., Aggregation kinetics in salt-induced protein precipitation, AIChE Journal, 35 (1989) 1779.

Qi, P., Volkin, D.B., Zhao, H., Nedved, M.L., Hughes, R., Bass, R., Yi, S.C., Panek, M.E., Wang, D., DalMonte, P., Bond, M.D., Characterization of the photodegradation of a human IgG1 monoclonal antibody formulated as a high-concentration liquid dosage form, J. Pharm. Sci., 98 (2008) 3117.

Ragone, R., Colonna, G., Balestrieri, C., Servillo, L., Irace, G., Determination of tyrosine exposure in proteins by second-derivative spectroscopy, Biochemistry, 23 (1984) 1871.

Raibekas, A.A., Bures, E.J., Siska, C.C., Kohno, T., Latypov, R.F., Kerwin, B.A., Anion binding and controlled aggregation of human Interleukin-1 receptor antagonist, Biochemistry, 44 (2005) 9871.

Randolph, T.W., Carpenter, J.F., Engineering challenges of protein formulations, AIChE Journal, 53 (2007) 1902.

Rathore, A.S., Sobacke, S.E., Kocot, T.J., Morgan, D.R., Dufield, R.L., Mozier, N.M., Analysis for residual host cell proteins and DNA in process streams of a recombinant protein product expressed in Escherichia coli cells, J. of Pharm. Biomed. Anal., 32 (2003) 1199.

Reifsnyder, D.H., Olson, C.V., Etcheverry, T., Prashad, H., Builder, S.E., Purification of insulin-like growth factor-I and related proteins using underivatized silica, J. Chromatogr. A, 753 (1996) 73.

Reithel, F.J., The dissociation and association of protein structures, Adv. Prot. Chem., 18 (1964) 123.

Rezwan, K., Meier, L.P., Gauckler, L.J., Lysozyme and bovine serum albumin adsorption on uncoated silica and AlOOH-coated silica particles: The influence of positively and negatively charged oxide surface coatings, Biomaterials, 26 (2005) 4351.

Riddiford, C.L., Jennings, B.R., Discussion on the shape of bovine plasma albumin, Biochim. Biophys. Acta, 126 (1966) 171.

Rivas, G., Fernandez, J.A., Minton, A.P., Direct observation of the self-association of dilute proteins in the presence of inert macromolecules at high concentration via tracer sedimentation equilibrium: Theory, experiment, and biological significance, Biochemistry, 38 (1999) 9379.

Robert, F., Bierau, H., Rossi, M., Agugiaro, D., Soranzo, T., Broly, H., Mitchell-Logean, C., Degradation of an Fc-fusion recombinant protein by host cell proteases: Identification of a CHO cathepsin D protease, Biotechnol. Bioeng., 104 (2009) 1132.

Roberts, P.L., Virus inactivation by solvent/ detergent treatment using Triton X-100 in a high purity factor VIII, Biologicals, 36 (2008) 330.

Roberts, P.L., Dunkerley, C., Effect of manufacturing process parameters on virus inactivation by solvent/ detergent treatment in a high-purity factor IX concentrate, Vox Sanguinis, 84 (2003) 170.

Robinson, A.B., Rudd, C.J., Deamidation of glutaminyl and asparaginyl residues in peptides and proteins, Curr. Top. Cell. Regul., 8 (1974) 247.

Robinson, A.B., Scotchler, J.W., McKerrow, J.H., Rates of nonenzymic deamidation of glutaminyl and asparaginyl residues in pentapeptides, J. Am. Chem. Soc., 95 (1973) 8156.

Roque, C.A., Lowe, C.R., Taipa, M.Â. Antibodies and genetically engineered related molecules: Production and purification, Biotechnol. Progr., 20 (2004) 639.

Ross, P.D., Minton, A.P., Hard quasispherical model for the viscosity of hemoglobin solutions, Biochem. Biophys. Res. Commun., 76 (1977) 971.

Rotter, M.A., Kwong, S., Briehl, R.W., Ferrone, F.A., Heterogeneous nucleation in sickle hemoglobin: Experimental validation of a structural mechanism, Biophys. J., 89 (2005) 2677.

Roy, S., Mason, B.D., Schöneich, C.S., Carpenter, J.F., Boone, T.C., Kerwin, B.A., Light-induced aggregation of type I soluble tumor necrosis factor receptor, J. Pharm. Sci. (2009) in press.

Rubin, D., Christy, C., Selecting the right ultrafiltration membrane for biopharmaceutical applications, Pharm. Technol. Europe, 1 (2002) 41.

Sablani, S., Goosen, M., Al-Belushi, R., Wilf, M., Concentration polarization in ultrafiltration and reverse osmosis: A critical review, Desalination, 141 (2001) 269.

Saldanha, J.W., Molecular engineering I: Humanization, in: Dübel, S. (Ed.), Handbook of therapeutic antibodies, volume I: Technologies, Wiley, Weinheim, 2007, pp. 119-144.

Salgin, S., Effects of ionic environments on bovine serum albumin fouling in a cross-flow ultrafiltration system, Chem. Eng. Technol., 30 (2007) 255.

Salinas, B.A., Sathish, H.A., Bishop, S.M., Harn, N., Carpenter, J.F., Randolph, T.W., Understanding and modulating opalescence and viscosity in a monoclonal antibody formulation, J. Pharm. Sci. (2009) in press.

Sandberg, H., Lütkemeyer, D., Kuprin, S., Wrangel, M., Almstedt, A., Persson, P., Ek, V., Mikaelsson, M., Mapping and partial characterization of proteases expressed by a CHO production cell line, Biotechnol. Bioeng., 95 (2006) 961.

Sasahara, K., McPhie, P., Minton, A.P., Effect of dextran on protein stability and conformation attributed to macromolecular crowding, J. Mol. Biol., 326 (2003) 1227.

Schellekens, H., Immunogenicity of therapeutic proteins, Nephrol. Dial. Transplant., 18 (2003) 1257.

Schellekens, H., Factors influencing the immunogenicity of therapeutic proteins, Nephrol. Dial. Transplant., 20 (2005) 3.

Schnabel, R., Langer, P., Controlled-pore glass as a stationary phase in chromatography, J. Chromatogr. A, 544 (1991) 137.

Scopes, R.K., Protein purification, Springer, New York, NY, 1994, pp. 380.

Shawler, D., Bartholomew, R., Smith, L., Dillman, R., Human immune response to multiple injections of murine monoclonal IgG, J. Immunol., 135 (1985) 1530.

Shire, S.J., Shahrokh, Z., Liu, J., Challenges in the development of high protein concentration formulations, J. Pharm. Sci., 93 (2004) 1390.

Shojaee, N., Patton, W.F., Lim, M.J., Shepro, D., Pyrogallol red-molybdate: A reversible, metal chelate stain for detection of proteins immobilized on membrane supports, Electrophoresis, 17 (1996) 687.

Shukla, A.A., Hinckley, P., Gupta, P., Yigzaw, Y., Hubbard, B.R., Strategies to address aggregation during Protein A chromatography, Bio Process Int., 3 (2005) 36.

Shukla, A.A., Hubbard, B., Tressel, T., Guhan, S., Low, D., Downstream processing of monoclonal antibodies-application of platform approaches, J. Chromatogr. B, 848 (2007) 28.

Sifton, D.W., Physicians desk reference, http://www.pdr.net/login/Login.aspx, 2002.

Sjoequist, J., Meloun, B., Hjelm, H., Protein A isolated from Staphylococcus aureus after digestion with lysostaphin, Eur. J. Biochem., 29 (1972) 572.

Sluzky, V., Tamada, J., Klibanov, A., Langer, R., Kinetics of insulin aggregation in aqueous solutions upon agitation in the presence of hydrophobic surfaces, PNAS, 88 (1991) 9377.

Smyth, D.S., Utsumi, S., Structure at the hinge region in rabbit immunoglobulin-G, Nature, 216 (1967) 332.

Stankovic, C.J., Delfino, J.M., Schreiber, S.L., Purification of gramicidin A, Anal. Biochem., 184 (1990) 100.

Stoner, M.R., Fischer, N., Nixon, L., Buckel, S., Benke, M., Austin, F., Randolph, T.W., Kendrick, B.S., Protein-solute interactions affect the outcome of ultrafiltration/diafiltration operations, J. Pharm. Sci., 93 (2004) 2332.

Strauss, D.M., Gorrell, J., Plancarte, M., Blank, G.S., Chen, Q., Yang, B., Anion exchange chromatography provides a robust, predictable process to ensure viral safety of biotechnology products, Biotechnol. Bioeng., 102 (2009a) 168.

Strauss, D.M., Lute, S., Brorson, K., Blank, G.S., Chen, Q., Yang, B., Removal of endogenous retrovirus-like particles from CHO-cell derived products using Q sepharose fast flow chromatography, Biotechnol. Progr. (2009b) in press.

Stulík, K., Pacáková, V., Tichá, M., Some potentialities and drawbacks of contemporary size-exclusion chromatography, J. Biochem. Biophys. Meth., 56 (2003) 1.

Suki, A., Fane, A.G., Fell, C.J.D., Flux decline in protein ultrafiltration, J. Membr. Sci., 21 (1984) 269.

Suki, A., Fane, A.G., Fell, C.J.D., Modeling fouling mechanisms in protein ultrafiltration, J. Membr. Sci., 27 (1986) 181.

Sulkowski, E., Controlled pore glass chromatography of proteins, in: Burgess, R.J. (Ed.), Protein purification: Micro to macro, Alan R. Riss, New York, NY, 1987, pp. 177-195.

Tanford, C., Physical chemistry of macromolecules, John Wiley & Sons, New York, NY, 1967, pp. 710.

Tarutani, T., Chromatographic studies in the field of silicate chemistry, J. Chromatogr. A, 313 (1984) 33.

Thirumangalathu, R., Krishnan, S., Brems, D.N., Randolph, T.W., Carpenter, J.F., Effects of pH, temperature, and sucrose on benzyl alcohol-induced aggregation of recombinant human granulocyte colony stimulating factor, J. Pharm. Sci., 95 (2006) 1480.

Thirumangalathu, R., Krishnan, S., Speed Ricci, M., Brems, D.N., Randolph, T.W., Carpenter, J.F., Silicone oil- and agitation-induced aggregation of a monoclonal antibody in aqueous solution, J. Pharm. Sci. (2009) in press.

Thomas, C.R., Nienow, A.W., Dunnill, P., Action of shear on enzymes: Studies with alcohol dehydrogenase, Biotechnol. Bioeng., 21 (1979) 2263.

Timasheff, S.N., Solvent effects on protein stability, Curr. Opin. Struct. Biol., 2 (1992) 35.

Timasheff, S.N., The control of protein stability and association by weak interactions with water: How do solvents affect these processes?, Ann. Rev. Biophys. Biomol. Struct., 22 (1993) 67.

Tran, R., Joseph, J.R., Sinclair, A., Bracewell, D., Zhou, Y., Titchener-Hooker, N.J., A framework for the prediction of scale-up when using compressible chromatographic packings, Biotechnol. Prog., 23 (2007) 413.

Treuheit, M.J., Kosky, A.A., Brems, D.N., Inverse relationship of protein concentration and aggregation, Pharm. Res., 19 (2002) 511.

Tsai, P.K., Bruner, M.W., Irwin, J.I., Ip, C.C.Y., Oliver, C.N., Nelson, R.W., Volkin, D.B., Middaugh, C.R., Origin of the isoelectric heterogeneity of monoclonal immunoglobulin h1B4, Pharm. Res., 10 (1993) 1580.

Turker, M., Hubble, J., Membrane fouling in a constant-flux ultrafiltration cell, J. Membr. Sci., 34 (1987) 267.

Tutunjian, R.S., Ultrafiltration processes in biotechnology, Ann. NY Acad. Sci., 413 (1983) 238.

Tyagi, A.K., Randolph, T.W., Dong, A., Maloney, K.M., Hitscherich, C., Carpenter, J.F., IgG particle formation during filling pump operation: A case study of heterogeneous nucleation on stainless steel nanoparticles, J. Pharm. Sci., 98 (2008) 94.

Tzannis, S.T., Hrushesky, W.J.M., Wood, P.A., Przybycien, T.M., Adsorption of a formulated protein on a drug delivery device surface, J. Colloid. Interf. Sci, 189 (1997) 216.

Umana, P., Jean-Mairet, J., Moudry, R., Amstutz, H., Bailey, J.E., Engineered glycoforms of an antineuroblastoma IgG1 with optimized antibody-dependent cellular cytotoxic activity, Nat. Biotechnol., 17 (1999) 176.

United States Pharmacopeial Convention, Particulate matter in injection, in: United States Pharmacopeial Convention (Ed.), United States Pharmacopeia, United States Pharmacopeial Convention, Rockville, MD, 2002, pp. 2046-2051.

Usami, A., Ohtsu, A., Takahama, S., Fujii, T., The effect of pH, hydrogen peroxide and temperature on the stability of human monoclonal antibody, J. of Pharm. Biomed. Anal., 14 (1996) 1133.

Valerio, M., Colosimo, A., Conti, F., Giuliani, A., Grottesi, A., Manetti, C., Zbilut, J.P., Early events in protein aggregation: Molecular flexibility and hydrophobicity/ charge interaction in amyloid peptides as studied by molecular dynamics simulations, Proteins, 58 (2005) 110.

Van Buren, N., Rehder, D., Gadgil, H., Matsumura, M., Jacob, J., Elucidation of two major aggregation pathways in an IgG2 antibody, J. Pharm. Sci. (2008) in press.

Van Deemter, J.J., Zuiderweg, F.J., Klinkenberg, A., Longitudinal diffusion and resistance to mass transfer as causes of nonideality in chromatography, Chem. Eng. Sci., 5 (1956) 271.

Van Reis, R., Brake, J.M., Charkoudian, J., Burns, D.B., Zydney, A.L., High-performance tangential flow filtration using charged membranes, J. Membr. Sci., 159 (1999) 133.

Van Reis, R., Goodrich, E.M., Yson, C.L., Frautschy, L.N., Dzengeleski, S., Lutz, H., Linear scale ultrafiltration, Biotechnol. Bioeng., 55 (1997) 737.

Van Stokkum, I.H.M., Linsdell, H., Hadden, J.M., Haris, P.I., Chapman, D., Bloemendal, M., Temperature-induced changes in protein structures studied by fourier transform infrared spectroscopy and global analysis, Biochemistry, 34 (2002) 10508.

Vermeer, A.W.P., Bremer, M.G.E., Norde, W., Structural changes of IgG induced by heat treatment and by adsorption onto a hydrophobic Teflon surface studied by circular dichroism spectroscopy, Biochim. Biophys. Acta, 1425 (1998) 1.

Vermeer, A.W.P., Norde, W., The thermal stability of immunoglobulin: Unfolding and aggregation of a multi-domain protein, Biophys. J., 78 (2000) 394.

Virkar, P.D., Narendranathan, T.J., Hoare, M., Dunnill, P., Studies of the effect of shear on globular proteins: Extension to high shear fields and to pumps, Biotechnol. Bioeng., 23 (1981) 425.

Vladisavljevic, G.T., Rajkovic, M.B., The effect on concentration dependent viscosity on permeate flux limitation in ultrafiltration, Facta Univers., 2 (1999) 9.

Von Hippel, P.H., Schleich, T., The effects of neutral salts on the structure and conformational stability of macromolecules in solution, in: Timasheff, S.N., Fasman, G.D. (Ed.), Structure and stability of biological macromolecules, Marcel-Dekker, New York, NY, 1969, pp. 416-574.

Von Vansant, E.F., Voort, P., Vrancken, K.C., Characterization and chemical modification of the silica surface, Elsevier Science, Amsterdam, 1995, pp. 572.

Walsh, G., Biopharmaceuticals: Biochemistry and biotechnology, Wiley, Chichester, 2003, pp. 448.

Walsh, G., Second-generation biopharmaceuticals, Eur. J. Pharm. Biopharm., 58 (2004) 185.

Wang, L., Ghosh, R., Fractionation of monoclonal antibody aggregates using membrane chromatography, J. Membr. Sci., 318 (2008) 311.

Wang, W., Instability, stabilization, and formulation of liquid protein pharmaceuticals, Int. J. Pharm., 185 (1999) 129.

Wang, W., Protein aggregation and its inhibition in biopharmaceutics, Int. J. Pharm., 289 (2005) 1.

Wang, W., Singh, S., Zeng, D.L., King, K., Nema, S., Antibody structure, instability, and formulation, J. Pharm. Sci., 96 (2007a) 1.

Wang, Z., Chu, J., Zhang, X., Study of a cake model during stirred dead-end microfiltration, Desalination, 217 (2007b) 127.

Webb, J.N., Webb, S.D., Cleland, J.L., Carpenter, J.F., Randolph, T.W., Partial molar volume, surface area, and hydration changes for equilibrium unfolding and formation

of aggregation transition state: High-pressure and cosolute studies on recombinant human IFN-gamma, PNAS, 98 (2001) 7259.

WHO Expert Committee, Requirements for the use of animal cells as in vitro substrates for the production of biologicals (Requirements for biological substances No. 50), in: World Health Organization (Ed.), WHO Technical Report Series, 878, WHO Press, Geneva, 1998, pp. 19-56.

Wierenga, D.E., Cogan, J., Petricciani, J.C., Administration of tumor cell chromatin to immunosuppressed and non-immunosuppressed non-human primates, Biologicals, 23 (1995) 221.

Wilkes, J.O., Fluid mechanics for chemical engineers, Prentice Hall PTR, Upper Saddle River, NJ, 2006, pp. 753.

Williams, A., Overview of conventional chromatography, Curr. Prot. Protein Sci., 8.1 (2005) 1.

Williams, A., Frasca, V., Ion-exchange chromatography, Curr. Prot. Protein Sci., 8.2 (2001) 1.

Wimmer, K., Harant, H., Reiter, M., Blueml, G., Gaida, T., Katinger, H., Two-dimensional gel electrophoresis for controlling and comparing culture supernatants of mammalian cell culture productions systems, Cytotechnology, 16 (1994) 137.

Winter, G., Griffiths, A.D., Hawkins, R.E., Hoogenboom, H.R., Making antibodies by phage display technology, Annu. Rev. Immunol., 12 (1994) 433.

Winzor, D.J., Protein charge determination, Curr. Prot. Protein Sci., 2 (2005) 210.

Winzor, D.J., Jones, S., Harding, S.E., Determination of protein charge by capillary zone electrophoresis, Anal. Biochem., 333 (2004) 225.

Wood, S.J., Wypych, J., Steavenson, S., Louis, J.-C., Citron, M., Biere, A.L., Alpha-synuclein fibrillogenesis is nucleation-dependent: Implications for the pathogenesis of Parkinson's disease, J. Biol. Chem., 274 (1999) 19509.

Woods, A.S., The mighty arginine, the stable quaternary amines, the powerful aromatics, and the aggressive phosphate: Their role in the noncovalent minuet, J. Prot. Res., 3 (2004) 478.

Wu, D., Howell, J.A., Field, R.W., Critical flux measurement for model colloids, J. Membr. Sci., 152 (1999) 89.

Yamane-Ohnuki, N., Satho, M., Production of therapeutic antibodies with controlled fucosylation, mAbs, 1 (2009) 230.

Yao, Y., Lenhoff, A.M., Pore size distributions of ion exchangers and relation to protein binding capacity, J. Chromatogr. A, 1126 (2006) 107.

Ye, H., Simultaneous determination of protein aggregation, degradation, and absolute molecular weight by size exclusion chromatography-multiangle laser light scattering, Anal. Biochem., 356 (2006) 76.

Yigzaw, Y., Hinckley, A., Hewing, A., Vedantham, G., Ion exchange chromatography of proteins and clearance of aggregates, Curr. Pharm. Biotechnol., 10 (2009) 421.

Youravong, W., Lewis, M.J., Grandison, A.S., Critical flux in ultrafiltration of skimmed milk, Food Bioprod. Process., 81 (2003) 303.

Zettlmeissl, G., Rudolph, R., Jaenicke, R., Reconstitution of lactic dehydrogenase. Noncovalent aggregation vs. reactivation. 1. Physical properties and kinetics of aggregation, Biochemistry, 18 (2002) 5567.

Zheng, J.Y., Janis, L.J., Influence of pH, buffer species, and storage temperature on physicochemical stability of a humanized monoclonal antibody LA298, Int. J. Pharm., 308 (2006) 46.

Zimmerman, S.B., Minton, A.P., Macromolecular crowding: Biochemical, biophysical, and physiological consequences, Ann. Rev. Biophys. Biomol. Struct., 22 (1993) 27.

Zippelius, R., Untersuchungen zum Einfrier- und Auftauverhalten pharmazeutischer Humanproteinlösungen im Großmaßstab, Department for chemistry and pharmacy, Ludwig-Maximilians-University, Munich, 2002, pp. 162.